# THE AMBIENT TEMPERATURE OXIDATION OF CARBON MONOXIDE BY COPPER-MANGANESE OXIDE BASED CATALYSTS

**CHRISTOPHER D. JONES**

**Ph.D Thesis** **March 2006**





ProQuest LLC
789 East Eisenhower Parkway
P.O. Box 1346
Ann Arbor, MI 48106-1346

DECLARATION

This work has not previously been accepted in substance for any degree and is not being concurrently submitted in candidature for any degree.

Signed ..... (candidate)

Date .....

STATEMENT 1

This thesis is the result of my own investigations, except where otherwise stated. Other sources are acknowledged by footnotes giving explicit references. A bibliography is appended.

Signed ..... (candidate)

Date .....

STATEMENT 2

I hereby give consent for my thesis, if accepted, to be available for photocopying and for inter-library loan, and for the title and summary to be made available to outside organisations.

Signed ..... (candidate)

Date .....

# Abstract

The catalytic oxidation of carbon monoxide is an important reaction both commercially and scientifically. Copper-manganese oxides in the form of hopcalite have formed a cheap and accessible carbon monoxide abatement catalyst for the last 80 years. This thesis outlines the robust and reproducible preparation methods necessary for the formation of highly active species, with the heat treatment applied during the catalyst drying steps being identified as crucial for the formation of active species.

The addition of metal cations ($Co^{3+}$, $Ni^{2+}$, $Fe^{3+}$, $Ag^{+}$) to the standard hopcalite formulation has given rise to many interesting properties including increased intrinsic activity, increased surface area and greater stability of catalytic activity with increased usage.

The results of doping with a small quantity of cobalt produced materials that were amorphous to X-Ray Diffraction studies and with increased surface areas over the standard hopcalite. The dual positive effects of increased activity and prolonged catalyst stability were also brought about by the addition of cobalt (1-5% with respect to the quantity of copper present). The joint effect of precipitate ageing time and level of cobalt doping is also probed. The poisoning effect of water on the hopcalite and cobalt-doped hopcalite is reported, with the effect being identified as temporary and reversible in many cases.

The mechanisms of oxidation and deactivation over hopcalite are probed using the Temporal Analysis of Products technique with the important relationship between lattice oxygen and catalytic activity being identified. The presence of cobalt is also shown to be important to the re-oxidation of a reduced hopcalite surface.

Catalysts were produced that rivalled and often improved on the activity and stability of a presently available commercial catalyst.

## Acknowledgements

Many people deserve thanks for providing support, guidance and friendship throughout the duration of this work. The years since undertaking this project have thrown up a variety of challenges, it has not always been easy progress, scientifically or personally, but the end product is testimony to those who have not faltered in their encouragement of my work or my life.

Whole-hearted thanks must go to Graham Hutchings and Stuart Taylor for shepherding me through the rocky paths of scientific research, for their useful discussion and the ever-trickling supply of fresh ideas. The Post Docs of the group Phil, Jon, Nianxue and Dan have all been a great source of knowledge, friendship and assistance during this work and I thank them.

As for the mass hoards with whom I have shared a lab, initially I must thank Charlie and Ash for keeping me sane as I adapted to life at Cardiff, Jon Neville for being himself and providing many stories of hilarity during our few years together. Graham Laing and Darragh Ryan, two guys who were always partial to a game of pool and a pint when the going was tough, or the sun was shining!- A culture that seems to be increasingly lost to the group today. We experienced highs and lows together but the laughs and camaraderie were second to none and I hope there are many great times to come in future years as we all move on to other things. Thanks lads! I have promised Graham Laing a personal acknowledgement for his help with some technical issues throughout this work, thanks Grah, but you'll have to make do with a couple of lines rather than the 2 pages as requested!

Not to forget Tom, Sarah, Jenny and Jo, Pete, Javi, Leng Leng, Hong Mei. Gerry, the list goes on. My liver is glad to have moved on but I miss the wind-ups and Friday afternoons. Kieran, keep up the good work, I expect to see some fruit being born of my labours!

None of this work would have been possible within an EPSRC case studentship in conjunction with Molecular Products Ltd. Thank you to both for the funding over the 3 years and especially to Graham Crickmore, Dave Jones and Mandy Crudace for their useful discussions. A special thank you should go to EPSRC for continuing to pay for my upkeep in the post Cardiff years offering gainful employment since November 2004.

No acknowledgement section would be complete without thanking those people who have had to put up with me outside of University, moping around as the going got tough, or suffering a two-day hangover after a Christmas Curry, or three-day hangover after my 25$^{th}$! Mum & Dad, thank you for everything from your encouragement to the roof you put over my head and 3 years of packed lunches. Sarah, I don't know what I'd do without you, you're the best result I had in my 3 years at Cardiff and I look forward to our future together. Let us hope for many happy times ahead.

To end with a quote by Sir Humphrey Davy, **"In science one tries to tell people, in such a way as to be understood by everyone, something that no-one ever knew before. But in poetry the exact opposite is true".** How very true! Those who know me well will testify that I was never very much of a poet.

# Contents

# Chapter 1 – Literature Survey

In this chapter, many issues relating to the oxidation of carbon monoxide over metal oxide catalysts, which have arisen in literature over the past century, are discussed. Special attention has been given to the potential applications of these catalysts, preparation of active species and promotion of catalysis in these systems. The limitations of using metal oxide based catalytic systems are also recognised and explored with the aim of introducing and giving an understanding of the experimental results contained in later chapters.

## 1.1 - Carbon Monoxide

CO is a colourless, odourless, tasteless but extremely poisonous gas. It is slightly soluble in water and burns with a characteristic blue flame to produce carbon dioxide. It is a useful reducing agent, removing oxygen from many compounds and is used extensively in the reduction of metals, e.g. in a blast furnace to remove iron from its ore. [1]

Carbon monoxide is formed by the combustion of carbon in oxygen at high temperatures but can also be formed from the decomposition of carbon dioxide at excessive temperatures (>2000°C). It is often present in the exhaust fumes of internal combustion engines but can also be generated in coal stoves, furnaces and gas heaters that do not get enough air.

Known as the "silent killer", carbon monoxide is a very poisonous gas. It is especially dangerous to humans because it is not easily detected by our senses. Breathing air that contains even small amounts of CO; as little as 0.1% carbon monoxide by volume, can

prove fatal. [2] A concentration of only 1% is enough to cause death in only a few minutes. When CO is inhaled it binds irreversibly to the protein haemoglobin in red blood cells, disabling the oxygen transfer mechanism in the body. This deactivation mechanism occurs readily as CO is attracted to the haemoglobin about 210 times as strongly as is oxygen. As a result, it takes the place of oxygen in the blood causing oxygen starvation throughout the body. Early signs of CO poisoning can often be mistaken for flu due to the similarity of their symptoms; headache, breath shortness, dizziness, disorientation, nausea and fainting. At high levels, vomiting, coma and eventually brain damage and death will occur. [3-5] The depletion of dangerous levels of CO from the air around us is obviously even more important in confined spaces.

### 1.1.1 - Oxidation of carbon monoxide

$$CO + 1/2O_2 \leftrightarrow CO_2$$

The oxidation of carbon monoxide in an oxygen rich atmosphere occurs readily at high T but will only occur at lower temperatures in the presence of certain materials. The reaction is thermodynamically irreversible at room temperature, with $\Delta G°$ for the reaction being equal to -256.9KJ/mole. The major contribution to $\Delta G°$ is the high negative value of $\Delta H°$ = -282.84 KJ/mole. The entropy for the reaction is -86.61 J/K/mol, so the negative value of $\Delta G°$ becomes smaller as temperature is increased. Even at very high temperatures, the equilibrium for the reaction always favours conversion to $CO_2$. [6]

Fundamentally, the oxidation of carbon monoxide is one of the most comprehensively studied and well understood reactions. The heterogeneous oxidation of CO has been widely studied over the last century by many investigators. [7, 9, 13, 14, 20, 22] Ever

since the early work of Langmuir investigating CO oxidation over platinum group metals, where the conversion was catalysed by a heated platinum sponge which became incandescent due to the heat of reaction, scientists have been captivated by the area. [8]

The poisonous nature of CO has stimulated a large amount of interest in the heterogeneous catalysis field, especially investigations in to contact agents which operate at ambient temperature. [9] Studies in recent years have yielded substantial information on activated adsorption, the concept of active sites, the nature of the active surface and the relationship between lattice instability and catalytic instability. The oxidation of CO has often been used as a catalytic test reaction due to fact that the chemisorption of carbon monoxide is facile and non-dissociative under normal catalytic conditions. The reaction has served to increase the understanding of the redox mechanism of catalytic oxidation, as well as helping to verify the electronic theory of chemisorption on catalysts.

The revival in the study of this field has been underpinned by the development of new, high-powered surface science techniques, which have offered new insight into chemisorbed species and the molecular model of carbon monoxide oxidation. Such is its importance to fundamental catalysis principles that it is still under much scrutiny, even today.

### 1.1.2 - Carbon monoxide oxidation catalysts

The role of a catalyst in a given reaction is to alter the rate of reaction at a given reaction temperature by lowering the activation energy barrier or by providing an alternative reaction route. Varieties of materials have been reported as active for the catalysis of carbon monoxide. Some of the most popular include:

- Transition metal oxides – Zn, Mn, Cu, Ti, Fe, Ni, Co, Mo
- Precious metal oxides – Ag, Au, Pt, Pd
- Some oxides of the rare earth elements – Ce, Th

This first chapter discusses the oxidation of carbon monoxide using copper containing catalysts. Firstly, the relevant applications of such catalysts are considered.

## 1.2 – Background to carbon monoxide oxidation abatement

In recent years, there has been substantial interest in the oxidation reaction of CO to produce $CO_2$. Carbon monoxide is a pollutant of industrial and domestic origin with a well publicised history of serious health implications. Reports of long term exposure at even ppm levels have been identified as being very concerning and have prompted the development of methods to reduce exposure levels in many environments. Emission control using catalytic oxidation has many advantages over adsorption methods in terms of size of equipment, cost and operating simplicity.

As a result, high activity, low temperature carbon monoxide oxidation catalysts are highly sort after with applications arising in:

- Air cleaning in building as well as in cars
- Gas masks in military & mining fields
- CO detectors
- $CO_2$ lasers
- Space exploration
- Selective oxidation of CO in reformer gas for fuel cell applications

In order to find optimum catalysts for CO oxidation, it was first necessary to look at potential uses to which the catalyst could be put to work.

### 1.2.1 - Air cleaning in building and in cars

Due to the dangerous nature of CO it is often necessary to remove it from the air around us. In many situations, the polluted air may be rich in water vapour and only be available at room temperature. Any useful catalyst should therefore be water tolerant and operate under ambient conditions

Much work carried out in the field has focussed on the removal of CO from vehicle emissions at quite high temperatures. Unfortunately, Hopcalite catalysts are moisture sensitive and deactivate on exposure to water. [10] Hence, it is most desirable to find moisture tolerant alternatives or to incorporate elements of moisture protection in hopcalite-containing systems.

### 1.2.2 - Purification of industrial gases

It has often proved difficult to separate CO from a gaseous mixture, therefore, measures have often been taken to convert it to the less toxic $CO_2$, due to the ease of its separation. [11] This process is of great importance in the world around us.

- **Diving**

  Deep sea welders may be required to work for long periods at depths of up to a few hundred metres. The air around them requires cleaning to remove $CO_2$, CO & $NO_x$ produced as a result of respiration and welding. "Scrubbing" of the air is carried out using precious metals supported on tin oxide, with any hydrocarbons or sulphur compounds being removed before the CO oxidation takes place.

### 1.2.3 - Public protection

Many governments have contingency measures in place, which in the event of war, would protect the general population. These often take the form of underground shelters which when populated, would require much air cleaning in order to prevent the build up of toxic gases from fires and also the by-products of respiration. Precious metals dispersed on tin oxides have been deemed suitable for this purpose due to their moisture tolerance and high regeneration properties

.

- **Smoke hoods**

  These pieces of personal protective equipment (PPE) have found many uses in both the mining and aviation industries. [12] Fires in confined spaces obviously have the power to kill, though it is a little known fact that more people will die as a result of inhaling toxic gases than from the exposure to the heat of the fire itself. In this situation, PPE in the form of a smoke hood containing CO busting catalysts is essential, providing valuable minutes to escape which in many cases can make the difference between life and death.

- **Gas masks**

  Towards the end of World War I, Lamb *et al.* discovered a 4-component catalyst for use in gas mask canisters. [9] Later work foccussed on developing the catalyst for use in coal mining & fire fighting situations. The catalysts were of two types, either $MnO_2$ with copper carbonate or $MnO_2$, CuO, CoO and AgO. [13-14] Both forms were found to be highly active at room temperature, readily converting carbon monoxide to carbon dioxide with a high specific activity. When moisture protection was incorporated by the addition of drying agents such as calcium chloride, longer life catalysts were obtained. [14]

### 1.2.4 - Other applications

Lasers are a part of everyday life with applications arising in surgery, welding, drilling, spectroscopy, photochemistry and meteorology, with the $CO_2$ laser being one of the most versatile in operation. In recent years, catalysts for ambient temperature CO oxidation have been sought for use in sealed $CO_2$ laser systems to assist in the recombination of the CO and $O_2$ formed during laser usage by the dissociation of $CO_2$.

$$CO_2 \rightarrow CO + 1/2O_2$$

Consumption of $CO_2$ and a build up of $O_2$ degrades the performance of the laser leading to a loss of power output. The presence of the $O_2$ causes a breakdown of the electrical field and a decrease in the laser activity. It is therefore essential that the amount of $O_2$ present in the sealed laser is kept at a minimum. The problem of $CO_2$ consumption and $O_2$ build up has been countered by the incorporation of a catalyst which is able to convert the dissociated products back to $CO_2$. [15]

Typically, hopcalite has had only limited success in laser systems due to both its tendency to degrade to dust and its deactivation upon $CO_2$ or $H_2O$ adsorption. [15] Other more successful laser systems developed have supported precious metals on both $Al_2O_3$ and $SnO_2$.

Other uses have arisen in strictly modern applications such as the CO sensor which can provide invaluable early warning signals of a build up of the potentially lethal CO gas. A variety of CO sensors have been developed. [16-17]

## 1.3 - Hopcalite

Hopcalite catalysts have long been used in the removal of environmentally damaging gases such as $CO_x$ and $NO_x$. The early research was carried out by researchers on behalf

of the US Naval Department through a series of co-operating laboratories. As long ago as 1917, researchers at the John Hopkins University, under the direction of J. C. W. Frazer, investigating a large number of oxidising agents, discovered the high activity of the $CuMn_2O_4$ phase, produced by the reaction of copper and manganese oxides, for the oxidation of CO at low temperature. [9] Ever since, Hopcalite has often been used to oxidise a range of environmentally damaging gases over a range of temperatures, from ambient through to 400°C. It is only at higher temperatures where their effectiveness lessens due to structural rearrangement. [18] Catalysts of this type are the catalysts of choice for respiratory protection. [19-21]

### 1.3.1 - Hopcalite – Early research

Investigation into CO oxidation by Stieglitz gave positive results at room temperature for the combustion of CO with oxygen from air. Finely divided palladium oxidised a 0.3-0.5% CO mixture when the gas was dried over soda lime & calcium chloride. Initially all the carbon monoxide was removed but the catalyst was observed to deactivate with time on stream. Despite the positive results it was decided that CO oxidation involving palladium based catalysts would ultimately prove too expensive. [9]

Not to be perturbed, research continued, this time focussing on the activation of metal oxides; especially on copper oxide, using small amounts of palladium. Copper oxide was impregnated with dilute palladium nitrate and the impregnated granules heated in air at 450 – 500°C for a short period of time. During tests of the single oxide, copper oxide alone removed 20 to 50 % of CO from a 1% mixture of CO with air. When doped with 0.25 to 0.4% palladium, 95 to 100% of the CO was removed initially with activity dropping to 80 to 85% after 2 to 3 hours of the experiment. The promotional behaviour

of precious metals in conjunction with basic metal oxide systems was highly evident at this early stage. It is an area of research that has fascinated researchers ever since.

Further work by Stieglitz realised that a silver oxide & sodium peroxide mixture was a potent oxidation system for CO removal at room temperature. The silver oxide was precipitated from a dilute solution of silver nitrate, washed then filtered. The two components were pressed together and dried at 85-120°C, then further dried at 200°C.

At CO concentrations between 0.5 & 4.5%, 98% of CO was adsorbed from a 500ml gas sample over 2 minutes. The reaction worked slowly at 0°C and involved a considerable start-up time. Neither sodium peroxide nor silver oxide singularly was able to oxidise CO at room temperature, so the level of their combined performance suggested a synergistic effect between the components. On the application of heat, at 40 to 50°C, the reaction started rapidly and continued without the addition of further heat due to the exothermic nature of the reaction. The theory behind the operation of this catalyst was that the sodium peroxide removed the $CO_2$ formed, thus preventing the formation of carbonates on the silver oxide surface. The presence of small amounts of moisture in the catalyst system was found to be beneficial to catalytic activity.

The follow up to this work investigated copper and silver oxides in combination. The copper oxide was specially prepared by precipitation and activated with 1% silver oxide. Initial activity was below 50%, the catalyst lifetime was short and the action appeared to be chemical rather than catalytic. It was not possible to promote activity by increasing the silver oxide loading.

### 1.3.2 - Cobalt oxide

Wright and Luff investigated a system containing cobalt oxide prepared by the treatment of cobalt sulphate with excess sodium hypochlorite and sodium hydroxide at room temperature. [22] The mixture was left for 30 minutes, during which time the excess of hypochlorite decomposed. The hydrated oxide was thoroughly washed and dried at 120°C. The cobalt oxide granules were tested for their behaviour towards a 1% carbon monoxide mixture. Any changes in the nature of the preparation greatly affected the physical nature of the granules. It was further evident that a highly porous, yet hard granule was a goal to be striven for, as had been indicated in some of the pioneering work in the area. [9] Better results were obtained for dry 1% CO than moist gas, leading to the conclusion that water, in some way was acting as a poison towards cobalt oxide. The usual lifetime of the catalyst was only an hour. Dry gas activity varied between 15 and 100% but inconsistencies occurred in the results with reproducibility being highlighted as a problem.

### 1.3.3 - Copper and cobalt oxide

A combination of copper and cobalt oxide in 60:40 mixture was prepared by an intimate mixture of the moist hydrated oxides. [9] The activity was partially catalytic since the decrease in available oxygen during the experiment was insufficient to account for all the carbon monoxide oxidised. The average lifetime of the catalytic system was 2 hours.

### 1.3.4 - Manganese dioxide and silver oxide

Frazer working at the John Hopkins University noted that neither manganese dioxide nor silver oxide reacted rapidly with CO at room temperature. [9] Sodium hydroxide was added to increase activity (up to about 15 to 23%). On the addition of a small amount of calcium chloride to the layers in the absorption tube, the lifetime of the

absorbent was increased dramatically with the calcium chloride thought to be acting as a desiccant. At room temperature, a 1% CO test mixture was completely oxidised with a catalyst lifetime of 30 to 40 minutes. In the absence of calcium chloride, the system operated for 10 – 15 minutes before efficiency fell below 90%. The presence of moisture in the gas increased the life of the absorbent. This result was similar to that seen when copper oxide was used in combination with silver oxide. At low temperature, 0°C, the system operated at high efficiency but only for a short time period. Typically a silver to manganese ratio of (1.5-2.5):1 was used.

More encouraging results were obtained with a three component mixture Co:Ag:Mn 1:1: (0.5-1). This system exhibited a lifetime of longer than 1h against dry gas. Silver oxide was identified as a crucial constituent as when smaller amounts of $Ag_2O$ were used, the materials produced were less active.

The promising results of this work led to further investigation of the topic. More active varieties of manganese dioxide were prepared by the omission of sodium hydroxide which lead to an increase in catalyst lifetime. The first really active manganese dioxide was prepared by reducing methyl alcohol with a cold solution of ammonium permanganate. A highly divided manganese dioxide was obtained. A 50:50 mixture of this and silver oxide had a lifetime of over 3 h.

Around the same time at Washington State University, Merrill, Bray and Scalione discovered a three-component mixture of cobalt, manganese and silver oxides (20:34:46), prepared by the interaction of silver permanganate with moist hydrated cobaltic oxide. Its behaviour towards a 1% mixture of CO was investigated, with the results indicating $MnO_2/Ag_2O$ to have an indefinite lifetime in dry gas, but to be

poisoned fairly rapidly by moisture. [121] It was observed that during the deactivation, the amount of $O_2$ available in the sample decreased. This suggested that the oxygen source for the reaction was drawn from within the mixed oxide system, i.e. either surface or lattice oxygen. It was reported that a return to normal activity occurred when the system was treated with dry gas. The behaviour of this species towards moisture was characteristic of all the samples prepared. The preparation involved the hydrated oxides being prepared separately, washed thoroughly, then intimately mixed. Impregnation with silver oxide then took place. The samples were dried slowly at 120°C, meshed then dried at 200°C. It was noted that the method of drying was very important as this step determined the water of hydration left in the granules, which was thought to be a determining factor in preparing active catalysts.

More active species were obtained when the samples were heated for a short time at 200°C after preliminary slow drying at 200°C. This was found to be most important in the cobalt containing catalysts. Cobalt oxide when prepared in this way was active at room temperature. This was the first example of a single metal oxide being active for carbon monoxide oxidation. Prolonged heat treatment, especially at high temperature spoiled the catalyst activity, this was attributed to the destruction of the porous nature of the granules. It was also evident that materials made largely of silver oxide catalysts were highly affected by rigorous heating.

It was postulated that the physical nature of the granules and the catalytic behaviour were determined by the size and composition of the particles from the catalyst precipitate. Fine precipitate particles which did not clump together before filtration gave hard, relatively non porous catalysts which were found to be less active catalysts than the more porous species. However, when the particles were too coarse, soft and

active particles were obtained, though these were not robust enough for use in canisters. Highly porous granules generally had a higher surface area, resulting in higher activity. However, this high porosity was thought, in part, to the ease the poisoning by water vapour, which was observed for all samples tested at room temperature.

The most active catalysts contained $MnO_2$ as the chief constituent, prepared by the Fremy Method. [23] Many mixtures of widely altering compositions were found to be active for CO oxidation. The chief constituent in all cases was $MnO_2$, with silver oxide also present, the upper limit of $Ag_2O$ for optimum performance was found to be 38% in the two component mixture, 15% in a three component mixture with copper oxide and 5% or less when cobalt oxide is also present.

The standard formulation of hopcalite was chosen in August of 1918. It was a four component mixture containing 50% $MnO_2$, 30% CuO, 15% $Co_2O_3$ and 5% $Ag_2O$. The substance was batch produced and given the name Hopcalite I. At around the same time a two-component mixture of $MnO_2$ (60%) and CuO (40%) was prepared from active manganese oxide and copper carbonate. The copper carbonate was completely converted into copper oxide upon calcination. A decision was taken as to which catalytic system should be mass-produced. The consensus was to go with the four-component mixture. However, it is interesting to note that the commercially mass produced hopcalite formulation of today tends to be based around a two-component mixture of CuO and $MnO_2$ combined with stabilisers and inert bulking materials. [24]

## 1.4 - Catalytic systems containing copper oxide

Catalysis over copper containing species is significant to many reactions, including the water-gas shift reaction, methanol synthesis as well as in air cleaning and in the control

vehicle emissions. In the water gas shift reaction, carbon monoxide removes surface hydroxyls or oxygen which are produced by the dissociation of water [25]. Studies have shown that the $CuO/ZnO/Al_2O_3$ precursor can be used for the production of a methanol synthesis catalyst. [26-30] Methanol was formed by the hydrogenation of carbon dioxide, but the catalyst enabled oxygen to scavenge any carbon monoxide left on the surface.

In the case of automobile catalysts, copper has been explored as a possible alternative to precious metals like platinum and palladium for the reduction of nitrogen oxides by carbon monoxide in catalytic converters. The reaction proceeded through the decomposition of $NO_x$ to deposit nitrogen gas and adsorbed oxygen on the catalyst surface, the oxygen was then available to react with the carbon monoxide to form $CO_2$.

The role of the copper in this reaction is not fully understood, it has been widely assumed that copper is active in a particular oxidation state or that it cycles between states in a redox reaction [31-32]. Jernigan and Somorjai were amongst the first to investigate how the oxidation state of copper affects the reaction rate. [33] They also reported the first high pressure study for CO oxidation on copper and oxidic copper surfaces. By adjusting the $CO/O_2$ partial pressures in the reaction mixture they could determine the oxidising power. Within certain ranges of $CO/O_2$ pressures they could isolate the copper species in oxidation states of zero, $^{+}1$ and $^{+}2$. At high pressure, the conversion of CO proceeded fastest over $Cu^0$, metallic copper at 300°C, followed by $Cu^+$ and $Cu^{2+}$, in order of increasing oxidation state.

Ethyl acetate and ethanol are some of the most dominating VOC's, especially in the printing industry and CO is one of the main components in the waste gas from

formaldehyde plants. Catalytic incineration is an important way to reduce both CO and VOC emission. Supported precious metal catalysts have most commonly been used in this process, but metal oxide catalysts, including those containing CuO have also found extensive applications. [34-37] Precious metal catalysts are in general more active and more tolerant to sulphur poisoning than metal oxides. However, metal oxides are much cheaper and allow for a higher catalyst load. [38] The provision of the higher surface area in metal oxide catalyst beds also makes the catalyst more resistant to non-selective poisoning, which is a common problem in emission control. [39] Liu *et al.* have shown the level of CO oxidation over ceria supported copper oxide to be similar in magnitude to oxidation over precious metal catalysts. [40] Both McCabe [41] and Yu Yao [42] have stated that $Pt/Al_2O_3$ catalysts are only slightly more active than metal oxide catalysts for ethanol oxidation.

On studying several mixed metal oxide systems, Rajesh and Ozkan [43] and Yu Yao [42] found $CuO/Al_2O_3$ to be the most active catalyst for the complete oxidation of ethanol. McCabe *et al.* have shown that the activity of hopcalite ($MnO_2$: CuO of 4:1) was comparable to a $Pt/Al_2O_3$ catalyst for the combustion of ethanol but was irreversibly deactivated at around 500°C. [44] This is the temperature at which the amorphous to crystalline phase transition as been reported to take place in hopcalite systems. [18]

## 1.5 - Recent work in to hopcalite catalysts

The effect of the preparation conditions on the activity of hopcalite catalysts has been shown to be of great importance. Variables such as precipitate ageing time, pH, temperature, Cu:Mn ratio of reactants as well as catalyst drying and calcination temperature and duration have all been shown to be crucial. [21] Optimum preparation

conditions have been identified in terms of producing the highest activity for the oxidation of CO at ambient temperature. A number of factors, which can be varied during the catalyst preparation procedure and subsequent calcination step, were found to be crucial in controlling the composition and activity of the copper manganese mixed oxide. Conditions for optimum activity were found by Hutchings *et al.* to be "1/2 [Cu]:[Mn] ratio at pH = 8.3 and 80°C for 12h ageing time, followed by calcination at 500°C for 17h".

The relationships between bulk phases and catalytic activity were found to be complex. Generally, the catalysts showed X-ray diffraction features corresponding to amorphous mixed copper manganese oxide phases. Catalysts that were calcined above 500°C were highly crystalline and displayed high specific activity, however this was found to be a consequence of the low surface areas of the material and not due to a high CO oxidation activity.

The un-aged precursors were largely composed of copper hydroxy nitrates and manganese carbonate. At the moment of precipitation, copper and manganese were observed in separate phases but on ageing the phases re-dissolved to give poorly crystalline manganese carbonate, exemplified by broad line spacing on XRD analysis. On calcination the metal carbonates were converted to yield the metal oxide catalyst. The un-aged calcined catalyst was found to comprise of copper manganese oxide $Cu_{1.4}Mn_{1.6}O_4$ with $Mn_2O_3$ and CuO. Ageing the precipitation mixture for 30 minutes produced a system containing a similar set of components.

Samples aged between 60 and 240 minutes comprised of $Cu_{1.4}Mn_{1.6}O_4$ , $Mn_2O_3$ and CuO. The CuO signal was weak and the $Mn_2O_3$ intensity decreased with increased

ageing time. The 300 minute aged catalysts were mainly $Cu_{1.2}Mn_{1.8}O_4$ with $Mn_2O_3$ and CuO present as minor phases. The 12h aged catalyst was less crystalline with $CuMn_2O_4$ and CuO the major phases present. No $Mn_2O_3$ was detected on XRD analysis. These results indicated that increasing the sample ageing time, the proportion of manganese which was incorporated within the mixed oxide phase was increased.

Typical surface areas for the catalysts produced were in the region of 25 - 31$m^2$/g. Activities of the catalysts aged for less than 30 minutes were thought to be due to the presence of CuO in the catalyst. On XRD analysis the relections due to the presence of CuO were observed to decrease for the catalysts aged between 60 and 240 minutes. It was during this ageing time period that the most inactive catalytic species appeared to be produced. The studies detailing ageing time were largely linked with the bulk phase properties of the catalyst system. These correlations could not be made for other preparation factors such as pH and temperature.

Doeff *et al.* have shown using XPS that the Cu/Mn ratio decreases with increased ageing time, this was consistent with the peak intensities recorded during XRD studies for species aged for different lengths of time. [45] A precipitate ageing time of 12h yielded the highest activity catalyst, where Cu/Mn was 0.5, as might have been expected for $CuMn_2O_4$.

On further XPS analysis, smaller Na/Mn ratios were observed for catalysts produced with longer ageing times. Experiments conducted at a higher pH resulted in the quantity of surface $Na^+$ decreasing and an associated increase in activity of the system. It was clear from this study that catalyst ageing time and calcination conditions were the factors of most significance in preparing highly active hopcalite species.

Recent work in the field of low temperature CO oxidation has increased since Haruta *et al.* demonstrated that gold highly dispersed on various oxides forms catalysts active at sub-ambient temperatures. [48-49] It was suggested that a synergistic mechanism was occurring at the gold and metal oxide interface, with the metal oxide not simply acting as an inert carrier, but playing a key role in the catalytic process. [50-51] CO oxidation was proposed to occur when CO adsorbs onto a metallic Au site adjacent to a metal oxide site occupied by an adsorbed $O_2$ molecule, with the catalytic reaction proceeding via an intermediate carbonate-like species that decomposed to $CO_2$; at which point it could desorb from the surface.

Systems involving other noble metals have also been found to give high activity but commercial catalysts of this type would prove expensive due to the rarity and the need for complex pre-treatment of the precious metals involved. [52-54]

The versatility and longevity of use of hopcalite catalysts has demonstrated that oxide catalysts can offer a viable alternative to precious metal based systems, despite often providing lower activity and inflated operating costs. Single component metal oxide catalysts have struggled to directly rival precious metal catalysts but activity can be vastly improved by combining several elements or by the addition of promoters. [55-57]

Catalytic oxidation of CO on transition metal surfaces has received significant interest in industrial chemistry and in emission control. [58-59] Manganese oxides have been widely applied as catalysts and structural promoters for heterogeneous reactions. [60] Mixed oxide catalysts have often contained manganese along with a polyvalent metal such as Cu, Co or Ag. It would seem that the main disadvantage of metal oxide catalysts

in commercial systems is their instability in gaseous media containing hydrocarbons, water and sulphur-containing species. [53]

The addition of precious metal promoters has often given rise to an increase in activity of hopcalite at elevated temperatures. Ferrandon *et al.* have carried out tests into Cu and Mn oxides singularly and in combination with Pt and Pd species. [53] Catalytic activity was described before and after hydrothermal treatment and the exposure to $SO_2$ in order to test the resistance of the catalyst towards potential poisons. The test mixture consisted of naphthalene, CO and $CH_4$ in order to best resemble the composition of flue gas from wood burners. In general, the activity of noble metal catalysts for the oxidation of CO was higher than the activity of the metal oxide catalysts alone. On addition of $MnO_x$ to Pt/Pd, the activity of the corresponding metal was observed to decrease for CO oxidation. However, mixed $CuO_x$-Pt and $CuO_x$-Pd systems were seen to retain the performance of the most active catalytic component.

After hydrothermal treatment, the Pd catalyst continued to display a higher activity than the Pt catalyst for CO oxidation. The same was found to be true on treatment with sulphur. Combining both the metal and noble metal oxides lead to more resistant catalysts when compared to the single oxide species alone. This enhancement of activity was thought to be due to the $MnO_x$ combining with $SO_2$ at low temperatures to form manganese sulphate, where the $MnO_x$ was acting sacrificially preventing Pd & Pt from being poisoned.

In summary, it was found that sulphur treatment increased the activity of $MnO_x$-Pt , with the increased activity on the surface thought to be due to the presence of sulphate which prevented the oxidation of Pt, thus enhancing the activity of the Pt catalyst for

CO oxidation. The $CuO_x$-Pd catalyst when exposed to sulphur, also exhibited an increase in activity with the activity being better then the Pd catalyst alone. The impediment of CO oxidation on $MnO_x$ and $CuO_x$ with sulphur treatment was thought to be due to an inhibiting effect of $SO_2$ on CO adsorption, where a fast poisoning of the carbonyl adsorption sites; which were necessary for CO oxidation to proceed, occurred.

## 1.6 - Cobalt oxide as a catalyst

Cobalt oxide has been shown to exhibit a very high activity towards CO oxidation at room temperature. [61] In a similar mode of behaviour to that of hopcalite catalysts, this activity was shown to decrease in the presence of $H_2O$ and hydrocarbons and with time on-line. Mergler reported $Pt/CoO_x/SiO_2$ to be the most active system out of three tested ($CoO_x$, $CeO_2$ or $MnO_2$). The mechanism proposed suggested that CO was adsorbed on Pt & $O_2$ was dissociated on $CoO_x$. The reaction of carbon monoxide and oxygen took place ($CO_{ads}$ and $O_{ads}$) either at the interface between Pt and $CoO_x$ or by $O_2$ spillover to Pt sites. [62]

Haruta investigated CO and $H_2$ oxidation over gold nano-particles supported on $Co_3O_4$, where oxidation was recorded at temperatures as low as -70°C. [63] Haruta suggested CO to adsorb on to Au particles with $O_2$ adsorption occurring on the metal oxide. The reaction then could have taken place at the interface between the Au particles and $Co_3O_4$.

The $Co_3O_4/Al_2O_3$ system exhibited a high activity towards CO oxidation even without the presence of a noble metal. Carbon monoxide was unable to block the cobalt oxide surface from $O_2$ adsorption as it had on platinum. An Infra Red Spectroscopy study into CO, $CO_2$ and $CO+O_2$ revealed that during exposure to CO, $CO_2$ was formed due to the

reaction of CO with surface oxygen. Surface carbonate groups were formed and attributed to $CO_2$ adsorption or possibly CO adsorption. Deactivation due to time on line was recorded and partially attributed to surface sites becoming saturated with carbonate species, hindering further reaction. The decline in activity could also have been due to carbon deposition formed by CO disproportionation. [61]

The model proposed for CO oxidation on $Co_3O_4$ was therefore:

- CO adsorbs on $Co_3O_4$ surface
- Adsorbed CO reacts with surface oxygen and desorbs as $CO_2$, a carbonate species may be formed as an intermediate
- The reduced cobalt is re-oxidised by gas phase $O_2$ or possibly further reduced by CO causing deactivation of the site
- $CO_2$ can then adsorb on the surface to form carbonate species.

Takita studied the adsorption of oxygen and water on cobalt oxide and the effects of co-adsorption of water on oxygen over $Co_3O_4$ using TPD techniques. He concluded that at least 3 types of oxygen were adsorbed on the surface of $Co_3O_4$ calcined at 823-973K. TPD experiments also revealed the presence of four types of water species on the oxide surface, all desorbing at temperatures between 300 and 700K. The adsorption of water onto the surface strongly affected the quantity of oxygen that could be co-adsorbed on to the surface. When the level of $H_2O$ reached a critical level, no further oxygen could adsorb on to the surface, having the effect of diminishing the oxidising power of the cobalt oxide catalyst in moist atmospheres. [64]

## 1.7 - Manganese dioxide based catalysts

It has been previously noted in this chapter that manganese oxide has long been a major component of oxidation catalysts. [14] During the early years of research in to the

oxidising ability of metal oxide systems, the chosen formulation for the Hopcalite I catalyst contained 50% $MnO_2$. Manganese oxide alone has not been reported as active for CO oxidation at ambient temperature; however, when combined with other metal oxides and especially when at elevated temperature, a potent oxidising system can be formed. [21,53]

Whitesell and Frazer were amongst the first to note the activity of manganese oxide, which represented the first example of an industrially important catalyst. [65] A material catalytically active at sub ambient temperatures was synthesised by treatment of potassium permanganate with sulphuric acid and subsequent treatment of the product with nitric acid. The hydrated oxide precipitate was washed thoroughly and oxidised using a drying process. As with many metal oxide catalytic systems, poisoning by water vapour was a problem. However, the regeneration of a water-deactivated species was achieved on prolonged heating.

The oxidation of carbon monoxide over manganese-based catalysts does not appear to be well understood and over the years, varieties of mechanisms have been postulated. The early work of Roginski and Zeldovich suggested the oxidation of carbon monoxide to proceed by the reaction of gas phase oxygen with chemisorbed CO. [66] Klier and Kuchyncka observed that oxidation of carbon monoxide by lattice oxygen occurred rapidly producing both surface adsorbed and gaseous carbon oxides. [67] In recent years Kobayashi and Kobayashi have been able to apply transient experiments to the reaction. Using a continuous flow catalytic reactor and sudden changes of the feed gas composition they have observed the variations in the make up of the outlet gases. Iodometric experiments have been applied to scope the oxidation power distribution of the surface adsorbed oxygen species. [67] The method revolved around the analysis of

the quanity of iodine produced from KI solutions at different pH values when in contact with the oxide surface. [69] Where the oxidation power was high, Iodine was produced in the solutions of higher pH. By applying this methodology it was shown that two types of oxygen were present on the $MnO_2$ surface; a species of high oxidising power consisting of only a fraction of the surface and a species of much lower oxidising power populating the vast majority of the surface. The high oxidising power species were thought to be either $O^{2-}$ or $O^-$ ions. The experiments concluded that gaseous CO reacted directly with the surface oxide species, forming a surface carbonate intermediate that decomposed to yield gaseous $CO_2$. Kinetic experiments have postulated that the RDS is the reaction between surface $O^{2-}$ ions and CO from the gas phase. Investigations by Davydov, utilising IR techniques have proven the reaction between chemisorbed oxygen and carbon monoxide as well as the formation of carbonate based intermediates. [70]

## 1.8 – Catalyst Preparation

The most common method for the preparation of mixed oxide catalysts is crystallisation or co-precipitation in solution of a precursor form (hydroxide, oxide, insoluble salt) of the catalyst. [71-72] A much studied case, and possibly the most successful, is that of the hydroxy carbonate for preparing catalysts containing copper, zinc or chromium along with additional elements (Co or Al). These studies were brought about by the practical importance of catalysts used in making synthesis gas and methanol.

The process of precipitation involves two main stages, nucleation and growth. During the nucleation process, the first minute crystals of the solid phase begin to form, these tend to have a high specific surface area and high free energy, so are considered as quite unstable. Below a certain critical size of nuclei, the free energy of formation of the solid

phase is less than its surface energy so the new phase is thermodynamically unstable. Above this critical size solid particles can grow. The growth step tends to be controlled by interface or diffusion phenomena. The first case involves the formation of complicated solid structures, while the second is more common in the precipitation processes used in catalyst preparation. [73]

In general, the following parameters are useful for nucleation:

- The higher the super saturation, the higher the nucleation rate
- Any interface may act as a heterogeneous nucleus by lowering the surface free energy of the new phase, thus increasing the rate of nucleation
- Elevated temperatures lower the nucleation rate by increasing the critical size of the nuclei

The following parameters are necessary for particle growth:

- The higher the super-saturation the higher the growth rate, but this is rapidly limited by diffusion processes
- Since an increase in temperature enhances the diffusion rates, the higher the temperature, the higher the growth rate of the new phase

Some general rules for obtaining a fine precipitate might include:

- Vigorous stirring during the addition of the precipitating agent. This is beneficial in two ways: firstly, each volume of solution rapidly reaches the highest degree of super-saturation; secondly, contact time with the agitator and the walls of the vessel is maximised, thereby promoting heterogeneous nucleation.
- Rapid addition of the precipitating agent. This ensures a rapid reaching of the highest degree of super-saturation in the whole volume of the solution, hence a

maximum nucleation rate is obtained. For the same reason, the best precipitating agent is often the one which gives the lowest solubility product.

- Precipitation is often advantageously made at the lowest practical temperature, as this often favours nucleation over growth

During the precipitation process, the multi-element product can be of three types:

- Metals combine in an insoluble single compound. Instances include the precipitations as chromates, molybdates and tungstates.
- Metals may precipitate into a single phase solid solution or a single phase mixed structure, e.g precipitation by sodium carbonate of aluminates or hydroxyl precursors of aluminates of Cu, Fe, Ni, Zn and Mg. Divalent metal oxalates can also be precipitated in this way.
- Metals may precipitate simultaneously, but in separate phases, e.g. metal hydroxides precipitated by NaOH, KOH and $NH_4OH$. Usually $NH_4OH$ is preferable for precipitation, especially when washing off all the alkali from the catalyst is a prerequisite for the preparation of the final catalyst.

Koleva has reported that most preparations of hopcalite involve the use of nitrate precursors because of their high solubility and the ease of removal of the nitrate anion during the calcination step [46]. In this way, the nitrate leaves no residue on the catalyst, unlike during the use of chlorides or sulphates which have commonly lead to the retention of the metal anion on the surface. These observations were echoed by Hutchings and Vendrine. [74] For alumina supported hopcalites, it has been found that the use of manganese acetate in place of the nitrate leads to a highly dispersed oxide phase. Another popular route to the hopcalite catalyst is the decomposition of the copper and manganese formates at 350 – 450°C. [75] Variations of the co-precipitation

method appear to be the most popular routes towards the final catalyst where the use of nitrate precursors predominates. Sol-gel precipitation is common in producing copper manganese oxides for use as cathode materials [45], with the $CuMn_2O_4$ spinel also being produced by more hi-tech methods including ultrasonic thermal decomposition.

The spray pyrolytic process for mixed oxides offered an attractive route to catalytically active materials. The one-step process from simple precursors produced finely dispersed and homogeneous powders of a regular shape. [47] Problems arising from unstable precursors, heterogeneous decomposition or partial loss of the precursor due to sublimation had to be avoided so the selection of suitable precursors was of crucial importance. The cationic and valency order of $CuMnO_x$ was changed as compared to the spinel synthesised by conventional solid state reactions. [21] The reasons for this behaviour were attributed to the reaction mechanism of this procedure with a quick reaction time and moderate decomposition temperature. Catalytic experiments identified the spinel as having high activity for CO oxidation, supporting the belief that spinel formation in amorphous Cu/Mn catalysts is a promoter of CO oxidation. Investigations also indicated that activity depends on calcination conditions supporting the views of Hutchings. [21]

## 1.9 - The Effect of Electronic Structure on CO Oxidation over Transition Metal Oxide Surfaces

Transition metals with d-bands are excellent catalysts for both hydrogenation and oxidation. [76] The electronic structure of the metal can be described using the band theory model, which states that a metal is a collective source of $e^-$ and $e^-$ holes. There are two regions of energetic states, namely the valence and conduction band, with mobile electrons and positive holes. The potential energy of the electron is characterised

by the Fermi level, corresponding to the electrochemical potential of the electrons and electron holes. The amount of electron density also dictates the position of the Fermi level. A metal has a certain number of free levels or d-holes available for bonding with adsorbates. At the surface, the free electrons or holes allow molecules to bind to the surface, with the strength of the binding depending on the position of the Fermi level, a lower Fermi level will gives stronger adsorption. Acceptor species e.g. ($O_2$) take electron density from the conduction band of the metal causing the Fermi level to drop. Donor species e.g. ($H_2$,CO,$C_2H_4$) give $e^-$ density to the conduction band. In general, metals have a narrow d-band, with the catalytic properties of the metal being influenced by the occupational density of the $e^-$ in this band. It is possible to see direct relationships between the catalytic activity of the transition metal and the electronic properties of the unfilled d-bands.

| **n-type** | **p-type** | **I-Type** |
|---|---|---|
| ZnO, $SnO_2$ | NiO, $Cr_2O_3$, **MnO** | $Fe_3O_4$, $Co_3O_4$ |
| | FeO, CoO,$Cu_2O$, $Ag_2O$ | **CuO** |

Oxides of the transition metals give the most active, selective & industrially important catalysts. Electronic theory predicts numerous other semiconductors to have catalytic activity though chemical factors also predominate.

Chemisorption is an important factor in oxidation reactions. CO oxidation has been thoroughly investigated with the p-type semi-conductor NiO & the n-type semi conductor ZnO as the catalyst. [73]

| | $E_a$[KJ/mol] | | $E_a$[KJ/mol] |
|---|---|---|---|
| NiO (p) | 63 | ZnO (n) | 118 |
| $Cr_2O_3$ doped | 80 | $Ga_2O_3$ doped | 84 |
| $Li_2O$ doped | 50 | $Li_2O$ doped | 134 |

The p-type NiO semiconductor was the better catalyst; an increase in p-type conduction due to $Li_2O$ was observed along with a decrease due to $Cr_2O_3$.

It has been widely reported that the donor step is rate determining, namely the chemisorption of CO.

$$CO + [+] \rightarrow CO^{+}_{ads}$$

The assumption is supported by the observation that the reaction is first order in CO.

The chemisorption of $O_2$, an acceptor step, is fast, and the reaction rate is not dependent on $P_{O2}$.

$$\tfrac{1}{2} O_2 \rightarrow O^{-}_{ads} + [+]$$

The final step is neutral and follows the Langmuir Hinshelwood mechanism

$$CO^{+}_{ads} + O^{-}_{ads} \rightarrow CO_{2\,(g)}$$

In the first instance, the influence of donors on ZnO looked remarkable; it might be expected that increasing the n-type conductivity by adding trivalent donors would lower the reaction rate. However, this is not reported, leading to the conclusion that in this case, an acceptor reaction was the rate-determining step. It is possible that the RDS is the chemisorption of $O_2$ owing to a considerable dependence of the reaction rate on the partial pressure of oxygen being observed.

Iron and chromium mixed oxides are important oxidation catalysts. Metal oxides with $d^0$ or $d^{10}$ electronic structures have often been reported to be useful oxidation catalysts. [76] Levels of activity have been correlated with:

- The strength of bonding of O to the surface
- The heat of formation of the metal oxide
- The availability of lattice oxygen

Catalytic activity during the oxidation of CO is reported to correlate with the bonding energy of $O_2$ on the surface. Other considerations such as surface geometry, orbital structures of catalyst & starting materials must also be taken into consideration.

## 1.10 – Promotion of Catalysis

Promoters are of great use in catalytic research due to their remarkable influence on reactivity and activity. In fact, the future of catalysis is likely to progress largely towards the use of promoters. The catalytic properties of pure substances are generally well known but the possibilities for improvement through the use of suitable promoters are widespread. A promoter can be defined as a substance added to the catalyst during its preparation in small amounts, usually less than 10%, which by itself has little activity but imparts either, better activity, stability or selectivity for the desired reaction than is realised without it. [77]

**Structural Promoters** – One of the most important types of promoter is the one where the surface area of the active component is increased. This usually involves stabilising the catalyst by inhibiting the loss of surface area during usage but can be by other methods.

**Electronic Promoters** - Dispersed in the active phase & influences the electronic chemical bonding to the adsorbate. The reaction depends on the ability of the metallic system to accept electrons from and give up electrons to the surface. Many metals have

vacant orbitals or "holes", thus possessing a high affinity for additional electrons. If a foreign substance is added, this effects the number of empty orbitals and consequently the catalytic activity. If the activity is improved more than expected from averaging because of the effect of the vacant orbital, the substance may be considered as an electronic promoter.

**Lattice Defect Promoters** - The active centres of many oxide catalysts can be strongly linked to the presence of lattice defects that occur near the surface. A small amount of impurity or additive can largely increase the number of lattice defects since each interstitial foreign atom may be at the centre of a lattice defect that extends for 10A or more. If the promoter increases the catalytic properties by affecting the number of lattice defects, it can be considered as a lattice defect promoter. In order for the interstitial substitution to take place, the foreign ion needs to be almost the same size as the one it is replacing. Also related to the defect formation is the electrical conductivity and valence state of the ion. Small amounts of impurities or promoters may affect the electrical conductivity of semi-conductor oxides and can change the stable valence state of neighbouring atoms if the impurity has a valance different from that of the ion it is replacing.

**Textural promoters** – These inhibit the growth of catalyst particles to form large, less active sites during the reaction. Thus, they prevent loss of active surface by sintering and increase the thermal stability of the catalyst.

E.g. $Cu/ZnO/Al_2O_3$, low T conversion, ZnO promoter gives decreased Cu sintering.

## 1.11 – Spinels of copper and manganese – Ionic Configuration and Structure

Over the years, there has been much interest in copper and manganese spinels. Interesting crystallographic properties were expected due to the presence of the two types of Jahn Teller ions, $Mn^{3+}$ and $Cu^{2+}$. In spite of the attention given to the subject, the distribution of the metal cations amongst tetrahedral and octahedral sites, as well as the valencies of the copper and manganese ions is still poorly understood.

In 1958, Sinha and co-workers were amongst the first to report that the hopcalite spinel, $CuMn_2O_4$, had a cubic structure. After considering x-ray intensities and bonding rules they proposed the formula, $Cu^{+}[Mn^{3+}Mn^{4+}]O_4$, where manganese was present in mixed oxidation states and its cations were present in an octahedral environment. [78] Miyahara disagreed and in 1962 published his own findings, proposing a configuration of $Cu^{2+}[Mn^{3+}]O_4$, based on the assumption that the local distortions caused by octahedral and tetrahedral $Cu^{2+}$ compensate for each other resulting in a macroscopic structure. [79]

A variety of authors have reported difficulty in preparing pure $CuMn_2O_4$. [80-82] A tetragonal spinel was obtained by Buhl *et al.* but involved heating to temperatures around 940°C. [82] At lower temperatures, the cubic spinel phase was obtained but it was found to contain significant quantities of impurities.

Vanderberghe reported the preparation of stoichiometric $CuMn_2O_4$ to be impossible at room temperature to broadly confirmed this theory. [83] He suggested that a cubic configuration could only arise with excess copper ($x = 0.05$) for $Cu_{1+x}Mn_{2-x}O_4$. Results

indicated that tetrahedral $Cu^{+}$ and octahedral $Mn^{4+}$ offer the most stable environment in copper manganite spinels.

The reaction between $Mn_2O_3$ and CuO was accompanied by electron transfer. Where:

$$CuO + Mn_2O_3 \rightarrow Cu^{+}[Mn^{3+}Mn^{4+}]O_4^{2-}$$

$$Cu^{2+} + Mn^{3+} \rightarrow Cu^{+} + Mn^{4+}$$

$Cu^{+}$ preferred a tetrahedral site due to its $d^{10}$ configuration, forming stable $sp^3$ bonds. Whereas the two types of manganese cation, $Mn^{3+}$ & $Mn^{4+}$ that had $3d^4$ and $3d^3$ electronic configurations respectively, would be stabilised in octahedral sites through forming $dsp^2$ & $d^2sp^3$ hybrid bonds.

As the fraction of $O_H$ sites occupied by distorting cations ($Mn^{3+}$) was reduced, the mutual interaction amongst the distorted $O_H$, responsible for parallel alignment was also reduced, randomising the orientation and preserving the cubic symmetry. [84]

Further discrepancies arise in the literature when considering the valencies of the copper and manganese ions in hopcalite. A series of magnetic and structural investigations of $CuMn_2O_4$ lead to a number of researchers suggesting $Cu^{2+}$ and $Mn^{3+}$ to be the most stable configuration of the mixed oxide. [85-86] Others suggested that $Cu^{+}$ in the presence of $Mn^{4+}$ was the most viable environment. [78,79,82] Both configurations have been supported by electronic measurements. [87-90]

Loeb and Goodenough report the absence of distortion where distorting cations occupy a quarter of the $O_H$ sites, with the phenomena being observed in manganites containing a mixed $Mn^{3+}/Mn^{4+}$ phase. With an increasing presence of $Mn^{4+}$ in the crystals, the

distortion from cubic symmetry decreases. [91] This arrangement would involve an oxygen ion surrounded by four cations: 3 x $O_H$ ($Mn^{3+}$ & $Mn^{4+}$) through mutually perpendicular bonds and one $T_D$ $Cu^+$ through a single bond at 125° to the Mn bonds, i.e. along the (111) direction from the quadrant formed by the 3 perpendicular bonds.

| | $CuMn_2O_4$ | CuO | $Cu_2O$ | $MnO_2$ | $Mn_2O_3$ | Calculated Bond Lengths |
|---|---|---|---|---|---|---|
| Cu-O | 2.04 | 1.95 | 1.84 | - | - | $Cu^+$-$O^{2-}$ 2.36<br>$Cu^{2+}$-$O^{2-}$ 2.10 |
| Mn-O | 1.95 | - | - | 1.88<br>1.89 | 2.00<br>2.01<br>2.03 | $Mn^{3+}$-$O^{2-}$ 2.02<br>$Mn^{3+}$-$O^{2-}$ 1.96 |
| O-O | 2.45<br>2.96<br>3.35 | 2.62<br>2.88<br>3.41 | 3.69 | | | 2.80 |

**Figure 1.11.1 - A table of predicted and actual bond lengths in a series of metal oxide catalysts [92]**

The $O^{2-}$ could form three p-bond orbitals and overlap with the three neighbouring $Mn^{3+}$/$Mn^{4+}$ cations or form $sp^3$ hybrid orbitals (as in $Cu_2O$) where Cu-O was covalent. The observed values of Cu-O and Mn-O were intermediate between those calculated from the covalent and ionic radii reported by Pauling. [93] Therefore indicating a resonating system where bonds were partially covalent and partially ionic.

The determination of the oxidation states of the components of hopcalite has also proved challenging to a number of other researchers. [78-80] Investigations have shown that the ionisation state of copper in copper manganite, $CuMn_2O_4$, was different from

that of copper in other iso-amorphous compounds such as $CuCr_2O_4$ and $CuFe_2O_4$ where it was $Cu^{2+}$. The Cr and Fe in these compounds was considered to be present as $M^{3+}$, where as in $CuMn_2O_4$, the consensus of findings points to $Mn^{4+}$. [94]

Buciuman *et al.* have used temperature programming methods to probe the different oxide phases present in active and deactivated hopcalite specimens. On consideration of the activation energies and reproducibility measured by TPR, it was concluded that oxidation reactions over CuO followed a redox mechanism using lattice oxygen while over $Mn_2O_3$, the mechanism is associative involving adsorbed oxygen species. Based on the TPR and kinetic results, the synergy between copper and manganese oxides in hopcalite was assigned to the spillover effect. [95]

## 1.12- Mechanism of electron transfer in copper manganese oxides

An insight into the understanding of the electron transfer processes in hopcalite spinels would of course be beneficial in the understanding of how hopcalite catalysts operate, in terms of their activation, reaction, deactivation and regeneration.

Using X-ray diffraction, Sinha *et al.* [78] have analysed the bulk structure at a variety of stages of the reaction:

$$CuO + Mn_2O_3 \longrightarrow Mn^{3+}[Cu^{2+}Mn^{3+}]O_4^{2-}$$

Although the spectra obtained were complex, using the intensity of the [400] and [422] lines, it was possible to determine that initially the $Cu^{2+}$ occupied $O_H$ sites from where they migrated to $T_D$ sites on receipt of an electron from $Mn^{3+}$.

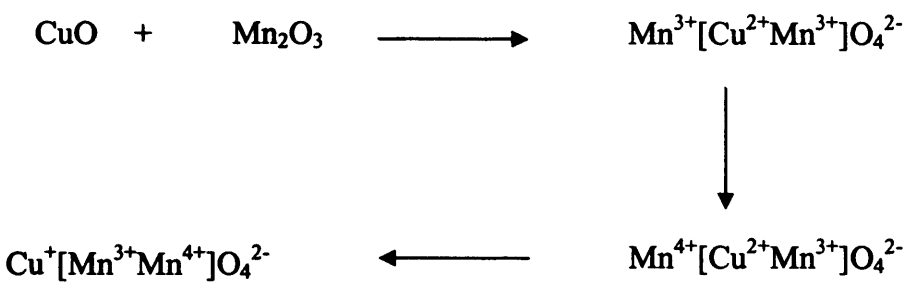


Sinha proposed two models for the electron transfer process:

**Model 1:**

Due to elevated temperatures, an $e^-$ from $Mn^{3+}$ *3d* orbital became excited to the *4s* conduction level. This had a spherical symmetry and could overlap with the empty *4s* orbital of the $Cu^{2+}$ anion. The activation energy for such a transfer would be higher, which rendered this explanation far less likely than model 2.

**Model 2:**

The anions provided a catalytic route in the oxidation/reduction reaction through the formation of a bridge facilitating the flow of $e^-$. [96] A mechanism where an $e^-$ was transferred through the p-orbital of an intervening $O_2$ ion was considered. Electron transfer was thought to take place simultaneously from $Mn^{3+}$ to $O^{2-}$, with the $e^-$ from the oxygen passing on to an adjoining octahedral $Cu^{2+}$ ion. [97]

This gave rise to two states: $\Psi_1 = Mn^{3+}O^{2-}Cu^{2+}$ and $\Psi_2 = Mn^{4+}O^{2-}Cu^{+}$

As $\Psi_2$ was the lower energy state, the e- transfer to copper was irreversible. It was more likely that the $T_D$ $Mn^{3+}$, rather than the $O_H$ $Mn^{4+}$ took part in the transfer. [98-99] After the electron transfer, the resulting $Cu^+$ ions had a tendency to form bonds to $sp^3$ orbitals and become stabilised in a $T_D$ environment. Similarly, the $Mn^{4+}$ ions that tended to form $d^2sp^3$ bonds also preferred an $O_H$ site. These ions were located at the wrong positions

but at sufficiently high T, they possessed enough mobility to migrate to their proper sites. This migration was thought to be slow compared to the $e^-$ transfer process, therefore acting as the rate determining step in the overall formation of $Cu^+[Mn^{3+}Mn^{4+}]O_4^{2-}$.

Work by Bernard Gillot, who investigated the oxidation mechanism and ionic configuration of $CuMn_2O_4$ spinels prepared at 850-930°C would appear to confirm these findings. [100] Results from his study indicate that $Cu^+$ and $Mn^{2+}$ ions were more likely to be present in tetrahedral sites, whereas $Cu^{2+}$, $Mn^{3+}$ and $Mn^{4+}$ were more likely to occupy octahedral sites.

## 1.13 - Mechanism of CO oxidation over hopcalite

Hopcalite is reported to activate above temperatures at which water loss occurs. At this temperature, it has been generally thought that MnOOH ($Mn^{3+}$) was oxidised to $Mn^{4+}$, which is known to be an active centre for $O_2$ adsorption. [96, 101] This suggestion did not disagree conceptually with either the acid base characteristics of the reactants or the relative basicity of the hydrated Cu and Mn oxide surfaces. In the Lewis sense, CO is basic and $O_2$ is acidic. [102-103] On considering a dehydration reaction between the hydrated Cu and Mn oxides, the hydrated manganese oxide was expected to de-protonate and the hydrated copper oxide to de-hydroxylate evolving water. However, this would have yielded a very unstable $Cu^{3+}$, with $Mn^{3+}$ remaining in the same state. An $e^-$ transfer between the metal ions, from $MnOO^-$ to $Cu^{3+}$ would have produced a very stable $Cu^{2+}$ cation.

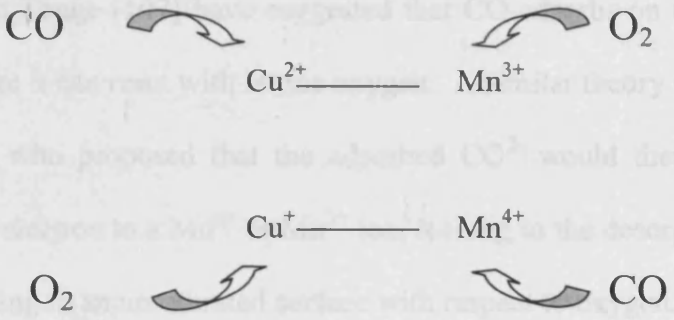


This model was supported by the fact that both $Cu_2O$ and $MnO_2$ are reported as active for the oxidation of carbon monoxide. [104] This was further supported by Kanungo [105-106] who states that the maximum activity occurred for a Cu mole fraction of 0.5, which coincided with a maximum $Cu_2O$ and a maximum $Mn^{3+}/Mn^{4+}$ ratio. Kanungo, in partnership with Schwab, attributed the oxidising power of hopcalite to the presence of $Mn^{4+}$ where:

$$CO + Mn^{4+} \rightarrow CO^{+}_{ads} + Mn^{3+}$$

And the promotion of copper was linked to the reduction of $O_2$

$$1/2O_2 + Cu^{+} \rightarrow Cu^{2+} + O^{-}_{ads}$$

with the oxidation occurring by the process:

$$O^{-}_{ads} + CO^{+}_{ads} \rightarrow CO_2$$

Schwab and Kanungo are amongst a number of researchers who have suggested that the following resonance system exists in hopcalite. When present it enabled the catalyst to return to its active state.

$$Cu^{2+} + Mn^{3+} \rightarrow Cu^{+} + Mn^{4+}$$

As long as this redox couple existed, it was thought to be difficult to attribute the deactivation process in hopcalite to the oxidation state of the metal cations.

Dollimore and Tonge [107] have suggested that CO adsorbs on the catalyst surface at $Cu^{+}$ sites where it can react with lattice oxygen. A similar theory was also suggested by Winter *et al.* who proposed that the adsorbed $CO^{2-}$ would then be oxidised by the transfer of an electron to a $Mn^{4+}$ or $Mn^{3+}$ ion, leading to the desorption of $CO_2$ from the surface, resulting in an unsaturated surface with respect to oxygen. [109]

Veprek *et al.* ascribed the high activity of the amorphous spinel phase in comparison with the crystallised spinel to the greater concentration of surface active centres in the former. [19]

## 1.14 - Deactivation of Hopcalite Catalysts

Much speculation exists in the literature as to the deactivation mechanism for $CuMn_2O_4$. Both Kanungo [105,109] and Dondur *et al.* [110-111] report that the activity of the catalyst decreased substantially above the temperature of the amorphous to crystalline phase transition. However, Kanungo points out that crystalline $CuMn_2O_4$ was still active for CO oxidation. [106] A study by Veprek has demonstrated that at the onset of phase transition, activity began to decrease and after heat treatment of the catalyst for 2h at 873K, deactivation was complete. [19] Supporting the copper manganese oxide on alumina had the effect of stabilising the catalyst with respect to high temperature heat treatment. [112]

Many researchers have postulated that hopcalite catalysts prepared using alkali metal species are prone to change at the phase change temperature where segregation of $K^{+}$ and $Na^{+}$ can occur. Veprek has reported $K^{+}$ segregation and migration over the surface at the phase change temperature [19] while Hutchings has reported that the presence of sodium in the final catalyst was linked to poor activity. When higher ratios of sodium to

copper were detected in the final catalyst, catalytic activity was profoundly decreased in all cases. [113]

It is a commonly reported fact that metal oxide catalysts are very susceptible to poisoning by water vapour. Investigations into the effect of water on hopcalite catalysts have been ongoing, ever since the early work in the 1920's, when the ease of poisoning of Hopcalite I by water was highly evident. [9,13] It is a problem that has plagued researchers over the years and limited the potential industrial applications of this otherwise very versatile catalyst. Any use of hopcalite in commercial systems needs to include a method of drying the reactant gas to ensure that catalyst deactivation does not occur due to water poisoning.

The mechanism of deactivation of hopcalite catalysts has been studied by a variety of surface-probing techniques. Work by Cocke *et al.* is particularly useful when considering deactivation of hopcalite. [114] Using XPS, the nature of the chemical shifts and the shake up of the satellite structures of the copper 2p signal indicated the deactivation of $CuMn_2O_4$ to be accompanied by a change in the copper oxidation state from $Cu^{2+}$ to $Cu^{+}$. Splitting of the Mn 3s signal provided evidence of a simultaneous change of state of the manganese from $Mn^{3+}$ to $Mn^{4+}$. These redox processes again lead to the postulation of the widely discussed coupling system of:

$$Cu^{2+} + Mn^{3+} \rightarrow Cu^{+} + Mn^{4+}$$

## 1.15 - Copper in catalysis

### 1.15.1 - Cu (I) based catalysts

Garner has comprehensively studied the reaction of CO & $O_2$ on the $Cu_2O$ surface. [115-117] The findings stated that no $CO_2$ was produced on passing CO over a fresh $Cu_2O$ surface at 25°C. However, if the surface was pre-covered with $O_2$, slow production of $CO_2$ was observed. Adsorption of CO in this case was thought to have created new adsorption sites for oxygen leading to the assumption that a $CO_3$ complex was formed on the oxygenated surface. On the decomposition of the carbonate complex at room temperature, $CO_2$ was desorbed and O adsorbed on the surface. Furthermore, the $CO_3$ complex could have reacted with excess CO in the gas phase, again liberating $CO_2$.

$$CO_{3\,(ads)} + CO_{(g)} \longrightarrow 2CO_{2\,(g)}$$

Garner also reported the formation of the $CO_3$ complex by the reaction of $CO_2$ with chemisorbed oxygen.

$$CO_{2\,(g)} + O_{(ads)} \longrightarrow CO_{3\,(ads)}$$

However, in this case oxygen could not be adsorbed after the final complex had formed. Further work by Winter into CO oxidation over $Cu_2O$ proposed a mechanism where CO first reacted to form a carbonate ion and an anion vacancy. This vacancy became filled by $e^-$ transfer from oxygen in a process that was considered as promoting the decomposition of the carbonate to $CO_2$. [118] Obviously, in the absence of adsorbed $O_2$, the formation of a carbonate complex would not have accounted for these results.

Garner *et al.* stated that during room temperature oxidation over $Cu_2O$, the reaction was not inhibited by the $CO_2$ product. This would be consistent with a Langmuir Hinshelwood type mechanism. [117] After probing the existence of a $CO_3^{2-}$ intermediate during this reaction the following model was proposed:

1. CO and $O_2$ adsorb on the surface of the copper oxide catalyst. Subsequent reaction at the surface forms a carbonate complex.
2. The adsorbed carbonate complex reacts with excess adsorbed CO yielding two molecules of carbon dioxide

On removal of the unreacted gas, the surface still held substantial amounts of the carbonate complex. On the application of heat to the catalyst, $CO_2$ and $O_2$ were desorbed from the surface following the breakdown of the carbonate intermediate.

### 1.15.2 - Cu (II) based catalysts

Oxidation catalysts containing poly-valent metals such as copper have long been used. Cu (II) has been a major component of the hopcalite catalyst, which has been used in connection with air pollution control and for the oxidation of waste industrial gases for more than 80 years. Taylor and Jones presented their initial findings in to oxidation by hopcalite catalysts as long ago as 1921. [13] Singularly, CuO was found to be poorly active for carbon monoxide oxidation, but in conjunction with other metal oxides and in appropriate proportions, some very active catalyst systems were obtained. [14] Many systems containing CuO mixed with other transition metal oxides have been studied over the years. Oxides of iron, nickel, cobalt and manganese have all been shown to enhance the activity of copper oxide under the appropriate conditions. [76,55-57] Copper based catalysts have been considered as possible substitutes for noble metal systems in automobile exhaust systems. [119] Chromium promoted copper oxides have

been investigated in both unsupported and alumina supported systems. Self propagating high temperature syntheses have produced some very active Cu-Cr-O systems. Traditional exhaust catalysts are often made of a small quantity of noble metal (Pt/Pd at 0.05-0.1%) dispersed on a high surface area support, e.g. alumina supported on corderite with honeycomb geometry. However, the complexity of these systems and the rarity of the raw materials make these systems expensive.

Transition metal oxide catalysts were found to be different to the noble metal systems in terms of the adsorption behaviour of the reactants and products. Catalytic oxidation of CO is often performed in a series of quick reaction steps, while the adsorption of CO proceeds quickly and is often limited only by the desorption of $CO_2$. The reaction of CO on CuO has often lead to the formation of carbonate intermediates upon the reaction of $O_2$ from the catalyst surface. Even at 298K, CO is reported to adsorb on the surface of CuO as a carbonyl complex that can be quickly oxidised to a carbonate species by reaction with $O_2$ both from the surface and from the atmosphere. It was thought that the interaction of CuO with CO might eventually lead to the reduction of the oxide to $Cu_2O$, but it was noted that the chromium ions present on the surface could moderate the reduction of CuO.

On optimisation of the chromium content in the catalyst, it was found that the activity of $CuCr_2O_4$ spinels could be controlled giving results comparable to those of Pt/Pd based catalysts while also being superior to the Pt/Pd based catalysts in terms of their thermal stability and chemical resistance to substances such as sulphur. One of biggest drawbacks of the CuO based systems investigated was again the ease of poisoning by water vapour. [13-14]

Cu-Zn-O systems are also regarded as effective CO oxidation catalysts that display a high specific activity. Hutchings *et al.* reported that copper and zinc in a 2:1 ratio gave appreciable activity at ambient temperature, decreasing with time on line. However, the initial activity at the time of print identified the catalyst as being more active than those used commercially. Preparation atmosphere and ageing time were strongly influential on the final catalyst structure. [120]

CuO/ZnO catalyst systems have been identified as being key in the synthesis of methanol at low temperature and pressure, as well as in the water gas shift reaction and in methanol steam reforming. [25] Ferrandon *et al.* have investigated precious metal and copper oxide systems as total oxidation catalysts. Particular interest was given to the oxidation of napthalene, methane and CO with some very active species recorded. [53]

## 1.16 – Aims of this thesis

This thesis is focussed at developing a robust and reproducible preparation method aimed at synthesising hopcalite based catalysts with increased catalytic activity and stability. It is hoped that the active species produced will be able to rival the performance of the commercial catalysts available. Particularly, the effect of ageing times and heat treatment will be probed, especially in relation to the incorporation of other elements in to the hopcalite system, which it is hoped will have a promotional and/or stabilising effect on activity.

The mechanism of carbon monoxide oxidation over hopcalite catalysts is well discussed. However, questions remain to be answered concerning the nature of the oxidising species. Many issues have been raised in the literature concerning the deactivation of hopcalite catalysts with time on stream and due to poisoning by water vapour and other species via blocking of surface active sites. The mechanism of

deactivation in hopcalite and doped hopcalite systems will also be probed, particularly in relation to poisoning by water vapour. Mechanistic insights will be offered both from steady state and transient response experiments encompassing the Temporal Analysis of Products (TAP) technique. The understanding of these parameters will be crucial to the design of experimental procedures involving precipitation as the method of catalyst preparation.

A variety of preparation methods and characterisation techniques will be used with the aim of producing the ultimate hopcalite-based CO oxidation catalyst. These methods are discussed at length in chapter 2.

## Chapter 1 - References


[1] http://www.nationmaster.com/encyclopaedia/Carbon-monoxide

[2] R. G. Adler, Carbon Monoxide in the Workplace, Occupational Safety and Health Administation, US department of Labour, March 1991.

[3] Department of the Environment, Expert Panel on Air Quality Standards, Carbon Monoxide. London, HMSO, 1994

[4] World Health Organisation. Air Quality Guidance for Europe. 2nd Edition. WHO Regional Publications, European Series, No 91.Copenhagen: WHO Regional Office for Europe, 2000.

[5] MRC Institute for Environment and Health (1998) Assessment on Indoor Air Quality in the Home (2): Carbon Monoxide (Assessment 5) Leicester. www.le.ac.uk/ieh/pdf/ExsumA5.pdf

[6] http://wine1.sb.fsu.edu/chm1045/notes/Energy/HessLaw/Energy04.htm

[7] P. A. Wright, S. Natarajan, J. M. Thomas, P. L. Gai-Boyes, J. Chem Mater. 4 (1992) 5

[8] I. Langmuir, J. Am Chem. Soc, 40 (1918) 1316

[9] A. Lamb, W. C. Bray, J. C. W. Fraser, J. Ind. & Chem. Eng. March 1920

[10] T. H. Rogers, C. S. Piggt, W. H. Bahlke, J. M. Jennings, J. Am. Chem Soc.9 (1921) 1973

[11] S. A. Solovev, G. M. Belokleitseva, V. M. Vlasenko, J. Appl. Chem. USSR, 65, 9 (1992) 1555

[12] E. J. Trimble, Toxicology 115, 1-3 (1996) 41-61

[13] H. A. Jones, H. S. Taylor, J. Am. Chem. Soc. 43, 10 (1921) 2179

[14] M. Brittan, H. Bliss, C. A. Walker, AICHE Journal, 16, 2 (1970) 305

[15] V. Y. Baranov, G. F. Drokov, V. A. Kuzmenko, V. S. Mezhevov, V. V. Pigulskaya, Kvantovaya Elektronika, 13, 5 (1986) 989

[16] N. Yamamoto, S. Tonomura, T. Matsuoka, H. Tsubomura, Jap. J. Appl. Phys, 20 (1981) 721

[17] N. Murakami, Y. Matsuura, K. Takahata, Proc. 2nd International meeting on Chemical Sensors, Bordeaux (1986) 268

[18] A. Zavadski, S. Kireev. V. Mukhin, S. Tkachenko, V. Chebykin, V. Klushin, D. Teplyakov, Russ. J. Phys Chem. 76, 12 (2002) 2072

[19] S. Veprek, D. L. Cocke, S. Kehl and H. R. Oswald, J. Catal, 100 (1986) 250

[20] S. H. Taylor, G. J. Hutchings, A. A. Mirzaei, Chem. Comm. (1999) 1373

[21] G. J. Hutchings, A. A. Mirzaei, R. W. Joyner, M. R. H. Siddiqui, S. H. Taylor, Appl. Cat. A: Gen 166 (1998) 143

[22] Wright, Luff, Z. Anorg. Chem. 27 (1901) 81

[23] E.F. Fremy, Comp. Rend. 82 (1876) 1231

[24] Moleculite Safety Data Sheet: Molecular Products Ltd, HOP2, 31st March 2000, Issue 6a

[25] G. E. Parris, K. Klier, J. Catal. 97 (1986) 374

[26] M. Bowker, K. Houghton, K. C. Waugh, J. Chem. Soc. Faraday Trans 1, 77 (1981) 3023

[27] G. C. Chinchen, P. J. Denny, D. G. Parker, M. S. Spencer, K. C. Waugh, D. A. Whan, Appl. Catal. 30 (1987) 333

[28] K. I. Slovetskaya, A. A. Greish, M. P. Vorobeva, K. M. Kustov, Russian Chem. Bull. Int. Ed, 50, 9 (2001) 1589

[29] J. C. J. Bart, R. P. Sneedon, Catal. Today 2 (1987) 1

[30] G. G. Xia, Y. G. Yin, W. S. Willis, J. Y Wang, J. Catal. 185 (1999) 91

[31] C. T. Campbell, K. A. Daube, J. Catal. 104 (1987)109

[32] E. Colbourn, R. A Hadden, H. D. Vandervell, K. C. Waugh, G. Webb, J. Catal. 130 (1991) 514

[33] G. G. Jernigan, G. A. Somorjai, J. Catal. 147 (1994) 567

[34] J. J. Spivey, Ind. Eng. Chem. Res. 26 (1987)

[35] I. Mazzarino, A. A Barresi, Catal. Today 17 (1993) 335

[36] S. Shelley, Chem. Eng. (1997) 57

[37] T. Lawton, Hydrocarbon Eng. (1997) 79

[38] R. J. Farrauto, C. H. Batholomew, Fund. of Ind. Cat. Proc, Blackie, Chapman & Hall, London, 1997, p160

[39] J. Chen, R. M. Heck, R. J.Farrauto, Catal. Today 11 (1992) 517

[40] W. Liu, M. Flytzani-Stephanopoulos, J. Catal. 153 (1995) 304

[41] R. W. McCabe, P. J. Mitchell, Ind. Eng. Chem. Prod. Res. dev. 22 (1983) 212

[42] Y. Yu Yao, Ind. Eng. Chem. Proc. Des. Dev. 23 (1984) 60

[43] H. Rajesh, U. S. Ozkan, Ind. Eng. Chem. Res. 32 (1993) 1622

[44] R. W. McCabe, P. J. Mitchell, Ind. Eng. Chem. Prod. Res. Dev. 23 (1984) 196

[45] M. M. Doeff, T. J. Richardson, J. Hollingsworth, C. Yuan, M. Gonzales, J. Power Sources, 112 (2002) 294

[46] V. Koleva, D. Stoilova, D. Mehandjiev, J. Solid State Chem, 133 (1997) 416

[47] P. Fortunato, A. Reller, H. R. Oswald, Solid State Ionics, 101-103 (1997) 85

[48] M. Haruta, T. Kobayashi, H. Sano, N. Yamada, Chem. Lett. (1987) 405

[49] M. Haruta, N. Yamada, T. Kobayashi, S. Iijima, J. Catal. 115 (1989) 301

[50] S. D. Lin, M. Bollinger, M. A. Vannice, Catal. Lett. 17 (1993) 245

[51] H. Sakurai, M. Haruta, Catal. Today, 29 (1996) 361

[52] P. Thormahlen, M. Skoglundh, E. Fridell, B. Andersson, J. Catal. 188 (1999) 300

[53] M. Ferrandon, J. Carno, E. Bjornbom, S. Jaras, Appl. Cat. A: Gen 180 (1999) 153

[54] N. A. Hodge, C. J. Kiely, R. Whyman, M. R. H. Siddiqui, G.J. Hutchings, Q. A. Pankhurst, F. E. Wagner, R. R. Rajaram, S. E. Golunski, Catal. Today, 72 (2002) 107

[55] A. V. Vorontsov, L. A. Kasatkina, Kinet. Katal, 21, (1980) 1494

[56] P. C. Liao, J. J. Carberry, T. H. Fleish and E. E. Wolf, J. Catal. 74, (1982) 307

[57] K. S. Murthy, J. Ghose, J. Catal, 147 (1994) 171

[58] Y. Yu Yao, J. T. Kummer, J. Catal. 46 (1977) 388

[59] F. Severino, J. Laine, Ind. Eng. Chem. Prod. Res. Dev. 22 (1983) 326

[60] R. Lin, W Liu, Y. Zhong, M. Luo, Appl. Cat. A: Gen 220 (2001) 165

[61] J. Jansson, M. Skoglundh, E. Fridell, P. Thormahlen, Top. in Catal. Vol 16-17, 1-4 (2001) 385

[62] Y. J. Mergler, A. van Aalst, J. van Delft, B. E. Nieuwenhuys, Appl. Catal. B, 10 (1996) 245

[63] M. Haruta, S. Tsubota, T. Kobayashi, H. Kageyama. M. J. Genet, B. Delmon, J. Catal. 144 (1993) 175

[64] Y. Takita, T. Tashiro, Y. Saito, F. Hori, J. Catal. 97 (1986) 25

[65] W. A. Whitesell and J. C. W. Frazer, J. Am. Chem. Soc. 45. (1923) 2841

[66] S. Z. Roginskii and Y. Zeldovich, Acta Physicochem, USSR, 1 (1934) 554

[67] M. Kobayashi, H. Matsumoto and H. Kobayashi, J. Catal. 21 (1971) 48

[68] K. Klier, K. Kuchynka, J. Catal. 6 (1966) 62

[69] M. Kobayashi, H. Kobayashi, J. Catal. 27 (1972) 108

[70] A. A. Davydov, Y. M. Shchekochikhin and N. P. Keier, Kinet. Katal, 11 (1970) 1230

[71] C. L. Thomas, Catalytic Principles and Proven Catalysts, Academic Pres, New York, 1970

[72] A. B. Stiles, Catalyst Manufacture – Laboratory and Commercial Preparations, Marcel Dekker, New York 1983

[73] Preparation of Solid Catalysts, Ed. by G. Ertl, H. Knozinger, J. Weitkamp, Wiley-VCH, 1999

[74] G. J. Hutchings and J. C. Vendrine in Basic Principles in Applied Catalysis, Springer Publications, Ed. M. Baerns (2004)

[75] D. Stoilova, R. N. N Nickolov, K. T. Cheshkova, J. Colloid and Interface Sci, 228 (2000) 24

[76] G. C. Bond, Heterogeneous Catalysis: Principles and Applications, Oxford Chemistry Series, Clarendon Press, 1974

[77] Handbook of Heterogenous Catalysis, Ed. by G. Ertl, H. Knozinger, J. Weitkamp, Wiley-VCH, 1997

[78] A. P. B. Sinha, N. R. Sanjana and A. B. Biswas, J. Phys. Chem, 62 (1958) 191

[79] S. Miyahara, J. Phys Soc. Japan, 17b-I, (1962) 181

[80] G. Glasse, J. Phys. Chem. Solids, 27 (1966) 383

[81] G. Rienacker and K. Werner, Zaorg. Allg. Chem. 327 (1964) 275

[82] R. Buhl, J. Phys. Chem. Solids, 30 (1969) 805

[83] R. E. Vanderberghe, Phys. Status Solid, 50 (1978) K85

[84] G. I. Finch, A. P. G. Sinha, Proc. Roy. Soc. (London) A242 (1956) 506 85

[85] C. Delorme, Bull. Soc. Franc. Miner. Crist. LXXXI (1958) 79

[86] P. K. Baltzer and E. Lopatin, Phys. Letters, 22 (1966) 380

[87] C. D. Sabane, A. P. B. Sinha and A. B. Biswas, Indian J. Pure Appli. Phys. 4 (1966)188

[88] M. V. Loginova, V. A. Stogova and I. T. Sheftel, Izv. Akad. Nauk. SSSR, Ser. Neorg. Mater. 7, (1971) 120

[89] S. T. Kshirsagar and C. D. Sabane, Japan J. Appl. Phys. 10 (1971) 794

[90] G. T. Bandage and H. V. Keer, J. Phys. Chem, 8 (1975) 501

[91] J. B. Goodenough, A. L. Loeb, Phys. Rev. 98 (1955) 391

[92] G. I. Finch, A. P. G. Sinha, Proc. Roy. Soc. (London) A242 (1956) 506

[93] L. Pauling, "The Nature of the Chemical Bond" Cornell Univ. Press, Ithaca, New York, 1945

[94] B. D. Naik and A. P. B. Sinha, Indian J. Pure Appli. Phys, 2 (1969) 170

[95] F. C. Buciuman, F. Patcas, T. Hahn, Chem. Eng and Proc. 38 (1999) 563

[96] B. J. Zwolinski, R. J. Marcus and H. Eyring, Chem. Rev, 55 (1955) 157

[97] C. Zener, Phys. Rev, 82 (1951) 403

[98] L. Neel, Ann. Phys. Paris, 3 (1948) 137

[99] P. W. Anderson, Phys. Rev, 79, 350 (1950) 705

[100] B. Gillot, S. Buguet, E. Kester, J. Mat. Chem. 7, 12 (1997) 2513

[101] N. K. Radhakrishnan and A. B. Biswas, J. Indian Chem. Soc. L1 (1974) 274

[102] H. Knozinger, "Advances in Catalysis", Academic Press, New York, Vol 25 (1976) 184

[103] H. Knozinger, Catal. Rev. Sci. Eng, 17 (1978) 31

[104] F. S. Stone, Adv. Catal. 5 (1962) 1

[105] S. B. Kanungo, J. Catal 58 (1979) 419

[106] G. M. Schwab, S. B. Kanungo, Z. Phys. Chem. N.F, 107 (1977) 109

[107] D. Dollimore and K. H. Tonge, J. Chem. Soc. A (1970) 1728

[108] E. R. S. Winter, Adv Catal. 10 (1958) 196

[109] S. B. Kanungo, Symposium on Science of Catalysis and its Application in Industry, Sindri, India (1979)

[110] V. Dondur, S. Lampa, D. Vukelic, Proc. 2nd Euro. Symposium on Thermal Analysis (Ed. by D. Dollimore) Heyden, London (1981)

[111] V. Dondur, S. Lampa, D. Vukelic, Heterogeneous Catalysis, Proc. 4th Int'l Symp. Part 2, Ed. by D. Dollimore, 1979

[112] Z. Jaworska-Galas, W.Mista, J. Wrzyszcz, M. Zawadski, Catal. Lett. 24 (1994) 133

[113] A. A. Mirzaei, H. R. Shaterian, R. W. Joyner, M. Stockenhuber, S. H. Taylor, G. J. Hutchings, Catal. Comm. 4 (2003) 17

[114] C. Yoon, D. L. Cocke. J. Catal. 113, (1988) 267

[115] F. S. Stone, in W. E. Garner, Chemistry of the Solid State, Butterworths, London, 1955

[116] W. E. Garner, T. J. Gray, F. S. Stone, Disc. Faraday Soc, 8 (1950) 246

[117] W. E. Garner, T. J. Gray, F. S. Stone, Proc. Royal Soc. London (1952) 472

[118] E. R. S. Winter, J. Chem Soc. (1955) 2726

[119] G. Xanthopoulou, G. Vekinis, Appl. Cat. B: Environ. 19 (1998) 37

[120] A. A. Mirzaei, H. R. Shaterian, S. H. Taylor, G. J. Hutchings, Catal. Lett. Vol 83, 3-4 (2003) 103

[121] D. R. Merrill, C. C. Scalione, J. Am. Chem. Soc. 43 (1921) 1982

# Chapter 2 – Experimental Techniques

This chapter details the experimental procedures used to synthesise the catalysts discussed in later chapters. Also explained here is the underlying theory behind the characterisation techniques applied to gain information about the catalyst structure and activity as well as their application to the work.

## 2.1 - Catalyst Preparation

### 2.1.1 - Batch precipitation procedure - Synthesis of hopcalite

Catalysts were prepared using a co-precipitation procedure. [1] Aqueous solutions of 0.25M $Cu(NO_3)_2.3H_2O$ and 0.25M $Mn(NO_3)_2.6H_2O$ were premixed in a 1:2 molar ratio of the metals (Cu:Mn). The resulting cold solution of nitrates was added to the reaction vessel. (See 2.1.1.1) Aqueous $Na_2CO_3$ (0.25M) was added to the nitrate mixture by burette until pH=8.3 was achieved, while stirring at 800rpm. The procedure took around 30 minutes to complete. The resulting precipitate was left under these conditions for a time period designated as the ageing time. This was typically between 30 minutes and 12 h. After ageing was complete, the precipitate was then filtered on a Buchner line and washed with hot distilled $H_2O$ to remove any remaining $Na^+$ ions; the presence of excess sodium in the catalyst is known to suppress activity. [2,3] The colour of the precipitate varied between green and brown depending on the ageing time used. As ageing times were increased, the precipitate colour altered from a light green through to a dark brown in colour. The precipitate was dried at 110°C for 16 h to give the material denoted as the catalyst precursor.

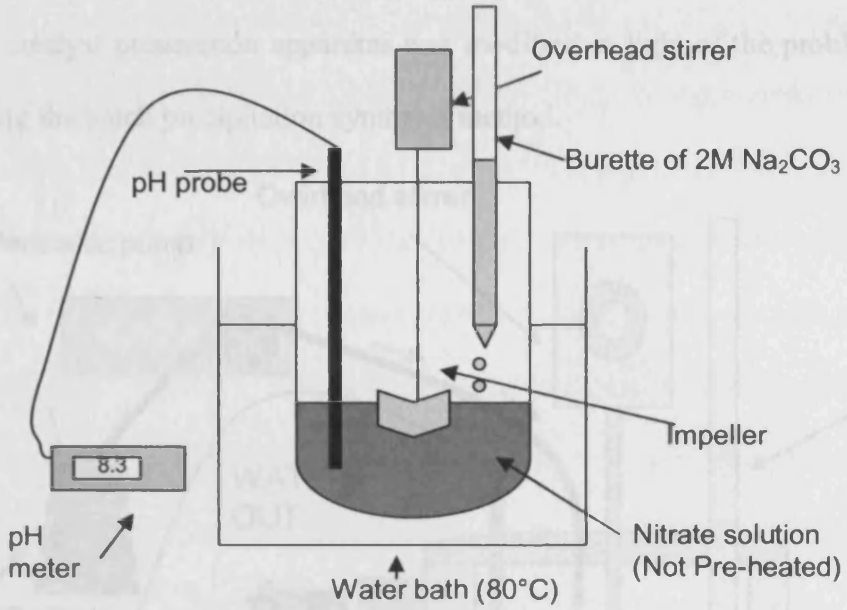


**Figure 2.1.1.1 – Diagram of original co-precipitation apparatus**

The original co-precipitation vessel proved problematic due to lack of reproducibility during the synthesis of catalysts. The major factors influencing the preparation were the lack of pH control during the precipitate ageing combined with the poor maintenance of temperature, thought to have arisen from heating the reaction vessel in an isothermally maintained water bath. This heating method proved inadequate as temperature differences were observed between the temperature of the water bath and the temperature of the precipitate within the reaction vessel throughout the ageing process. These temperature differences could be attributed to a time effect whereby the mixture took a period of time to come to the desired temperature after precipitation occurred. This temperature fluctuation was undesirable as effective temperature control has been identified to be an influencing factor in the preparation of active species. [4]

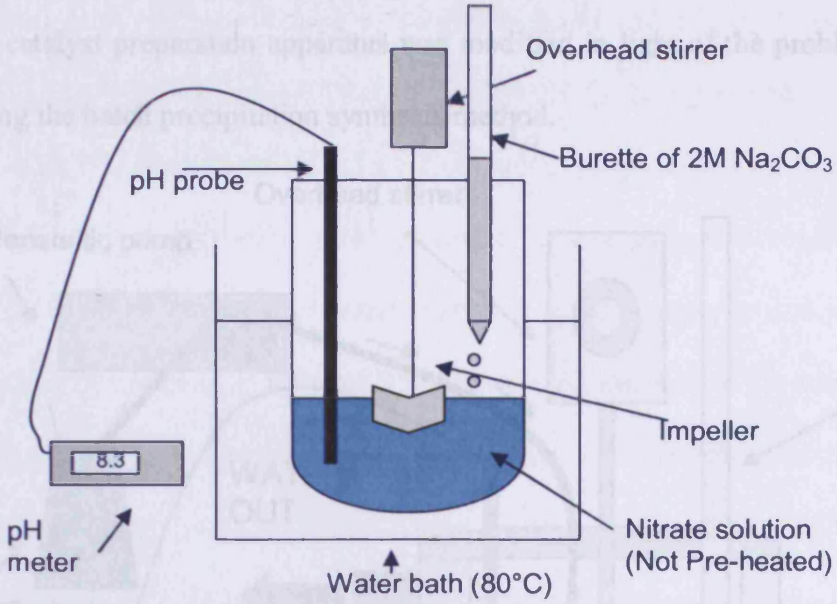


**Figure 2.1.1.1 – Diagram of original co-precipitation apparatus**

The original co-precipitation vessel proved problematic due to lack of reproducibility during the synthesis of catalysts. The major factors influencing the preparation were the lack of pH control during the precipitate ageing combined with the poor maintenance of temperature, thought to have arisen from heating the reaction vessel in an isothermally maintained water bath. This heating method proved inadequate as temperature differences were observed between the temperature of the water bath and the temperature of the precipitate within the reaction vessel throughout the ageing process. These temperature differences could be attributed to a time effect whereby the mixture took a period of time to come to the desired temperature after precipitation occurred. This temperature fluctuation was undesirable as effective temperature control has been identified to be an influencing factor in the preparation of active species. [4]

## 2.1.2– Pumping method of co-precipitation

The catalyst preparation apparatus was modified in light of the problems that occurred during the batch precipitation synthesis method.

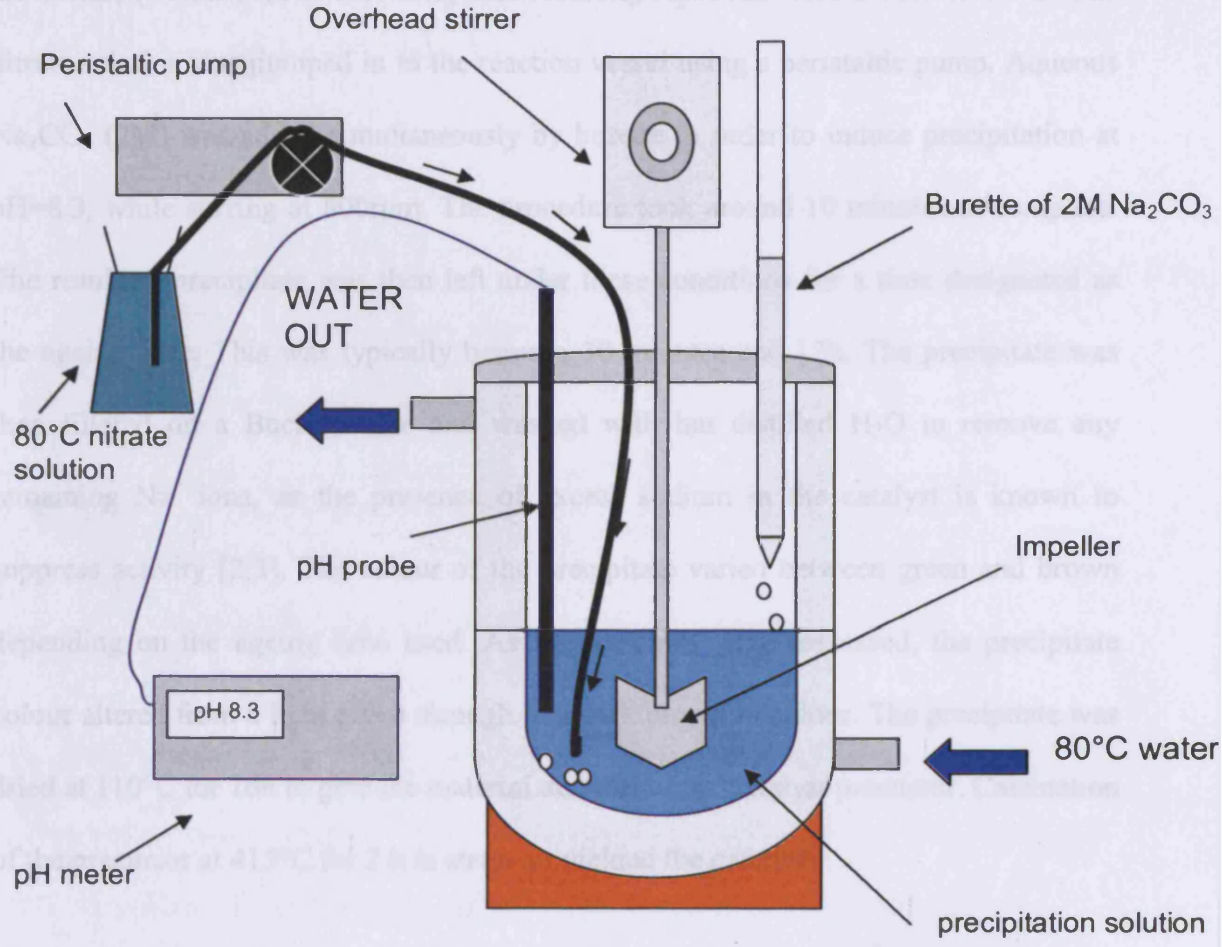


**Figure 2.1.2.1 – Diagram of modified co-precipitation apparatus**

Advantages of new co-precipitation set up:

- Enables better control of experimental variables
- pH maintained by addition of acid/base during precipitate ageing
- T (°C) maintained by water heated, double walled reaction vessel.
- Nitrate reagents pre-heated to 80°C before use.
- Simultaneous addition of nitrates and carbonates gives simultaneous precipitation.

## 2.1.3 - Preparation of hopcalite catalysts (modified procedure)

Catalysts were prepared using a co-precipitation procedure. Aqueous solutions of 0.25M $Cu(NO_3)_2.3H_2O$ and 0.25M $Mn(NO_3)_2.6H_2O$ were premixed in a 1:2 wt ratio of the metals (Cu:Mn). (Tab 2.1.4.1.1) The resulting solutions were heated to 80°C. The nitrate solution was pumped in to the reaction vessel using a peristaltic pump. Aqueous $Na_2CO_3$ (2M) was added simultaneously by burette in order to induce precipitation at pH=8.3, while stirring at 800rpm. The procedure took around 10 minutes to complete. The resulting precipitate was then left under these conditions for a time designated as the ageing time. This was typically between 30 minutes and 12h. The precipitate was then filtered on a Buchner line and washed with hot distilled $H_2O$ to remove any remaining $Na^+$ ions, as the presence of excess sodium in the catalyst is known to suppress activity [2,3]. The colour of the precipitate varied between green and brown depending on the ageing time used. As ageing times were increased, the precipitate colour altered from a light green through to a dark brown in colour. The precipitate was dried at 110°C for 16h to give the material denoted as the catalyst precursor. Calcination of the precursor at 415°C for 2 h in static air yielded the catalyst.

## 2.1.4 - Preparation of doped hopcalite catalysts

In an attempt to modify the $CuMnO_x$ hopcalite catalyst, with the intention of increasing catalytic activity, some of the copper nitrate present in the starting reagent mixture was replaced with another nitrate of element (M). The ratio of Cu to element M was manipulated so that the overall starting reactant stoichiometry was 2:1, Mn : (Cu+M).

## 2.1.4.1 – Reagents for producing doped catalysts

Catalysts were synthesised using the modified co-precipitation method discussed in Chapter 2.1.2. Copper, manganese and M nitrates (0.25M) were premixed in the desired ratio (Figs 2.1.4.(1-4)). The remainder of the synthesis process was identical to that used in producing hopcalite itself (chapter 2.1.3).

| Co:Cu ratio | $Co(NO_3)_2$ 0.25M | $Cu(NO_3)_2$ 0.25M | $Mn(NO_3)_2$ 0.25M |
|---|---|---|---|
| 100:0 | 41.5 ml | - | 100ml |
| 50:50 | 20.8 | 30.1 | 100 |
| 20:80 | 8.3 | 48.2 | 100 |
| 10:90 | 4.2 | 54.2 | 100 |
| 5:95 | 2.1 | 57.3 | 100 |
| 2:98 | 0.8 | 59.1 | 100 |
| 1:99 | 0.4 | 59.7 | 100 |
| 0:100 | - | 60.3 | 100 |

**Table 2.1.4.1.1 – Reagent volumes used in cobalt doping experiments**

The source of cobalt was $Co(NO_3)_2.6H_2O$. A 0.25M solution was used to dope the copper and manganese nitrate mixture. Precipitates were always a very deep brown in colour regardless of the ageing time used.

| Ag:Cu | $Ag(NO_3)_2$ 0.25M | $Cu(NO_3)_2$ 0.25M | $Mn(NO_3)_2$ 0.25M |
|---|---|---|---|
| 100:0 | 50ml | - | 100ml |
| 50:50 | 25 | 30.1 | 100 |
| 20:80 | 10 | 48.2 | 100 |
| 10:90 | 5 | 54.2 | 100 |
| 5:95 | 2.5 | 57.25 | 100 |
| 1:99 | 0.5 | 59.65 | 100 |
| 0:100 | - | 60.3 | 100 |

**Table 2.1.4.1.2 – Reagent volumes used in silver doping experiments**

The source of silver was $Ag(NO_3)$. A 0.25M solution of silver nitrate was used in the doping experiments

| Fe:Cu | $Fe(NO_3)_3$ 0.25M | $Cu(NO_3)_2$ 0.25M | $Mn(NO_3)_2$ 0.25M |
|---|---|---|---|
| 100:0 | 49.99ml | - | 100ml |
| 50:50 | 24.99 | 30.1 | 100 |
| 20:80 | 9.99 | 48.2 | 100 |
| 10:90 | 4.99 | 54.2 | 100 |
| 5:95 | 2.5 | 57.25 | 100 |
| 2:98 | 1 | 59.05 | 100 |
| 1:99 | 0.5 | 59.65 | 100 |
| 0:100 | - | 60.25 | 100 |

**Table 2.1.4.1.3 – Reagent volumes used in iron doping experiments**

| Ni:Cu | $Ni(NO_3)_2$ 0.25M | $Cu(NO_3)_2$ 0.25M | $Mn(NO_3)_2$ 0.25M |
|---|---|---|---|
| 100:0 | 50ml | - | 100ml |
| 50:50 | 25 | 30.1 | 100 |
| 20:80 | 10 | 4.2 | 100 |
| 10:90 | 5 | 54.2 | 100 |
| 5:95 | 2.5 | 57.25 | 100 |
| 2:98 | 1 | 59.05 | 100 |
| 1:99 | 0.5 | 59.65 | 100 |
| 0:100 | - | 60.25 | 100 |

**Table 2.1.4.1.4 – Reagent volumes used in nickel doping experiments**

## 2.1.5 - Calcination of precursor

**Calcination profile 1** – Calcination of the precursor in a carbolite tube furnace at 500°C for 17h in static air yielded the hopcalite catalyst. The sample was loaded into the pre-heated furnace at 500°C in a quartz calcination boat

**Calcination profile 2** - Calcination of the precursor in a carbolite tube furnace at 415°C for 2h in static air yielded the hopcalite catalyst. The sample was loaded at room temperature in a quartz calcination boat and ramped to the desired temperature at 20°C/min.

# 2.2 - Catalyst Testing

## 2.2.1 - CO/He/$O_2$ test mixture

The catalysts were tested for CO oxidation using a fixed-bed laboratory microreactor. Typically CO (10% in He, 2.5ml/min) and $O_2$ (20ml/min) were fed to the reactor at controlled rates using the mass flow controllers and passed over the catalyst at 25°C; the products were analysed using on-line gas chromatography with a 3m carbosphere column in a Varian 3600X Gas Chromatograph. This equated to gas mixture of 1.1/88.9/10 ($CO/O_2$/He) and a gas hourly space velocity of $6750h^{-1}$.

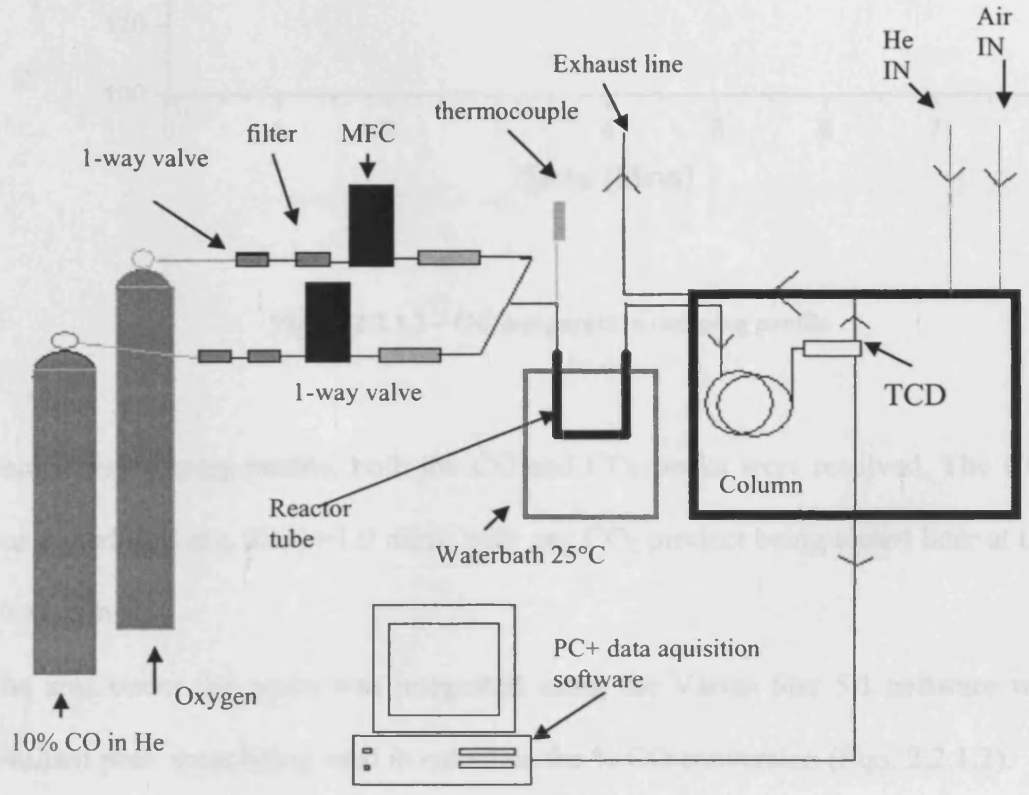


**Figure 2.2.1.1 - Schematic of the microreactor system**

During the GC separation, the column was held at 145°C for 1 minute, then ramped to 195°C at 10°C/min, and held isothermally for a further 2 minutes (see fig 2.2.1.2)

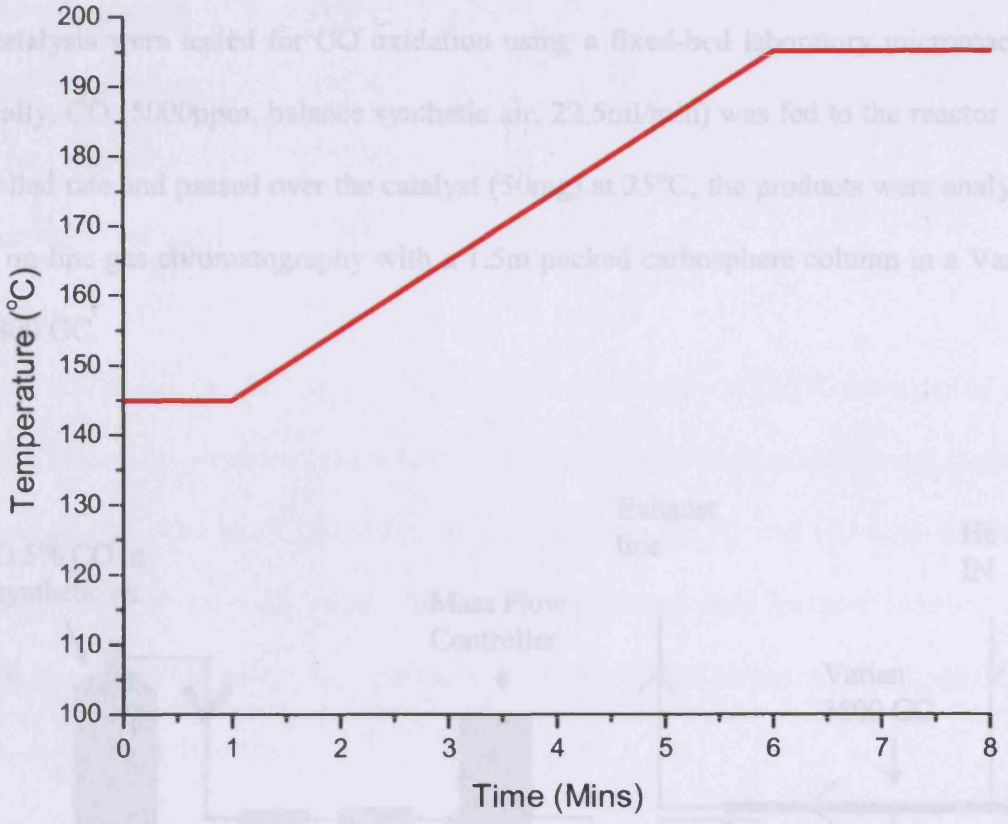


**Figure 2.2.1.2 – GC temperature ramping profile**

Using this ramping profile, both the CO and $CO_2$ peaks were resolved. The CO peak was eluted first at $t_r$ (CO) =1.9 mins, with any $CO_2$ product being eluted later at $t_r$ ($CO_2$) =6.86 mins.

The area under the peaks was integrated using the Varian Star 5.1 software with the resultant peak areas being used to calculate the % CO conversion (Eqn. 2.2.1.2).

$$\% \text{ conversion} = \frac{\text{Area } CO_2 \text{ peak}}{\text{Area CO peak} + \text{Area } CO_2 \text{ peak}}$$

**Equation 2.2.1.2 – Conversion equation**

## 2.2.2 – Catalyst testing – CO/Air test mixture

The catalysts were tested for CO oxidation using a fixed-bed laboratory microreactor. Typically, CO (5000ppm, balance synthetic air, 22.5ml/min) was fed to the reactor at a controlled rate and passed over the catalyst (50mg) at 25°C; the products were analysed using on-line gas chromatography with a 1.5m packed carbosphere column in a Varian CP-3800 GC.

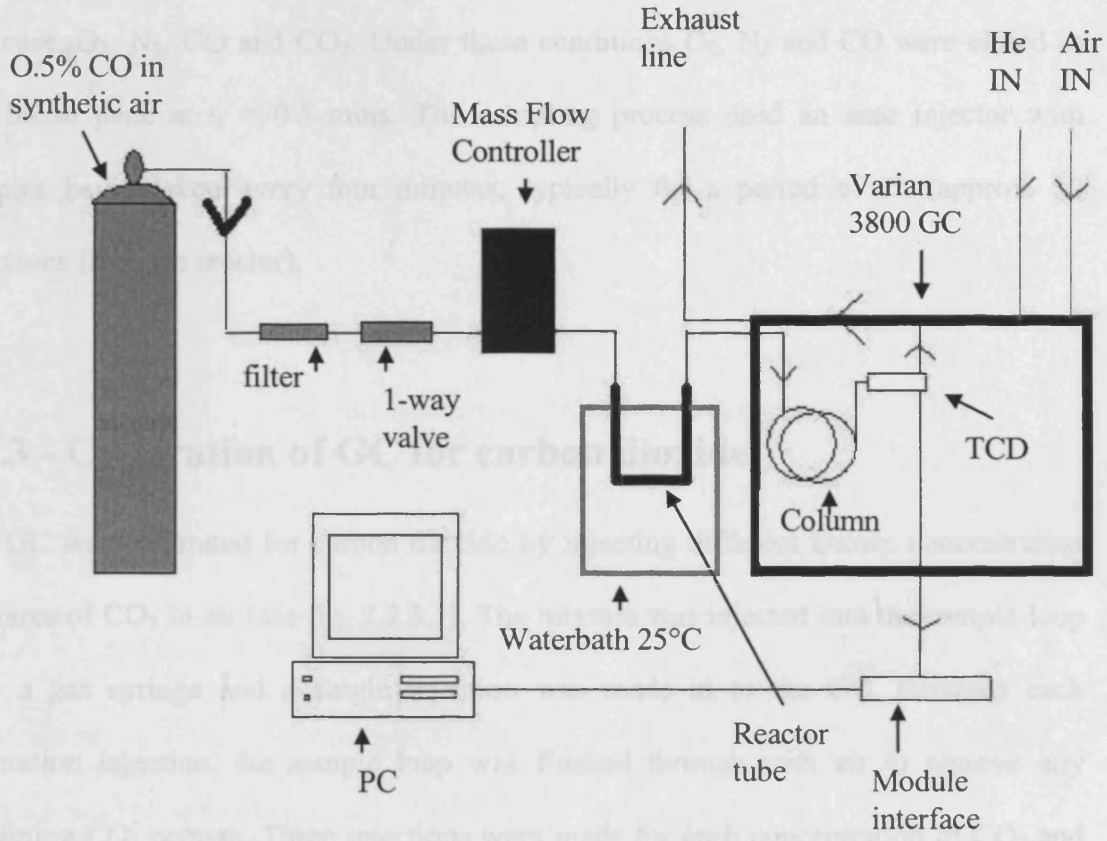


**Fig 2.2.2.1 – Schematic of the micro reactor system for the CO/Air test mixture**

**Gas Chromatograph temperature settings**

| | |
|---|---|
| Injector temperature: | 165°C |
| Detector temperature: | 195°C |
| Filament temperature: | 225°C |
| Column conditions: | 195°C |

During the analysis, the GC column was heated isothermally at 195°C for a period of 4 minutes. The carbosphere column was suitable for the separation of permanent gases, in this case, $O_2$, $N_2$, CO and $CO_2$. Under these conditions $O_2$, $N_2$ and CO were eluted as one broad peak at $t_r$ = 0.5 mins. The sampling process used an auto injector with samples being taken every four minutes, typically for a period of 2h (approx. 30 injections from the reactor).

## 2.2.3 - Calibration of GC for carbon dioxide

The GC was calibrated for carbon dioxide by injecting different known concentration mixtures of $CO_2$ in air (see fig. 2.2.3.1). The mixture was injected into the sample loop with a gas syringe and a single injection was made in to the GC. Between each calibration injection, the sample loop was flushed through with air to remove any remaining $CO_2$ present. Three injections were made for each concentration of $CO_2$ and the results averaged. The results were graphed with concentrations (% $CO_2$) plotted against peak area (number of counts), a line of best fit was set against the data to allow us to convert between the number of counts of product determined by GC analysis and the % $CO_2$ present.

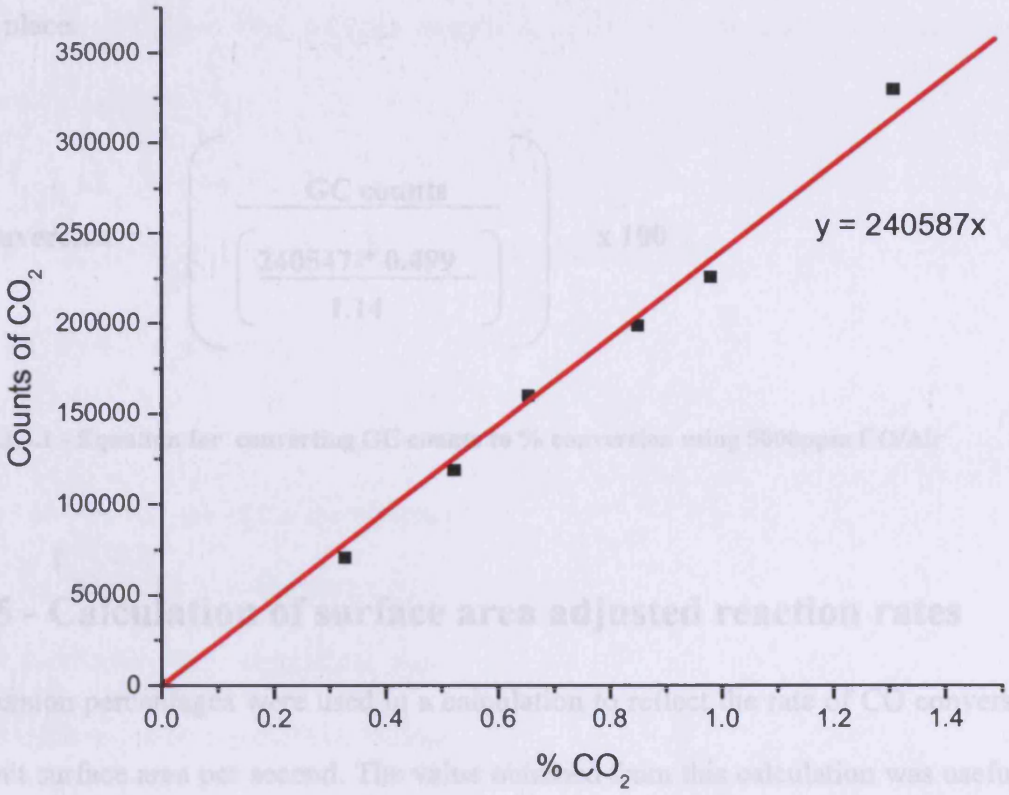


**Figure 2.2.3.1 – Calibration of GC using mixtures of known $CO_2$ concentration**

## 2.2.4 - Conversion of CO to $CO_2$

The conversion for the oxidation of CO to $CO_2$ was carried out using the peak area of the $CO_2$ peak which is resolved $t_r$=1.4 minutes.

The counts of $CO_2$ produced was manipulated to a percentage value of CO converted with the use of a response factor (1.14) allowing the conversion between $CO_2$ to CO. The response factor was calculated from calibration curves and the published data. [5-6] Also taken into account was the exact concentration of the CO mixture used. In the example below, the actual mixture concentration was 4990ppm. The final result, percentage conversion of CO, was obtained by dividing the peak area of the $CO_2$ by the

peak area which would be expected should 100% conversion of the CO mixture have taken place.

$$\% \text{ conversion} = \left( \frac{\text{GC counts}}{\left( \frac{240547 * 0.499}{1.14} \right)} \right) \times 100$$

**Eqn 2.2.4.1 - Equation for converting GC counts to % conversion using 5000ppm CO/Air**

## 2.2.5 - Calculation of surface area adjusted reaction rates

Conversion percentages were used in a calculation to reflect the rate of CO conversion per unit surface area per second. The value obtained from this calculation was useful in comparing catalyst systems with respect to differences in surface areas (SA).

$$\text{Conversion rate} = 7.8125 \times 10^{-8} \times \left[ \frac{\% / 100}{(1/20 \times SA)} \right]$$

**Eqn 2.2.5.1 - Equation for converting % conversion of CO to rate of CO conversion (Mol/m$^2$/s)**

The value, $7.8125 \times 10^{-8}$ was the quantity, in moles of CO, passed over the catalyst in one second. This was calculated from 22.5ml of 0.5% CO being passed over the catalyst during one minute, equating to 0.1125ml/min of CO. Assuming that one mole of gas occupies a volume of 22414cm$^3$, this equated to $4.6875 \times 10^{-6}$ Mol/min or $7.8125 \times 10^{-8}$ Mol/s of carbon monoxide.

(1/20 x SA) was related to the level of surface area present within the catalyst bed where 50mg of catalyst was used, i.e. one twentieth of the BET surface area measured per gram of the catalyst.

## 2.3 – Catalyst Characterisation Techniques

### 2.3.1- Gas chromatography

The key parts of a gas chromatograph include:

- a source of gas as the mobile phase
- an inlet to deliver the sample to the column
- a column where separations occur
- an oven to thermostat the column
- a detector to register the presence of a chemical in the column effluent
- a data system to record and display the chromatograph

The arrangement of these components is typical to most GC systems (fig 2.3.1.1)

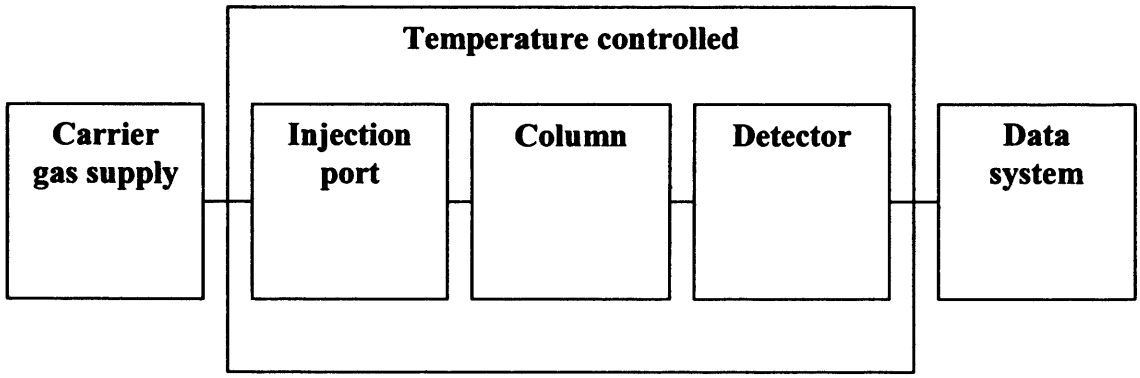


**Figure 2.3.1.1 – Block diagram of a gas chromatograph**

### 2.3.1.1 - Selection of carrier gas

The gas or mobile phase is an essential but limiting, facet in separations. The carrier gas facilitates the movement of the constituents of a sample through the column. The choice of carrier gas is restricted, unlike in Liquid Chromatography (LC) where altering the mobile phase can provide better separations, in GG very little can be gained by altering the composition to influence the partition co-efficient or separation factor. The choice of carrier gas is limited to nitrogen, argon or helium. The best results are achieved when the carrier gas is of high purity, free of water and oxygen which can reduce the lifetime of some columns.

### 2.3.1.2 - Injection port

The chromatographic analysis begins when the sample is introduced to the column, ideally without disrupting the flows in the column. The delivery of the sample in to the column should be controlled, reproducible and rapid.

The most common method for delivering samples to the GC column is injecting through a plastic membrane with a gas tight syringe. In this method, a gas tight seal is maintained and sample is deposited into the heated zone. The sample is volatilised and swept into the column, for a manual injection this can take approximately 1s. Syringe injections are a convenient and effective method of sample delivery to the GC. However, fatigue of the plastic septum limits the number of injections before it needs to be replaced.

Rotary gas sampling valves offer huge advantages for GC instruments. Precision switching allows a gas sample to be measured in precise volume and introduced to the carrier gas without disrupting the flow. The sample is loaded into the loop (Fig

2.3.1.2.1) and then, with a change in valve position, is swept in to the column under flow of the source gas (Fig 2.3.1.2.2)

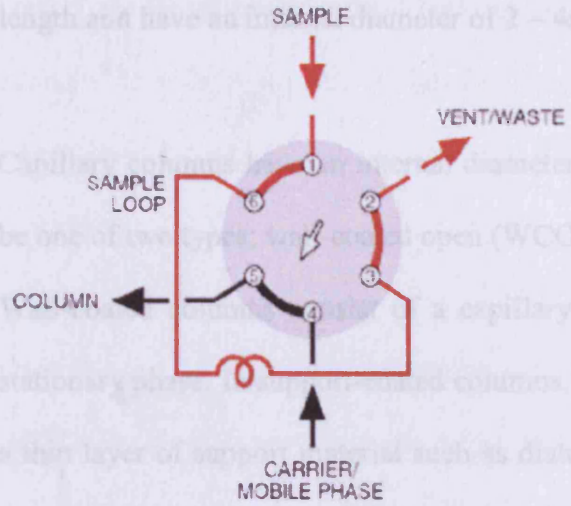


**Figure 2.3.1.2.1- Position A: Auto injector "FILL" mode**

With the valve in Position A, sample flows through the external loop while the carrier flows directly through to the detector. When the valve is switched to Position B, the sample contained in the sample loop and valve flow passage is injected onto the detector.

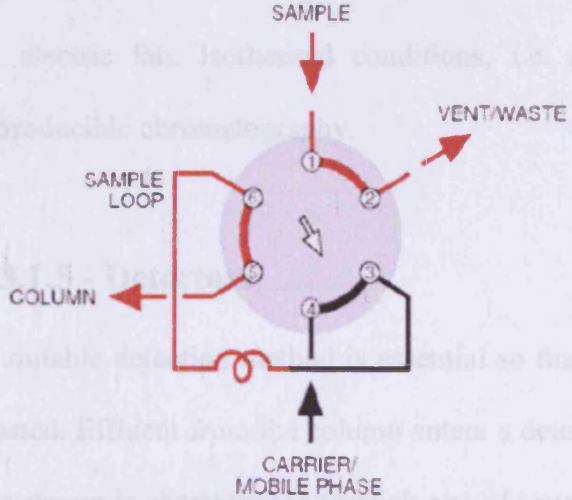


**Figure 2.3.1.2.2- Position B: Auto injector "INJECT" mode**

### 2.3.1.3 - Columns

There are two general types of column, packed and capillary. Packed columns contain finely divided, inert, solid support material. Most packed columns are 1.5 – 10m in length and have an internal diameter of 2 – 4mm.

Capillary columns have an internal diameter of a few tenths of a millimetre. They can be one of two types; wall-coated open (WCOT) or support-coated open tubular (SCOT). Wall-coated columns consist of a capillary tube whose walls are coated with liquid stationary phase. In support-coated columns, the inner wall of the capillary is lined with a thin layer of support material such as diatomaceous earth, on to which the stationary phase has been adsorbed. SCOT columns are generally less efficient than WCOT columns. However, both types of capillary column are seen as more efficient than packed columns.

### 2.3.1.4 - Temperature control

Samples must be in the vapour state throughout GC separation. All modern GCs contain temperature programmed ovens that allow separations of chemicals spanning a range of vapour pressures in a single analysis. Heat is spread evenly throughout the oven using an electric fan. Isothermal conditions, i.e. no thermal gradients, are essential for reproducible chromatography.

### 2.3.1.5 - Detectors

A suitable detection method is essential so that the separation processes have not been wasted. Effluent from the column enters a detector where the composition of the carrier gas stream is characterised through one of several physical or chemical properties of the

molecules. The most commonly used detectors are the thermal conductivity detector (TCD), flame ionisation detector (FID) and the electron capture detector (ECD). The TCD is based upon changes in the heat absorbing properties of the gas effluent when the carrier gas composition is altered with analyte gas: the FID relies upon the formation of gaseous ions from organic molecules combusted in a hydrogen-air flame: the ECD response is controlled by the ability of species to attract and remove thermalised electrons.

Over the last 20 years, mass-selective detectors (MSDs) have transformed the practise of GC. The development of these robust and inexpensive detectors when combined with the knowledge that analytical confidence is highest with a mass spectrometer as a detector has resulted in the general availability of GCMS equipment.

### 2.3.1.6 - Data systems

With the ongoing development of computers and software, the acquisition of data from GC is a very simple procedure. Signals from the detector amplifier are digitized and stored to disk allowing facile data retrieval. Software allows the results to be displayed in an automatic manner and standard reports can be generated.

## 2.3.2 - Bulk structure analysis - X-Ray diffraction

XRD is the classical technique for the determination of the bulk structure of crystalline solids. [7] Powder X-ray diffraction patterns are characteristic of the material analysed so the technique can be used to identify the phases present by comparison with literature or computer database.

Patterns were obtained using an Enraf Nonius FR590 X-Ray generator, with a $CuK_{\infty}$ source and a CPS 120 hemispherical detector. Radiation was generated at 40kV and 20mA. The sample was spun through 360° for the duration of the analysis to ensure a random arrangement of crystallites; the hemispherical detector enabled all angles to be measured simultaneously.

**Theory of XRD**

Electrons are fired at a copper target to create X-rays. These are directed on to a powder sample at a glancing angle and detected after diffraction by a detector positioned at an angle $\theta$ to the sample. The final powder pattern corresponds to a plane of atoms in the sample that satisfy the Bragg equation:

$$n\lambda = 2d \sin\theta$$

Where n is an integer, $\lambda$ is the X-ray wavelength, d is the particular lattice plane spacing and $\theta$ is the Bragg diffraction angle (half the deviation of the diffracted beam from the incident beam)

The primary use of Bragg's law is the determination of the spacing between layers in the lattice, for once the angle corresponding to a reflection has been determined, d may

be readily calculated. The spacing of the planes defined by the lattice points in a crystal is an important quantitative aspect of its structure and its investigation by X-ray diffraction.

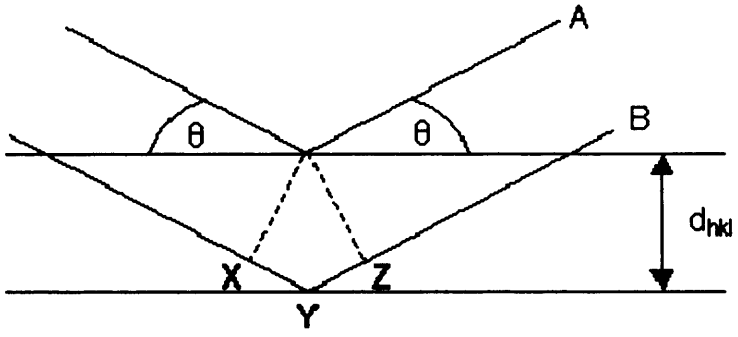


**Figure 2.3.2.1 – Diagram of Bragg's Law**

Consider a simple crystal such as that illustrated below, with lattice planes separated by a distance $d_{hkl}$. As illustrated above the scattered X-rays from this crystal will travel in random directions. For this to happen the extra distance travelled by ray B must be an exact multiple of the wavelength of the radiation. This means that the peaks of each wave are aligned with each other. The geometry of the Bragg condition is remarkably simple, and leads to the powerful result of the Bragg law:

The extra distance that ray B must travel is the distance X-Y-Z.

Thus: $\mathbf{X\text{-}Y\text{-}Z = n\lambda}$

But, $\mathbf{X\text{-}Y = Y\text{-}Z = d \sin \theta}$

Hence, $\mathbf{n \lambda = 2d \sin \theta}$

In order to consider the general case of hkl planes, the equation can be rewritten as:

$$\lambda = 2\, d_{hkl} \sin \theta_{hkl}$$

Since the $d_{hkl}$ incorporates higher orders of diffraction i.e. n greater than 1.

The angle between the transmitted and Bragg diffracted beams is always equal to $2\theta$ as a consequence of the geometry of the Bragg condition. This angle is readily obtainable in experimental situations and hence the results of X-ray diffraction are frequently given in terms of $2\theta$. However, it is very important to remember that the angle used in the Bragg equation *must* always be that corresponding to the angle between the incident radiation and the diffracting plane, i.e. $\theta$.

There are a number of complications with this technique:

- A minimum amount of material is necessary for detection
- Diffraction lines broaden as crystallite size decreases: discrimination is difficult with crystallites less than 5nm in diameter.
- Lines from different components often occur in similar positions, or overlap and interfere with each other

Particle size can be calculated from line width. As crystallite size decreases, the signal becomes broader. The extent of line broadening is governed by the Scherrer equation:

$$d = k\lambda / B\cos\theta$$

**d = diameter of crystallite (nm)**
**k = constant, equal to 0.57**
**$\lambda$ = X-Ray wavelength**
**$\theta$ = diffraction angle**
**B = line width**

## 2.3.3 - Surface Area Determination - The BET technique

The physisorption of an inert gas on to porous materials is the most popular approach to surface area measurement. [8] Nitrogen physisorption is independent of the material in the sense that at low temperatures $N_2$ molecules tend to form a layer which depends

only on the size of the $N_2$ molecule, this is known to be $0.16nm^2$, with the molecules packing together as tightly as they can, independent of the surface structure.

This approach was derived by Brunauer, Emmett and Teller, who recognised that multilayers of physisorbed adsorbate can form as the monolayer is being filled. The basis of the approach is formed by the BET equation:

$$\frac{P}{V(P_0-P)} = \frac{1}{V_m.c} + \frac{(c-1)}{V_m.c} \cdot \frac{P}{P_0}$$

In this equation $V$ is the volume of gas adsorbed, $P$ is the pressure of gas, $P_0$ is the saturated vapour pressure of the liquid adsorbate at the temperature of the experiment and $V_m$ is the volume equivalent to an adsorbed monolayer (calculated from the adsorption isotherm). The BET constant $c$ is given by:

$$c = \frac{\exp(H_1-H_L)}{RT}$$

Where $H_1$ is the heat of adsorption of the first layer absorbed, the second and subsequent layers are all characterised by heats of adsorption equal to the latent heat of evaporation, $H_L$. The empirical constant $c$ reflects the difference in heat of adsorption between the first and second adsorbed monolayer. The larger the value of $c$, the stronger the adsorption. If $c$ falls below 2, the isotherm changes from a type II to a type

III or IV. The BET equation can only be applied to type II and type IV isotherms (Fig 2.3.3.1 and fig 2.3.3.2), as these are the only two isotherms in which point $\mathbf{V_m}$ can be determined.

The BET equation makes many assumptions. These are:

- Adsorbed molecules stay on the catalyst surface
- Energy of adsorption is the same for layers other than the first
- A new layer can start before another is finished

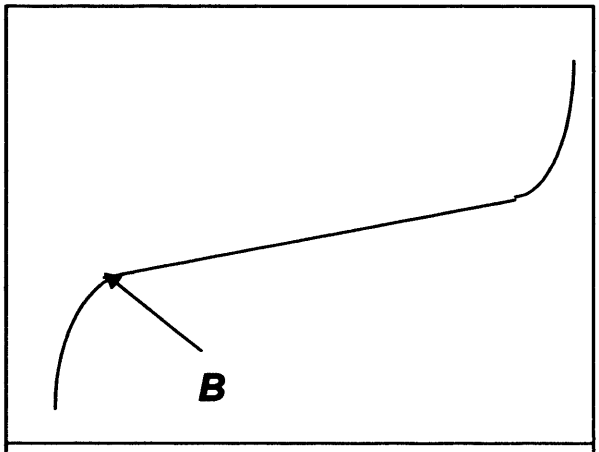


**Figure 2.3.3.1- BET Isotherm Type II**

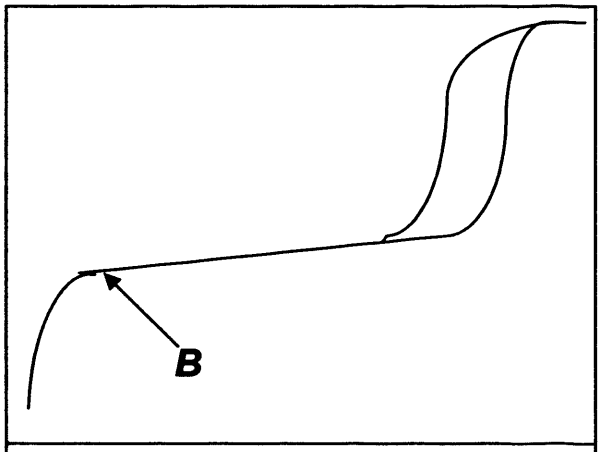


**Figure 2.3.3.2 – BET Isotherm Type IV**

The experiment is carried out by measuring the amount of $N_2$ adsorbed on the sample at 77K as a function of the pressure of the $N_2$ over the sample. The final surface area is determined by assuming that each molecule of adsorbed nitrogen occupies an area of $0.165nm^2$. BET plots are normally carried out in the range $(P/P_0)$= 0.05 to 0.35 with 1, 3 or most commonly 5 points in the isotherm range.

If the plot is not linear or if all the points selected do not lie on the best fit line then the data is not valid for analysis by BET. The c value obtained can also indicate the validity of the application to a particular substance. A high c value (>350) indicates the pressure

corresponding to monolayer coverage is low, $(P/P_0)>0.05$ and point $V_m$ is well defined. A low c (<20) indicates the pressure corresponding to monolayer coverage is high $(P/P_0)>0.18$ and point $V_m$ is ill defined. For metal oxides, typical c values obtained by $N_2$ adsorption at 77K are in the region of 80 to 150.

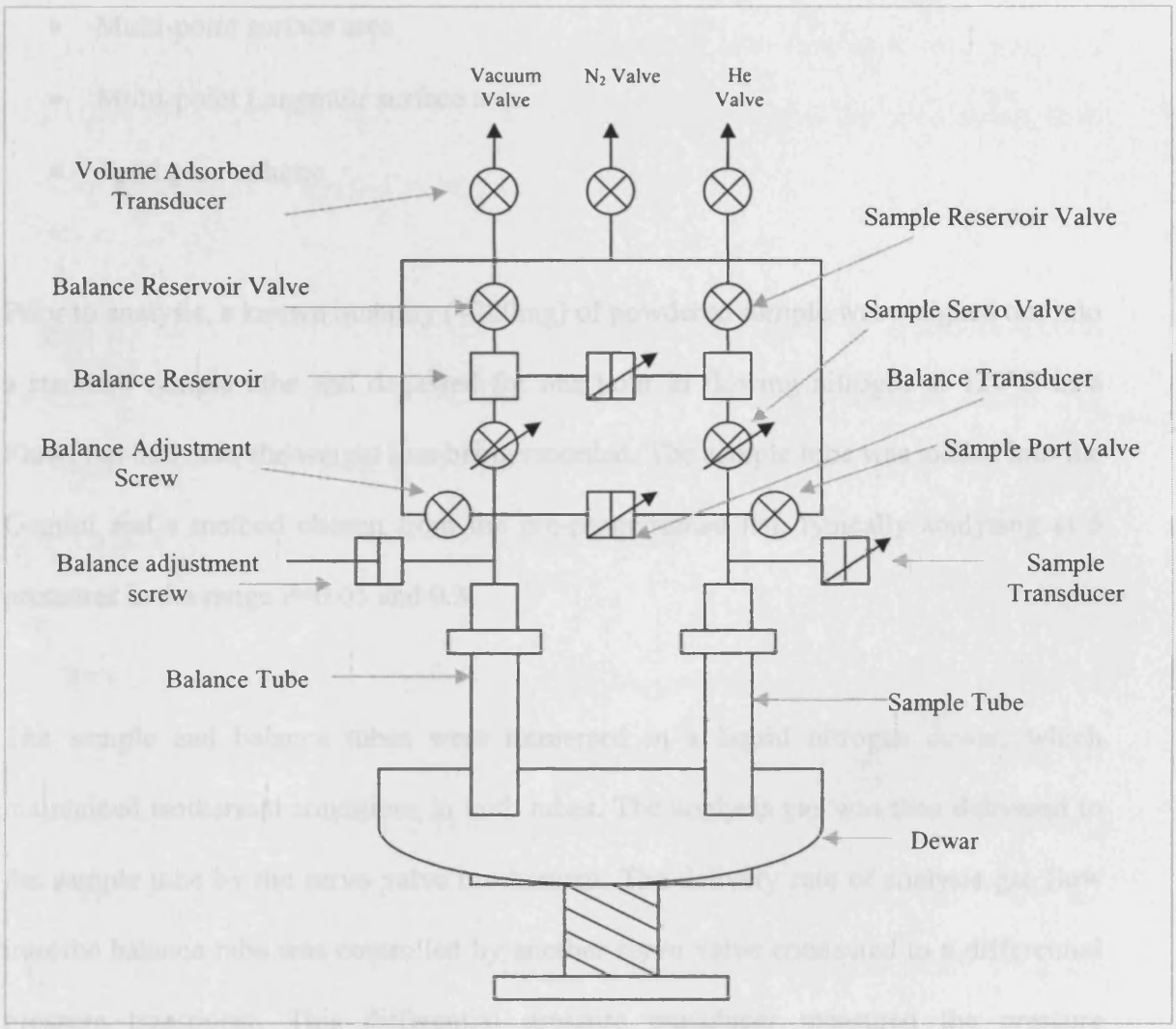


**Figure 2.3.3.3 – Schematic of Gemini 2360 analyser**

**Procedure**

Surface area analysis was carried out using a Micromeritics Gemini 2360 analyser, controlled by a PC. The Gemini provides rapid and accurate sample analysis, including selectable calculation of the following:

- Single-point BET
- Multi-point surface area
- Multi-point Langmuir surface area
- Total pore volume

Prior to analysis, a known quantity (~200mg) of powdered sample was weighed out into a standard sample tube and degassed for one hour in flowing nitrogen at 120°C in a FlowPrep 060 unit, the weight loss being recorded. The sample tube was loaded into the Gemini and a method chosen from the pre-programmed list, typically analysing at 5 pressures in the range P=0.05 and 0.3.

The sample and balance tubes were immersed in a liquid nitrogen dewar, which maintained isothermal conditions in both tubes. The analysis gas was then delivered to the sample tube by the servo valve mechanism. The delivery rate of analysis gas flow into the balance tube was controlled by another servo valve connected to a differential pressure transducer. This differential pressure transducer measured the pressure imbalance between the sample and balance tubes, which was caused by the adsorption of the analysis gas onto the sample. As the sample adsorbed analysis gas, the pressure dropped in the sample tube. The result was that the Gemini maintained a constant pressure of analysis gas over the sample while varying the rate of analysis gas delivery to exactly match the rate at which the sample could adsorb the gas.

Analysis started when gas entered the system and was admitted into the two reservoirs: the sample reservoir and the balance reservoir. From there it flowed into the sample and balance tubes. The flow of gas through the system was controlled by three transducers and a series of valves.

### 2.3.4 - TPR (Temperature Programmed Reduction)

The term TPR (Temperature Programmed Reduction) was first used in a paper by Robertson *et al* but the basic idea of characterising catalysts by monitoring their reducibility was first suggested by Holm and Clark. [9]

TPR is a technique which can be used to determine the number of reducible species present in a material and to reveal the temperature at which reduction occurs. An important aspect of TPR analysis is that the sample need not have any special characteristics other than containing reducible metals. [10]

The TPR analysis begins by flowing the analysis gas (typically a blend of two gases with vastly different thermal conductivities), in this case 10% $H_2$ in Ar, through the sample at ambient temperature to establish a base line reading. While the gas is flowing the temperature of the sample is increased linearly with time ($10^oC\ min^{-1}$) and the consumption of $H_2$ by adsorption/reaction is monitored. Hydrogen reacts with the oxygen in the sample to form $H_2O$ which is then trapped in the cold trap, changing the composition of the gas passing over the detector and hence its thermal conductivity. Since argon has a lower thermal conductivity than $H_2$, the thermal conductivity of the gas blend consequently decreases. The flowing gas removes heat from the filament more slowly, requiring less electricity to maintain a constant filament temperature. The instrument records the electrical demand as it changes. The detector signal is recorded

over a range of temperatures, when these are graphed, the data forms one of move peaks.

**Equipment**

The AutoChem 2910 Automated Catalyst Characterisation System was able to perform an array of high precision temperature programmed and chemisorption studies including pulse chemisorption, temperature programmed reduction (TPR), desorption (TPD), oxidation (TPO), and reaction analyses as well as BET surface area measurements.

**TPR Procedure**

Typically, the catalyst (50mg) was weighed and suspended on a plug of silica wool in the U-shaped TPR sample tube. The tube was loaded in to the AutoChem 2910 analyser and reaction parameters including sample weight, flow rates and temperature ramping rates. Typically, the catalyst was heated from ambient through to 450°C at 10°C/min while under the flow of a reducing gas mixture of 10% $H_2$ in argon. Changes in the reactant gas stream on reaction with the catalyst surface were detected by TCD.

## 2.3.5 - XPS (X-Ray Photoelectron Spectroscopy)

XPS provides information about the elemental surface composition. The principle of photoelectron spectroscopy is the excitation of electrons in an atom or molecule by means of X-Ray in a vacuum. The photoelectrons have a kinetic energy $E_{kin}$ equal to:

$E_{kin} = h\upsilon - E_B$

Where $h\nu$ is the energy of the incident X-rays and $E_B$ is the binding energy of the ejected electron. One of the most important additional applications of XPS is the determination of the oxidation state of elements of surface.

The electronic binding energies for inner shell electron shifts can be seen in nitrogen, indicating the photoelectron energy for various chemical environments. These energy shifts of the core $e^-$ are closely related to charge transfer in the outer electronic level. The charge redistribution of valence $e^-$ induces changes in the binding E of the core $e^-$, so that information on the valence of the element is readily available. A loss of negative charge (oxidation) is usually accompanied by an increase in the binding energy $E_B$ of the core electrons.

The surface sensitivity of photoelectron spectroscopy is increased by collecting the emitted electrons that emerge at small angles to the surface plane. These electrons must travel a long distance in the solid, and therefore they are more likely to be absorbed unless they are generated at the surface or in the near surface region. Photo emission of electrons from inner shells (eV = $4.8 \times 10^{-18}$ = $1.6 \times 10^{-15}$ J) is used in photoelectron spectroscopy to identify the surface composition and the oxidation states of surface atoms. The diffraction of X-Ray photoelectrons yields information about the surface structure.

**Equipment**

XPS studies were carried out during this study using an Escalab 220 spectrometer. Studies were completed with the grateful help of Dr Albert Carley, Cardiff University.

## 2.3.6 – AAS (Atomic Absorption Spectroscopy)

When a sample is burned in a flame, the atoms of the sample are released to form a cloud inside the flame. Each of the atoms consists of a positively charged nucleus surrounded by a number of electrons in rapid motion around the nucleus. For each of these electrons in the atom, there is a discrete set of energy levels that the electron can occupy. The distance between energy levels is different for each electron in the atom, but for similar atoms corresponding electrons have identical spacing. The energy levels range from $E_0$ at the ground state to $E\infty$; at which point the electron has enough energy to break away from the atom, this is the known as the ionisation energy.

In an unexcited atom, each electron is in the ground state. To excite the atom, one or more electrons can be raised to the first or higher energy levels by absorption of energy by the atom. This energy can be supplied by photons or by collisions due to heat.

Therefore, the appropriate energy is supplied by the flame to excite the electrons from the ground state to higher energy levels. It is the process by which these electrons fall back to the ground state that produces the signal.

The basic principles of atomic absorption spectroscopy can be expressed by three simple statements:

1. All atoms absorb light
2. Each element absorbs light at a specific wavelength, unique to that element. If a sample containing copper, for example, together with elements such as manganese and cobalt is exposed to light at the characteristic wavelength for copper, then only copper atoms will absorb light.

3. The amount of light absorbing is proportional to the concentration of absorbing atoms

In an atomic absorption spectrometer, these basic principles are combined and applied to practical quantitative analysis. The instrument consists of:

- A light source to generate light at the wavelength which is characteristic of the analyte element
- An atomiser to create a population of analyte atoms
- A monochromator to separate light from the source through the atom population and into the detector.
- A light sensitive detector
- PC and software to measure the detector response and translate it into useful analytical measurements

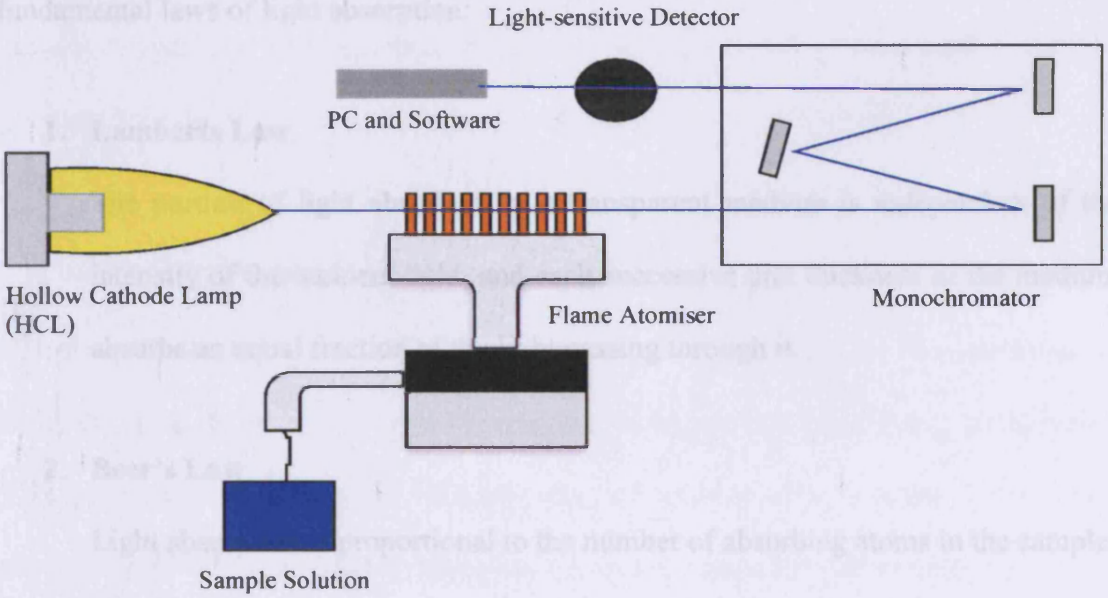


**Figure 2.3.6.1 – Schematic of a typical Atomic Absorption Spectrometer**

The general analytical procedure is very straightforward:

- Convert the sample in to a liquid
- Make up a blank solution containing no analyte element
- Make a series of calibration solutions containing exactly known concentrations of analyte element (5 – 150ppm)
- Atomise the blank and the standards in turn and measure the response for each solution
- Plot a calibration graph of concentration vs absorbance.
- Atomise the unknown solution and measure the response
- Refer to the calibration graph. Read off the concentration measurement for the absorption measured

**Relationship between light absorption and analyte concentration**

The relationship between light absorption and analyte concentration is defined in the fundamental laws of light absorption:

1. **Lamberts Law**

   The portion of light absorbed by a transparent medium is independent of the intensity of the incident light, and each successive unit thickness of the medium absorbs an equal fraction of the light passing through it.

2. **Beer's Law**

   Light absorption is proportional to the number of absorbing atoms in the sample.

The joint Beer-Lambert law is defined mathematically as:

$$I_t = I_0(10)^{abc}$$

Thus: $$\log_{10}\left(\frac{I_0}{I_t}\right) = abc$$

Where: $I_0$ = *Incident radiation power*

$I_t$ = *transmitted radiation power*

$a$ = "*absorption coefficient*" (*absorptivity*)

$b$ = *length of absorption path*

$c$ = *concentration of adsorption atoms*

Therefore, the absorbance is proportional to the concentration of the element for a given absorption path length at any given wavelength. Therefore, if a sample of concentration c gives a certain measured absorbance, a sample of concentration 2c will give double the absorbance. The Beer-Lambert law allows us to relate the measured absorbance to the concentration of the analyte element in the sample.

## 2.3.7 – TEM (Transmission Electron Microscopy)

Microscopy is a technique which can be invaluable in determining the size and shape of particles. [11-12] The most common type of microscope is a magnifying glass, which uses a ground lens to focus the light reflecting off an object into a larger image. Light microscopes of a more complex nature use a series of lenses for further magnification of the object. However, conventional light microscopes have a resolution limit of approximately 250nm (1 nm = $1 \times 10^{-9}$ m), approximately the wavelength of the

incoming light used to illuminate the sample. This resolution means that features on the sample smaller than this distance cannot be differentiated from each other. In order to observe the smaller details, a microscope that uses an illumination source with a smaller wavelength is needed. High voltage electrons are the most commonly used source, although x-rays and neutrons could theoretically be used as well.

Electron microscopy can yield information on phase composition and the internal structure of particles as specimens in the TEM are examined by passing the electron beam through them, revealing more information of the internal structure of specimens. There are two common types of electron microscopes: scanning (SEM) and transmission (TEM).

The technique applied to catalysts during this study was TEM. TEM produces an image that is a projection of the entire object, including the surface and the internal structures. The incoming electron beam interacts with the sample as it passes through the entire thickness of the sample. Therefore, objects with different internal structures can be differentiated because they give different projections. However, the projection is of necessity two-dimensional against the view screen and relations in the z-axis between structures are lost. Furthermore, the samples need to be thin, or they will absorb too much of the electron beam.

**Theory behind the TEM**

The TEM is an evacuated metal cylinder (the column) about two metres high with the source of illumination, a tungsten filament (the cathode), at the top. If the filament is heated and a high voltage (the accelerating voltage) of between 40,000 to 100,000 volts is passed between it and the anode, the filament will emit electrons. These negatively charged electrons are accelerated to an anode (positive charge) placed just below the

filament, some of which pass through a tiny hole in the anode, to form an electron beam which passes down the column. The speed at which they are accelerated to the anode depends on the amount of accelerating voltage present.

Electro-magnets, placed at intervals down the column, focus the electrons, mimicking the glass lenses on the light microscope. The double condenser lenses focus the electron beam onto the specimen which is clamped into the removable specimen stage, usually on a specimen grid.

As the electron beam passes through the specimen, some electrons are scattered whilst the remainder are focused by the objective lens either onto a phosphorescent screen or photographic film to form an image. Unfocussed electrons are blocked out by the objective aperture, resulting in an enhancement of the image contrast. The contrast of the image can be increased by reducing the size of this aperture. The remaining lenses on the TEM are the intermediate lens and the projector lens. The intermediate lens is used to control magnification. The projector lens corresponds to the ocular lens of the light microscope and forms a real image on the fluorescent screen at the base of the microscope column.

In a sense, a transmission electron microscope works in much the same way as an optical microscope. At the top of the column, there is a high voltage electron emitter that generates a beam of electrons that travel down the column. These electrons pass through the sample and a series of magnifying magnetic lenses, to where they're ultimately focused at the viewing screen at the bottom of the column. Different lenses can be used to change the magnification and focal point of the image. Apertures along the column can be used to change the contrast and resolution of the image. The column

itself is at a very high vacuum to minimize interactions between the electron beam and air molecules.

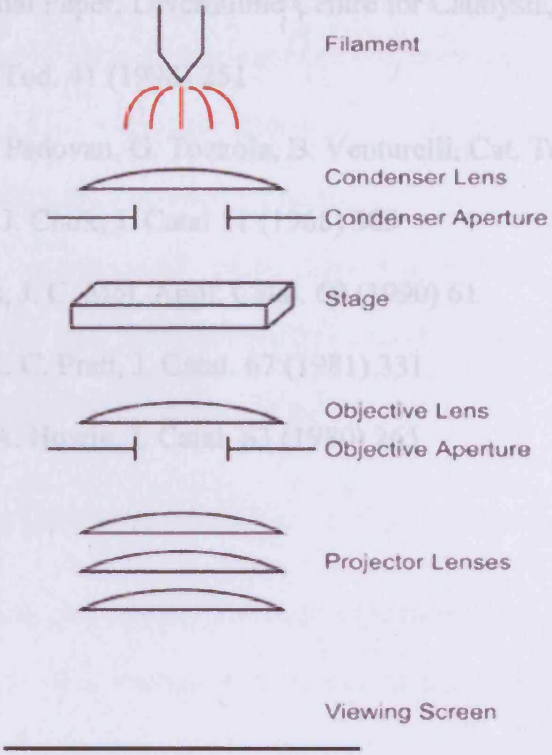


**Figure 2.3.7.1 – Schematic of an electron microscope**

TEM analyses were carried out at Lehigh University, Bethlehem, USA with the grateful collaboration of Prof Chris Kiely and Dr Andy Burrows.

## References

[1] A.A.Mirzaei, PhD Thesis, "The Low Temperature Oxidation of CO by copper containing catalysts", Liverpool University, 1998

[2] M. M. Doeff, T. J. Richardson, J. Hollingsworth, C. Yuan, M. Gonzales, J. Power Sources, 112 (2002) 294

[3] A. A. Mirzaei, H. R. Shaterian, R. W. Joyner, M. Stockenhuber, S. H. Taylor, G. J. Hutchings, Catal. Comm. 4 (2003) 17

[4] G. J. Hutchings, A. A. Mirzaei, R. W. Joyner, M. R. H. Siddiqui, S. H. Taylor, Appl. Cat. A: Gen. 166 (1998) 143

[5] W. A. Dietz, J. Gas Chrom. (1967) 68

[6] R. Joyner, Internal Paper, Leverhulme Centre for Catalysis, Liverpool (1992)

[7] G. Perego, Cat. Tod. 41 (1998) 251

[8] G. Leofanti, M. Padovan, G. Tozzola, B. Venturelli, Cat. Tod. 41 (1998) 207

[9] V. C. Holm, A. J. Clark, J. Catal 11 (1968) 305

[10] W. R. Robinson, J. C. Mol, Appl. Catal. 60 (1990) 61

[11] J. V. Sanders, K. C. Pratt, J. Catal. 67 (1981) 331

[12] M. M. Treacy, A. Howie, J. Catal. 63 (1980) 265

# Chapter 3 – Initial Experimental Studies of Ambient Temperature CO Oxidation over Hopcalite Catalysts

This chapter focuses on initial experiments aimed at producing highly active catalysts while developing a reproducible preparation route. Key factors that might affect the catalyst synthesis procedure are discussed especially with respect to the importance of the drying and calcinations steps in the formation of the final catalyst. Thermal treatment has been has been linked to the bulk phase and surface area characteristics of the catalysts and therefore is highly influential on catalyst activity.

## 3.1 – Initial Experimental Studies of Hopcalite Catalysts

The hopcalite sample was prepared by the co-precipitation batch production method, as outlined in Chapter 2.1.1. This method was developed by Mirzaei and has figured in a previous study of CO oxidation. [1]

Aqueous solutions of the copper and manganese nitrates were mixed and added to the reaction vessel while adding aqueous $Na_2CO_3$. The mixture was stirred continuously at 80°C and sodium carbonate added until pH 8.3 was achieved. The mixture was left under these conditions for a time period designated as the ageing time. The resulting pale green suspension was filtered and drying took place at 100°C for 16h, to give the material denoted as the catalyst precursor. This was followed by calcination at 500°C in static air for 17h to give the final catalyst.

### 3.1.1 - CO Oxidation Activity

The catalyst (100mg) was tested for its ambient temperature CO oxidation ability using gas chromatography. The total gas flow used was 22.5ml/min (20ml/min $O_2$ and 2.5ml/min of 10% CO in He), these conditions equated to a molar ratio of gases of 1.1: 88.9:10 ($CO:O_2$: He). The Gas Hourly Space Velocity (GHSV) for the experiment was $6750h^{-1}$, with a residence time of 0.533s

Under these conditions and a test period of 12 hours, no $CO_2$ was produced. The CO peak was observed at $t_r$ = 1.67mins, but no $CO_2$ was detected at the expected $t_r$ = 6.5mins.

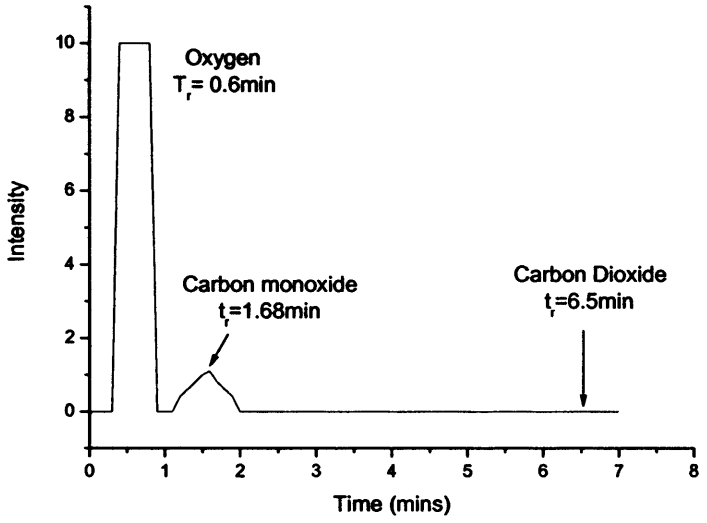


**Figure 3.1.1.1 – A typical gas chromatogram showing the separation of the reactants and products**

### 3.1.2 - Atomic Adsorption Spectroscopy

The ratio of metals present in the catalyst was measured by AAS and found to be 2.04:1 (Mn:Cu). See chapter 2.3.6 for full experimental details.

### 3.1.3 - X-Ray Diffraction Analysis

The catalyst showed many crystalline phases on analysis by powder X-Ray diffraction. (Fig. 3.1.3.1). The major phases were identified as $CuMn_2O_4$, $Cu_{1.2}Mn_{1.8}O_4$, $Cu_{1.4}Mn_{1.6}O_4$ and $Mn_2O_3$ with a small amount of CuO.

It would seem that the calcination conditions employed here have resulted in a highly crystalline complex mix of phases in the final catalyst. This crystallinity is undesirable, as reported by many authors who have observed a loss of activity in hopcalite catalysts due to crystallisation to the spinel after heat treatment at 873K. [2] The most active catalysts produced have been shown to possess an amorphous structure with respect to X-Ray Diffraction. [3-4] Kanungo has reported that the high temperature calcination of hopcalite is deleterious to catalytic performance. [5]

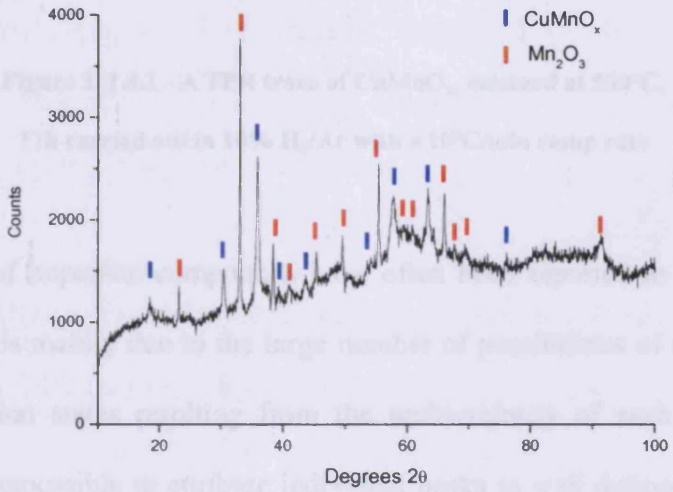


**Figure 3.1.3.1– XRD pattern of CuMnOx, calcined at 500°C, 17h**

## 3.1.4 - Temperature Programmed Reduction

The catalyst was investigated using temperature programming techniques. Typically, the catalyst (50mg) was analysed with the furnace temperature being ramped from ambient through to 450°C at 10°C/min while passing a reducing gas mixture (10%$H_2$/Ar) over the sample at 50ml/min. A full explanation of the TPR procedure is given in chapter 2.

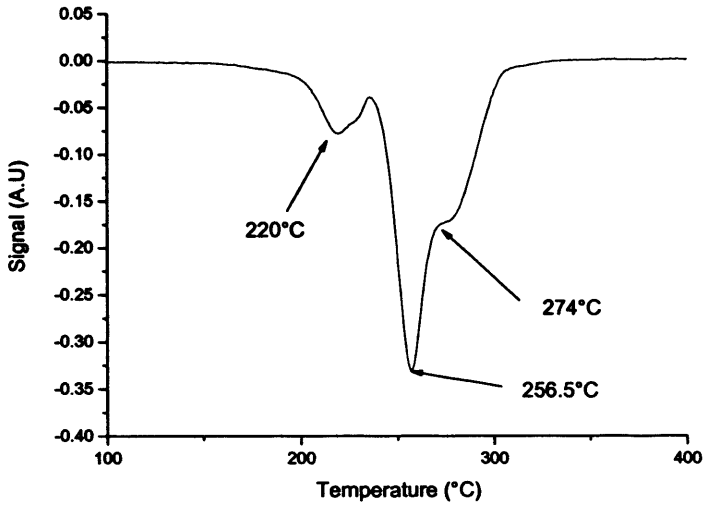


**Figure 3. 1.4.1 - A TPR trace of $CuMnO_x$, calcined at 500°C, 17h carried out in 10% $H_2$/Ar with a 10°C/min ramp rate**

The TPR profile of hopcalite compounds have often been reported as being difficult to interpret. [6] This is mainly due to the large number of possibilities of mixed copper and manganese oxidation states resulting from the multi-valency of each element. It was, therefore, almost impossible to attribute individual peaks to well defined redox reactions. However, it was expected that the lower temperature peaks were more likely to correspond to the reduction of $Cu^{2+}$ as copper is reported to have a higher reducibility than manganese in mixed compounds. [7] This was due to the more negative free energy of formation of the manganese oxides as compared to the copper oxide.

Further supporting evidence comes from the fact that manganese oxides are not expected to reduce at lower temperatures than CuO. [8] Mirzaei also concluded that the presence of manganese retards the reduction of CuO, extenuated by the fact that a shift to higher temperatures of the CuO reduction peak was observed where higher Mn:Cu ratios were present in the catalyst. This was a theory supported by Leith and Howden. [9] Mirzaei reported that CuO reduced in a two-step process from $Cu^{2+}$ to $Cu^{+}$ and $Cu^{+}$ to metallic $Cu^{0}$, with a typical peak at lower temperature followed by a shoulder at higher T. However, Fierro stated that CuO reduces in one step and that the second, shoulder signal was an artefact due to the sublimation of metallic copper on the unreduced CuO particles. [6]

Manganese oxide $Mn_2O_3$ is reported to reduce in one-step to MnO. Due to thermodynamic constraints, MnO does not further reduce to $Mn^{0}$. [9] It concludes that the high T reduction peaks were therefore due to the reduction of manganese as these were observed to almost disappear when a high copper content was used. The middle temperature reduction peaks could therefore be assigned to the presence of a mixed copper and manganese oxidic phase with a general formula $Cu_{1+x}Mn_{2-x}O_4$.

In the sample tested here, four reduction peaks were present, at 220, 227, 256.5 and 274°C. Based on previous publications, the two lower temperature peaks would therefore have resulted from the reduction of CuO. The highest temperature peak at 274°C would therefore be due to the reduction of $Mn_2O_3$ and the intermediate reduction peak must due to the reduction of the mixed $CuMnO_x$ phase, which by XRD was shown to be a mixture of $CuMn_2O_4$, $Cu_{1.2}Mn_{1.8}O_4$, $Cu_{1.4}Mn_{1.6}O_4$.

### 3.1.5 - Surface Area Studies

The material (0.100g) was analysed to determine its BET surface area using a Micromeritics Gemini analyser with $N_2$ as the adsorbate. (See Ch. 2.2.3) The 5 point surface area for the catalyst was measured as $14m^2/g$. This figure was much lower than the 23-31 $m^2/g$ reported by Mirzaeii [10], $27m^2/g$ reported by Porta [11] and the $35m^2/g$ reported by Wright [12] in their studies of CO oxidation by precipitated mixed copper manganese catalysts, synthesised under similar conditions.

The very low surface area, combined with the undesirable crystalline nature of the catalyst contributed to explaining the zero activity for this catalyst towards the CO oxidation test reaction.

## 3.2 - Calcination Investigation

It was necessary to modify the calcination procedure to produce a series of less crystalline or amorphous catalyst systems with greater active surface areas. It was thought that this could be achieved by alteration of the calcination conditions.

### 3.2.1 - Effect of Calcination Temperature on Catalytic Activity

The calcination conditions employed previously were thought to be too harsh, i.e. the calcination time was too long or the temperature of calcination was too high. It has previously been suggested that high temperature treatment might destroy the porous nature of the material, affecting it's catalytic properties. [13]

When shorter calcination times were employed, the resulting catalysts were immediately found to be active for CO oxidation. This holds true the theory of Veprek who states that only amorphous hopcalite systems are active as ambient temperature CO oxidation catalysts. [14]

The first active catalysts were produced in this study by heating the catalyst precursor from ambient to a variety of temperatures between 200 and 400°C (at 20°C/min) in static air and calcining for a period of 2 hours.

### 3.2.2 - Lower Temperature Calcination Conditions – XRD Data

On XRD analysis, it was interesting to look at the effect of heating the precursor at a variety of temperatures for a constant period of time. The original catalyst precursor comprised of a mixture of semi-crystalline phases including copper and manganese hydroxy carbonates, along with evidence of the copper manganese mixed phase, $CuMnO_x$.

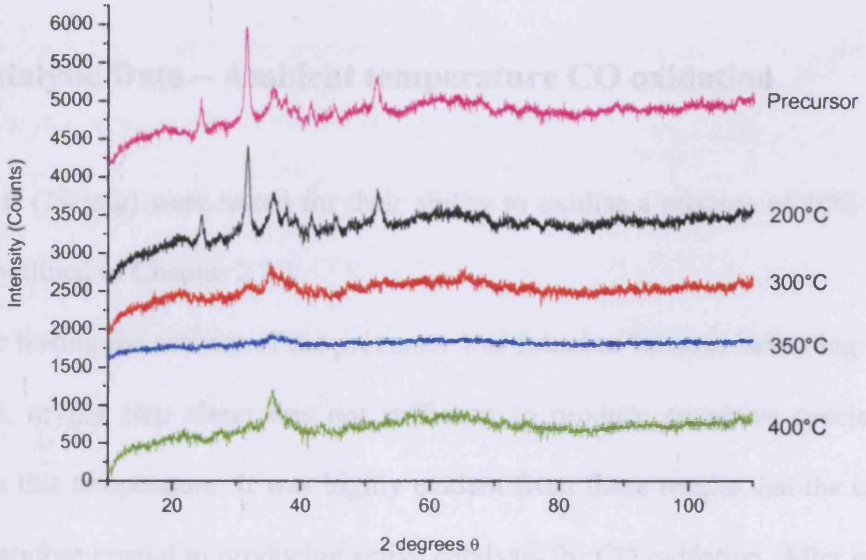


**Fig 3.2.2.1- XRD data of $CuMnO_x$ catalyst as a function of calcination temperature (2h in air)**

On heating the precursor in air for 2h at 200°C, very little change in bulk structure was was evident on XRD analysis from that of the precursor. The catalyst produced under these calcination conditions still displayed many of the crystalline phases that were present in the precursor. On raising the calcination temperature to 300°C, a loss of crystallinity occurred with the catalyst taking on an amorphous composition. This trend continued through 350°C, where the material obtained was almost completely amorphous to XRD. On further increasing the temperature to 400°C, a slight return of crystallinity was observed with strong evidence of the microcrystalline $CuMn_2O_4$ hopcalite phase reported by many researchers along with small amounts of copper and manganese oxides. [10-12, 15] It was these phases, occurring from calcination conditions of 400°C for 2h that have previously been reported as highly active for CO oxidation. [1] As was demonstrated in fig 3.1.3.1 earlier in this chapter, prolonged heating of the precursor at higher temperatures only served to produce highly crystalline, low surface area catalysts which were inactive for CO oxidation at ambient temperature.

### 3.2.3 - Catalytic Data – Ambient temperature CO oxidation

The catalysts (100mg) were tested for their ability to oxidise a mixture of 10% CO/He in oxygen as outlined in Chapter 2.2.1.

On catalytic testing the activity of the precursor was found to be zero, indicating that a low temperature, drying step alone was not sufficient to produce an active species for CO oxidation at this temperature. It was highly evident from these results that the calcination step was therefore crucial to producing active catalysts for CO oxidation. After calcination in air for 2h at 200°C, a catalyst was produced that was active for CO oxidation. Activity

was observed to rise to a maximum of 30% after approximately 30 minutes on stream at ambient temperature.

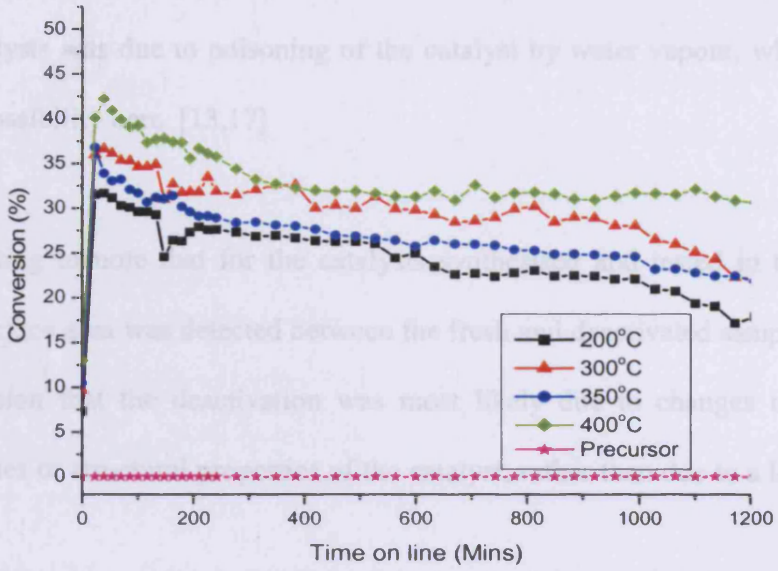


**Figure 3.2.3.1 – Activity of $CuMnO_x$ catalysts calcined for 2h at a variety of temperatures**

This species was shown to be rich in manganese carbonate on XRD analysis, as compared to the catalysts calcined at higher temperature, where a greater proportion of the carbonate phases of the precursor were converted to oxide species.

As the calcination temperature was increased further, an apparent increase in the initial activity of the catalyst could be observed, reaching a maximum of 43% for the sample calcined at 400°C. In each case, the maximum activity was observed early on in the lifetime of the catalyst, followed by slow deactivation with increasing time on-line. The deactivation with increased usage had previously been reported for hopcalite catalysts where some authors have attributed the phenomenon to the blocking of active sites on the catalyst surface. [16] It was likely that the deactivation observed for the catalysts discussed

in this chapter with increasing time-on-line, was due to an increasing number of the surface active sites becoming blocked, decreasing the ability of the catalyst to catalyse CO. Other authors have proposed that the gradual decrease in activity commonly observed in hopcalite catalysts was due to poisoning of the catalyst by water vapour, which may also have been a possibility here. [13,17]

It was interesting to note that for the catalysts synthesised and tested in this study, no decrease in surface area was detected between the fresh and deactivated samples. This lead to the conclusion that the deactivation was most likely due to changes in the surface adsorbed species or structural properties of the catalyst, rather than due to a loss of surface area. [14]

### 3.2.4 - Surface area adjusted rate of CO conversion

Surface areas were measured by the adsorption of $N_2$ using the BET technique as outlined in chapter 2.

The surface area of the precursor was substantially lower than those of the calcined catalysts. On calcination of the precursor for 2h in air, the surface area of the final catalyst increased from that of the precursor with increasing calcination temperature. A maximum surface area occurred for the 400°C calcined catalyst having a BET surface area of $82m^2/g$. These observations were in general agreement with the results of Veprek *et al.* who reported surface area to decrease on the amorphous-to-spinel transition. [14] The activity of the catalyst was observed to increase on activation (calcination of precursor) and decrease on the amorphous to crystalline phase transition. Activation by calcination

involved water removal, thereby generating adsorption sites for $O_2$ and creating small pores which increased the surface area and activity of the catalyst system.

| Catalytic System | Surface area ($m^2/g$) | C - value | Cu/Mn ratio |
|---|---|---|---|
| CuOx - 400°C | 24 | 85 | n/a |
| $MnO_x$- 400°C | 46 | 110 | n/a |
| $CuMnO_x$ Precursor | 48 | 36 | 0.47 |
| $CuMnO_x$ - 200°C | 65 | 49 | 0.48 |
| $CuMnO_x$ - 300°C | 73 | 65 | 0.48 |
| $CuMnO_x$ - 350°C | 77 | 48 | 0.49 |
| $CuMnO_x$ - 400°C | 82 | 64 | 0.50 |

**Table 3.2.4.1 – Surface areas of catalysts calcined at different temperatures**

All of the catalysts tested displayed surface areas higher than either of the single $CuO_x$ and $MnO_x$ components. The c-values measured for each of the catalysts were within the expected range for metal oxide catalysts. Both calcined $CuO_x$ and $MnO_x$, along with the mixed copper manganite precursor, displayed zero activity under these conditions for CO oxidation.

On adjustment of the activities for differences in surface areas, the catalyst calcined at 300°C, 2h displayed the highest conversion rate of CO in $Mol/m^2/s$. The maximum conversion rate observed during the calcination study also occurred for the species calcined under these conditions. In terms of stability with time on line, all catalysts suffered depreciation in conversion levels over the duration of the test period. The greatest

level of stability was observed for the catalyst calcined at 400°C, however, this higher stability correlated with a lower CO conversion rate in general.

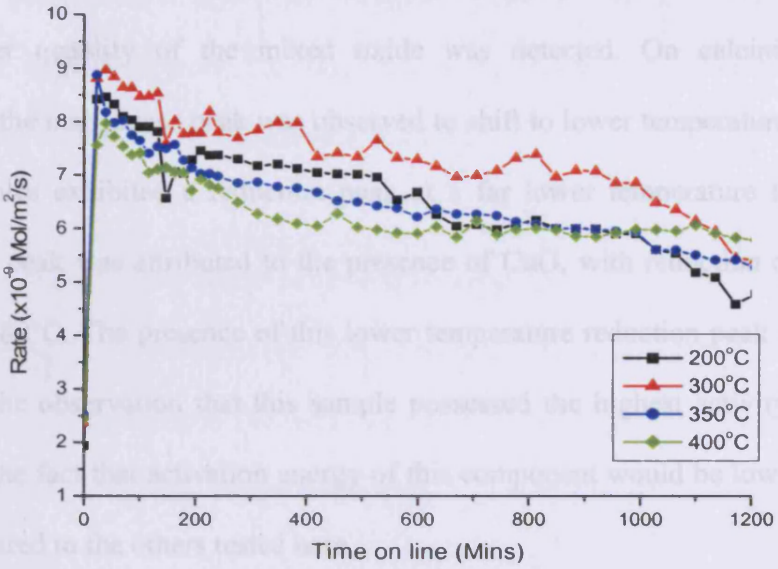


**Figure 3.2.4.2 – Surface area adjusted reaction rates for CO oxidation at 25°C as a function of calcination temperature**

## 3.2.5 – Temperature Programmed Reduction Studies

Temperature programmed reduction analysis of the samples showed significant differences between the profiles for each sample. It was interesting to note the phase change between the precursor and the 200°C calcined sample and those calcined at higher temperatures. The precursor and sample treated at 200°C exhibited a peak at lower temperature with a shoulder than can be attributed to CuO and a peak due to the reduction of manganese oxide at higher temperature. A less intense signal was detected at an intermediate temperature to the copper and manganese oxide peaks that can be assigned to the reduction of the mixed copper manganese oxide phase. The presence of only a small amount of the mixed,

catalytically active oxide, $CuMnO_x$, after drying of the precipitate at 100°C might explain why the activity of the precursor towards CO oxidation was zero. Likewise, the activity of the samples increased on raising the calcination temperature from 200°C through to 400°C, when a larger quantity of the mixed oxide was detected. On calcining at higher temperatures, the manganese peak was observed to shift to lower temperatures. The 400°C calcined samples exhibited a reduction peak at a far lower temperature than the other samples. This peak was attributed to the presence of CuO, with reduction of this species occurring at 180°C. The presence of this lower temperature reduction peak could perhaps be linked to the observation that this sample possessed the highest activity towards CO oxidation by the fact that activation energy of this component would be lower than in this catalyst compared to the others tested here.

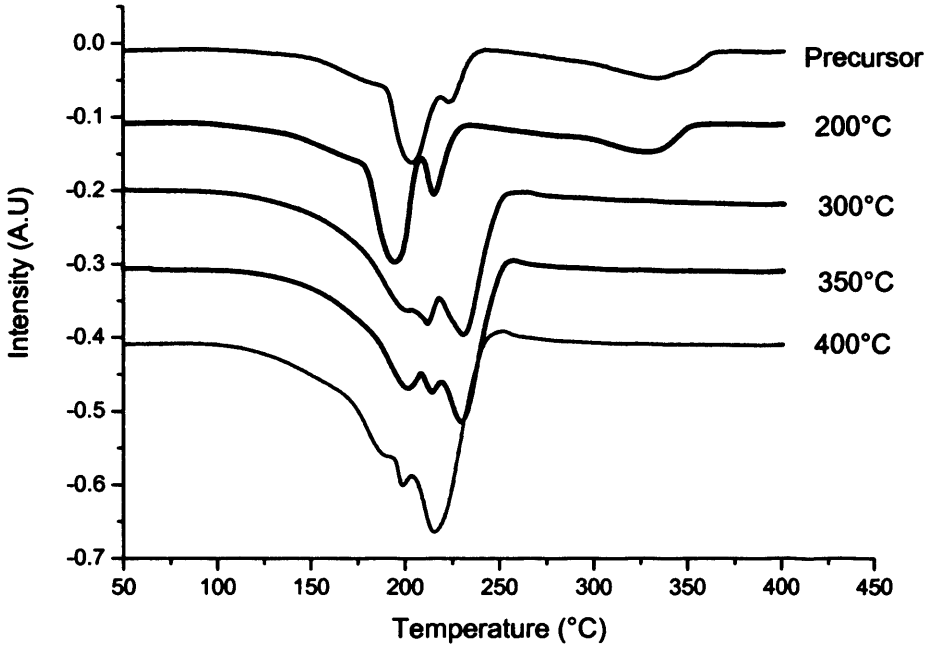


**Figure 3.2.5.1 – TPR trace of $CuMnO_x$, calcined at a range of temperatures for 2h carried out in 10% $H_2$/Ar with a 10°C/min ramp rate**

## 3.3 - Further Work on Effect of Calcination T and Time on Surface Area

A detailed investigation was carried out to determine the calcination conditions necessary to produce the most active catalysts. The precursor (1g) was calcined at 400°C for differing lengths of time in order to probe the effect that calcination time at a constant temperature had on the catalyst structure, surface area and activity.

### 3.3.1 - Highest performance batch produced catalyst

The most active batch produced catalyst was obtained using an ageing time of 5h. The activity of this catalyst towards CO oxidation rivalled that of the commercially available catalysts at the time. The ratio of the metals used in the preparation of this catalyst was 2:1 (Mn:Cu) compared to a 1.5:1 ratio used commercially.

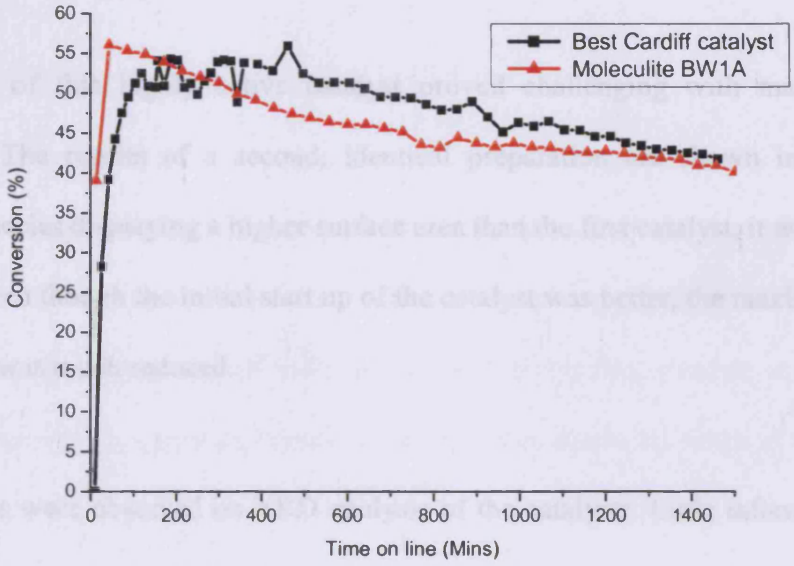


**Figure 3.3.1.1 – A comparison of catalytic performance of the best Cardiff produced catalyst vs. the industrial catalyst, Moleculite BW1A at 25°C**

Despite the lower surface area of the best Cardiff catalyst (63-77$m^2/g$ cf. 88-93$m^2/g$ for the commercial catalyst), the activity rivalled that of the Moleculite BW1A industrial catalyst. The initial start up of the Cardiff catalyst was slower but activity increased steadily with time on line, out performing Moleculite from a time of 200 minutes through to the end of the test period (1400 mins).

| Catalytic System | Surface area ($m^2/g$) | C - value | Cu/Mn ratio |
|---|---|---|---|
| Moleculite™ | 88 | 85 | 0.63 |
| E33a | 77 | 110 | 0.51 |
| E33b | 63 | 36 | 0.47 |

**Figure 3.3.1.2 – Best Cardiff produced vs Industrial oxidation catalyst BET and AAS data**

Reproduction of this highly active catalyst proved challenging with many problems encountered. The results of a second, identical preparation are shown in fig 3.3.1.3. Despite the species displaying a higher surface area than the first catalyst, it was interesting to note that even though the initial start up of the catalyst was better, the maximum activity level reached was much reduced.

No differences were observed on XRD analysis of the catalysts. Little information of the catalyst bulk structure could be drawn from the patterns owing to the samples being amorphous to XRD or micro-crystalline in nature; in which case the particle size would have been too small for XRD to yield useful structural information.

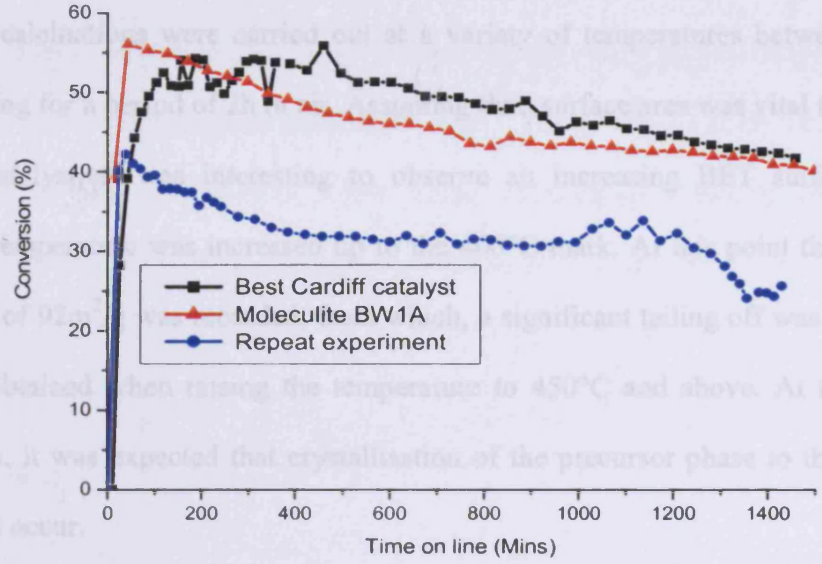


**Figure 3.3.1.3 – A graph of activity indicating the irreproducibility in synthesis of the best Cardiff produced catalyst versus Moleculite BW1A at 25°C**

## 3.4 - Optimisation of Calcination Conditions

As long ago as the 1920s, the drying and calcining steps of the hopcalite precursor were recognised as crucial in preparing catalytically active species. [13] Other researchers over the years have also paid particular attention to the drying steps. [10] A number of authors have discussed the importance of moisture content to the final catalyst activity. Where drying has occurred at high temperature, catalysts often displayed lower activity towards the test reaction. [1]

A range of calcination conditions were investigated and their products characterised by TPR, AA, XRD and BET analysis before testing against the standard CO oxidation reaction.

### 3.4.1 - Investigation of surface area

A range of calcinations were carried out at a variety of temperatures between 100 and 600°C, heating for a period of 2h in air. Assuming that surface area was vital to producing an active catalyst, it was interesting to observe an increasing BET surface area as calcination temperature was increased up to the 400°C mark. At this point the maximum surface area of $92m^2/g$ was recorded, from which, a significant tailing off was observed in the values obtained when raising the temperature to 450°C and above. At these higher temperatures, it was expected that crystallisation of the precursor phase to the $CuMn_2O_4$ spinel would occur.

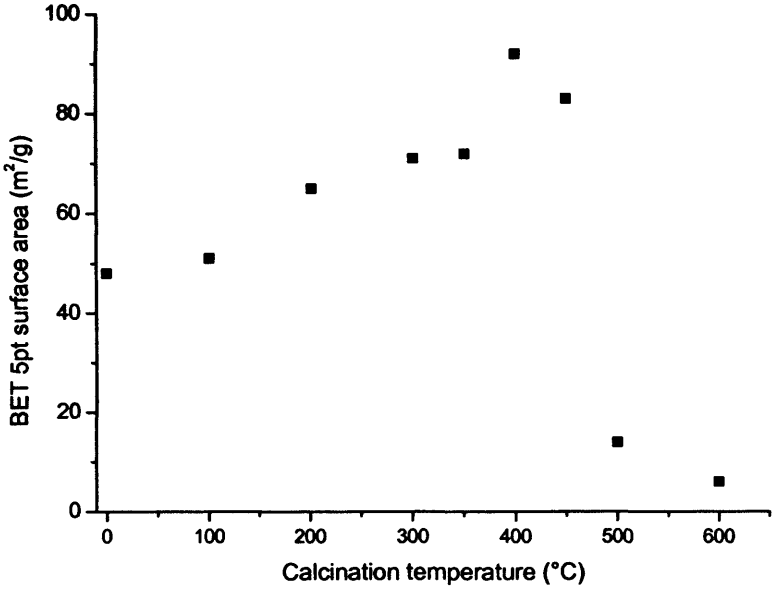


**Figure 3.4.1.1– Investigation into calcination conditions**

Veprek has reported the $CuMn_2O_4$ spinel as catalytically inactive for CO oxidation. [14] A similar trend in loss of surface area when increasing the calcination time at high temperature was reported by Wright *et al.* in their study of catalytic systems containing oxides of manganese and copper. [12]

The effect of calcination time was investigated by heating precursor samples at 400°C for a range of times between 0.5 and 6h. A bell-shaped distribution of points could be plotted for the resultant surface area against calcination time. The precursor at 0h calcination time (dried at 100°C for 16h) displayed a low surface area, rising to $92m^2/g$ for the sample calcined for 2 hours, with values tailing off as the calcination time was lengthened.

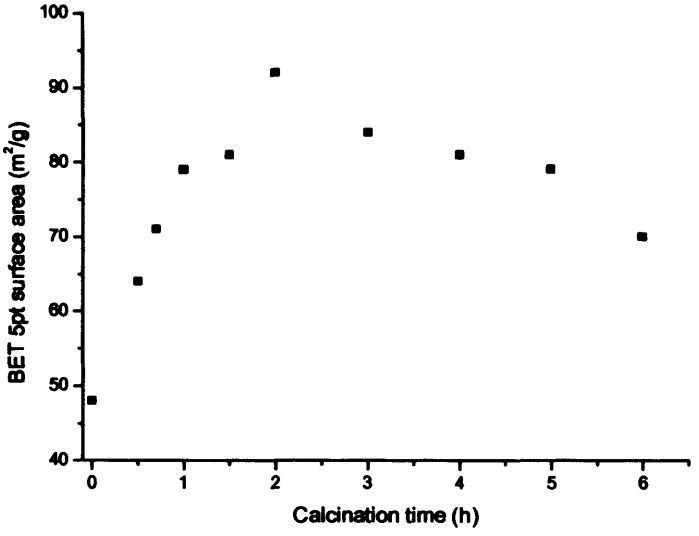


**Figure 3.4.1.2 – Catalyst surface areas as a function of calcination time at 400°C**

The calcination procedure was further probed by investigating conditions in the region 400°C for 2h in order to optimise the potential surface area levels available during later preparations.

### 3.4.2 - TPR analysis

The effect of calcining for 2h in the 400-500°C range was probed as it had previously been observed that heating to 500°C (18h) was too harsh a calcination environment, producing

inactive, crystalline catalysts. It was confidently thought that 400°C (2h) would produce the amorphous, active catalysts that this study was striving for.

On close analysis of the TPR data, some important trends were evident. As calcination temperature and time were increased, more $H_2$ was consumed during the reduction process, indicating an increase in the quantity of reducible material present in the catalyst. It concluded that the more heat treatment that the catalyst was exposed to, the greater the oxide content in the catalyst. However, this did not necessarily lead to more active catalysts as other factors such as bulk structure needed to be considered.

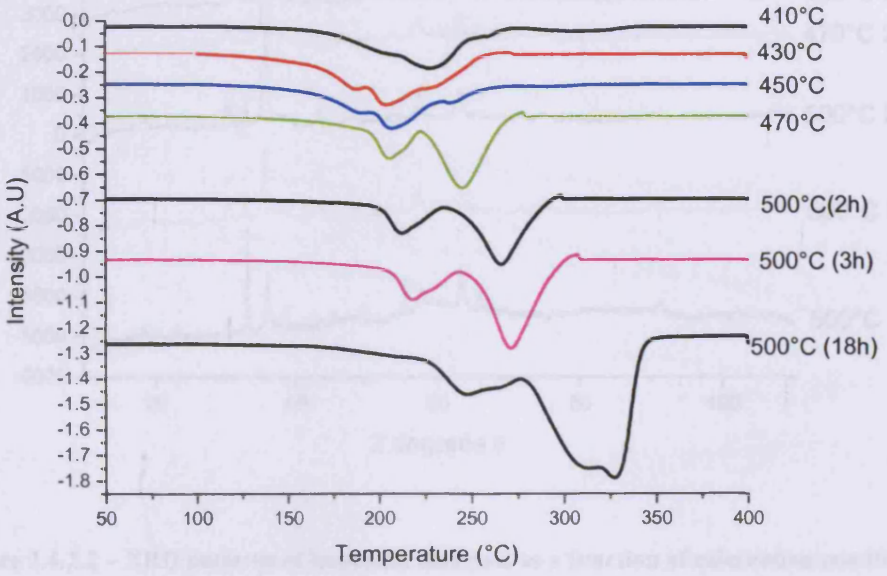


**Figure 3.4.2.1 – TPR profiles as a function of calcinations temperature and time**

Of the samples tested, the lowest temperature reduction peak occurred for the catalyst calcined at 430°C. As calcination temperature and time were further increased, a general shift of all the reduction peaks to higher temperature was observed. When calcining at 500°C 18h, the characteristic four-reduction peak system that related to crystalline

$CuMn_2O_4$ was produced; the presence of this phase was further confirmed on XRD analysis. For the catalysts calcined at lower temperatures, it was not possible to detect the standard four-reduction peak system expected for the hopcalite spinel. A strong signal due to the reduction of CuO was present at low temperature, but the $CuMnO_x$ and $Mn_2O_3$ peaks were small and overlapping. These peaks were only resolved when higher temperature calcinations were employed and a greater quantity of the oxide was present.

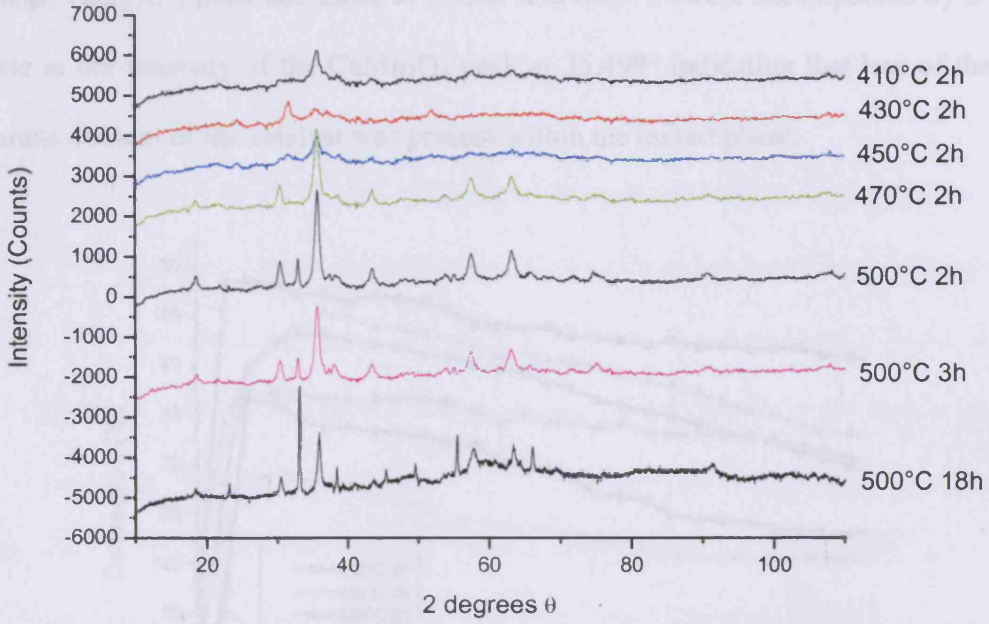


**Figure 3.4.2.2 – XRD patterns of hopcalite catalysts as a function of calcination conditions**

Figure 3.4.2.2 highlights that as calcination time and temperature were increased, the catalysts produced became more crystalline in nature. The most pertinent point of transition between the production of amorphous and crystalline catalysts occurred between the sample calcined at 450°C/2h and that at 470°C/2h. This point occurred at a lower temperature than might have been expected for the amorphous to crystalline transition as

reported by Wright *et al.* who identified the transition temperature as being 500°C. [12] At 470°C it was possible to detect an increase in intensity of signals due to the $CuMnO_x$ phase (57.336°, 62.991°) in conjunction with those due to the $Mn_2O_3$ phase. Striking differences were evident between the catalyst diffraction patterns of the sample calcined at 500°C for an extended period compared to those calcined at lower temperatures and for a shorter time. It was also interesting to note the increase in intensity of the $Mn_2O_3$ peaks between the 3h calcined sample and the 18h calcined sample at 500°C. This increase in the size of the $Mn_2O_3$ (32.396°) peak and those at 55.361 and 65.975° were accompanied by a slight decrease in the intensity of the $CuMn_2O_4$ peak at 35.499° indicating that less of the total manganese content of the catalyst was present within the mixed phase.

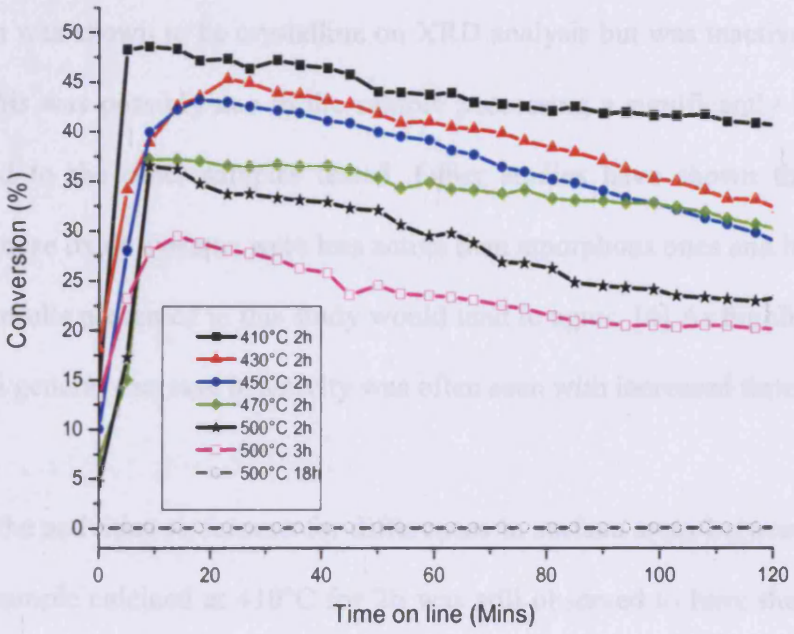


**Figure 3.4.2.3 – Activity towards CO oxidation as a function of the calcination conditions in air**

Each of the samples analysed against the test reaction displayed a gradual increase in the catalyst activity during the early minutes on line, generally leading up to the point of

maximum conversion; this is often referred to during this study as the start-up activity. The best start-up activity was observed for the sample calcined at 410°C for 2h in air. Start-up efficiency decreased, in general, as the calcination time and temperature was increased. The activity of the catalyst towards CO oxidation appeared to correlate with the XRD patterns shown in figure 3.4.2.2. At the lower calcination temperatures, a poorly crystalline XRD pattern was observed but was often related to a good level of CO oxidation. As calcination temperature and time were increased, it followed that an increase in the crystallinity of the catalyst was observed along with a general decrease in surface area.

These characteristics were often accompanied by a general decrease in catalytic activity towards the test reaction. This was exemplified by the fact that the sample calcined at 500°C for 18h was shown to be crystalline on XRD analysis but was inactive towards CO oxidation. This was possibly due to the sample possessing a significantly lower surface area compared to the other samples tested. Other studies have shown that crystalline copper manganese oxide systems were less active than amorphous ones and based on these findings, the results presented in this study would tend to agree. [4] As highlighted already in this study, a general decrease in activity was often seen with increased time on line.

On adjusting the activities to account for differences in surface areas between the catalyst samples, the sample calcined at 410°C for 2h was still observed to have the best start-up activity rate. The rates of CO conversion of the other 2h calcined catalysts were quite similar towards the start of their use but a tailing off of conversion rates was observed with increasing time-on-line. This deactivation may have been due to the blocking of catalyst active sites by the adsorption of species, such as carbonates, on to the catalyst surface, in a

similar fashion to the results reported by Gardner. [18] For the 500°C calcined samples the decrease of conversion rate with time on-line was more pronounced. This was further extenuated when the length of calcination time was increased from two to three hours.

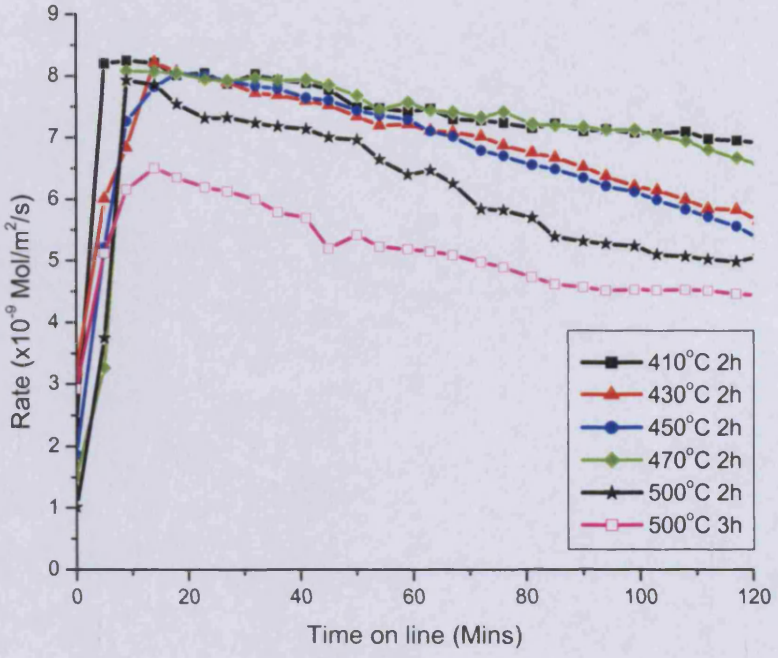


**Figure 3.4.2.4 – CO conversion rates adjusted for surface area as a function of calcinations conditions**

A replica set of catalysts, mirroring those shown in fig.3.4.2 were synthesised in order to check the reproducibility of the preparation method.

The TPR profiles of the replica set of catalysts were a good match to those shown in fig. 3.4.2.1. It was also interesting to note that no discernable differences were detected between the TPR of a fresh catalyst sample and that of a used one. This may provide an indication that the $O_2$ consumed in the oxidation process over these catalysts might have been provided from the gas phase, rather than from surface adsorbed or lattice sources. Alternatively, continual replenishment of lattice oxygen might have occurred during the

oxidation of CO by the catalyst surface with the overall effect being no change in the amount of $O_2$ present. In either of these cases, the level of oxide species present in the catalyst before and after use might have remained broadly the same.

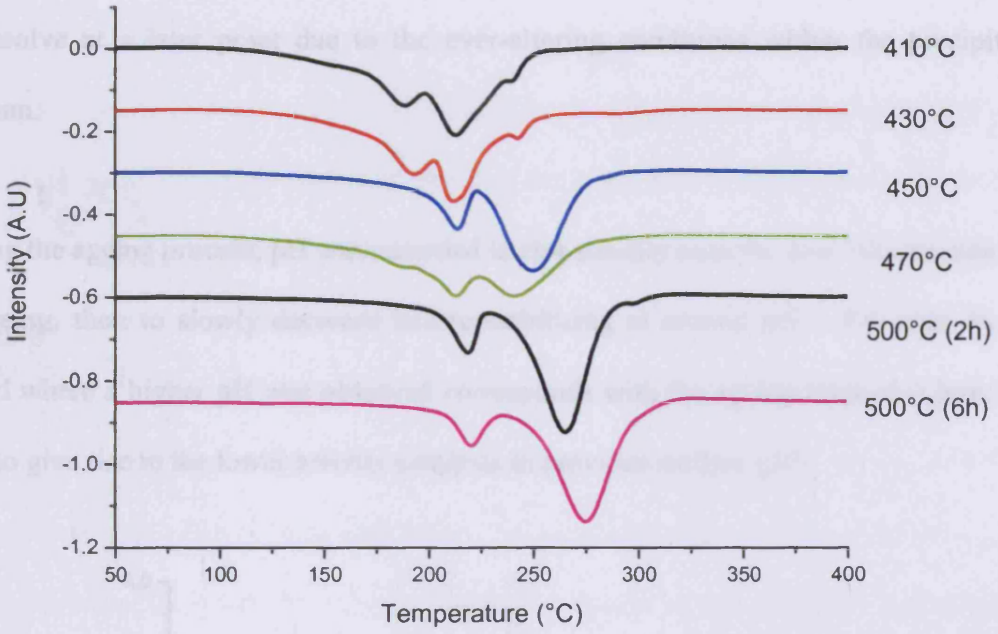


**Figure 3.4.2.5 – TPR analysis of hopcalite as a function of calcination conditions**

## 3.5 - Other Factors Influencing Reproducibility

As with any chemical synthesis, a reproducible route for the preparation of active catalysts was paramount. Without it, it would not be fully possible to understand the effects that altering preparation parameters would have on the structure and behavior of the final product. The level of variation existing within the preparation methods of catalysts synthesized in this chapter were further probed in terms of pH variation with ageing time along with the effect of fluctuation in temperature during the aging process.

### 3.5.1- Investigation into pH drift

During many of the co-precipitation syntheses, the pH of the precipitation suspension was observed to fluctuate during the ageing process after the initial pH=8.3 had been achieved by the addition of $Na_2CO_3$ to the nitrate mixture. This feature has not been uncommon to co-precipitation processes, as species have often been thought to precipitate out but then to re-dissolve at a later point due to the ever-altering conditions within the precipitation medium.

During the ageing process, pH was recorded to rise steadily over the first 100 minutes or so of ageing, then to slowly decrease before stabilising at around pH = 8.8 after 4h. The period where a higher pH was observed corresponds with the ageing times that have been seen to give rise to the lower activity catalysts in previous studies. [10]

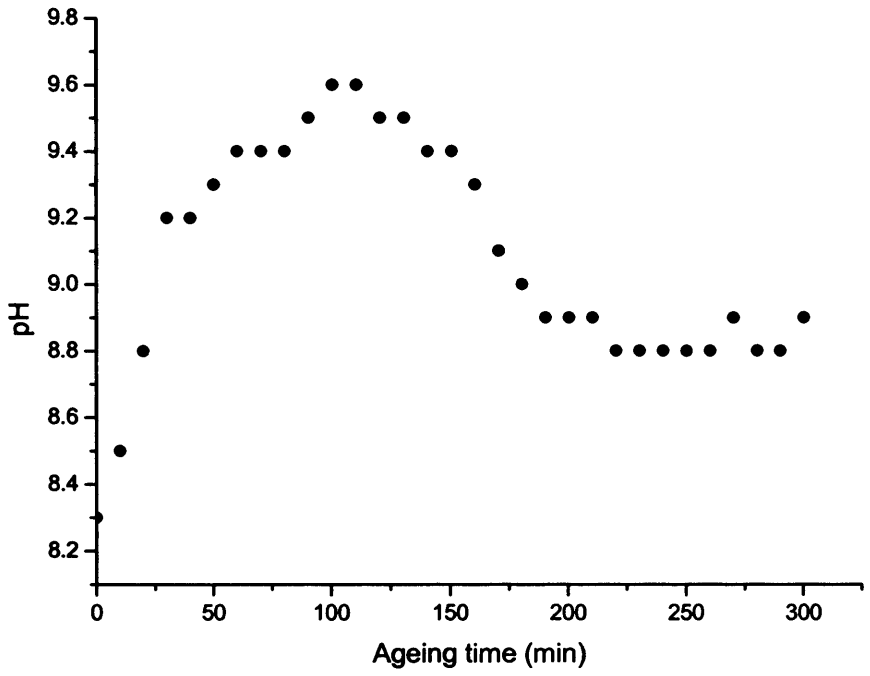


**Figure 3.5.1.1- pH drift profile during the precipitate ageing process**

Strict pH control was added to the catalyst preparation procedure in order to minimise variations between syntheses, therefore increasing the probability of generating reproducible species on a regular basis.

### 3.5.2 - Temperature control

The initial temperature control used in the set up shown in chapter 2.1.1 was poor. Reagents were added at room temperature to the precipitation vessel at 70°C. This predictably gave rise to a period of time at the start of the ageing process where the reagents were below the required temperature of the reaction vessel, and hence below the temperature reported to produce active catalysts. Temperature variation during catalyst preparation has been reported to have a strong influence towards phase changes and textural properties of the final species produced by precipitation processes. [19] Future preparations were tailored to include the use of preheated nitrates and carbonates, as well as a double-walled, water heated, glass reaction vessel to ensure isothermal conditions during the ageing process. An ageing temperature of 80°C was decided on as this was identified by Mirzaei as being the highest practical operating temperature for a precipitation process involving the use of a water heated reaction vessel. Mirzaei also concluded that higher temperature preparations often lead to catalysts that were more active. [10]

## 3.6 - Conclusions

The results presented in this chapter have provided strong evidence as to how the final catalyst structure and activity can be influenced by factors during the preparation procedure. Some highly active species were produced that could match the activity of the

commercial catalyst Moleculite, but discrepancies in the preparation method of the catalysts meant that consecutive batches of material were rarely of the same composition or activity.

Some optimum conditions have been identified to address this, particularly in terms of the heat treatment required to produce amorphous, active species. A calcination temperature of 410°C for 2h in air was found to produce the most active catalysts. An explanation of the high activity of this species might be offered by the presence of a higher BET surface. Studies in to surface areas obtained over a range of calcinations conditions in air also indicated that a temperature between 410 and 420°C was optimum to producing catalysts of high relative surface areas.

Where higher calcination temperatures and longer heating times were used, inactive, crystalline species with relatively low surface areas were often produced. This was exemplified by the amorphous-to-spinel transition temperature occurring between 450 and 470°C. A loss of both surface area and activity was associated with the onset of this phase change. Conversely, where the calcination temperature was too low, poorly crystalline manganese carbonate predominated on XRD analysis with the presence of this species being linked to poorly catalytically active species.

The importance of pH control during the precipitate ageing process has also been identified as crucial, more so during the first 200 minutes of ageing when stark increases of pH in the precipitation medium were observed where no pH control was in place. For the catalysts discussed later in this thesis, preparations involved the addition of small amounts of acidic

or alkaline species were added during the ageing process to maintain a constant pH = 8.3 in the reaction vessel.

The limitation of temperature variation during ageing has also been identified as being crucial to obtaining a reproducible catalyst preparation procedure. The catalysts produced and discussed later in this thesis involved the use of pre-heated reagents as well as superior insulation of the precipitation vessel in order to counter temperature fluctuations that may have been influencing catalyst structure. Some of these preparation differences were outlined in chapter 2.1.2.

In summary, a reproducible preparation method has been formulated which has been applied during the remainder of this thesis with the goal of synthesising catalysts able to consistently match the oxidising ability of the commercial catalyst Moleculite.

## References


[1] A. A. Mirzaei, PhD Thesis, Low T Carbon Monoxide Oxidation Catalysts, University of Liverpool, June (1998)

[2] A. Zavadski, S. Kireev. V. Mukhin, S. Tkachenko, V. Chebykin, V. Klushin, D. Teplyakov, Russ. J. Phys. Chem. 76, 12 (2002) 2072

[3] S. B. Kanungo, J. Catal. 58 (1979) 419

[4] P. Fortunato, A. Reller, H. R. Oswald, Solid State Ionics, 101-103 (1997) 85

[5] S. B. Kanungo, J. Catal. 58 (1979) 419

[6] G. Fierro, M. Lojacono, M. Inversi, G. Moretti, P. Porta, P. Lavecchia, in: Proceedings of the 10$^{th}$ International Congress on Catalysis, Budapest (1992)

[7] H. R. Oswald, W. Feitknecht and M. J Wampetich, Nature (London), 207 (1965) 72

[8] J. Frazer, J. Phys. Chem. 38 (1934) 735

[9] I. R. Leith and M. G. Howden, Appl. Catal. 37 (1988) 75

[10] G. J. Hutchings, A. A. Mirzaei, R. W. Joyner, M. R. H. Siddiqui, S. H. Taylor, Appl. Cat. A: Gen. 166 (1998) 143

[11] P. Porta, G. Moretti, M.Musicanti, A. Nardella, Sol. State Ionics, 63-65 (1993) 257

[12] P. A. Wright, S. Natarajan, J. M. Thomas, Chem. Mater. 4 (1992) 1053

[13] A. Lamb, W. C. Bray, J. C. W. Fraser, J. Ind. & Chem. Eng. 12 (1920) 213

[14] S. Veprek, D. L. Cocke, S. Kehl and H. R. Oswald, J. Catal. 100 (1986) 250

[15] V. Koleva, D. Stoilova, D. Mehandjiev, J. Sol. State Chem. 133 (1997) 416

[16] J. Janson, M. Skoglundh, E. Fridell, P. Thormahlen, Top. in Catal. Vol 16-17, 1-4 (2001) 385

[17] H. A. Jones, H. S. Taylor, J. Am. Chem. Soc. 43, 10 (1921) 2179

[18] W. E. Gardner, T. Ward, J. Chem. Soc. 857 (1939)

[19] G. C. Bond, Heterogeneous Catalysis: Principles and Applications, Oxford Chemistry Series, Clarendon Press (1974)

# Chapter 4 – Promotion of Hopcalite by Doping with Cations

In chapter 4, the effect of adding small quantities of other elements to the standard hopcalite preparation is investigated. 1, 2, 5, 10 and 20% of a metal M were added, relative to the quantity of copper used. The aim of this section of work was to identify any possible promoters of hopcalite catalysts. The results of the most successful experiments, namely those catalysts doped with cobalt are expanded upon in chapter 5.

Catalysts were produced using the standard preparation technique outlined in chapter 2. The ratio of Cu to element M was varied so that the overall reactant stoichiometry remained at 2:1, Mn : (Cu+M). The mixture was precipitated using 2M $Na_2CO_3$. A 30-minute ageing time was utilised in each case as these conditions had given rise to some most active species in a previous study. [1-3]

| Metal ion | Ionic radius (pm) |
|---|---|
| $Cu^{2+}$ | 87 |
| $Mn^{3+}$ | 75.3 |
| $Co^{2+}$ | 83.8 |
| $Co^{3+}$ | 71.8 |
| $Ag^{+}$ | 129 |
| $Ni^{2+}$ | 83 |
| $Fe^{3+}$ | 73.8 |

**Figure 4.1.1 – Table of ionic radii of dopant metal ions [4]**

Promoters are added to catalysts with the intention of imparting better activity, stabilisation or selectivity on the catalyst. They are usually added in quantities of less

than 10%, as they have been in this study with the hope they might take part in institial replacement, increasing the number of lattice defects present and therefore influencing the catalytic properties of the material.

When deciding on which additional elements to incorporate into the catalyst, the relative atomic radii of each metal ion was considered. The $Co^{3+}$ and $Ni^{2+}$ anions were similar in radius to the $Cu^{2+}$ ion that was being replaced. The premise was that these could be included without causing too much disruption to the hopcalite framework. The $Ag^{+}$ ion was much larger in ionic radius than the $Cu^{2+}$ ion so it was thought that incorporating this might result in a breakdown in the standard hopcalite structure and this in turn might lead to some interesting catalytic properties. Kanungo has previously shown that the addition of small quantities of copper to metal oxide systems, caused the metal ions to interchange in their coordination sites, resulting in an increase in metal-oxygen bond lengths of both oxides and an alteration in the exchange interaction. [5-7]

## 4.1 – Doping of Hopcalite using Nickel

A series of nickel-doped catalysts were prepared using standard co-precipitation methods. In each case, an ageing time of 30 minutes was employed. The catalyst precursor synthesised was dried and calcined as described in chapter 2.

### 4.1.1 – X-Ray Diffraction

X-ray diffraction studies were carried out on the nickel doped hopcalite catalysts using an Enraf Nonius diffractometer in a method outlined in chapter 2. The nickel-doped catalyst precursors all displayed very similar XRD patterns, however it was possible to observe a promotion of intensity of CuO peak at 31.53° in the 1% Ni doped system compared to the un-doped precursor. This peak was observed to decrease in intensity as

greater quantities of nickel were added. Subtle differences could be observed between the XRD pattern of the non-doped hopcalite precursor and those of the Ni doped systems, mainly in terms of a slight increase in crystallinity in the nickel-doped species. The un-doped catalyst displayed the most amorphous XRD pattern when compared to the nickel-doped catalyst precursors. However, in the 20% Ni doped catalyst, some of the amorphous character observed in the hopcalite precursor was seen to return. Perhaps the relatively high catalytic activity of this catalyst, compared to the other nickel-doped systems, can be attributed to the amorphous nature of this material.

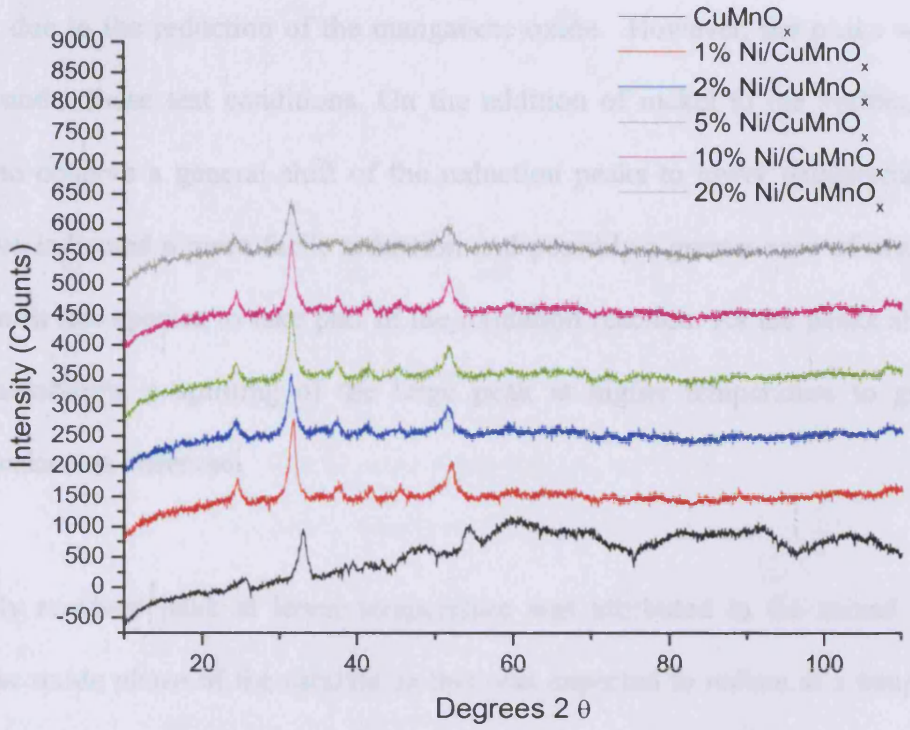


**Figure 4.2.1 – X-ray diffraction data of Ni doped $CuMnO_x$ as a function of % Ni doping (Precursors dried at 100°C for 16h in air)**

## 4.1.2 - Temperature Programmed Reduction

A temperature programmed reduction analysis of the Ni doped systems, calcined for 2h at 415°C, was carried out using a reducing gas mixture of 10%$H_2$/Ar. The reducing gas

mixture was flowed over the catalyst bed at 50ml/min while the temperature of the sample was ramped from 25°C, through to 500°C at 10°C/min. A more detailed explanation of the TPR procedure is given in chapter 2.

The standard TPR profile of the 30 minute aged hopcalite displayed a 3-peak system. The peak at the lower temperature with a small shoulder peak could be attributed to the reduction of $Cu^{2+}$ to $Cu^0$ (via $Cu^+$), the larger peak at higher temperature was therefore assigned to the reduction of a manganese oxide species. It was possible that the reduction of the $CuMn_2O_4$ component of the catalyst was also contained coincident with the peak, due to the reduction of the manganese oxide. However, the peaks were not resolved under these test conditions. On the addition of nickel to the system, it was possible to observe a general shift of the reduction peaks to lower temperature. This might have indicated a more facile reduction and possibly a greater ease of availability of oxygen in this species to take part in the oxidation reaction. As the peaks shifted to lower temperature, a splitting of the large peak at higher temperature to give two smaller peaks was observed.

The newly resolved peak at lower temperature was attributed to the mixed copper-manganese oxide phase of the catalyst as this was expected to reduce at a temperature intermediate to those of the individual copper and manganese oxides. As the Ni:Cu ratio was increased in the catalyst, it was possible to see a reduction in size of the lowest temperature peak, as the quantity copper oxide in the system had decreased. As greater quantities of nickel were incorporated in the system, it was possible to see the emergence of a peak that could be attributed to the reduction of a nickel oxide species. This peak occurred at higher temperature, in the region of 293°C. This peak was first

observed in the 5% Ni doped system and was seen to increase in size as larger Ni:Cu ratios were used.

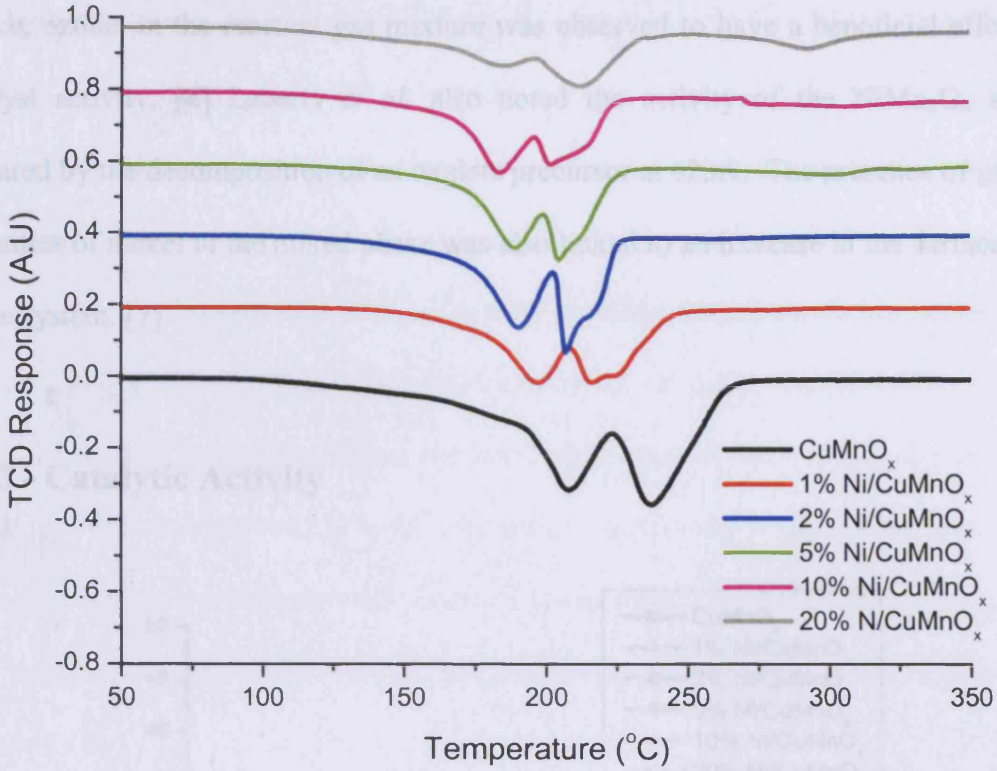


**Figure 4.1.2.1 - TPR profiles of nickel-doped $CuMnO_x$ catalysts calcined at 415°C for 2h as a function of % cobalt doping**

In this case, the lowering of the reduction temperature of the copper oxide with increasing nickel content did not correlate with the CO oxidation activity with no enhancement of activity being observed. However, the presence of NiO in the catalyst, where a Ni:Cu ratio of 20% was utilised, did have the effect of increasing catalytic activity. It may not be the case here that nickel was promoting the activity of the hopcalite catalyst, but that the presence of nickel in the catalytic system (in larger amounts) caused the formation of nickel oxide which was acting as a catalyst in its own right; thereby enhancing the total catalytic activity for CO oxidation. Other authors have discussed the catalytic activity of the $NiMn_2O_4$ spinel for CO oxidation where the spinel

was prepared from carbonate precursors. The activity was attributed to the metal cations being in positions with an octahedral coordination. Activity of this system at room temperature was low, around 15% conversion, however the presence of an oxygen source, ozone, in the reactant gas mixture was observed to have a beneficial effect on catalyst activity. [6] Laberty *et al.* also noted the activity of the $NiMn_2O_4$ spinel prepared by the decomposition of an oxalate precursor at 623K. The presence of greater quantities of nickel in the mixed phase was also linked to an increase in the surface area of the system. [7]

## 4.1.3 - Catalytic Activity

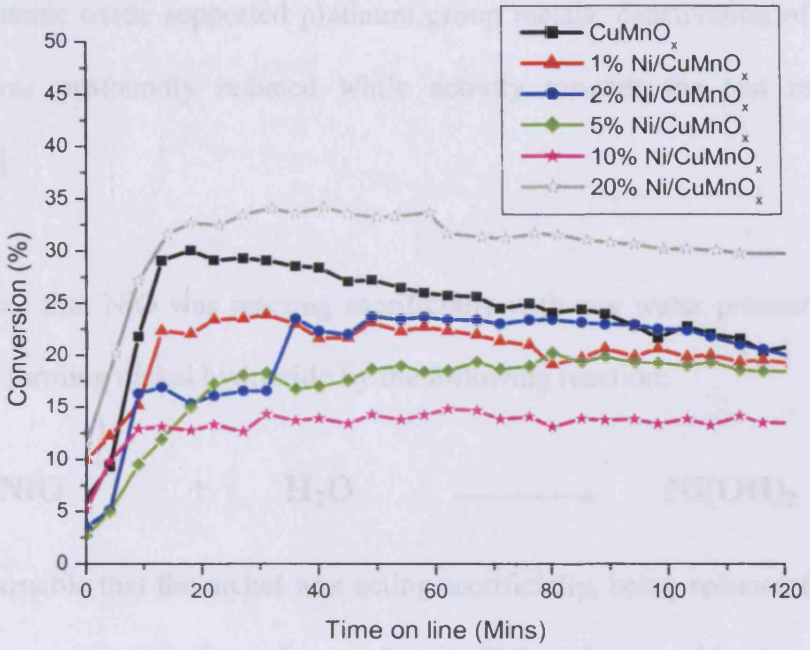


**Figure 4.1.3.1 – CO oxidation activity a series of Ni doped $CuMnO_x$ catalysts aged for 30 minutes**

The nickel-doped hopcalite catalysts were tested for their activity against the 5000ppm CO to air test mixture. The results of the catalytic testing are shown in figure 4.1.1. It was apparent that the addition of nickel in small quantities to the standard hopcalite

formulation had little positive effect on the oxidising ability of the catalyst towards carbon monoxide. Only in the case of the 20% doped example was an increase in activity over the standard hopcalite example observed. The 20% nickel doped hopcalite also displayed a very stable level of activity as opposed to the $CuMnO_x$ catalyst which exhibited the standard deactivation profile expected for hopcalite with decreased activity being linked to increased time on-line. It was interesting to note that all the nickel-doped samples appeared to be more stable in terms of activity vs. time on line than the standard hopcalite. It was, of course, possible that although not acting as a promoter of activity, the nickel was contributing to stabilising the hopcalite catalyst during the oxidation reaction. Nickel has previously been reported to stabilise catalytic systems for the oxidation of CO to $CO_2$ by acting sacrificially. When added to systems containing stannic oxide supported platinum group metals, deactivation of the system with time was profoundly reduced while activity towards the test reaction was increased. [8]

It was possible that NiO was reacting sacrificially with any water present in the feed gas, possibly forming nickel hydroxide by the following reaction:

$$NiO + H_2O \longrightarrow Ni(OH)_2$$

It was also possible that the nickel was acting sacrificially, being reduced from $Ni^{2+}$ to $Ni^{3+}$ thereby preventing the hopcalite catalyst itself from being oxidised to an inactive state. [9]

When the CO oxidation activity was adjusted to take into account the quantity of CO oxidised per square metre of catalyst in the period of a second, the standard hopcalite and the 20% Ni doped catalysts displayed similar start-up activity profiles. The activity

of the Ni doped catalyst remained high during the early stage of the lifetime of the catalyst, i.e. the stage when activity is most important for use in commercial systems such as breathing apparatus. Again, it was interesting to note the possible stabilising influence that the presence of the nickel dopant had on the rate of CO conversion of the catalysts. Zero deactivation was observed within the first two hours on stream for nearly all the systems containing nickel in their formulation, the one exception was the 20% Ni doped catalyst. This was in direct contrast to the results displayed for standard hopcalite catalysts in chapter 3, where considerable depreciation was observed during the test-period when the non-optimised preparation method was used.

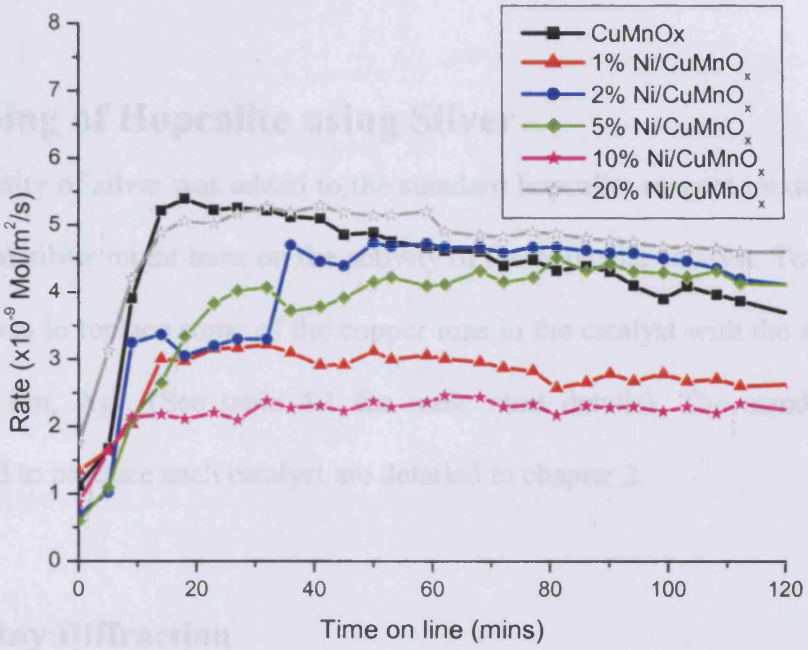


**Figure 4.1.3.2 – Surface area adjusted reaction rates for CO oxidation over Ni doped $CuMnO_x$ catalysts aged for 30 minutes**

In many instances, the presence of nickel in the catalyst had the effect of increasing the surface area over that of the standard hopcalite. However, the increases observed in this study brought on by increasing the nickel content were not as great as those observed by Laberty (>200m$^2$/g) where the nickel-manganese mixed oxides were prepared by a

decomposition of the mixed metal oxalates rather than the decomposition of the metal carbonates. [7]

| Catalytic System | Surface area ($m^2/g$) | C - value | Ni/Cu ratio |
|---|---|---|---|
| $CuMnO_x$ | 87 | 85.02 | 0.000 |
| 1% $Ni/CuMnO_x$ | 116 | 79.02 | 0.013 |
| 2% $Ni/CuMnO_x$ | 78 | 86.89 | 0.028 |
| 5% $Ni/CuMnO_x$ | 70 | 81.93 | 0.071 |
| 10% $Ni/CuMnO_x$ | 94 | 99.03 | 0.101 |
| 20% $Ni/CuMnO_x$ | 101 | 102.73 | 0.205 |

**Table 4.1.3.3 – BET surface area and Atomic Absorption data**

## 4.2 – Doping of Hopcalite using Silver

A small quantity of silver was added to the standard hopcalite reagent mixture to probe any effect that silver might have on the activity of the hopcalite catalyst. The aim of the experiment was to replace some of the copper ions in the catalyst with the substantially larger silver ion, $Ag^+$. (See table 4.1 for ionic radii details). The standard reagent mixtures used to produce each catalyst are detailed in chapter 2.

### 4.2.1 – X-Ray Diffraction

X-ray diffraction studies were carried out on the silver-doped hopcalite catalysts using an Enraf Nonius diffractometer in a method outlined in chapter 2.

The XRD patterns obtained for the silver-doped catalysts were all very similar in their composition. All the samples tested were amorphous in nature after drying at 100°C for 16h, the main phases present being traces of manganese and copper carbonate. On

calcination of the precursors at 415°C for 2h in air, a further loss of crystallinity of the copper and manganese components was observed on XRD analysis. It was not possible to detect any silver oxide in the samples doped to less than 5% silver, this might have been due to any $Ag_2O$ formed being finely dispersed through the catalyst. This was a feature of doping manganese oxide catalysts with silver that was also observed by Lin *et al.* [10]

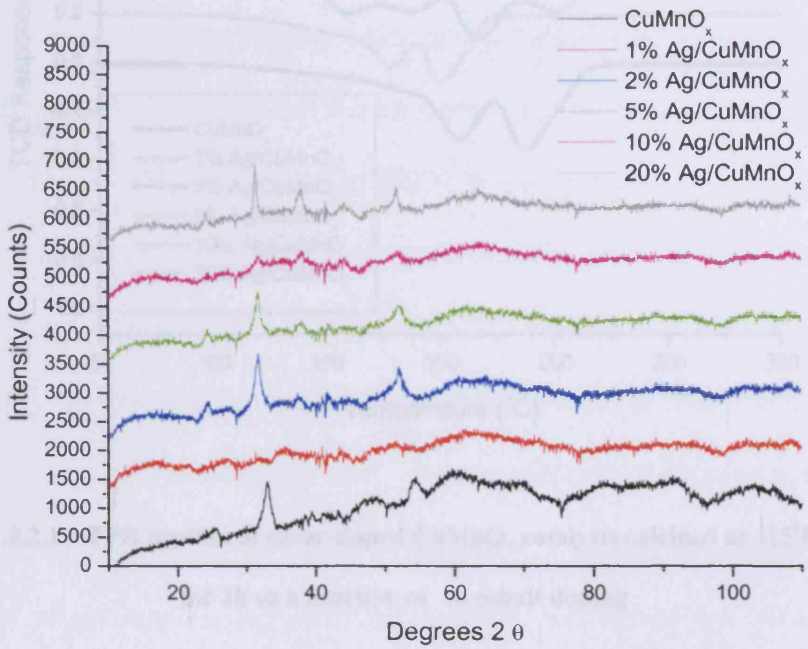


**Figure 4.2.1.1 – X ray diffraction patterns of Ag doped $CuMnO_x$ precursors**

Where larger Ag:Cu ratios were used, the calcination of the precursor gave rise to the emergence of a crystalline phase on XRD analysis that were due to presence of $Ag_2O$ in combination with the amorphous manganese and copper oxide phases observed previously.

## 4.2.2 - Temperature Programmed Reduction

Temperature programmed reduction analyses of the silver-doped systems were carried out using the standard TPR procedure outlined in chapter 2.

Addition of silver to hopcalite provided some interesting results on TPR analysis of the catalysts. It was possible to observe a general shift to lower temperature of the TPR peaks due to the reduction of $CuO_x$ and $MnO_x$.

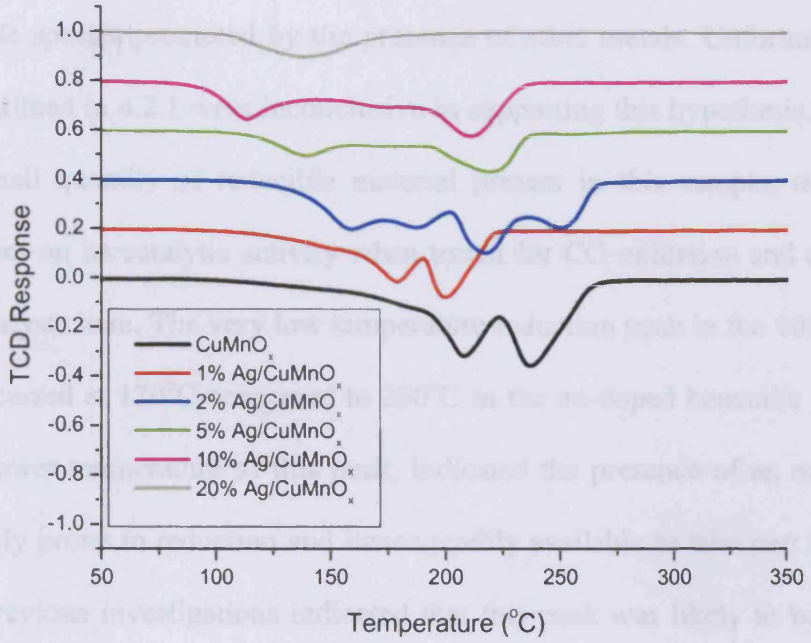


**4.2.2.1 – TPR profiles of silver-doped $CuMnO_x$ catalysts calcined at 415°C for 2h as a function of % cobalt doping**

The 2% Ag doped species exhibited a very different profile to those seen up to this point in the study. Four distinct reduction peaks were observed due to the presence of four different types of oxide present in the sample. The 5, 10 and 20% doped catalysts offered different features again on TPR analysis. The shift of reduction peaks to lower temperature on increasing the silver content from 2 > 5 > 10 continued, although with this decrease in reduction temperature came a general decrease in the total content of reducible material (e.g. oxide) in the catalyst; as calculated by the quantity of $H_2$ consumed during the experiment.

The 20% doped catalyst was interesting as it contained very little reducible material at all. When compared to the other samples tested in this study, its TPR profile was not standard, having only one visible reduction peak occurring at 140°C. It was probable that this catalyst was not an $Ag/CuMnO_x$ catalyst due to the nature of this profile, rather a single oxide species promoted by the presence of other metals. Unfortunately, XRD studies as outlined in 4.2.1 were inconclusive in supporting this hypothesis. Despite the relatively small quantity of reducible material present in this sample, there was no negative effect on its catalytic activity when tested for CO oxidation and compared to the other catalysts here. The very low temperature reduction peak in the 10% Ag doped example, occurred at 120°C compared to 200°C in the un-doped hopcalite By its very nature, the lower temperature of this peak, indicated the presence of an oxide species that was easily prone to reduction and hence readily available to take part in oxidation processes. Previous investigations indicated that this peak was likely to be due to the reduction of copper oxide, occurring at a lower temperature than expected due to the promotion of its reduction by the presence of silver. This ease of availability of this oxide species might explain the excellent start-up activity of the 10% Ag doped hopcalite observed in 4.2.3.

### 4.2.3 - Catalytic Activity

In an opposite mode of behaviour to that observed when doping with nickel, when silver was added to the standard formulation for hopcalite synthesis, it appeared to have a beneficial effect on final catalyst activity in many of the doping strengths investigated. The addition of 1, 2, 5 and 10 % silver all resulted in an increase of CO oxidation against the test mixture when compared to the standard 30-minute aged $CuMnO_x$ sample. In each case, the initial start up activity was quicker than in hopcalite.

When stability with time on line was considered, the catalysts did not appear to be as stable as those produced during the nickel doping experiments. The deactivation profiles of the majority of the silver-doped species were similar to that observed for the $CuMnO_x$ catalyst. The most active silver-doped catalyst was the 10% doped sample, where the early catalytic activity reached over 50%. This was one of the highest activities observed during the study of promoters of hopcalite catalysts to this point.

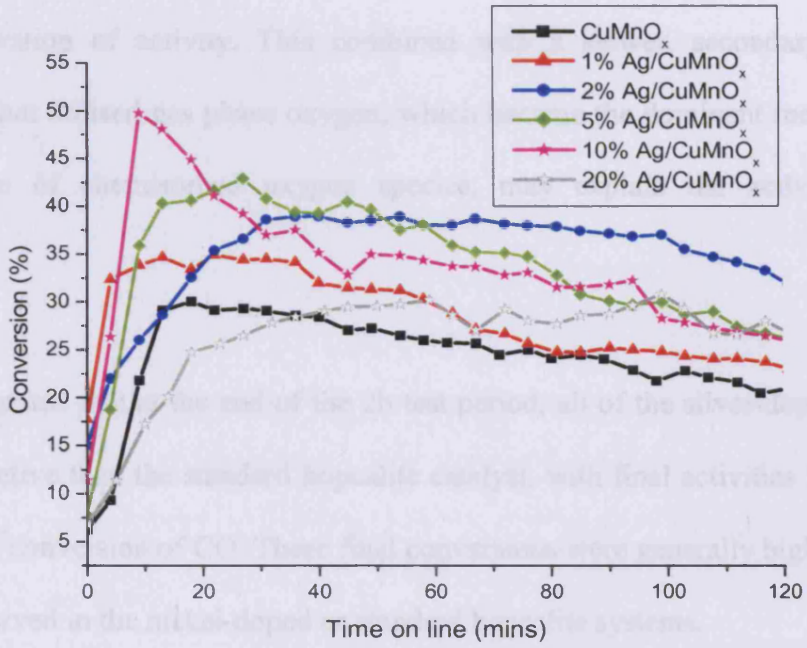


**Figure 4.2.3.1 – CO oxidation activity of silver-doped $CuMnO_x$ catalysts aged for 30 minutes as a function of percentage silver doping**

The 10% Ag doped catalyst deactivated to a large degree over the 2h test period, with activity falling below 30% at the final measurement. Lin *et al.* have also reported that silver oxide in quantities of up to 5% can promote reduction in manganese oxides and increase activity towards CO oxidation. However, reaction temperatures used in their study were in the region of 50°C. It should also be noted that where greater quantities of silver were used, reduction and therefore activity levels were inhibited. [10]

The results of silver doping were encouraging when searching for catalysts active early on in usage rather than those whose activity builds up to a maximum level after some time on line. Both properties could find use in commercial systems.

It was possible that the high initial start-up activity of the silver-doped catalyst might have been linked to two oxidation processes occurring on the catalyst. The start-up activity may have been fuelled by chemisorbed oxygen, which when used up resulted in rapid deactivation of activity. This combined with a slower, secondary oxidation mechanism that utilised gas phase oxygen; which became the dominant mechanism on the depletion of chemisorbed oxygen species, may explain the activity profiles observed.

It should be noted that at the end of the 2h test period, all of the silver-doped catalysts were more active than the standard hopcalite catalyst, with final activities in the range of 25 to 35% conversion of CO. These final conversions were generally higher than any of those observed in the nickel-doped or standard hopcalite systems.

Silver, supported on reducible metal oxides has been well investigated in recent years. Imamura identified a 70:30, Mn:Ag mixed oxide as being an excellent CO oxidation catalyst, with the mixed oxide being considerably more active than the individual components. [11-12] Gardner, however, reported that low loaded (Ag<1%) silver manganese oxide was highly active at very low temperatures for the oxidation of carbon monoxide. [13] Work by Tanielyan and Augustine confirmed the promotional effect of silver towards metal axtivity over metal oxides where the addition of ~10% Ag to cobalt oxide supported on Alumina and synthesised by Sol-gel impregnation, produced highly

active species at low temperature where an excess of $O_2$ was present. [14] An increased silver loading resulted in an increased activity towards the test reaction.

On analysing the surface area of the silver-doped catalysts, there was a marked difference in the values for the silver-doped catalysts compared to the hopcalite sample. Each of the silver-doped samples displayed higher and sometimes significantly higher BET 5 point surface areas than the un-doped sample. A trend appeared to be present that as the silver content of the doped catalyst is increased, surface area tended to decrease back towards the value of the un-doped sample.

| Catalytic System | Catalyst surface area ($m^2/g$) | C - value | Ag/Cu ratio |
|---|---|---|---|
| **$CuMnO_x$** | 87 | 82.05 | 0.001 |
| **1% $Ag/CuMnO_x$** | 107 | 81.23 | 0.010 |
| **2% $Ag/CuMnO_x$** | 98 | 89.08 | 0.021 |
| **5% $Ag/CuMnO_x$** | 94 | 63.32 | 0.048 |
| **10% $Ag/CuMnO_x$** | 89 | 59.65 | 0.098 |
| **20% $Ag/CuMnO_x$** | 92 | 63.98 | 0.210 |

**Table 4.2.3.2 – BET surface area data and Atomic Absorption data**

On synthesis and analysis of a 50% doped silver catalyst, this trend continued, with a surface area of $54m^2/g$ being presented. On analysis of a 100% doped catalyst, i.e. no copper being present in a $CoMnO_x$ system, the surface area measured was even lower at $24m^2/g$. The corresponding CO oxidation activities of the 50 and 100% doped catalysts were very low (~15%). This was attributed to the significant lowering of surface area observed in these catalysts when compared to the more active, higher surface area (and low percentage silver doped) samples. Gulari *et al.* have reported silver oxide, prepared by the decomposition of the metal carbonate at 500°C, as possessing a low surface area

and to be composed of large silver crystallites (~300A), which were inactive towards CO oxidation. [15]

On adjusting the activity of the silver-doped catalysts to account for differences in surface area, the 10% silver doped catalyst still exhibited a very good start-up activity, closely followed by the 5, 1 and 2% doped species, all of which displayed a higher rate of CO conversion than the $CuMnO_x$ catalyst. The majority of the Ag doped species displayed a decrease in CO conversion rate with time on-line, in the same way as hopcalite has tended to become less active with increasing time on-line. The rate of conversion displayed by the 10% Ag doped $CuMnO_x$ catalyst was higher than both that displayed by the standard hopcalite example and that of the most active nickel-doped hopcalite species.

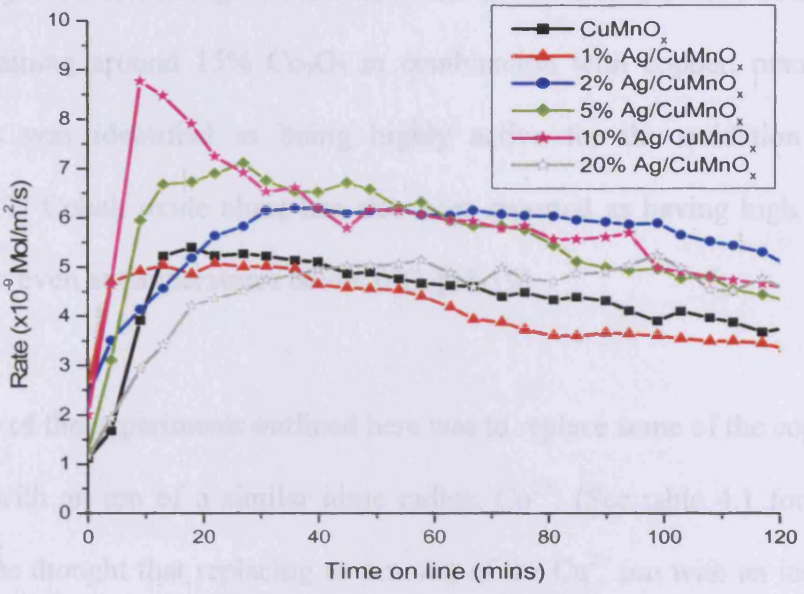


**Figure 4.2.3.3 – Surface area adjusted reaction rates over Ag /$CuMnO_x$ catalysts**

These factors lead to the conclusion that the addition of silver to the standard hopcalite formulation might be beneficial to conversion rates. It was not possible to observe the same stabilising property when doping with silver as was evident with nickel. In part,

this might have been due to the chemisorbed $O_2$ present on the silver-doped catalyst surface being quickly consumed during the early minutes on line. Thus, when the surface $O_2$ was fully consumed a drop in activity was observed, corresponding with a change to a slower mechanism of oxidation in which $O_2$ was adsorbed on to the catalyst surface from the gas phase before being available to react. This hypothesis would have been consistent with the observations of Gulari for catalysts prepared by a similar method. [15]

## 4.3 – Doping of Hopcalite using Cobalt

Small quantities of cobalt were added to the standard hopcalite reagent mixture in the form of cobalt (II) nitrate with the aim of probing any effect that it may have on the activity of the hopcalite catalyst. Lamb and Bray observed some interesting properties of hopcalite systems containing amounts of cobalt oxides during a study of the 1920s. A catalyst containing around 15% $Co_2O_3$ in combination with copper, manganese and silver oxides was identified as being highly active for the oxidation of carbon monoxide. [17] Cobalt oxide alone has also been reported as having high activity for CO oxidation, even at temperatures below 0°C. [18-19]

The principle of the experiments outlined here was to replace some of the copper ions in the catalyst with an ion of a similar ionic radius, $Co^{2+}$. (See table 4.1 for ionic radii details). It was thought that replacing an amount of the $Cu^{2+}$ ion with an ion of similar ionic size but possessing a different charge might give rise to some interesting properties by creating defects in the lattice structure of the catalyst. The standard reagent mixtures used to produce each catalyst are detailed in chapter 2.

### 4.3.1 - X-Ray Diffraction

X-ray diffraction studies were carried out on the cobalt-doped hopcalite catalysts using an Enraf Nonius diffractometer in a method outlined in chapter 2. All the patterns produced were symptomatic of a material that was amorphous to XRD or microcrystalline in nature. It was not possible to detect any emergent peaks due to the the presence of cobalt oxide as the ratio of cobalt to copper was increased in the starting reagent mixture. However, the presence of cobalt in the mixture was proved by AAS studies that are outlined in table 4.3.3.3.

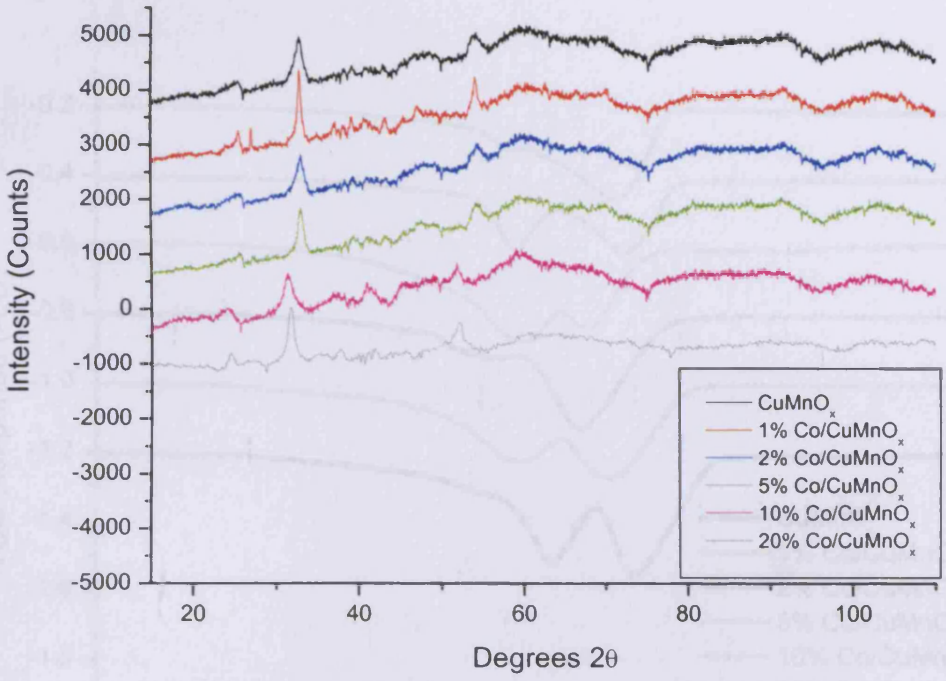


**Figure 4.3.1.1 – X-ray diffraction data of cobalt-doped $CuMnO_x$ as a function of % Co doping**

**(Precursors dried at 100°C for 16h in air)**

### 4.3.2 - Temperature Programmed Reduction

A temperature programmed reduction analysis of the copper-doped systems was carried out using the standard method. Each of the cobalt-doped hopcalite catalysts produced

similar patterns on TPR analysis; in the sense that two major reduction peaks were present in each case. The lowest temperature peak was attributed to the reduction of CuO, a peak that was generally observed to decrease in size as the Co:Cu ratio was increased. A shift in the reduction temperature of CuO compared to that in hopcalite was recorded for the 1 and 2% cobalt doped samples. This shift to lower temperature was not as pronounced as that observed during doping with either nickel or silver. As the Co:Cu composition was increased to 5% and upwards, the CuO peak was seen to move towards higher temperature, with the positions of both major peaks in this sample being similar to those in hopcalite.

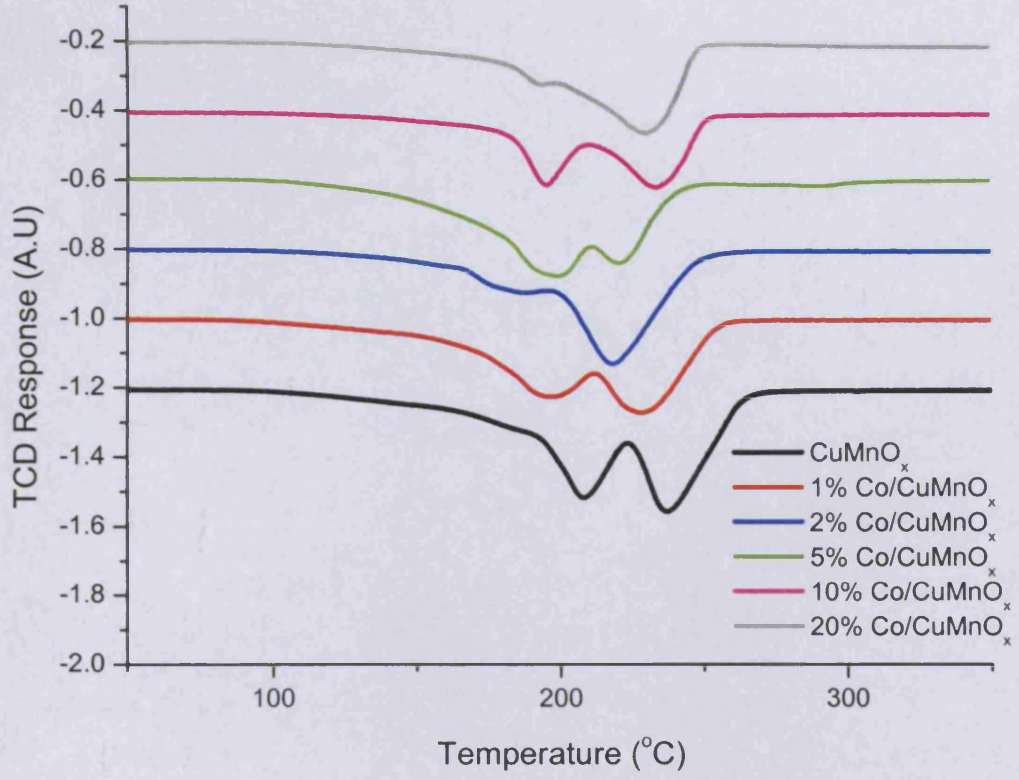


**4.3.2.1 – TPR profiles of cobalt-doped $CuMnO_x$ catalysts calcined at 415°C for 2h as a function of % cobalt doping**

It was possible that the presence of small quantities of cobalt in the catalyst system served to facilitate the reduction of the copper species from Cu (II) to Cu (I). As the proportion of cobalt relative to copper was increased, the TPR profiles of the catalysts

produced did not show huge variation from each other or that of hopcalite as far as general content was concerned. This was perhaps a benefit of including an ion of similar ionic radius to copper within the catalyst, resulting in a facile replacement of copper ions. Therefore huge distortions in the catalyst structure would not have been expected, hence the similar TPR patterns obtained.

### 4.3.3 - Catalytic Activity

Doping the hopcalite catalyst with cobalt provided some very interesting results. Not only was an increase is the CO oxidation ability of the catalyst observed, but for the first time, the dopant seemed to result in an increased stability in parallel. The start-up activity of the 1, 2% Co doped and the undoped catalyst were very similar. The results of the 1% Co doped catalyst were perhaps most impressive as the level of initial activity continued to rise for the first 20 minutes on-line before levelling out at the 45% conversion mark; a point at which the activity remained at throughout the 2h test period. Virtually zero deactivation was observed throughout the test period, any deviations might be attributed to variations in temperature and/or gas flow rates.

Cobalt oxide has been shown to be an excellent catalytic species when used in conjunction with precious metals such as Pt [20] or Au[21]. In these studies, the authors propose that CO adsorbed on to the Pt or Au sites, while the cobalt oxide supplied the oxygen needed to convert the CO to $CO_2$. It was possible in our study that the small quantities of cobalt were providing surface adsorbed oxygen for the CO oxidation reaction. However, the consumption of surface $O_2$ might have occurred leaving the surface in a reduced state. As oxygen was present in the gas phase during the experiments described in this chapter, it was possible that the cobalt was continually re-oxidising the catalyst surface throughout the test period leading to minimal deactivation

being observed. Jansson *et al.* have reported similar findings to support this theory. [22] However, they observed that where gas phase oxygen was not supplied during the reaction, the surface cobalt sites became deeply reduced, drastically reducing the activity of the system. Many of the deactivated catalysts showed the presence of carbonate species on the surface, which would have been consistent with activity loss through the blocking of active sites.

The 10% cobalt-doped hopcalite also displayed a very stable performance throughout the test period, however the start-up activity of this catalyst was poor in comparison with the others tested. When comparing the performance of cobalt-doped catalysts to those doped with Ag or Ni, the cobalt-doped samples appeared to be more desirable both in terms of relative activity as well as in terms of stability with time on-line.

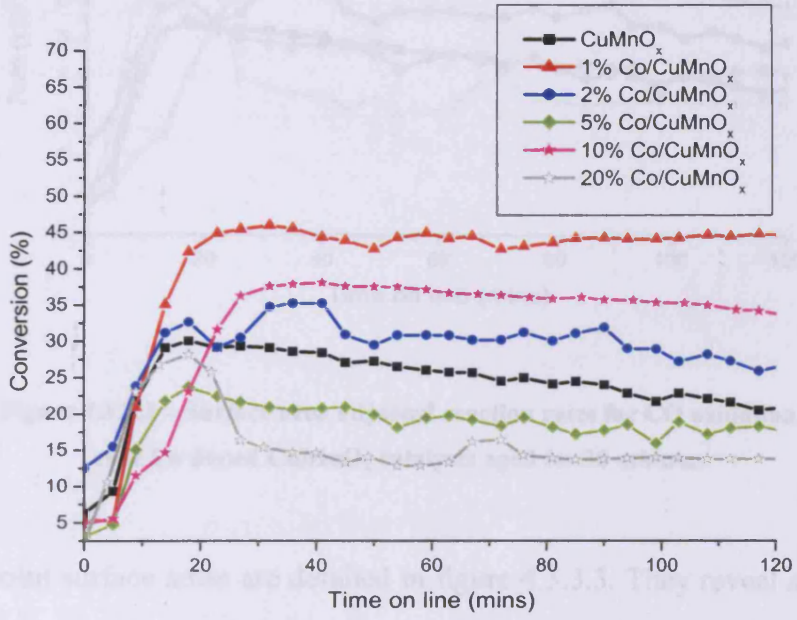


**Figure 4.3.3.1 – CO oxidation activity a series of Co doped $CuMnO_x$ catalysts aged for 30 minutes**

When activities were adjusted to take into account differences in surface areas, four out of the five cobalt-doped catalysts displayed a comparable or higher rate of CO conversion than the hopcalite catalyst. The 1% Co doped catalyst offered the highest

When activities were adjusted to take into account differences in surface areas, four out of the five cobalt-doped catalysts displayed a comparable or higher rate of CO conversion than the hopcalite catalyst. The 1% Co doped catalyst offered the highest rate of CO conversion of the cobalt doped catalysts tested. An additional positive feature was the encouragingly stable conversion rate of this species. The rate of CO conversion of this catalyst was the highest displayed by any of the catalyst systems reported up to this point and significantly higher than that of hopcalite.

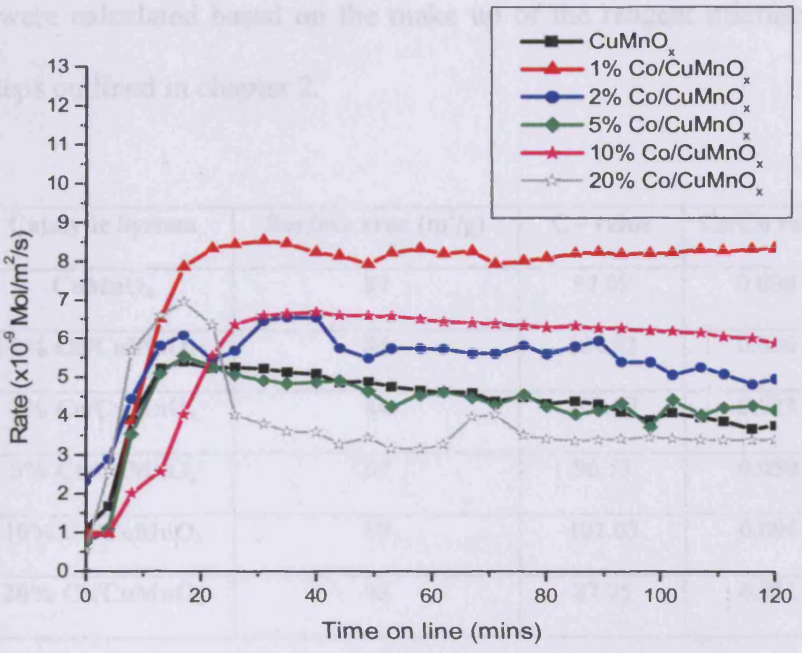


**Figure 4.3.3.2 – Surface area adjusted reaction rates for CO oxidation over Co doped $CuMnO_x$ catalysts aged for 30 minutes**

The BET 5-point surface areas are detailed in figure 4.3.3.3. They reveal all the cobalt-doped catalysts to have surface areas of similar magnitude, in the region of 63-89$m^2$/g. This range showed the cobalt-doped catalysts to generally have lower surface areas compared to that of the standard hopcalite catalyst (87$m^2$/g). Wright *et al.* observed cobalt to have a positive effect on surface area in 1:1:1 (Co:Cu:Mn) catalyst calcined at 500°C, compared to 39$m^2$/g for the $CuMn_2O_4$ prepared at the same temperature. [23]

temperature and calcination temperature. The surface areas reported here for cobalt-containing hopcalites were all significantly higher than those reported for hopcalite catalysts in the study by Mirzaei, where typically the catalyst surface area was much lower in the region of $25m^2/g$. [3,16]

It was not possible to correlate any differences in surface area measurements with the variations in cobalt to copper ratios used. The results of the AAS experiments proved the presence of cobalt in each of the samples at levels with a high degree of accuracy to those which were calculated based on the make up of the reagent mixture during the preparation steps outlined in chapter 2.

| Catalytic System | Surface area ($m^2/g$) | C - value | Co/Cu ratio |
|---|---|---|---|
| $CuMnO_x$ | 87 | 82.09 | 0.000 |
| 1% $Co/CuMnO_x$ | 84 | 104.93 | 0.010 |
| 2% $Co/CuMnO_x$ | 84 | 109.32 | 0.023 |
| 5% $Co/CuMnO_x$ | 67 | 96.53 | 0.050 |
| 10% $Co/CuMnO_x$ | 89 | 101.03 | 0.094 |
| 20% $Co/CuMnO_x$ | 63 | 87.75 | 0.211 |

**Table 4.3.3.3 – BET surface area data and Atomic Absorption data**

## 4.4 - Doping of Hopcalite using Iron

A small quantity of iron was added to the standard hopcalite reagent mixture to probe the effect that iron had on the activity of the hopcalite catalyst. The aim of the experiment was to replace some of the copper ions in the catalyst with the smaller $Fe^{3+}$ ion (see table 4.1 for ionic radii details). The source of iron used was $Fe(NO_3)_2.\ xH_2O$. The standard reagent mixtures used to produce each catalyst are detailed in chapter 2.

### 4.4.1 -X-Ray Diffraction

X-ray diffraction studies were carried out on the nickel-doped hopcalite catalysts using an Enraf Nonius diffractometer in a method outlined in chapter 2.

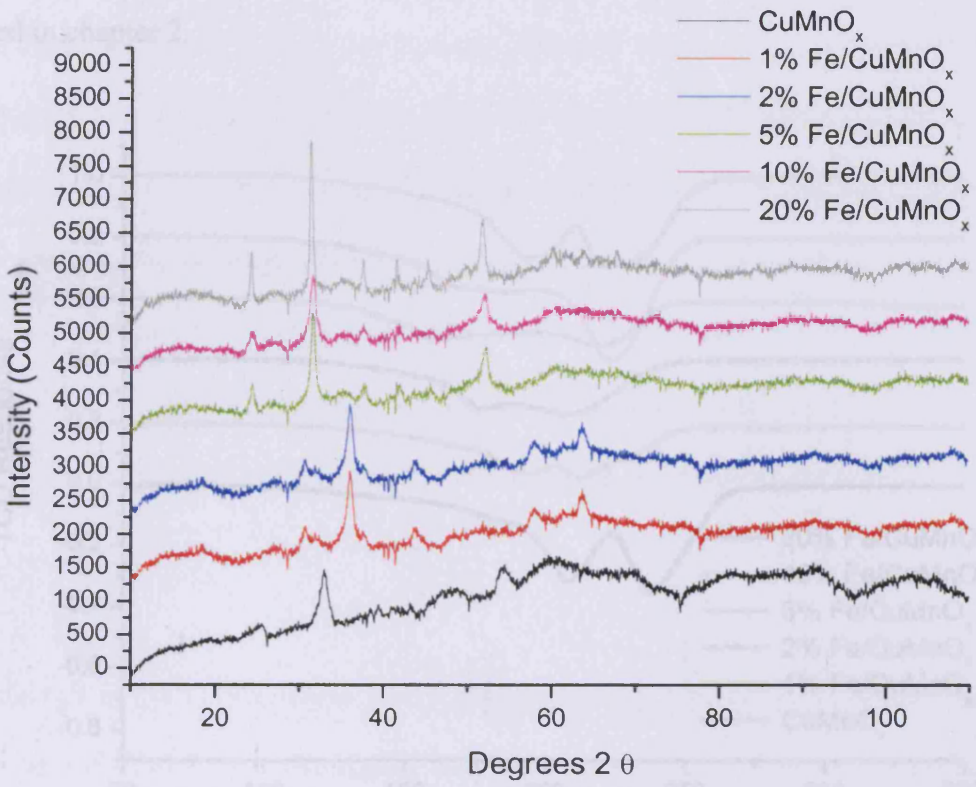


**Figure 4.4.1.1 – X ray diffraction patterns of Fe doped $CuMnO_x$**

Some obvious differences were present between the precursors on XRD analysis. The low iron content precursors generally exhibited an amorphous XRD pattern, similar to that of the hopcalite precursor. Iron was found to be present in these samples on AAS analysis, so it was likely that the iron oxide particles were micro-crystalline and therefore below the detection limit of the XRD technique. On increasing the Fe content from 5% through to 20% relative to the quantity of copper, an increase in the crystallinity of the precursors was observed. It was possible that the presence of

increasing quantities of iron in the catalyst was responsible for this enhancement in crystallinty as compared to the lower and undoped samples

## 4.4.2 - Temperature Programmed Reduction

A temperature programmed reduction analysis of the iron-doped systems was carried as detailed in chapter 2.

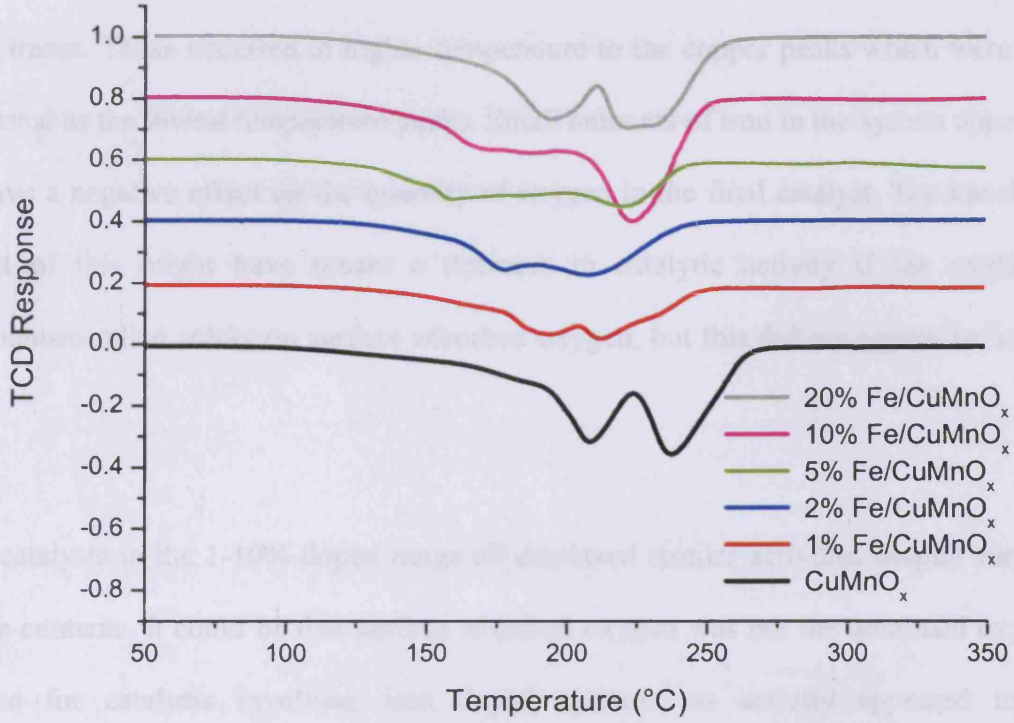


**Figure 4.4.3.1- TPR profiles of iron-doped $CuMnO_x$ catalysts calcined at 415°C for 2h as a function of % cobalt doping**

The TPR profile of the un-doped hopcalite catalyst displayed two major peaks, one with a shoulder to lower temperature. The peak occurring at 204°C and its corresponding shoulder can be attributed to the 2-stage reduction of CuO to Cu ($Cu^{2+}$ to $Cu^{+}$ and $Cu^{+}$ to $Cu^{0}$). As quantities of iron were introduced to the catalyst, the TPR profiles changed shape. It was possible to observe a general shift in peak position to lower temperature, indicating that with the incorporation of iron in to the catalyst, the oxide species present

were reduced more easily. This fact meant that the reduction of the iron-containing species would require less energy and potentially that the oxygen associated with this species might be readily available to take part in a reaction with CO. The incorporation of iron in the system coincided with an apparent decrease in the quantity of reducible material present in the catalysts. This was evident by analysing the area of the TPR peaks. The presence of iron in the system, although connected to a decrease in the quantity of oxide species present also resulted in the presence of additional peaks in the TPR traces. These occurred at higher temperature to the copper peaks which were still observed as the lowest temperature peaks. Small amounts of iron in the system appeared to have a negative effect on the quantity of oxygen in the final catalyst. The knock on effect of this might have meant a decrease in catalytic activity if the oxidation mechanism relied solely on surface adsorbed oxygen, but this did not appear to be the case.

The catalysts in the 1-10% doped range all displayed similar activities despite varying oxide contents. It could be that surface adsorbed oxygen was not the dominant oxygen source for catalysis involving iron doped systems, as activity appeared to be independent of total oxide content.

When larger quantities of iron were present in the catalyst (10 and 20%), the effect was an apparent shift of the copper oxide peaks back to higher temperature. This might indicate that although small quantities of iron were a beneficial additive to the hopcalite system in terms of lowering the reduction temperatures of the copper and manganese species, thereby making the provision of oxygen for the CO oxidation reaction more facile, larger quantities of iron might have an inhibiting, negative effect. It was, perhaps, possible to link the TPR profiles of the iron doped catalysts to the activity data shown in

chapter 4.4.3 as well as to the XRD profiles detailed in chapter 4.4.1.1. The iron-doped systems which contained lower quantities of the dopant metal (1, 2 and 5%) displayed a more superior surface area adjusted rate of CO conversion to any of the other iron-doped systems or the un-doped hopcalite catalyst.

## 4.4.3 – Catalytic Activity

Four of the iron-doped catalysts displayed a similar or enhanced start-up activity to the $CuMnO_x$ catalyst. The 2% Fe doped catalyst displayed the best start-up activity out of the Fe doped catalyst set. The 1,2,5 and 10% doped catalysts all were more active for CO oxidation than hopcalite. In a similar mode of behaviour to that observed when doping with cobalt, these four iron-doped catalysts displayed a very stable activation profile over the 2h test period.

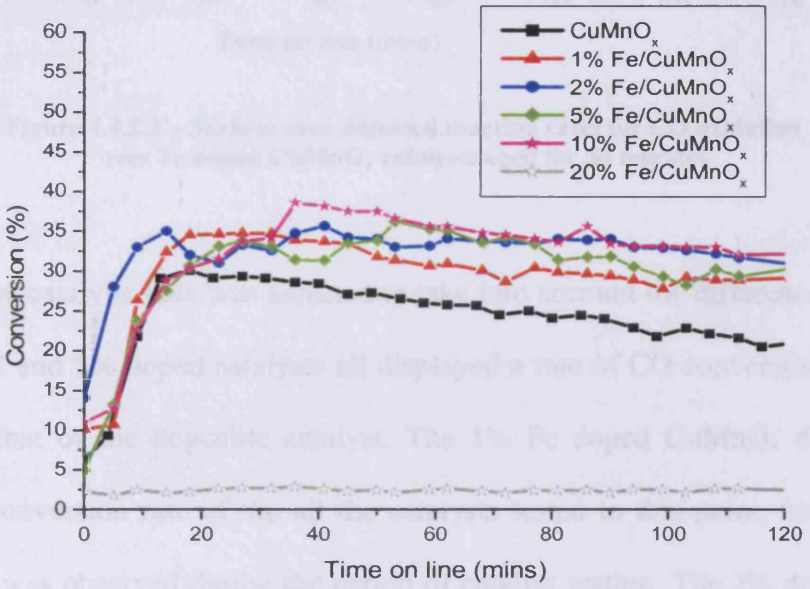


**Figure 4.4.2.1 – CO oxidation activity of iron-doped $CuMnO_x$ catalysts aged for 30 minutes**

The 20% Fe doped hopcalite catalyst was a case apart, in that its activity towards the test reaction was negligible throughout the test period. This can perhaps be explained by the fact that the BET 5 point surface area for this catalyst was measured at $26m^2/g$

compared to values in the range of 46-89$m^2/g$ observed for the other Fe doped samples. Therefore, the low of surface area for this catalyst compared to the others might offer an explanation for activity.

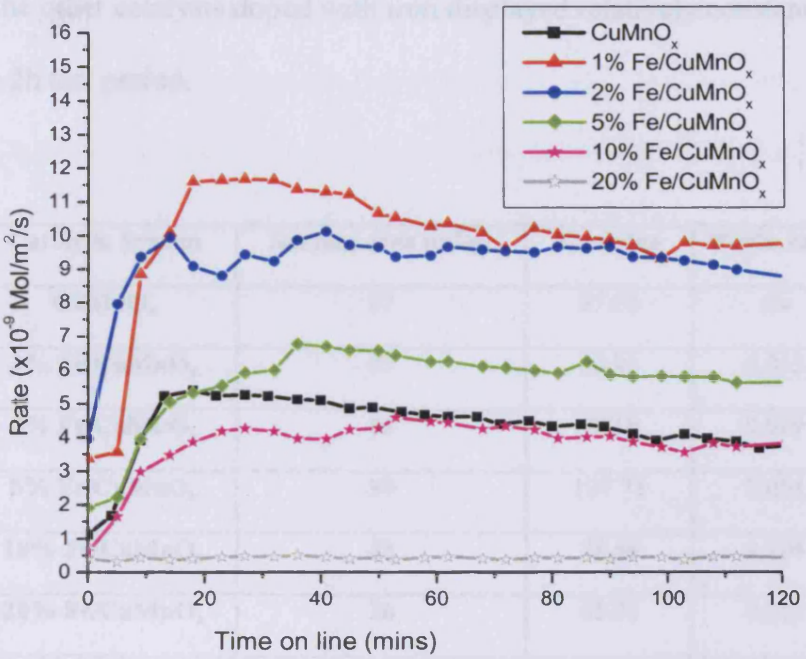


**Figure 4.4.2.2 – Surface area adjusted reaction rates for CO oxidation over Fe doped $CuMnO_x$ catalysts aged for 30 minutes**

When the raw catalytic data was adjusted to take into account the differences in surface area, the 1, 2 and 5% doped catalysts all displayed a rate of CO conversion which was superior to that of the hopcalite catalyst. The 1% Fe doped $CuMnO_x$ displayed the fastest CO conversion rate of the all the catalysts tested to this point, however some deactivation was observed during the period of catalyst testing. The 2% doped catalyst also displayed a conversion rate comparable to the quickest observed and detailed previously in this chapter. Many of the Fe doped catalysts tested benefited from the conversion of activity percentages to the rate of CO conversion per unit surface area of catalyst as the BET surface areas measured were significantly lower than for the other metal oxide catalysts investigated (see Table 4.4.2.3). As previously outlined, the

addition of iron to the catalyst may have contributed to reducing levels of deactivation with time on line.

Significant deactivation was observed in this sample set only for the 1% Fe doped catalyst. All the other catalysts doped with iron displayed relatively constant conversion rates over the 2h test period.

| Catalytic System | Surface area ($m^2/g$) | C - value | Fe/Cu ratio |
|---|---|---|---|
| $CuMnO_x$ | 87 | 85.02 | n/a |
| 1% $Fe/CuMnO_x$ | 47 | 63.83 | 0.012 |
| 2% $Fe/CuMnO_x$ | 63 | 93.19 | 0.019 |
| 5% $Fe/CuMnO_x$ | 90 | 101.72 | 0.054 |
| 10% $Fe/CuMnO_x$ | 88 | 78.48 | 0.104 |
| 20% $Fe/CuMnO_x$ | 26 | 65.91 | 0.211 |

**Table 4.4.2.3 – BET surface area data and Atomic Absorption data**

## 4.5 – Discussion

### 4.5.1 – Nickel doping experiments

The doping experiments where quantities of nickel were used in the production of the hopcalite catalyst in place of some of the copper in the standard formulation produced some interesting results. X-Ray diffraction studies did not provide adequate confirmation as to the bulk structure make up of the catalyst precursor, however it was possible to distinguish the Ni doped precursors from hopcalite as they were slightly more crystalline. The major peaks that could be identified from the XRD patterns were those relating to CuO, it was also possible to detect a slight decrease in the intensity of the major peaks as the nickel to copper ratio in the reagents was increased.

Temperature programmed reduction studies yielded some useful information. On the addition of nickel to the catalyst, the reduction temperature of the copper oxide species in the catalyst was seen to reduce, exemplified by a shift in the TPR profile to lower temperature. These lower temperature reduction peaks indicated a more energetically favourable oxidation process, where oxygen from the catalyst bulk or surface was more easily available to react catalytically with the CO reagent in the production of $CO_2$. The reduction temperature of the most easily reduced species (CuO) was noted to decrease from that in hopcalite in the 1, 2, 5 10% doped species. When 20% Ni was used in relation to the amount of copper, the signal due to the lowest temperature reducible species increased in reduction temperature. Furthermore, in the sample which contained the greatest quantity of Ni by AA analysis, a decrease in total amount of reducible species present in the catalyst was detected, indicating a lower oxide content in this catalyst. It was interesting to note that this catalyst system displayed the highest activity of all the nickel doped catalysts. This might have been due to the presence of NiO in catalyst system, which unlike the single oxides of copper and manganese was identified in our study as being catalytically active when prepared and tested under the standard conditions. Unfortunately, it was not possible to detect NiO on XRD analysis, so this theory remained conjecture. In terms of outright catalytic activity, none of the lower % doped Ni catalysts exhibited an activity rivalling that of the standard hopcalite catalyst or the 20% Ni doped species. The relative stable activity with time on line of the nickel containing systems should be noted as a very positive outcome of these tests, thereby dispelling the perceived standard decrease of activity with time, which can be observed in many hopcalite catalytic systems. [24] On adjusting for differences in the surface area between the catalyst samples, the 20% Ni doped catalyst displayed an initial activity comparable to that of hopcalite, but was far more impressive in terms stability of

conversion rate of CO to $CO_2$. The added stability might have been due to any nickel oxide present acting sacrificially with any moisture present, forming Ni ($OH_2$) and preventing poisoning of the copper-manganese oxide component by water.

The surface area measurements of the nickel doped catalyst set were in the range of 70-115$m^2$/g. All values recorded were greater than for the hopcalite sample alone, so this was another positive result in terms of producing more active hopcalite-type species. The ratios of Ni:Cu as recorded by AAS analysis were accurate to the values expected from the relative ratios of the metals in the nitrate reagent mixture, calculated during the synthesis step.

### 4.5.2 – Silver doping experiments

The addition of small amounts of silver to the catalyst formulation produced some interesting results in terms of catalytic activity. The 1, 2, 5 and 10% doped samples all produced an increase in activity over the standard hopcalite catalyst. Although the addition of silver to the formulation did not increase the stability of activity in the same way as when doping with nickel, there was still a slight stabilising effect evident when compared to the standard hopcalite catalyst. In some cases, adding silver did have a beneficial effect on the start-up activity of the catalyst. This start-up time was a crucial period in the lifetime of the hopcalite catalyst; traditionally it had determined its use in terms of commercial applications. Merrill *et al.* suggested long ago that oxidation over a $MnO_2/Ag_2O$ mixed catalyst occurred with the use of lattice $O_2$. [25] This observation would explain the high activity early in the lifetime of the silver-doped catalysts reported here. When the available lattice $O_2$ was totally consumed, a secondary oxidation mechanism took over which involved the reaction of gas phase oxygen.

As in the case of the Ni doped catalysts, it was not possible to distinguish between the doped samples and the hopcalite using XRD due to the amorphous nature of the

samples tested. Little could be determined in the way of the bulk structure of the precursors using this technique, though it was accurate to conclude that the patterns did not vary greatly, indicating similar materials being produced regardless of silver content. Surface area measurements identified all the silver-doped catalysts to have increased surface area when compared to the standard hopcalite catalyst and generally increased over the nickel-doped set. This could in part be responsible for the increased activity observed for the Ag doped samples as compared to hopcalite alone. Even when activity was adjusted to provide a CO conversion rate based on the surface area of the catalysts, the 2, 5 and 10% Ag doped samples possessed a higher conversion rate than the hopcalite catalyst. This trend continued with time on-line, even at the end of the 2 h test period the silver-doped species mentioned were still outperforming the hopcalite catalyst despite an element of deactivation in all of the cases. The 2, 5 and 10% Ag doped samples displayed a higher rate of CO conversion than any of the Ni doped species as well as the standard hopcalite. It should be noted that the best start-up activity and initial CO conversion rate observed so far in this study was seen in the 10% Ag doped sample, but the level of deactivation exhibited in this sample, was also the greatest observed in any catalyst to this point. Atomic Absorption Spectroscopy measurements confirmed that the M:Cu ratios intended from the different catalyst formulations used, were accurate to the intended levels.

### 4.5.3 – Cobalt doping experiments

The addition of a cobalt source during the hopcalite preparation stage again produced a catalyst that exhibited a decrease in the reduction temperature of the most readily reduced species of those present in the $Co/CuMnO_x$ catalyst set on TPR analysis. This trend was similarly observed in the catalysts doped with small percentage quantities of Ni and Ag. It was also possible to record a general decrease in the size of this signal;

which corresponded to the reduction of CuO, to the Co:Cu in the starting formulation was increased. It was not however possible to detect a corresponding emerging signal due to the reduction of any $CoO_x$ as this ratio was increased. This peak would however be small in most of the cases here due to the quantities of cobalt that were involved. Tests into a 100% $CoO_x$ catalyst produced and tested under standard conditions indicated that a pure sample of $CoO_x$ would reduce in two steps. It is possible that these signals were masked in the study by the much larger signals emanating from the reduction of $CuO_x$ and $MnO_x$ species.

In terms of catalytic activity towards the CO oxidation test reaction, the presence of cobalt in the catalyst make up had a positive effect. Activity levels observed were, in the most part, higher than in the standard hopcalite and those displayed by the catalysts doped with either nickel or silver. The presence of small quantities of cobalt also seemed to contribute to an increase in stability of activity as compared to hopcalite. The 1% doped sample in particular combined the two desirable attributes of high activity and stability with time on line, reaching an impressive maximum activity of 46% within 10 minutes of testing and maintaining this high activity constantly for the test period of 2h.

Doping with cobalt produced some exciting results in terms of matching the stability provided by doping the hopcalite with nickel, but also causing an increase in catalytic activity, as observed when doping with silver. When activities were adjusted for surface area differences, the 1% Co doped catalyst displayed a conversion rate similar to that of the 10% Ag doped $CuMnO_x$ – the best observed until this point, $8.5 \times 10^{-9}$ mol/m$^2$/s vs. $9 \times 10^{-9}$ mol/m$^2$/s. However as outlined already, this conversion rate was constant through the test period whereas for the silver doped catalyst the conversion rate

decreased throughout the test period, ending at $4.8x10^{-9}$ mol/$m^2$/s after 2h. Therefore, the cobalt-doped catalyst was a more attractive target for future study than the silver-doped catalyst. The ability of $CoO_x$ alone to oxidise CO was also an influencing factor in the decision to carry out further analysis in to hopcalite catalysts. [18] It seemed likely here that the cobalt was taking part in the reoxidation mechanism of the catalyst surface. The continuous reoxidation of the surface had the effect of limiting deactivation due to time on-line resulting in a very stable set of catalysts.

In terms of surface area, measured the BET analysis, the values obtained were very much in the region that might have been expected from metal oxide catalysts of this type in (63-89$m^2$/g). There was no apparent correlation between surface area and % cobalt doping unlike observed by Wright, who reported cobalt to have appositive effect on surface areas when added to copper and manganese oxides. [23] The ratios of Co:Cu determined by atomic adsorption spectroscopy were close on the desired ratios calculated during the preparation of the metal nitrate mixture before the co precipitation step.

### 4.5.4 – Iron doping experiments

XRD studies of the iron-doped samples again did not yield much in the way of conclusive data. The results merely acted as a confirmation that all the catalysts produced were similar in structure to each other. One conclusion that it was possible to draw was that the Fe doped precursors displayed more in the way of a crystalline character than the hopcalite catalyst. After TPR analysis, it was again possible to observe a shift in the position of the signal due to the most readily reduced species in the catalyst to lower temperature. This was true for the 1,2 and 5 % iron doped samples. On increasing the Fe: Cu to 10 and 20%, a return to higher temperature of these peaks

could be detected, though they still occurred at lower temperature than in the hopcalite sample. It should also be noted that in general, the iron-doped catalyst set did not consume as much hydrogen during the TPR process than the hopcalite catalyst, leading to the conclusion that less oxide species would be available from these catalysts; either surface adsorbed or from the lattice, to take part in the CO oxidation reaction. Despite apparently containing less oxide species than the hopcalite sample, the 1-10% iron-doped catalysts possessed CO oxidation activity at a similar level, or higher than that of hopcalite alone. These catalysts also displayed a good start-up activity. In the 2% doped sample the start-up activity was the best, with the activity in the 1,5 and 10% doped species being equal to that of hopcalite. The 20% doped species proved to be a bit of an anomaly as it showed no activity towards CO oxidation, a fact that may be linked to its significantly lower surface are than the other samples tested ($26m^2/g$). On adjustment of activities for differences in surface areas, both the 1 and 2% iron-doped $CuMnO_x$ systems displayed a significantly higher conversion rate of CO than hopcalite or any other of the other Fe or M-doped species tested up to this point. This was obviously a consequence of the lower surface areas of these species with the 1% Fe-doped sample displaying some decrease in conversion rate with time on line, dropping from $1.2x10^{-8}$ $Mol/m^2/s$ initially, to $1x10^{-8}$ $Mol/m^2/s$ at the end of the 2h test period. This was a very encouraging result despite the deactivation, as even this end conversion rate was higher than the best conversion rate observed at the end of test period to this point of $8.5x10^{-9}$ $Mol/m^2/s$ by the 1% cobalt-doped sample.

### 4.5.5 – Final Conclusions on Doping Experiments

The doping experiments gave rise to some very interesting results and certainly doping with any of the metals chosen offered some favourable characteristics over hopcalite alone. The most attractive feature discovered during this study was the increased

catalytic stability which arose from doping with nickel and with cobalt, as well as the promotion of catalytic activity which was observed during doping with silver and with cobalt. Iron doping also provided some interesting properties in terms of a highly competitive activity from a relatively low surface area catalyst. The results obtained from the cobalt doping experiments offered the dual advantage of increased stability combined with increased activity, so cobalt doping seemed the most promising path to investigate in terms of improving the formulation of hopcalite catalysts. The results of this further investigation, particularly looking at the effect of the concentration of cobalt and the important role that catalyst ageing time plays are discussed at length in chapter 5.

## References


[1] A.A. Mirzaei, H. R. Shaterian, R. W. Joyner, M. Stockenhuber, S. H. Taylor, G. J. Hutchings, Catal. Comm. 4 (2003)17

[2] A. A. Mirzaei, H. R. Shaterian, S. H. Taylor, G. J. Hutchings, Catal. Lett. 83, 3-4 (2003) 103

[3] G. J. Hutchings, A. A. Mirzaei, R. W. Joyner, M. R. H. Siddiqui, S. H. Taylor, Appl. Cat. A: Gen 166 (1998) 143

[4] Elemental data at: http://www.scescape.net/~woods/elements

[5] S. B. Kanungo, J. Catal. 58 (1979) 419

[6] D. Mehandjiev, A. Naydenov, G. Ivanov, Appl. Cat. A: Gen. 206 (2001) 13

[7] C. Laberty, C. Marquez-Alvarez, C. Drouet, P. Alphonse, C. Mirodatos, J. Catal. 198 (2001) 266

[8] A. Holt, M. Cheek, E. Clegg, US Patent 4,639,432 (1983)

[9] S. Veprek, D. L. Cocke, S. Kehl and H. R. Oswald, J. Catal. 100 (1986) 250

[10] R. Lin, W. Liu, Y. Zhong, M. Luo, Appl. Cat. A: Gen. 220 (2001) 165

[11] S. Imamura, H. Sawada, K. Uemura, S. Ishida, J. Catal. 109 (1988) 198

[12] S. Imamura, H. Yamade, K. Utani, Appl. Cat. A 192 (2000) 221

[13] S. D. Gardner, G. B. Hoflund, B. T. Upchurch, D. R. Schryer, E. J. Kielin, J. Schryer, J. Catal. 129 (1991) 114

[14] R. L. Tanielyan, R. Augustine, J. Chem. Eng. Comm.190 (2003) 986

[15] E. Gulari, C. Guldur, S. Srivannavit, S. Osuwan, Appl. Catal. A: Gen. 182 (1999) 147

[16] A. A. Mirzaei, PhD Thesis, Low T Carbon Monoxide Oxidation Catalysts, University of Liverpool (1998)

[17] A. Lamb, W. C. Bray, J. C. W. Fraser, J. Ind. Eng. Chem. 12 (1920) 213

[18] D. A. Cunningham, T. Kobayashi, N. Kamijo, M. Haruta, Catal. Lett. 25 (1994) 257

[19] P. Thormahlen, M. Skoglundh, E. Fridell, B. Andersson, J.Catal. 188 (1999) 300

[20] Y. Mergler, A. van Aalst, J. van Delft, B. E. Nieuwenhuys, Appl. Cat. B 10 (1996) 245

[21] M. Haruta, S. Tsubota, T. Kobayashi, H. Kageyama, M. J. Genet, B. Delmon, J. Catal. 144 (1993) 175

[22] J. Jansson, M. Skoglundh, E. Fridell, P. Thormahlen, Top. in Catal. Vol. 16/17, 1-4, (2001) 385

[23] P. A. Wright, S. Natarajan, J. M. Thomas, Chem. Mater. (1992) 4, 1053

[24] J. Jansson, M. Skoglundh, E. Fridell, P. Thormahlen, Top. in Catal. Vol 16-17, 1-4 (2001) 385

[25] D. R. Merrill, C. C. Scalione, J. Am. Chem. Soc. 43 (1921) 1982

# Chapter 5 – Effect of Ageing Time and % Cobalt Doping on Catalyst Structure and Activity

In this chapter, the dual effect of precipitate ageing time and % cobalt doping is investigated. The work presented in chapter 4 is extended where initial suggestions were that incorporating a small amount of cobalt in to the catalyst was beneficial to both catalytic activity and stability with time on-line.

Catalysts were produced with a range of cobalt doping levels (0, 1, 2 and 5%) and over a variety of catalyst ageing times (0h, 0.5h, 1h, 2h, 4h 6h, 12h). In each study the catalyst samples were synthesised using the standard procedure outlined in chapter 2, then characterised with a range of analytical techniques before being tested for their activity against the CO oxidation test reaction. Also discussed is the effect of water on the reaction system, in terms of changes in activity and stability.

## 5.1 – Cobalt-doped Catalysts produced with an Ageing Time of 0h

A series of cobalt-doped catalysts were prepared using standard co-precipitation methods. In each case, an aging time of 0h was employed. The catalyst precursor synthesised was dried and calcined as described in chapter 2 to give the final catalyst.

### 5.1.1 – X-Ray Diffraction

X-ray diffraction studies were carried out on the 0h aged, cobalt-doped hopcalite precursors using an Enraf Nonius diffractometer in a method outlined in chapter 2. On XRD analysis it was not possible to differentiate between the four samples. However, similarities could be drawn to the extent that all the samples were either poorly or microcrystalline and that all patterns were similar regardless of their cobalt content. The unaged precursors showed evidence of comprising of copper hydroxy nitrates along

with manganese carbonate. Therefore, it was likely that immediately after precipitation the copper and manganese components of the catalyst were present in separate species as opposed to a mixed oxide phase such as $CuMn_2O_4$. (Fig 5.1.1.1). It was not possible to deduce any further structural information from the XRD patterns of either the cobalt doped or the hopcalite precursors.

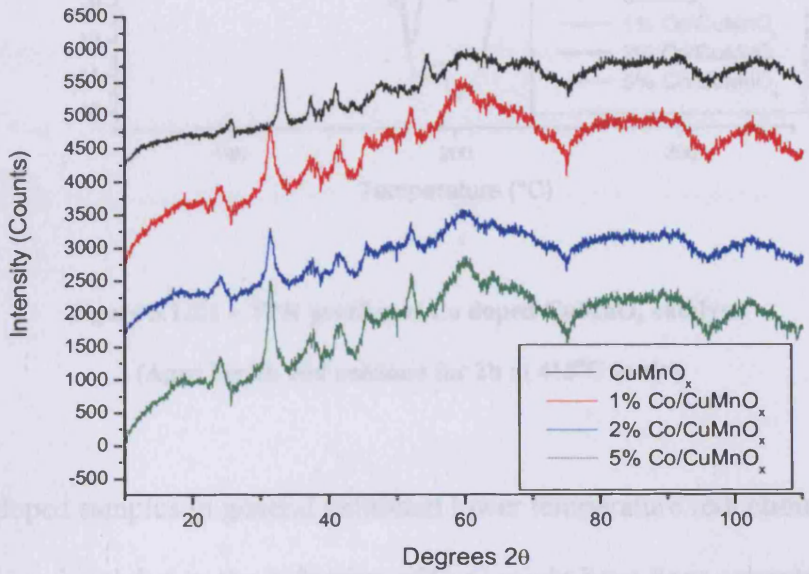


**Figure 5.1.1.1 – X-Ray Diffraction patterns of Co doped $CuMnO_x$ as a function of % Co doping (Ageing time 0h, Precursors dried at 100°C for 16h in air)**

## 5.1.2 - Temperature Programmed Reduction

The TPR patterns for each of the catalysts aged for 0h were similar in their shapes and relative position of the component peaks indicating similar species to be present in each. (Fig 5.1.2.1) The temperature where the consumption of hydrogen first started has been shown to coincide with the temperature where the catalytic reaction in the presence of oxygen would commence. [1] The TCD response was related to the quantity of reducible material (i.e. oxide) present in the catalyst sample. It followed that the more intense the TCD response, the greater the quantity of $H_2$ consumed during reduction, hence the larger quantity of oxide species reduced.

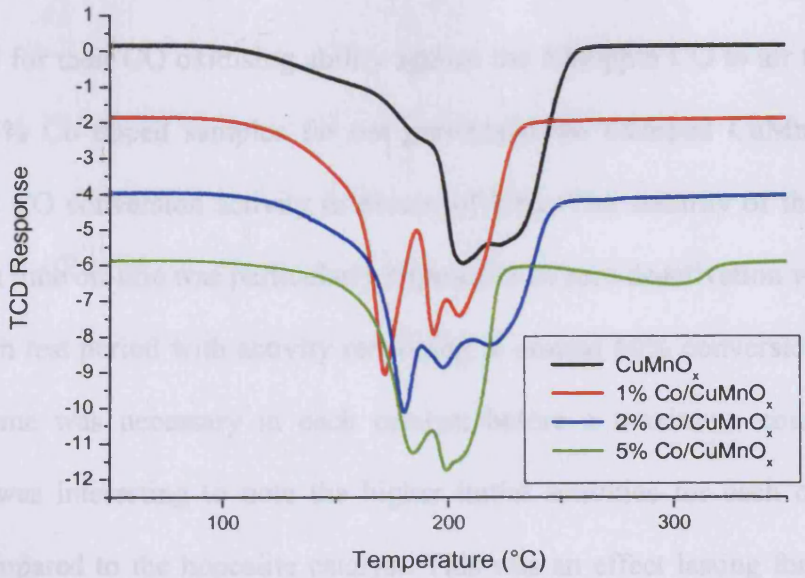


**Figure 5.1.2.1 – TPR profiles of Co doped $CuMnO_x$ catalysts**

**(Aged for 0h and calcined for 2h at 415°C in air)**

The cobalt-doped samples in general exhibited lower temperature reduction peaks in the region where a signal due to the reduction of CuO might have been expected. The same shift to lower temperature was observed for the less easily reduced $CuMn_2O_4$ and $Mn_2O_3$ components. This observation might have indicated that the reduction of the catalyst surface; that is widely believed to occur during the oxidation of CO, was energetically more facile when the hopcalite sample had been doped with a small quantity of cobalt. [2] It was evident that a much stronger signal was present for the CuO reduction in the doped samples than for the un-doped catalyst. Therefore, the possibility existed that the presence of cobalt in the sample served to ease the reduction of the copper oxide. The promotional effect of cobalt applied to all three of the doped samples but it was most evident when doping to 1% with respect to amount of copper.

### 5.1.3 - Catalytic Activity

When tested for their CO oxidising ability against the 5000ppm CO to air test mixture, the 1 and 5% Co doped samples far out performed the undoped $CuMnO_x$ catalyst, displaying a CO conversion activity in excess of 50%. The stability of the 1% doped catalyst with time on-line was particularly impressive as zero deactivation was observed during the 2h test period with activity remaining at around 60% conversion. An initial activation time was necessary in each catalyst before a maximum conversion was reached. It was interesting to note the higher initial activities for each of the doped catalysts compared to the hopcalite catalyst. This was an effect lasting for the first 10 minutes of testing.

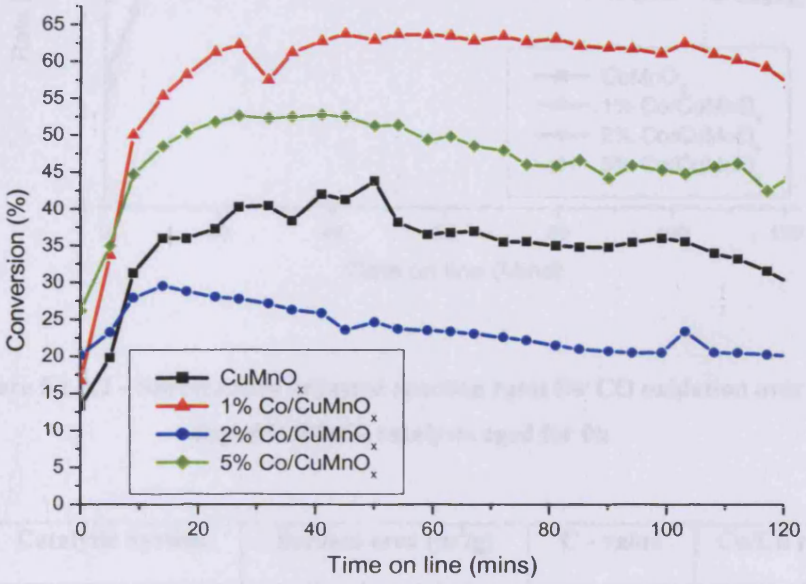


**Figure 5.1.3.1 – CO oxidation activity a series of Co doped $CuMnO_x$ catalysts aged for 0h**

When activity was adjusted for differences in the surface area of the catalysts, the 5% doped catalyst displayed the most impressive CO conversion rate while also possessing the highest start-up conversion over the first 10 minutes. The 1 and 2% cobalt-doped, as well as the un-doped samples, all had very similar start-up conversion rates. (Fig.

5.1.3.1). The most stable conversion rate was observed for the 1% cobalt-doped sample. A level of deactivation was observed in each of the other catalysts tested but was most pronounced in the hopcalite catalyst and the 2% cobalt doped sample. The rate of CO conversion exhibited by the 5% cobalt-doped catalyst was excellent when compared to the other catalysts produced with a 0h ageing time. The best start-up conversion rate was also observed for this catalyst, with only minimal deactivation observed over the 2h test period.

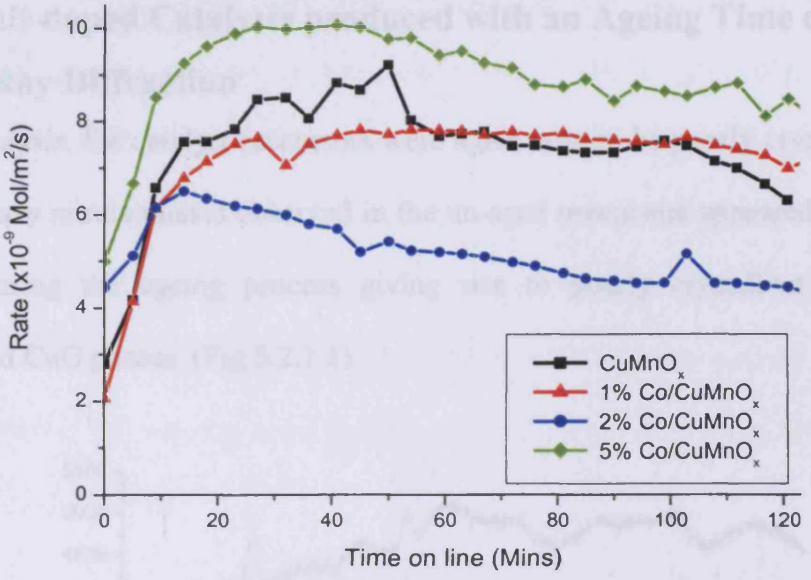


**Figure 5.1.3.2 – Surface area adjusted reaction rates for CO oxidation over Co doped $CuMnO_x$ catalysts aged for 0h**

| Catalytic System | Surface area ($m^2$/g) | C - value | Co/Cu ratio* |
|---|---|---|---|
| **$CuMnO_x$** | 74 | 82.09 | 0.000 |
| **1% $Co/CuMnO_x$** | 127 | 104.93 | 0.010 |
| **2% $Co/CuMnO_x$** | 51 | 109.32 | 0.023 |
| **5% $Co/CuMnO_x$** | 82 | 96.53 | 0.050 |

* measured by Atomic Absorption Spectroscopy

**Table 4.3.3.3 – BET surface area data and AAS data of 0h aged catalysts**

On measurement of surface areas using the BET technique a wide spread of values was obtained for the cobalt-doped catalysts (51-127$m^2$/g). The highest surface area for this ageing time was measured for the 1% doped sample which was significantly higher than any other observed under identical preparation conditions. This might explain the high activity of this catalyst towards the test reaction when compared to the others investigated. There was little correlation between the surface area values of the other catalysts and their intrinsic activity.

## 5.2 – Cobalt-doped Catalysts produced with an Ageing Time of 0.5h

### 5.2.1 – X-Ray Diffraction

On XRD analysis, the catalyst precursors were again seen to be poorly crystalline. The copper hydroxy nitrate phases observed in the un-aged precursors appeared to have re-dissolved during the ageing process giving rise to poorly crystalline manganese carbonate and CuO phases. (Fig 5.2.1.1)

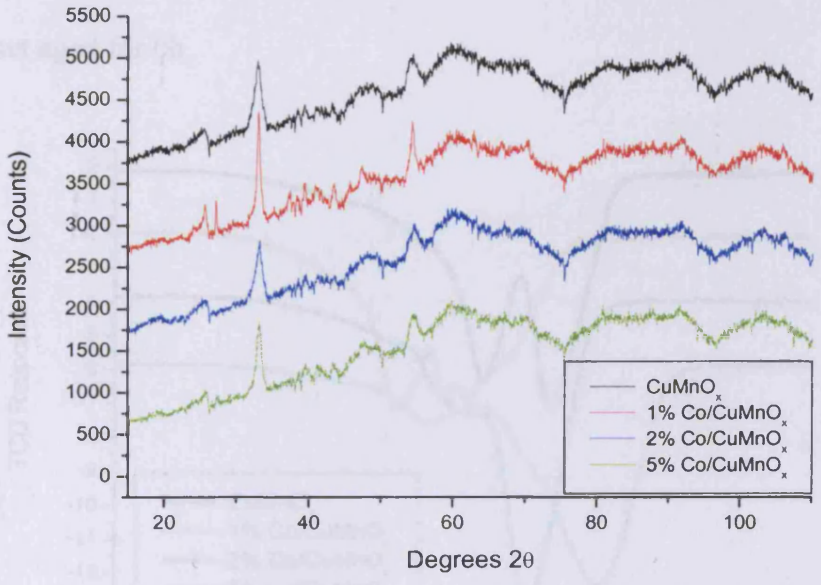


**Figure 5.2.1.1 – X-ray diffraction patterns of Co doped $CuMnO_x$ as a function of % Co doping**

**(Ageing time 0.5h, Precursors dried at 100°C for 16h in air)**

An emerging trend was that as the catalyst ageing time was increased, the XRD pattern displayed less crystalline character. This trend was later observed to continue for catalyst produced with longer ageing times.

## 5.2.2 - Temperature Programmed Reduction

On increasing the ageing time from zero to 0.5h, it was interesting to observe the differences in the TPR profiles for these catalysts compared to those synthesised with shorter ageing time. The change in bulk composition was a strong indicator of the influence that ageing can have on the final catalyst. The biggest single difference appeared to be a shift from a catalyst which contained large quantities of CuO to a catalyst where the $CuMnO_x$ and $MnO_x$ components, reduced at higher temperature, were more predominate. It was interesting to note that the temperature of the peaks due to the reduction of the most easily reduced species in each catalyst occurred in the order 1%<2%<5%<0%. This was the same peak order as that seen during the TPR studies of the catalyst set aged for 0h.

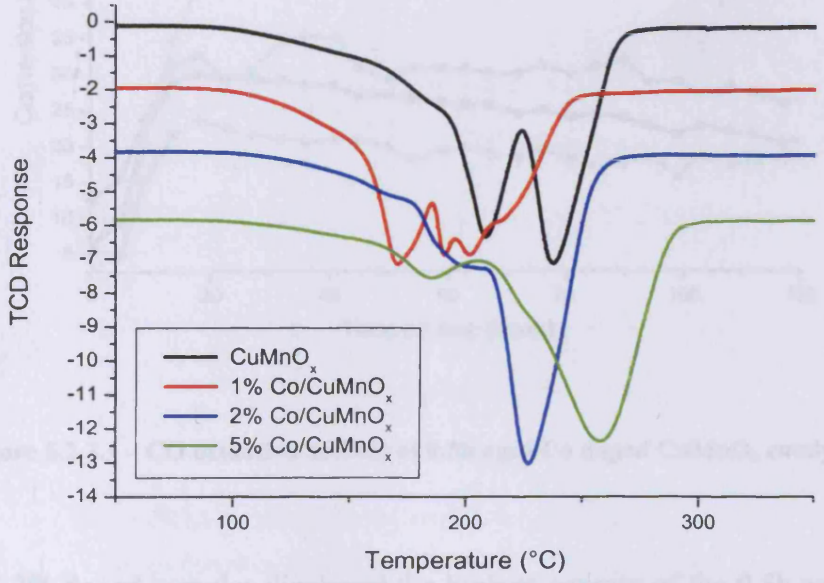


**Figure 5.2.2.1 – TPR patterns of 0.5h aged Co doped $CuMnO_x$ catalysts**

A point for comparison was the differences in $H_2$ consumption between the 1% Co-doped and the other catalysts. The 1% doped sample consumed less $H_2$ during the TPR reaction; this was indicative of a lower total composition of reducible material in this catalyst compared to the other three produced with this ageing time. This did not affect its CO oxidising power, exemplified by the 1% cobalt-doped sample displaying the best catalytic activity of the 0.5h aged catalysts. The $H_2$ usage during the reduction of the other three samples was of similar magnitude, indicating similar quantities of reducible species to be present in each.

## 5.2.3 - Catalytic Activity

When considering the CO oxidising ability of the catalyst (Fig 5.2.3.1), activity was generally reduced from that of the 0h aged samples.

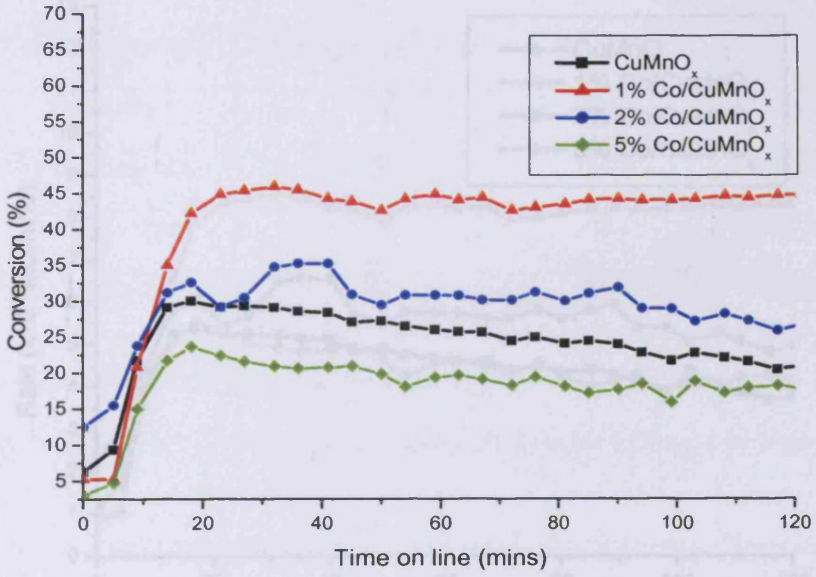


**Figure 5.2.3.1 – CO oxidation activity of 0.5h aged Co doped $CuMnO_x$ catalysts**

The 1% and 2% doped samples displayed the highest activity of the 0.5h aged set, with the initial start-up activity of both samples being better than, or at least comparable to

that of the undoped sample, as was the maximum activity displayed by these species. The deactivation of the catalyst with time on-line in all instances was not pronounced. However, it would seem that the most stable activity was observed for the 1% doped sample; a trend also common in the 0h aged catalyst set in figure 5.1.2. The largest loss of activity over the test period was observed for the hopcalite catalyst where a decrease of 8% from the maximum activity reached was recorded over the 2h test period.

When activities were adjusted to account for surface area differences between samples, the 1% cobalt-doped sample gave rise to the highest rate of CO conversion of the catalysts synthesised with a 0.5h aging time. In this case a maximum conversion rate of $8.5x10^{-9}$ $Mol/m^2/s$ was achieved, a rate at which conversion remained constant throughout the 2h test period.

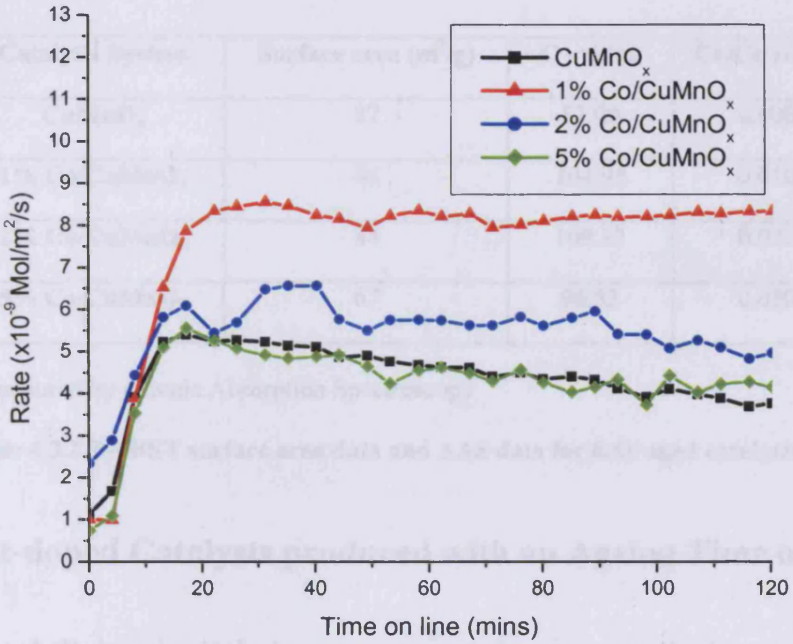


**Figure 5.2.3.2 – Surface area adjusted reaction rates for CO oxidation over 0.5h aged Co doped $CuMnO_x$ catalysts**

The 2% cobalt-doped sample also displayed a good rate of CO conversion (5.8 $x10^{-9}$ $Mol/m^2/s$) with the 5% and un-doped samples performing very similarly (5 $x10^{-9}$ $Mol/m^2/s$). However, the surface area adjusted CO conversion rates displayed by the 0.5h catalyst set were generally lower than those achieved for the 0h aged samples. This offered a general indication that the species produced after ageing for 30 minutes were less active than those produced where no ageing of the precipitate took place.

On measurement of the BET surface areas of the catalysts, there was little difference between the values obtained for the un-doped catalyst compared to the 1 and 2% doped samples as all were measured in the range 84-87$m^2/g$. The surface area of the 5% cobalt-doped catalyst was the lowest at 67$m^2/g$; this lower surface area also correlated with the lowest level of activity towards CO oxidation of the catalysts synthesised with an ageing time of 30 minutes.

| Catalytic System | Surface area ($m^2/g$) | C - value | Co/Cu ratio* |
|---|---|---|---|
| **$CuMnO_x$** | 87 | 82.09 | 0.000 |
| **1% $Co/CuMnO_x$** | 84 | 104.93 | 0.010 |
| **2% $Co/CuMnO_x$** | 84 | 109.32 | 0.023 |
| **5% $Co/CuMnO_x$** | 67 | 96.53 | 0.050 |

* measured by Atomic Absorption Spectroscopy

**Table 4.3.3.3 – BET surface area data and AAS data for 0.5h aged catalysts**

## 5.3 – Cobalt-doped Catalysts produced with an Ageing Time of 1h

A series of cobalt-doped catalysts were prepared using standard co-precipitation methods. In each case, an aging time of 1h was used. The catalyst precursor synthesised was dried and calcined as described in chapter 2 to give the catalyst.

## 5.3.1 – X-Ray Diffraction

On XRD analysis, a loss of crystallinity was again evident on cobalt doping, in a mode of behaviour similar to that of the shorter ageing time samples (Fig. 5.3.1.1). This was exemplified by a reduction in the intensity of the reflection at 33°. The XRD patterns indicated that the samples mainly consisted of material that was either amorphous to XRD or microcrystalline in nature. Similar results were observed for the other cobalt-doped catalysts studied at different ageing times to this point, but little in terms of detailed bulk structure composition could be determined from the XRD analysis. The major phases detected were carbonates of manganese and copper, which are known to have poor activity towards CO oxidation. [3]

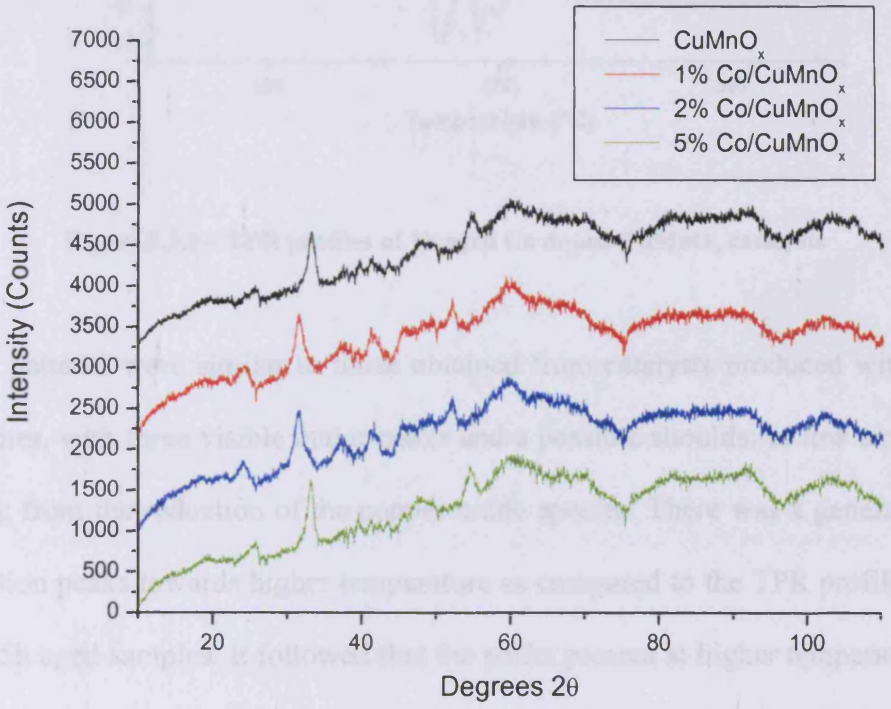


**Figure 5.3.1.1 – XRD pattern of 1h aged Co doped $CuMnO_x$ catalysts**

## 5.3.2 - Temperature Programmed Reduction

A temperature programmed reduction analysis of the 1h aged, cobalt-doped systems was carried out. On analysis of the relative peak areas of the TPR plot, it was evident from the quantities of hydrogen consumed during the experiments that each catalyst sample contained a similar quantity of reducible material.

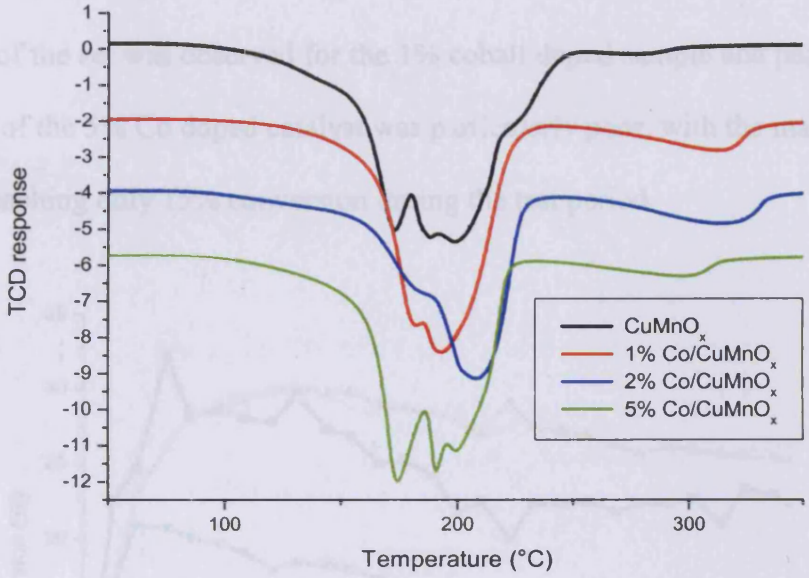


**Figure 5.3.1 – TPR profiles of 1h aged Co doped $CuMnO_x$ catalysts**

The TPR patterns were similar to those obtained from catalysts produced with shorter ageing times, with three visible major peaks and a possible shoulder at low temperature emanating from the reduction of the copper oxide species. There was a general shift of the reduction peaks towards higher temperature as compared to the TPR profiles for the 0h and 0.5h aged samples. It followed that the peaks present at higher temperature were due to the reduction of species which would require a larger amount of energy to liberate their oxide component. This observation might be linked to any differences that occurred in catalytic activity towards CO oxidation as it would mean if the bulk of the

reducible species in the sample could be reduced at high temperature, the oxygen from this species would be less readily available to take part in the oxidation reaction.

### 5.3.3 - Catalytic Activity

Activities for the 1h aged catalyst set were generally lower than has been reported previously in this study for cobalt-doped catalysts. The maximum conversion for the most active of the set was observed for the 1% cobalt doped sample and peaked at 30%. The activity of the 5% Co doped catalyst was particularly poor, with the maximum level of activity reaching only 15% conversion during the test period.

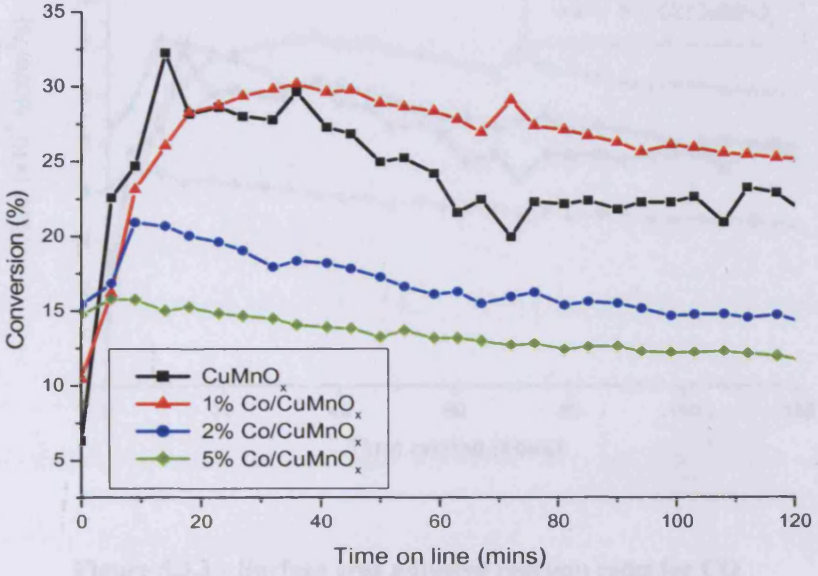


**Figure 5.3.3.1 – CO oxidation activity of 1h aged Co doped $CuMnO_x$ catalysts**

The hopcalite catalyst displayed the fastest start-up activity of the 1h aged cobalt-doped catalyst, but was also seen to deactivate to the highest degree over the test period. Deactivation with time on-line took place in all of the catalysts, the most appreciable deactivation was observed for the $CuMnO_x$ catalyst with a loss of 8% from its initial maximum activity during the test period. The cobalt-doped catalysts all deactivated at a

similar level in the region of 2 to 4% over the same period, with rates of deactivation being significantly lower in the cobalt doped samples than for the hopcalite catalysts tested.

When surface area adjusted CO conversion rates were calculated, the 2% cobalt-doped sample benefited from having a much lower surface area than the other samples. (See fig 5.3.3.2)

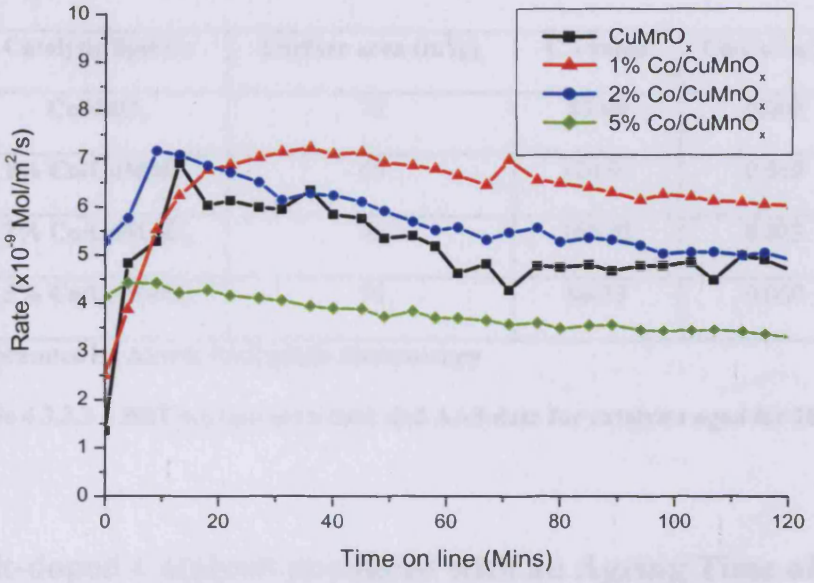


**Figure 5.3.3 – Surface area adjusted reaction rates for CO oxidation over 1h aged Co doped $CuMnO_x$ catalysts**

The start-up of the 2% doped catalyst was best in terms of the rate of CO conversion ($Mol/m^2/s$). The start-up rates of the 1% and undoped catalyst were both very similar; however, an appreciable deactivation was observed in the case of the undoped sample. The 1% and 5% doped catalysts both exhibited an increased stability; deactivation occurred but to a lesser extent. The conversion rate of the 5% doped catalyst was poor,

not simply in relation to this specific ageing time, but also when compared to previously tested samples in this study.

When considering the BET surface area measurements of the 1h aged catalyst samples, all three of the doped samples had a lower surface area than the hopcalite catalyst. Surface areas decreased in the order $CuMnO_x$ > 1% Co > 5% Co > 2% Co. The c values for the samples were all in the range that might be expected for metal oxide samples ( 82-110$m^2/g$).

| Catalytic System | Surface area ($m^2/g$) | C - value | Co/Cu ratio* |
|---|---|---|---|
| **$CuMnO_x$** | 72 | 82.09 | 0.000 |
| **1% Co/$CuMnO_x$** | 65 | 104.93 | 0.010 |
| **2% Co/$CuMnO_x$** | 45 | 109.32 | 0.023 |
| **5% Co/$CuMnO_x$** | 55 | 96.53 | 0.050 |

* measured by Atomic Absorption Spectroscopy

**Table 4.3.3.3 – BET surface area data and AAS data for catalysts aged for 1h**

## 5.4 – Cobalt-doped Catalysts produced with an Ageing Time of 2h

A series of cobalt-doped catalysts were prepared using standard co-precipitation methods. In each case, an ageing time of 2h was used. The catalyst precursor synthesised was dried and calcined as described in chapter 2 to give the catalyst.

### 5.4.1 – X-Ray Diffraction

On XRD analysis of the catalyst precursors obtained using a 2h ageing time, little information on the phases present in the catalyst bulk structure could be drawn due to the amorphous nature of the samples. Evidence pointed at a system containing poorly crystalline manganese carbonate phase along with copper oxide (CuO). Line spacings

were however broad, so it was difficult to ascertain any changes in line spacings between samples to which the Scherrer equation could have be applied and the particle size calculated. On calcination of the precursors, a XRD pattern was obtained which was either amorphous or microcrystalline to XRD analysis. It was not possible to detect peaks due to the reflections of the $CuMn_2O_4$ phase. The intensities of the peaks present here were overall, lower than those observed for shorter ageing times. This might have been indicative of a sample with a smaller crystallite size than that observed for the shorter ageing times.

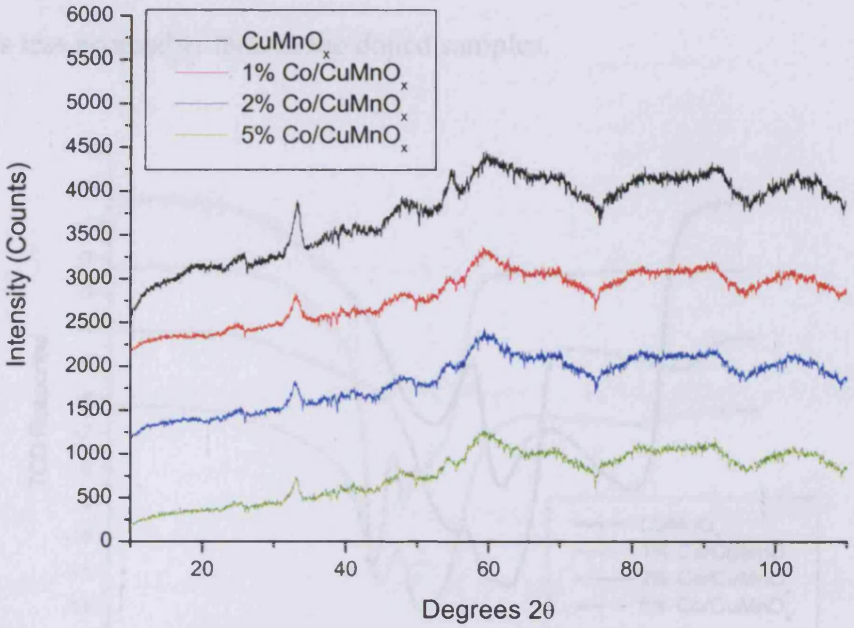


**Figure 5.4.1.1 - XRD pattern of 2h aged Co doped $CuMnO_x$ catalyst precursors dried at 100°C, 16h**

No differences were observed between the XRD data obtained before and after the catalyst was tested for the oxidation of carbon monoxide.

## 5.4.2 - Temperature Programmed Reduction

On analysis of the catalysts using TPR, some interesting trends could be drawn. The components of the doped catalysts were all reduced at lower temperature relative to the

hopcalite sample. Only the 1% doped sample appeared to consist mainly of CuO, whereas in the other three samples, the manganese oxide and mixed copper-manganese phase predominated. In the case of the undoped catalyst, the TPR pattern took on a significantly different appearance to the others observed for this ageing time. The uptake of hydrogen during the TPR experiment for this sample was the greatest of all the catalysts produced with a 2h ageing time, indicating the presence of a much larger quantity of reducible material compared to the others. Although the oxide content was greater in the undoped catalyst compared to the cobalt-doped samples, the higher reduction temperature associated with its component peaks might have indicated that its oxygen was less accessible than in the doped samples.

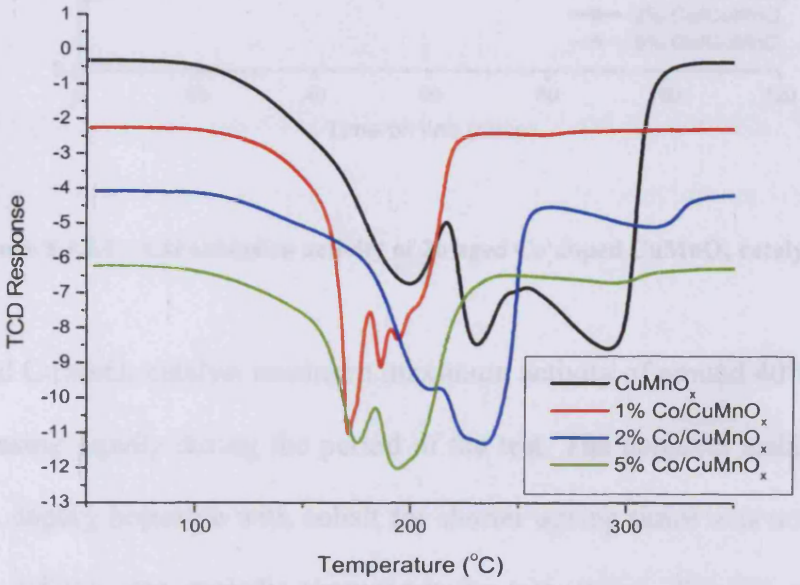


**Figure 5.4.2.1 - TPR patterns of 2h aged Co doped $CuMnO_x$ catalysts**

## 5.4.3 - Catalytic Activity

The final catalysts differed widely in their activity towards CO oxidation at ambient temperature. A different activity profile was observed for the 2 and 5% Co doped samples as compared to those observed up to this point in the study. In both these

samples, the characteristic catalyst "start-up" period leading up a maximum activity that had become a common factor in the behaviour of hopcalite and doped-hopcalite catalysts to this point was not observed. This feature was exemplified for the 2h aged catalysts by both the un-doped and 1% Co doped samples.

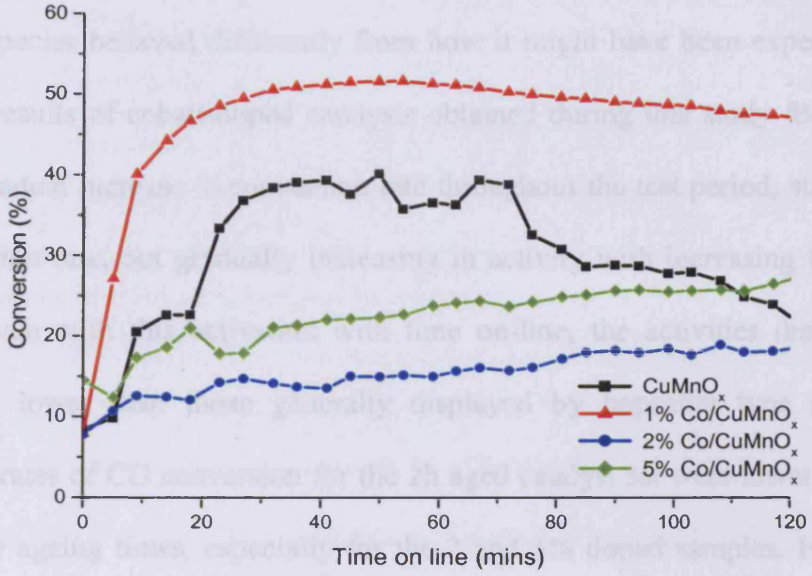


**Figure 5.4.3.1 – CO oxidation activity of 2h aged Co doped $CuMnO_x$ catalysts**

The un-doped $CuMnO_x$ catalyst reached a maximum activity of around 40% conversion before decreasing rapidly during the period of the test. The apparent stability increase prompted by doping hopcalite with cobalt for shorter ageing times was not present for this sample; activity was sporadic throughout the test period. The 1% cobalt doped hopcalite achieved the highest activity for this ageing time reaching a maximum activity of ~50% conversion after 20 minutes of the test period. Activity remained steady around this level for the remainder of the test period. The start-up activity of the 1% doped sample was only the best of all the catalysts produced with a 2h ageing time.

On adjusting the activities for differences in surface areas, it was possible to demonstrate that the 1% Co doped catalyst displayed a far superior start-up rate of CO

conversion per unit surface area per second than any of the other catalysts produced at this ageing time. The rate of CO conversion in the 1% doped sample remained high and relatively stable throughout the test period; compared to that of the hopcalite catalyst which tailed off rapidly after an initial activation period. The rate of CO conversion offered by this catalyst was the highest of all the catalysts tested to this point. The 2 and 5% doped species behaved differently from how it might have been expected judging from other results of cobalt-doped catalysts obtained during this study. Both catalysts showed a gradual increase in conversion rate throughout the test period, starting with a low conversion rate, but gradually increasing in activity with increasing time on-line. However, even with this activation with time on-line, the activities displayed were significantly lower than those generally displayed by hopcalite type catalysts. In general, the rates of CO conversion for the 2h aged catalyst set were lower than for the other shorter ageing times, especially for the 2 and 5% doped samples. However, the 1% cobalt-doped sample possessed an encouragingly high, relatively stable conversion rate.

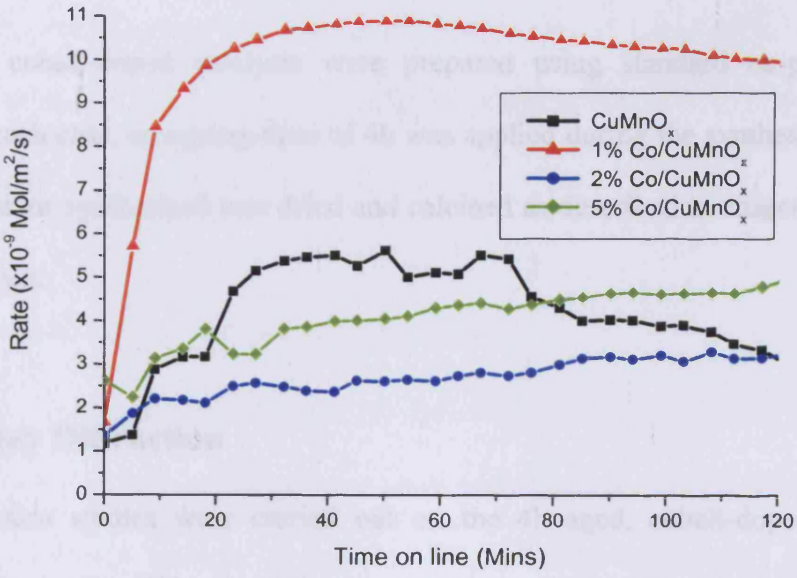


**Figure 5.4.3.2 – Surface area adjusted reaction rates for CO oxidation over 2h aged Co doped $CuMnO_x$ catalysts**

On the measurement of BET surface areas, the cobalt-doped catalysts all displayed surface areas in the region of 73-88$m^2/g$. This was significantly lower than the 110$m^2/g$ measured for the undoped sample produced with a 2h ageing time.

| Catalytic System | Surface area ($m^2/g$) | C - value | Co/Cu ratio* |
|---|---|---|---|
| $CuMnO_x$ | 110 | 63.28 | 0.000 |
| 1% $Co/CuMnO_x$ | 73 | 87.93 | 0.013 |
| 2% $Co/CuMnO_x$ | 88 | 98.32 | 0.021 |
| 5% $Co/CuMnO_x$ | 85 | 105.71 | 0.055 |

* measured by Atomic Absorption Spectroscopy

**Table 5.4.3.3 – BET surface area data and AAS data for catalysts aged for 2h**

On analysis of the catalysts by AAS, cobalt was measured to be present in the samples at the intended level, relative to the quantity of cobalt nitrate used during the catalyst synthesis step. (Table 2.1.4.1.1)

## 5.5 – Cobalt-doped Catalysts produced with an Ageing Time of 4h

A series of cobalt-doped catalysts were prepared using standard co-precipitation methods. In each case, an ageing time of 4h was applied during the synthesis step. The catalyst precursor synthesised was dried and calcined as described in chapter 2 to yield the final catalyst.

### 5.5.1 – X-Ray Diffraction

X-ray diffraction studies were carried out on the 4h aged, cobalt-doped hopcalite precursors using an Enraf Nonius diffractometer in a method outlined in chapter 2.

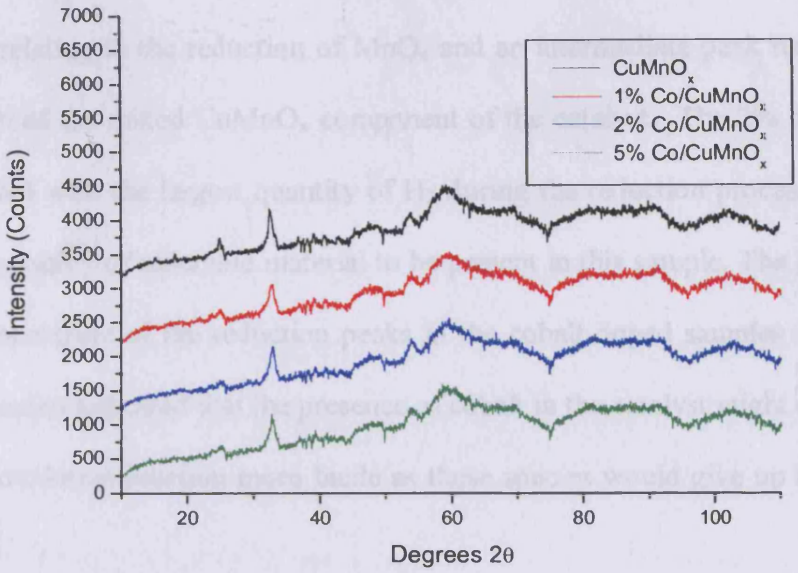


**Figure 5.5.1.1 – XRD pattern of 4h aged Co doped $CuMnO_x$ catalyst precursors dried at 100°C, 16h**

On XRD analysis, it was not possible to differentiate between the four samples. However, similarities could be drawn to the extent that all the samples were poorly or micro- crystalline and that all patterns were similar regardless of their cobalt content. The major crystalline peak in each of the samples tested was reflected at 33° and was due to the presence of copper oxide in the catalyst precursor. Other evidence pointed to the presence of manganese carbonate in all of the samples, however no cobalt oxide was detected in any of the precursors.

## 5.5.2 - Temperature Programmed Reduction

A temperature programmed reduction analysis was carried out using the method outlined in chapter 2. On analysis of the relative peak areas of the TPR plot it was again possible to observe a general decrease in the reduction temperature of the most reducible species in the catalysts as cobalt content was increased compared to that species in hopcalite. In each of the catalysts three distinct reduction peaks could be

observed, one at low temperature with a shoulder relating to the reduction of CuO, one at higher T relating to the reduction of $MnO_x$ and an intermediate peak resulting from the reduction of the mixed $CuMnO_x$ component of the catalyst. The 2% cobalt-doped sample reacted with the largest quantity of $H_2$ during the reduction process, indicating the highest quantity of reducible material to be present in this sample. The general shift to lower temperature of the reduction peaks in the cobalt-doped samples compared to those in hopcalite indicated that the presence of cobalt in the catalyst might contribute to making the oxidation reaction more facile as these species would give up their oxygen more readily.

Another feature of note was a set of reduction peaks in the hopcalite sample where the mixed copper-manganese oxide phase predominated as compared to the cobalt-doped samples where the single copper and manganese oxides were present in greatest quantities relative to the mixed oxide phase.

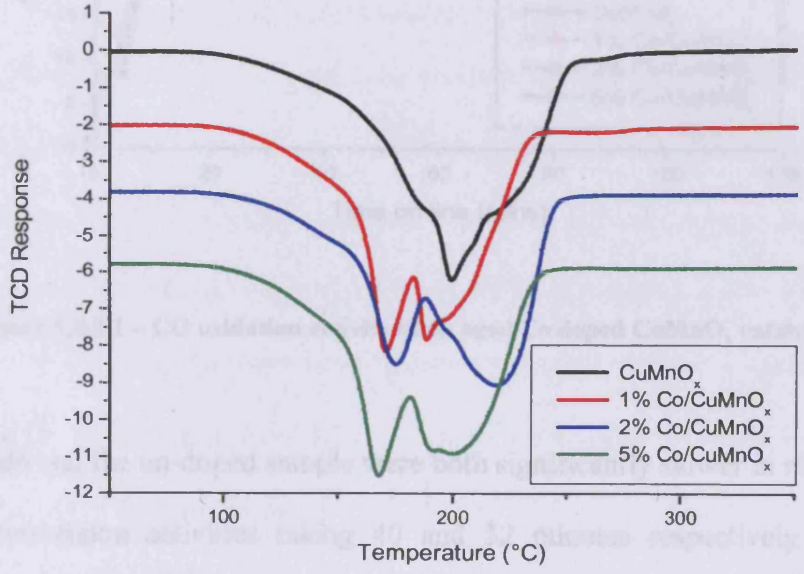


**Figure 5.5.2.1 – TPR patterns of 4h aged Co doped $CuMnO_x$ catalysts**

### 5.5.3 - Catalytic Activity

The cobalt-doped catalysts aged for 4h were tested for their oxidising ability of the standard 5000ppm CO to air text mixture. The hopcalite, 1% & 2% cobalt doped catalysts all exhibited similar levels of maximum activity during the test period, but start-up activities and the stability of the activity with time on-line differed markedly. The 2% cobalt-doped sample displayed a rapid start-up activity, reaching an impressive maximum conversion of over 50% within the first 10 minutes of testing. From this initial high level, there was a degree of deactivation over the test period, with activity dropping to ~43% at the end of the test period.

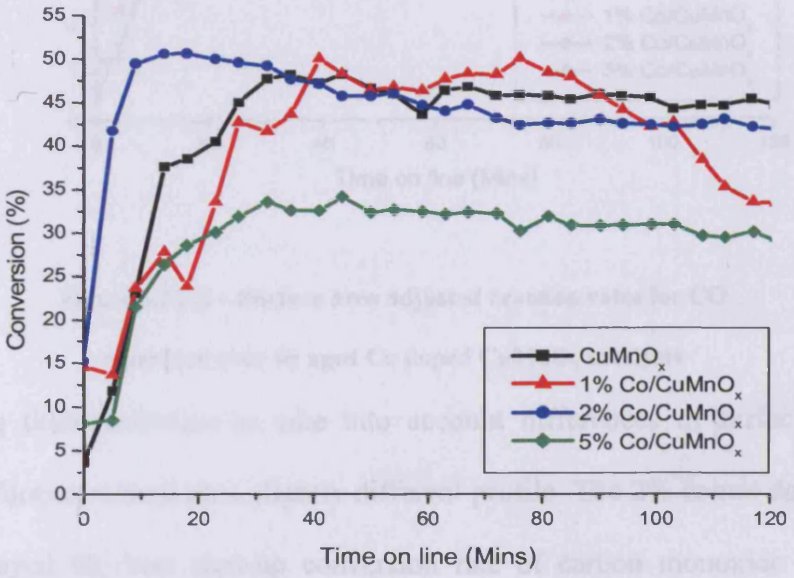


**Figure 5.5.3.1 – CO oxidation activity of 4h aged Co doped $CuMnO_x$ catalysts**

The 1% doped and the un-doped sample were both significantly slower in reaching their maximum conversion activities taking 40 and 32 minutes respectively to reach a similarly high activity. The activity of the hopcalite catalyst was the most stable of these catalysts with almost zero deactivation present observed once the maximum activity had been reached. The 5% cobalt-doped catalyst exhibited a start-up activity similar to those

of the 0 and 1% doped catalysts during the first 10 minutes of testing, but its maximum activity reached was only 34%; much lower than the other catalysts aged for 4h. However, the stability that the 5% doped catalyst showed to towards the test reaction was most impressive, with virtually no deactivation observed over the 2h test period.

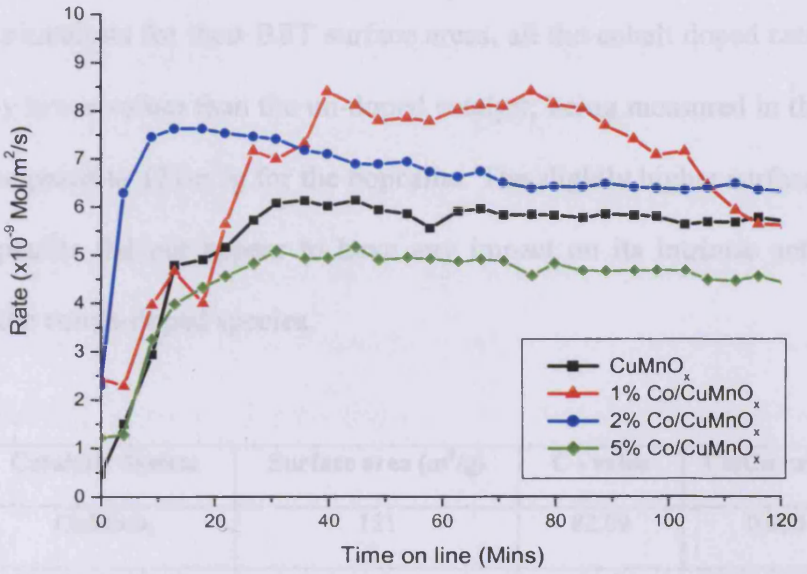


**Figure 5.5.3.2 – Surface area adjusted reaction rates for CO oxidation over 4h aged Co doped $CuMnO_x$ catalysts**

On adjusting these activities to take into account differences in surface areas, the catalytic performance took on a slightly different profile. The 2% cobalt-doped catalyst by far displayed the best start-up conversion rate of carbon monoxide in terms of Mol/m$^2$/s. The start-up conversion rates of the other three catalysts tested for this ageing time were all very similar and significantly slower than that of the 2% doped sample. In terms of stability with time on line, the conversion rates of the un-doped and 5% doped sample were stable throughout the 2h test period after the maximum rate had been achieved after 30 minutes on line. The maximum conversion rates achieved were of similar magnitude to those of the 2h, 1h and 0.5h aged catalyst sets but not as high as those produced by the 0h catalyst.

The 2% cobalt$_T$doped catalyst displayed a low amount of steady deactivation over the 2h test period, whereas the conversion rate of the 1% cobalt doped system was shown to ungulate throughout the test period but also to deactivate to the greatest extent of the catalysts tested for this ageing time.

On testing the catalysts for their BET surface areas, all the cobalt doped catalysts gave rise to slightly lower values than the un-doped catalyst; being measured in the range 92 – 104m$^2$/g compared to 121m$^2$/g for the hopcalite. The slightly higher surface are of the un-doped hopcalite did not appear to have any impact on its intrinsic activity when compared to the cobalt-doped species.

| Catalytic System | Surface area (m$^2$/g) | C - value | Co/Cu ratio* |
|---|---|---|---|
| **$CuMnO_x$** | 121 | 82.09 | 0.000 |
| **1% $Co/CuMnO_x$** | 92 | 104.93 | 0.009 |
| **2% $Co/CuMnO_x$** | 96 | 109.32 | 0.021 |
| **5% $Co/CuMnO_x$** | 104 | 96.53 | 0.056 |

* measured by Atomic Absorption Spectroscopy

**Table 5.5.3.3 – BET surface area data and Atomic Absorption data for catalysts aged for 4h**

## 5.6 – Cobalt-doped Catalysts produced with an Ageing Time of 6h

A series of cobalt-doped catalysts were prepared using standard co-precipitation methods. In each case, an ageing time of 6h was used during the synthesis. The catalyst precursor synthesised was dried and calcined as described in chapter 2 to yield the final catalyst.

## 5.6.1 – X-Ray Diffraction

X-Ray Diffraction studies were carried out on each of the 6h aged cobalt-doped catalyst precursors. The XRD patterns produced indicated that each or the samples were either amorphous with respect to X-Ray Diffraction or microcrystalline in structure. Few differences could be drawn between the traces; however, one point of difference was the peak at 33° of weak intensity for the 1% Co doped sample as compared to the other precursors. This signal was thought to relate to the presence of CuO in the final catalyst, it was therefore possible that a larger quantity of the copper in the final catalyst was present in the mixed oxide species rather than as a single metal oxide species. The intensity of this peak was also low in the 5% doped precursor indicating a lower level of CuO to be present in these samples compared to either the un-doped or 2% doped precursor.

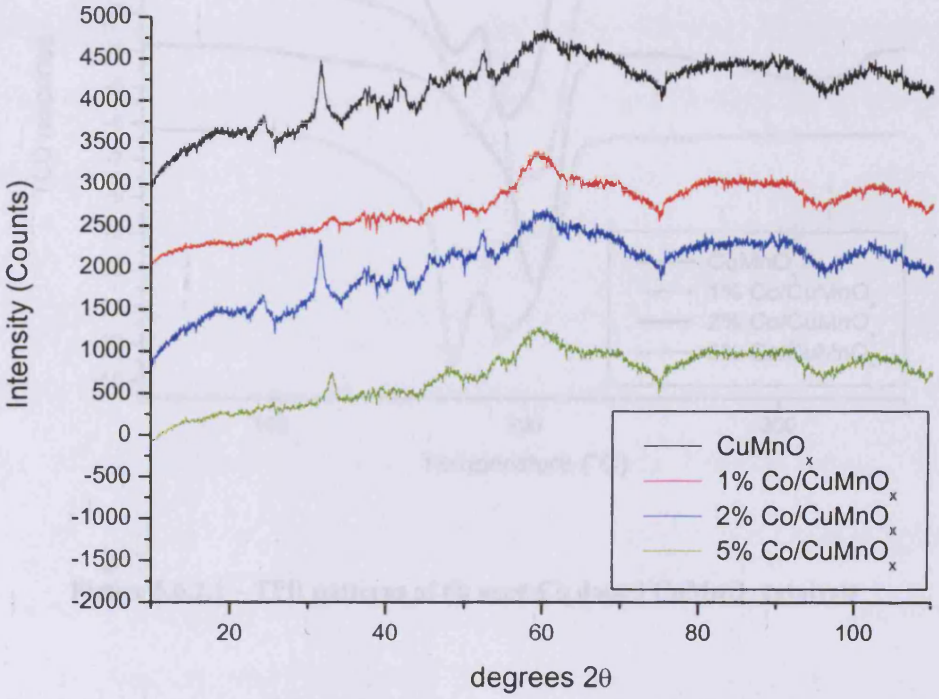


**Figure 5.6.1.1 – XRD patterns of 6h aged Co doped $CuMnO_x$ catalyst precursors dried at 100°C, 16h**

On XRD analysis of the calcined catalysts, the samples were totally amorphous to the technique so that no structural information could be determined from the patterns.

## 5.6.2 - Temperature Programmed Reduction

On TPR analysis of the 6h aged catalyst set some interesting differences could be drawn from the resulting data. The general shift of the reduction peaks to lower temperature as the cobalt to copper ratio was increased was not as evident here as it has been during the previous experiments using shorter ageing times. Only in the case of the 5% doped catalyst there was a reduction in the temperature of the most reducible species in the catalyst when compared to the standard hopcalite.

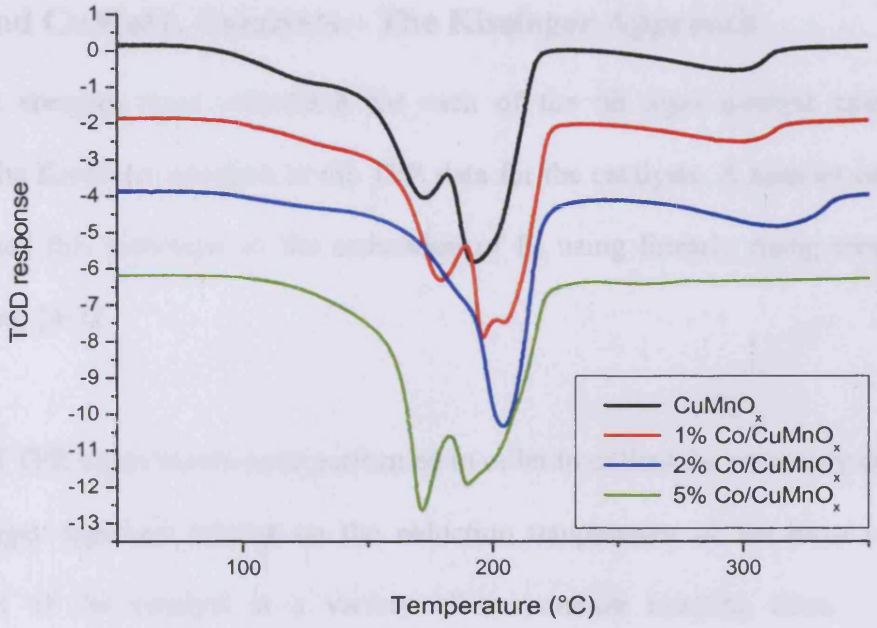


**Figure 5.6.2.1 – TPR patterns of 6h aged Co doped $CuMnO_x$ catalysts**

However, this lack of migration to lower temperatures had little bearing on the relative activities of the catalysts, with the four catalysts tested here producing some of the highest activities observed throughout the whole study. The 2% doped catalyst appeared to contain the greatest quantity of the mixed copper manganese oxide species. However,

the components in this species were generally less easily reduced than in the other three samples tested for this ageing time.

The TPR profiles of the other doped catalysts tested for this ageing time were of a standard appearance, composing of a mixture of the single copper and manganese oxides along with some of the mixed copper-oxide species. The pattern due to the reduction of the 2% Co/$CuMnO_x$ sample appeared to contain a smaller quantity of the copper oxide species providing an indication that a greater amount of the copper was present in the mixed $CuMnO_x$ phase.

### 5.6.3 - Calculation of Activation Energies of Reduction, of cobalt-doped and $CuMnO_x$ Catalysts – The Kissinger Approach

Activation energies were calculated for each of the 6h aged catalyst systems by applying the Kissinger equation to the TPR data for the catalysts. A number of authors have applied this technique to the estimation of $E_a$ using linearly rising temperature experiments. [4-7]

A series of TPR experiments were performed in order to collect the necessary data, with the Kissinger approach relying on the reduction temperature of the most reducible component of the catalyst at a variety of temperature ramping rates. In each experiment, the quantity of sample and the particle size of the catalyst were kept broadly the same while the ramp rate of the TPR furnace was varied. Measurements were recorded while ramping the furnace from ambient through to 500°C at heating rates of 2, 5, 10 and 20°C/min.

The Kissinger equation and its parameters are outlined below:

$$-\ln\left(\frac{\beta}{T_m^2}\right)=\frac{E_d}{RT_m}-\ln\left(\frac{AR}{E_d}\right)$$

$\beta$ = *Heating rate* $(^{o}C/\min)$

$T_m^2$ = *Most rapidly decomposed peak* $(K)$

$E_d$ = *Thermal decomposition activation energy* $(kJ/mol)$

$A$ = *Cons tant*

$R$ = *Gas cons tant*

Thermal decomposing activation energy wa s determined by a plot of $-\ln\left(\frac{\beta}{T_m^2}\right)$ against $\frac{1}{T_m}$, according to the Kissinger equation.

The slope of the plot was equal to $\frac{-E_d}{R}$.

From this value, the thermal reduction activation energies were estimated and are shown in table 5.6.3.3. The data used to calculate this value is detailed below in tables 5.6.3.1 and 5.6.3.2.

| $\beta$ | $CuMnO_x$ | 1% $Co/CuMnO_x$ | 2% $Co/CuMnO_x$ | 5% $Co/CuMnO_x$ |
|---|---|---|---|---|
| **2°C/min** | -11.4015972 | -11.4110312 | -11.3968635 | -11.4015972 |
| **5°C/min** | -10.6001486 | -10.5777016 | -10.5777016 | -10.5458466 |
| **10°C/min** | -9.8845544 | -9.9114607 | -9.9291992 | -9.9900734 |
| **20°C/min** | -9.3097331 | -9.3224585 | -9.2580061 | -9.2840368 |

**Table 5.6.3.1 – Details of $-\ln\left(\frac{\beta}{T_m^2}\right)$ for the 6h aged cobalt doped catalysts as a function of TPR ramp rate**

| $\beta$ | $CuMnO_x$ | 1% $Co/CuMnO_x$ | 2% $Co/CuMnO_x$ | 5% $Co/CuMnO_x$ |
|---|---|---|---|---|
| **2°C/min** | 423 | 425 | 422 | 423 |
| **5°C/min** | 448 | 443 | 443 | 436 |
| **10°C/min** | 443 | 449 | 453 | 467 |
| **20°C/min** | 470 | 473 | 458 | 464 |

**Table 5.6.3.2 - Details of $T_m$ (K) for the 6h aged cobalt doped catalysts as a function of TPR ramp rate**

| Catalyst | $E_a$ (kJ/mol) |
|---|---|
| $CuMnO_x$ | 70.1 |
| 1% $Co/CuMnO_x$ | 88.5 |
| 2% $Co/CuMnO_x$ | 73.9 |
| 5% $Co/CuMnO_x$ | 63 |

**Table 5.6.3.3 - Table of estimated activation energies for the cobalt doped catalysts aged for 6h**

Differences in the activation energies of this first peak were evident between the samples based on the calculations using the reduction temperature of the most reducible component in the sample. For the cobalt-doped catalysts, the activation energy of reduction, was calculated to decrease as the cobalt content in the catalyst was increased. The value recorded for the hopcalite catalyst was intermediate to the activation energies of the 2 and 5% doped sample. In summary, activation energy increased in the order:

$$E_a(5\%\ \text{doped}) < E_a(CuMnO_x) < E_a(2\%\ \text{doped}) < E_a(1\%\ \text{doped})$$

The 5% cobalt-doped catalyst was the only doped sample investigated which possessed a lower activation energy barrier than that of hopcalite. The 2% doped $CuMnO_x$ which exhibited the highest estimated activation energy of reduction also was observed to be the most active catalyst in terms of CO conversion (See Chapter 5.6.4 for catalytic activity data). It therefore did not seem probable that the enhanced activity of the 2% doped catalyst was due to a lowering of energy of activation that may have resulted from the addition of cobalt to the sample, as the estimated $E_a$ values did not support this hypothesis. It should be noted here that the 2% $Co/CuMnO_x$ catalyst contained a significantly smaller quantity of the species reduced at lowest temperature compared to the others tested.

## Thermal Reduction Activation Energies of $CuO_x$ and $MnO_x$

For the sake of comparison, samples of copper and manganese oxide were prepared using the same co-precipitation procedure that was used to synthesise the mixed oxides. The single metal oxide precursors were dried and calcined as outlined in chapter 2 to produce a single oxides of copper and manganese. TPR experiments were carried out on these catalysts in the same way as for the cobalt doped mixed oxides to yield values for the activation energy of reduction for $CuO_x$ and $MnO_x$.

| $\beta$ | $CuO_x$ | $MnO_x$ |
|---|---|---|
| 2°C/min | -9.4193443 | -9.943092807 |
| 5°C/min | -8.72013403 | -9.284036831 |
| 10°C/min | -8.41529888 | -8.148320725 |
| 20°C/min | -8.14476 | |

**Table 5.6.3.4 - $-\ln\left(\frac{\beta}{T_m^2}\right)$ for $CuO_x$ and $MnO_x$ catalysts aged for 6h as a function of TPR ramp rate**

| $\beta$ | $CuO_x$ | $MnO_x$ |
|---|---|---|
| 2°C/min | 430 | 477 |
| 5°C/min | 448 | 505 |
| 10°C/min | 485.5 | 524 |
| 20°C/min | 535.5 | |

**Table 5.6.3.5 - $T_m$ (K) for $CuO_x$ and $MnO_x$ catalysts aged for 6h as a function of TPR ramp rate**

On plotting the graph to calculate activation energy, it results that $CuO_x$ has an $E_a$ of 20.3 kJ/mol and $MnO_x$ an $E_a$ of 52.3 kJ/mol. Errors in the estimated $E_a$ values were likely to be in the order of 10% after inter analysis variations were considered. The values of $E_a$ estimated for the single metal oxide catalysts indicated that the mixed oxide species were unlikely to be a simple mixture of the individual oxides as the $E_a$ values of the mixed species were not a simple additive effect of the individual oxide values.

## 5.6.4 - Catalytic Activity

The cobalt-doped catalysts aged for 6h were tested for their oxidising ability of the standard 5000ppm CO to air text mixture. The levels of activity shown by all the samples in this ageing time were consistently high and amongst the best observed for any of ageing times investigated. The start-up activity of the hopcalite catalyst was encouragingly high with a maximum activity of greater than 70% achieved within the first five minutes of testing. This maximum activity was followed by a period of steady deactivation throughout the 2h test period, by the end of which, the activity had decreased to 58% conversion. The end conversion levels of the 1 and 5% cobalt-doped catalysts were similar to that of the 6h aged hopcalite sample as was the rate of deactivation with time on-line, however, the start-up activity of these two doped catalysts was slower than for the undoped catalyst and the maximum conversion reached was also at a slightly lower level.

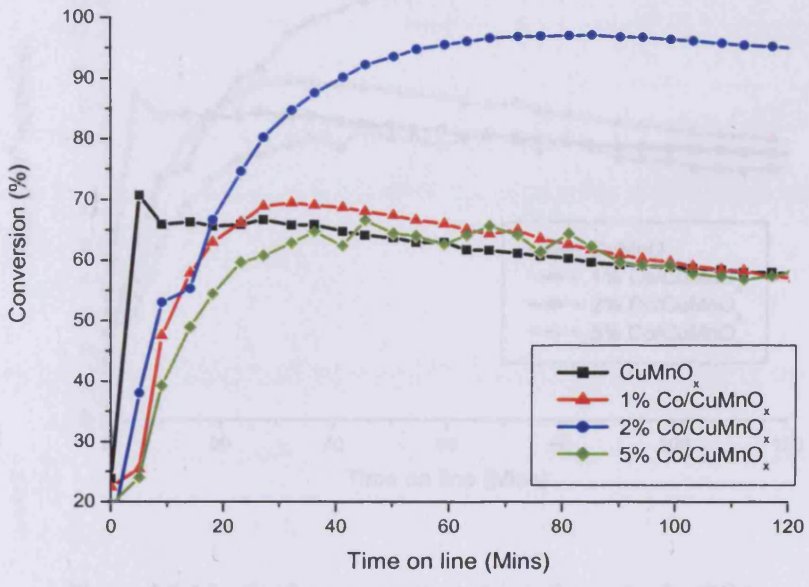


**Figure 5.6.4.1 – CO oxidation activity of 6h aged Co doped $CuMnO_x$ catalysts**

Perhaps the most interesting result observed for this catalyst set was that of the 2% cobalt-doped catalyst. The start-up activity was intermediate to those of the un-doped and the 1% doped hopcalite, however, the catalyst continued to increase in activity with increasing time on-line. This mode of behaviour was significantly different from what had come to be regarded as normal behaviour from the systems tested to this point. The 2% doped catalyst reached an initial conversion of 53% after the first 10 minutes of tested, however during the next 50 minutes on-line, the activity rose steadily to a maximum level of CO conversion of >95%, a level at which it stayed for the remainder of the test period with little deactivation recorded. The 6h aged 2% cobalt-doped catalyst possessed the highest maximum activity of all the catalysts tested to this point, as well as possessing the highest end activity of all the catalysts investigated after the 2h test period.

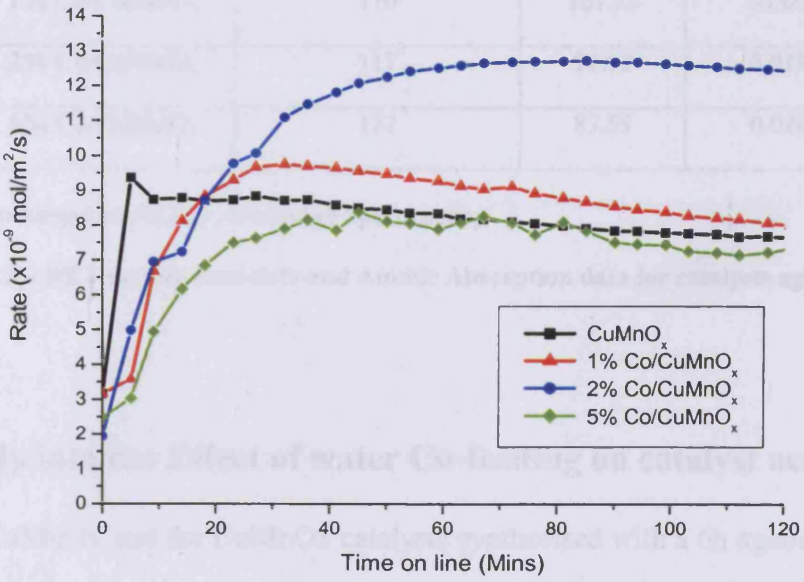


**Figure 5.6.4.2 – Surface area adjusted reaction rates for CO oxidation over 6h aged Co doped $CuMnO_x$ catalysts**

The BET 5-point surface areas of the four samples were all generally higher than those observed for the samples of other ageing times, being measured in the region of 110-122m$^2$/g. On adjusting the activities for the small differences in surface areas, the

maximum conversion exhibited by the 2% doped sample was in the region of $1.3x10^{-8}$ $Mol/m^2/s$. This was the highest surface area adjusted, rate of CO conversion exhibited by any of the catalytic systems tested throughout the study of the effects of ageing times and percentage cobalt doping. The start-up CO conversion rate of the hopcalite sample aged for 6h was the highest initial CO conversion rate observed during the test reaction regardless of ageing time, with a conversion of $9.4 \times 10^{-9}$ $Mol/m^2/s$ reached after less than 5 minutes on-line.

On analysis of the catalyst samples by AAS, the cobalt to copper ratios calculated were conducive with the intended values.

| Catalytic System | Surface area ($m^2/g$) | C - value | Co/Cu ratio* |
|---|---|---|---|
| $CuMnO_x$ | 116 | 73.32 | 0.000 |
| 1% $Co/CuMnO_x$ | 110 | 101.53 | 0.009 |
| 2% $Co/CuMnO_x$ | 117 | 91.92 | 0.019 |
| 5% $Co/CuMnO_x$ | 122 | 87.59 | 0.048 |

* measured by Atomic Absorption Spectroscopy

**Table 5.6.4.3 – BET surface area data and Atomic Absorption data for catalysts aged for 6h**

## 5.6.5 - Study into the Effect of water Co-feeding on catalyst activity

The 2% Co/CuMnOx and the CuMnOx catalysts synthesised with a 6h ageing time both produced some interesting results for CO oxidation. These active species were tested for their response towards the addition of small amounts of water to the reactant feed gas. In order to moisten the 5000ppm CO to air mixture, the test gas was passed through a water saturator at room temperature and then at 0°C. At room temperature, the gas stream would contain typically 3% $H_2O$, while at 0°C, the gas feed typically contained

<1% water. A placebo test was also carried out where the feed gas was passed through a molecular sieve, in order to give results using a totally "dry gas". Typically, each of the active catalysts had reached its maximum activity after a period of 40 minutes on-line under normal testing conditions, at which point water was introduced to the feed gas.

### 5.6.5.1 - Water co-feeding experiments over 2% Co/CuMnO$_x$

During the co-feeding with water experiments, the feed gas was first passed through the water saturator then over the catalyst after 40 minutes of testing. Deactivation was almost instantaneous, after only 8 minutes of passing the moistened gas over the catalyst, the carbon monoxide conversion was effectively zero. Under normal conditions, where the feed gas used was not dried before use, experiments took place with gas straight from the cylinder. In the dry gas experiments, the feedstock mixture was passed through a molecular sieve trap in order to remove any $H_2O$ present that might impact on activity.

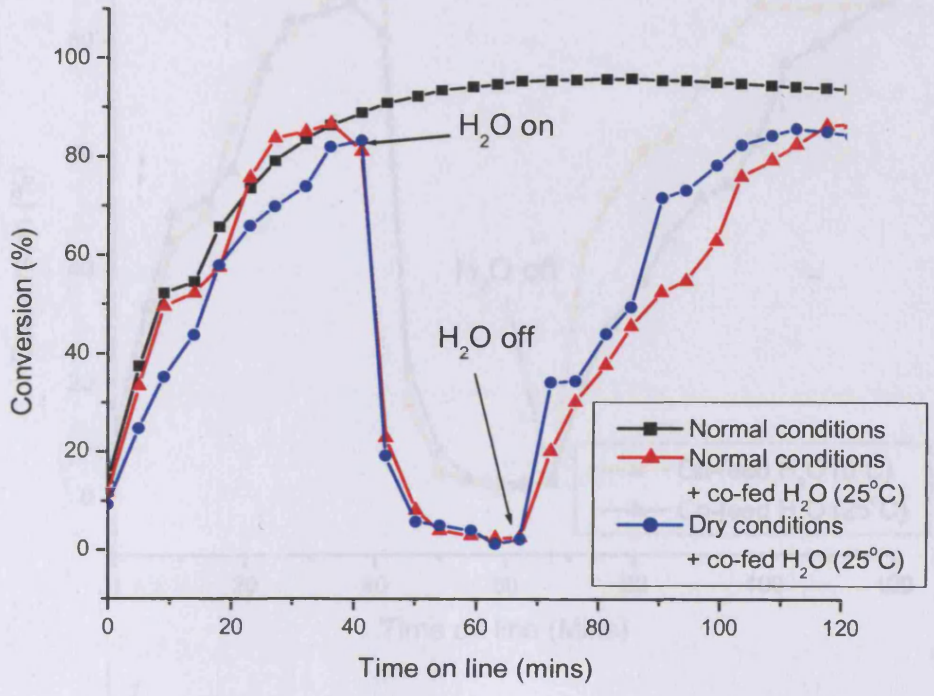


**Figure 5.6.5.1.1 – Water co-feeding experiments over 2% cobalt doped CuMnO$_x$, 6h aged**

When looking at the first 40 minutes on-line, no increase in activity was observed when using the dry gas over the normal test conditions, leading to the conclusion that little water vapour was present in the reactant feed gas . Deactivation was equally as rapid for both the dry gas and the normal conditions when water vapour was introduced. After almost 30 minutes of co-feeding water vapour over the catalyst, water ceased to be added to the feed gas, resulting in the catalyst starting to reactivate. The rate of reactivation was slightly quicker where the dry gas was used as compared to the normal reaction conditions. In both cases, when water was withdrawn from the test conditions, the catalyst activity returned almost to the level of conversion displayed by the catalyst system where no water vapour had been introduced. It was possible to conclude from this that the poisoning of hopcalite due to the presence of water vapour was only a temporary effect.

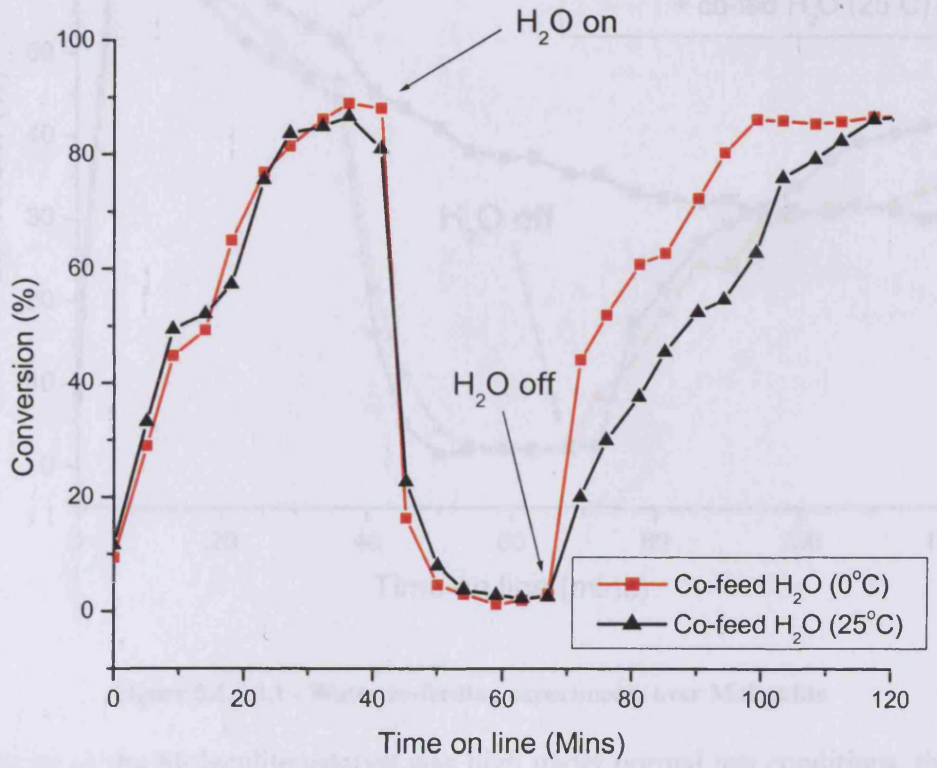


**Figure 5.6.5.1.2 - Water co-feeding experiments over 2% cobalt doped $CuMnO_x$, 6h aged**

A further experiment was carried out with the water saturator at 0°C where a lower percentage of the gas stream would have been saturated. It was interesting to observe an equally as rapid deactivation of the catalyst, leading to the conclusion that the catalyst system was very sensitive to the presence of water vapour, even at very low levels. When the water co-feeding was ceased, it was possible to observe a substantially quicker return to the original activity where the reactant gas was co-fed with water at 0°C as compared to co-feeding at 25°C.

### 5.6.5.2 - Water co-feeding experiments over Moleculite

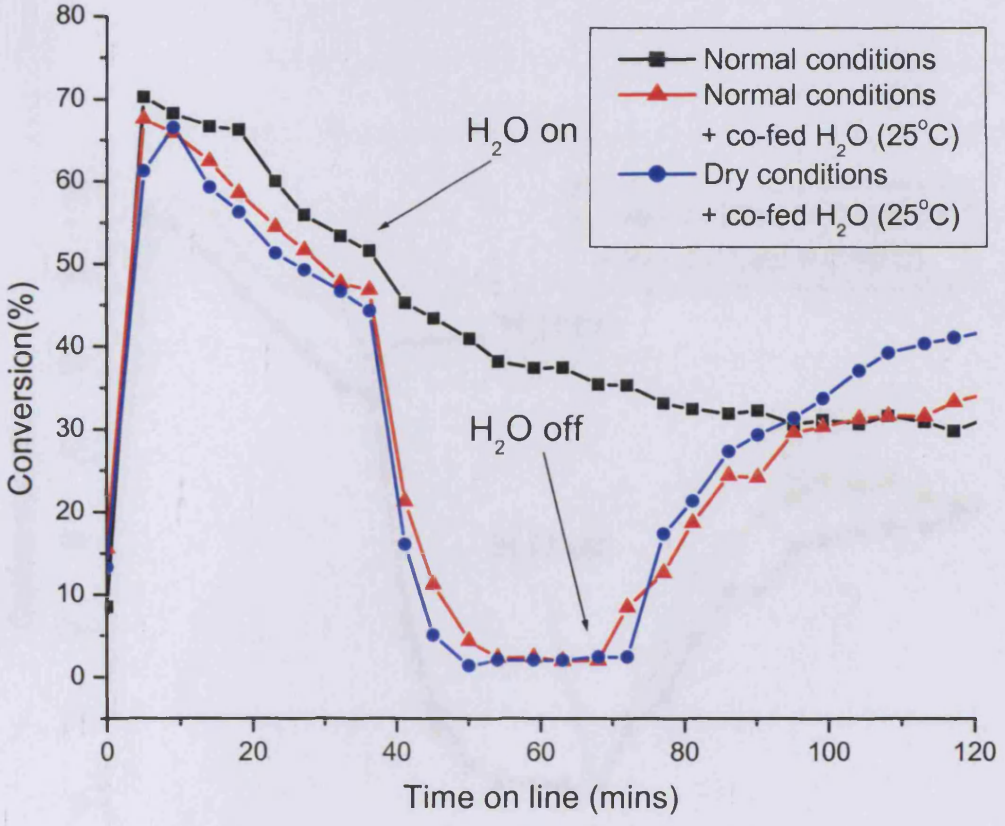


**Figure 5.6.5.2.1 - Water co-feeding experiments over Moleculite**

The activity of the Moleculite catalyst was high under normal test conditions, though it was seen to decrease rapidly with time on-line over the 2h test period. On the addition of water to the feed gas, the catalytic activity rapidly declined to zero. After almost 30

minutes of water co-feeding, the water saturator was turned off and reaction conditions reverted to normal. A return to the expected activity under normal conditions was observed. A marginally quicker reactivation of the catalyst was evident where a dry feedstock gas was used as compared to the normal test conditions.

Water co-feeding experiments also took place over the Moleculite catalyst at 0°C, where the feed gas would have contained <1% water vapour. As with the 2% $Co/CuMnO_x$ catalyst, an equal deactivation was observed for the co-fed gases at 0 and 25°C. It was again evident that the reactivation of the catalyst towards its level under standard conditions was quicker where the less moist gas feed was used.

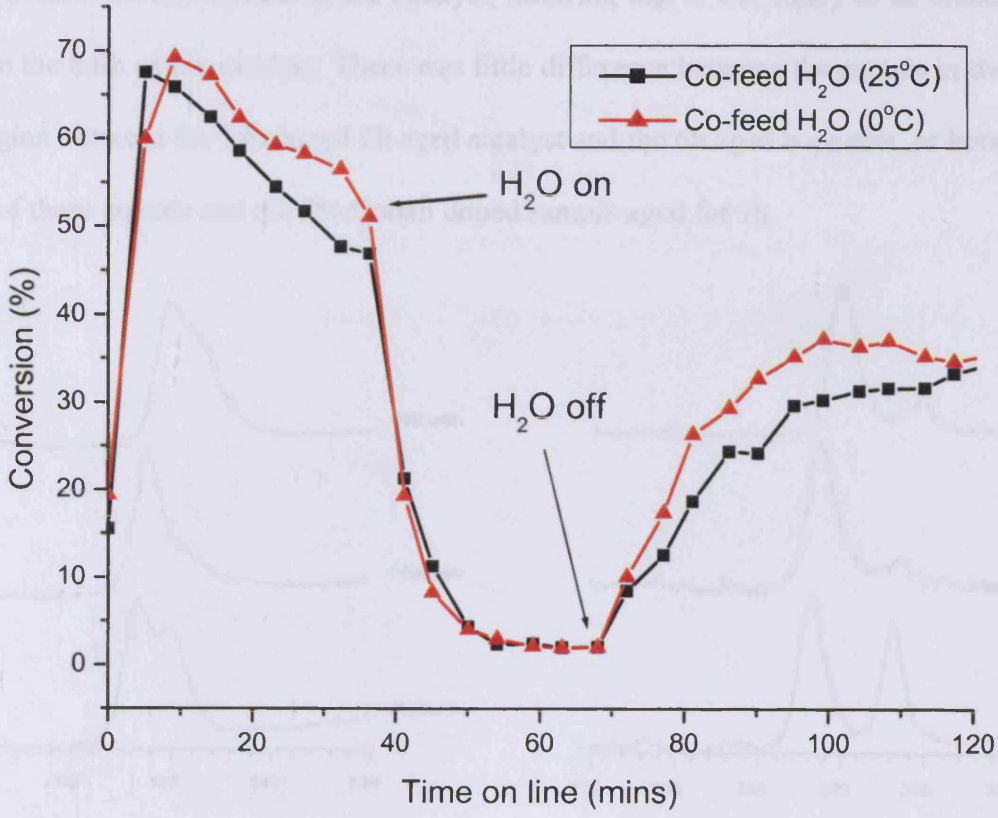


**Figure 5.6.5.2.2 - Water co-feeding experiments over Moleculite**

## 5.6.6 - XPS Studies on the 6h Aged Catalysts

XPS studies were carried out on the most active cobalt doped species produced. Details of the XPS procedure are outlined in chapter 2. Results from XPS indicated a large quantity of carbonate on the catalyst surface. This however, was unlikely to be responsible for the high activity of the 6h aged species as when compared to the relatively less active 2% cobalt-doped catalyst aged for 1h, a similar amount of carbon was observed in this system too. Surface carbonates have previously been reported to be deletrious to catalytic activity by blocking surface active sites.

XPS studies provided some interesting information about the position of cobalt within the catalyst. AAS studies had already shown that cobalt was present in the 2% doped hopcalite at the expected level, however XPS analysis showed that cobalt was unlikely to be present on the surface of the catalyst, inferring that it was likely to be contained within the bulk of the catalyst. There was little difference between the signals in the Co 2p region between the 2% doped 6h aged catalyst and the 6h aged hopcalite, or between both of these signals and the 2% Cobalt doped sample aged for 1h.

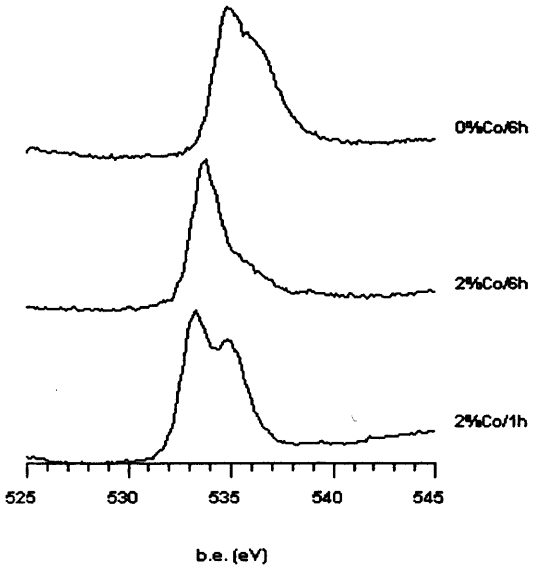


Figure 5.6.6.1 – XPS analysis of O 1s region

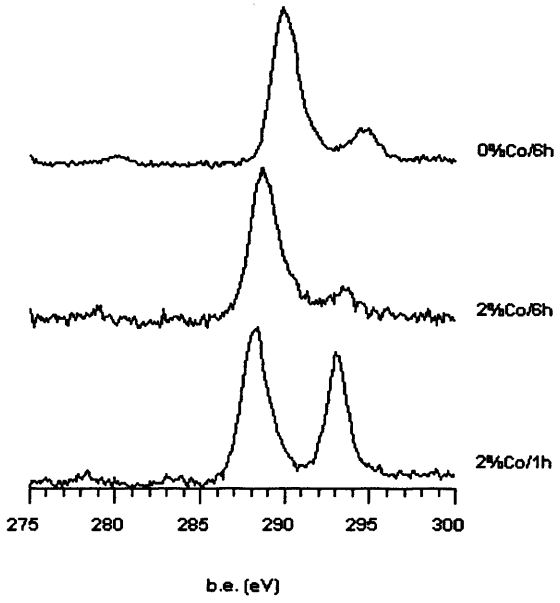


Figure 5.6.6.2 – XPS analysis of C 1s region

On further analysis of the spectral region containing information of the copper content on the catalyst surface, the signals for each of the catalysts tested were very similar, indicating copper to the present in a plus two oxidation state on the catalyst surface regardless of the ageing time or cobalt content used.

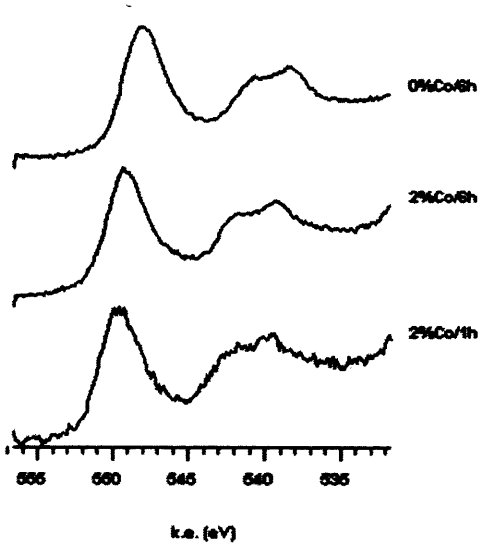


Figure 5.6.6.3 – XPS analysis of Cu 2p region

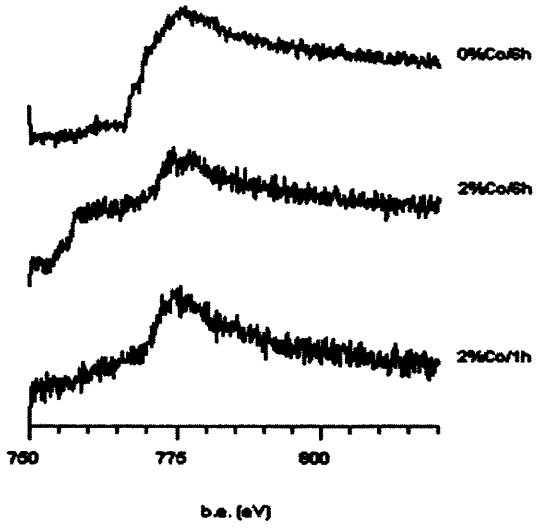


Figure 5.6.6.4 – XPS analysis of Co 2p region

XPS analysis indicated manganese to be present in a mixed oxidation state of +3 and +4. These results echoed the findings of many authors who have investigated the

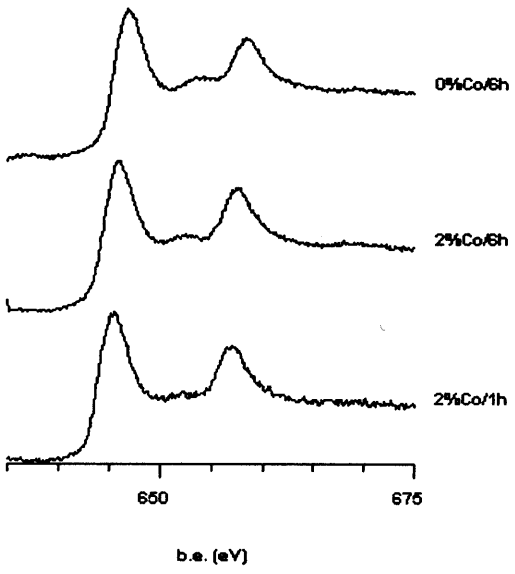


Figure 5.6.6.5 – XPS analysis of Mn 2p region

## 5.7 – Cobalt-doped catalysts produced with an Ageing Time of 12h

A series of cobalt-doped catalysts were prepared using standard co-precipitation methods. In each case, an ageing time of 12h was used during the synthesis. The catalyst precursor synthesised was dried and calcined as described in chapter 2 to yield the final catalyst.

### 5.7.1 – X-Ray Diffraction

X-ray diffraction studies were carried out on the 12h aged, cobalt-doped hopcalite precursors using an Enraf Nonius diffractometer in a method outlined in chapter 2. As for the other ageing times, it was not possible to determine the bulk structure of the species tested using XRD, as the samples were either amorphous to x-ray diffraction or microcrystalline in nature.

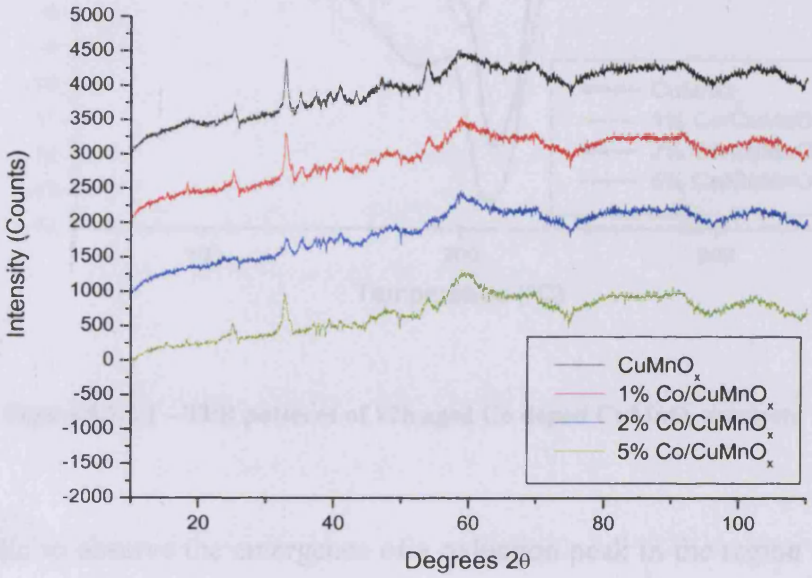


**Figure 5.7.1.1 – XRD of 12h aged Co doped $CuMnO_x$ catalyst precursors dried at 100°C, 16h**

Broadly, there were little in the way of differences between the XRD patterns of the 12h catalyst precursors, except to note that the reflection due to presence of CuO in the 2%

cobalt-doped sample was less intense than in the other samples tested. The similarity in the XRD patterns for each of the 12h aged samples indicated that the all the samples were similar in composition regardless of cobalt content.

## 5.7.2 - Temperature Programmed Reduction

On analysis of the TPR profiles of the 12h aged catalysts, a general shift of the reduction peaks to lower temperature with increasing cobalt content; as was observed for the majority of the other ageing times, was not as obvious for this sample set.

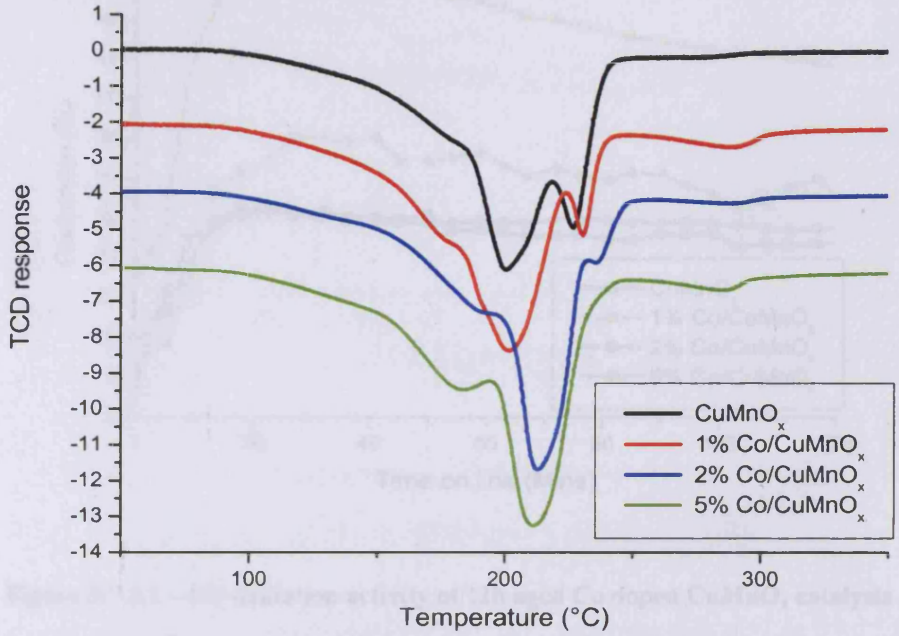


**Figure 5.7.2.1 – TPR patterns of 12h aged Co doped $CuMnO_x$ catalysts**

It was possible to observe the emergence of a reduction peak in the region of 280°C as the cobalt content was increased, this peak may have been due to the reduction of a small amount of $CoO_x$. An obvious difference between the TPR patterns of the un-doped and 1% doped species compared to the 2 and 5% doped catalysts was the relative ratios of the reduction peak areas. In all cases the peak due to the reduction of the mixed

$CuMnO_x$ species predominated, however in the 0 and 1% doped catalysts, the peaks due to the reduction of $MnO_x$ were larger than those due to the reduction $CuO_x$, but in the 2% and 5% doped samples, the opposite was true.

### 5.7.3 - Catalytic Activity

The cobalt-doped catalyst aged for 12h were tested for their oxidising ability of the standard 5000ppm CO to air text mixture.

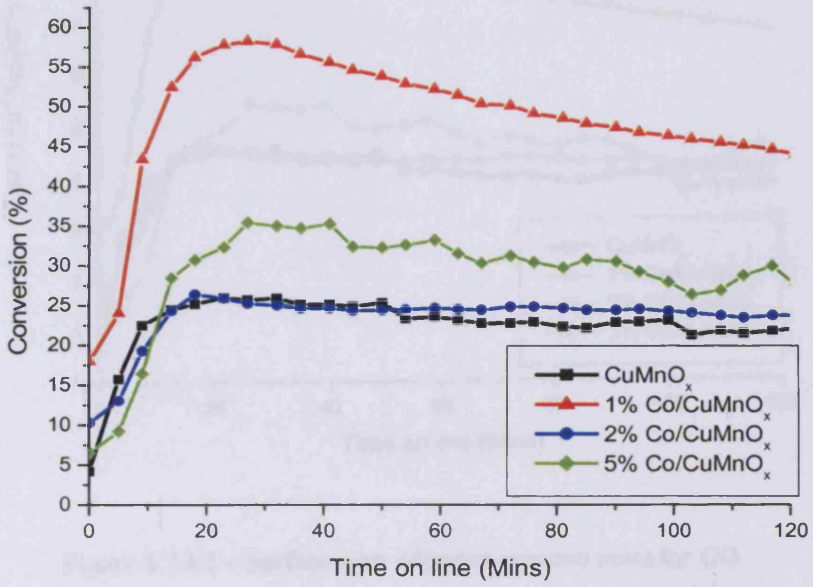


**Figure 5.7.3.1 – CO oxidation activity of 12h aged Co doped $CuMnO_x$ catalysts**

In general, levels of activity were lower than for the catalysts aged for a shorter period. The undoped and 2% cobalt-doped sample both displayed similar start up activities, maximum conversion levels and an even level of stability throughout the 2h test period. The stability of these two systems with time on line was excellent` with little deactivation observed, however the maximum conversions reached were only in the region of 27%; a low level in comparison to other results observed to this point. The 5% doped sample displayed a slightly higher maximum conversion level during the test

period but its start-up activity and level of stability were poorer than those observed for the 0 and 2% doped samples. The most active catalyst of this set was the 1% doped with activity reaching a maximum activity of 58% after 20 minutes on line. This catalyst deactivated substantially over the 2h test period, ending with an activity level of just over 45% conversion.

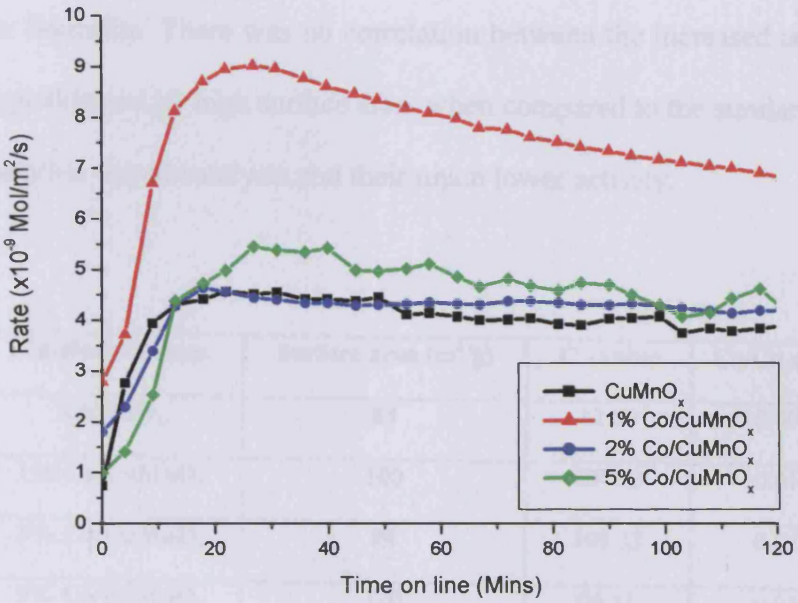


**Figure 5.7.3.2 – Surface area adjusted reaction rates for CO oxidation over 12h aged Co doped $CuMnO_x$ catalysts**

On adjusting the activity of the catalysts to take into account differences in surface areas, the rate of CO conversion per square metre per second of the catalyst was calculated. The values calculated for the 2 and 5% cobalt-doped hopcalite as well as the hopcalite itself were low in comparison to those already discussed in this study with a conversion level of around $4.5 \times 10^{-9}$ Mol/m$^2$/s. Catalyst stability in all three cases was satisfactory with little in the way of deactivation observed throughout the test period. The start-up conversion activity of the 1% doped hopcalite was competitive towards others investigated in this study, however substantial deactivation occurred throughout

the test period, decreasing from the maximum conversion rate of $9.1x10^{-9}$ $Mol/m^2/s$ to $7x10^{-9}$ $Mol/m^2/s$ at the end of 2h test period.

On comparison of the BET surface area of the 12h aged catalysts set, it was apparent that the cobalt-doped catalysts possessed slightly higher surface areas than the un-doped hopcalite. Surface areas of the doped catalysts were in the range 94-120$m^2/g$ compared to 88$m^2/g$ for hopcalite. There was no correlation between the increased activity of the 1% doped hopcalite and its high surface area, when compared to the similar surface area values for the other doped catalysts and their much lower activity.

| Catalytic System | Surface area ($m^2/g$) | C - value | Co/Cu ratio* |
|---|---|---|---|
| $CuMnO_x$ | 88 | 82.09 | 0.000 |
| 1% $Co/CuMnO_x$ | 100 | 104.93 | 0.010 |
| 2% $Co/CuMnO_x$ | 94 | 109.32 | 0.023 |
| 5% $Co/CuMnO_x$ | 120 | 96.53 | 0.050 |

* measured by Atomic Absorption Spectroscopy

**Table 5.7.3.3 – BET surface area data and Atomic Absorption data for catalysts aged for 12h**

## 5.7.4 – TEM Analysis

A selection of catalysts and precursors were analysed using Transmission Electron Microscopy experiments. The intention was to probe any differences in the structure of the materials that were not evident from the XRD experiments. An introduction to the TEM technique is given in chapter 2.

On TEM analysis, the cobalt doped catalysts were typically seen to comprise of needle like particles, which were more often than not decorated with small irregularly shaped particles and spindly material (Figure 5.7.4.1)). A clear difference evident between the cobalt-doped catalyst precursor (Figure 5.7.4.3) and the calcined catalysts was that in the later the needles were more crystalline and appeared to be composed of separate particles while retaining the overall shape of the needle.

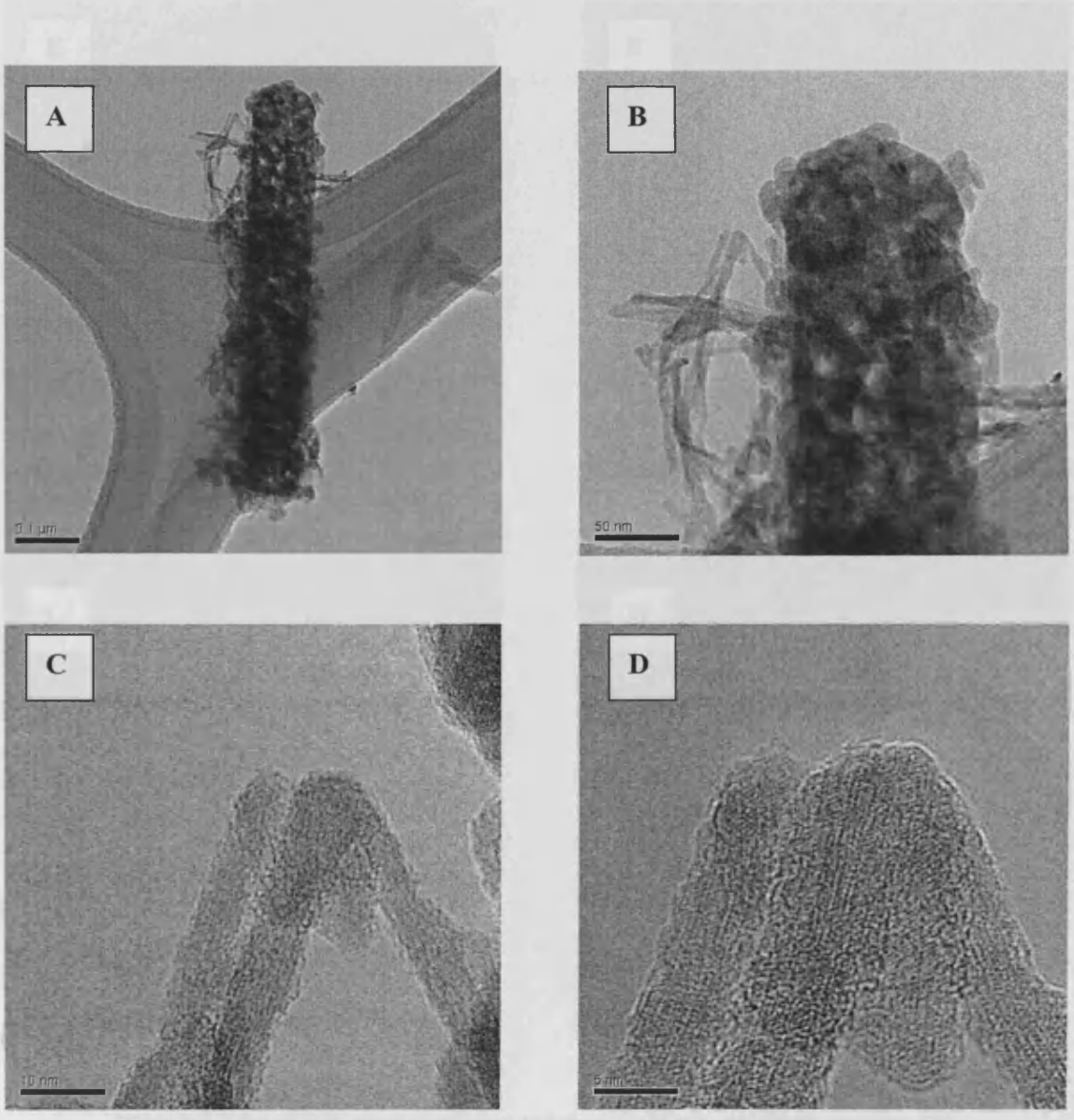


**Figure 5.7.4.1 –TEM analysis of 1% cobalt doped catalysts aged for 12h**

It was difficult to determine the precise location of the cobalt in the 1% doped $CuMnO_x$ sample however, it was thought to be present in the needle like particles of the cobalt doped catalysts. (C-D) Estimated particle size from the TEM micrograph data were in the region of 5-10nm, this might explain the difficulty of applying XRD to these samples as this crystallite size was at the far end of the sensitivity level associated with the technique

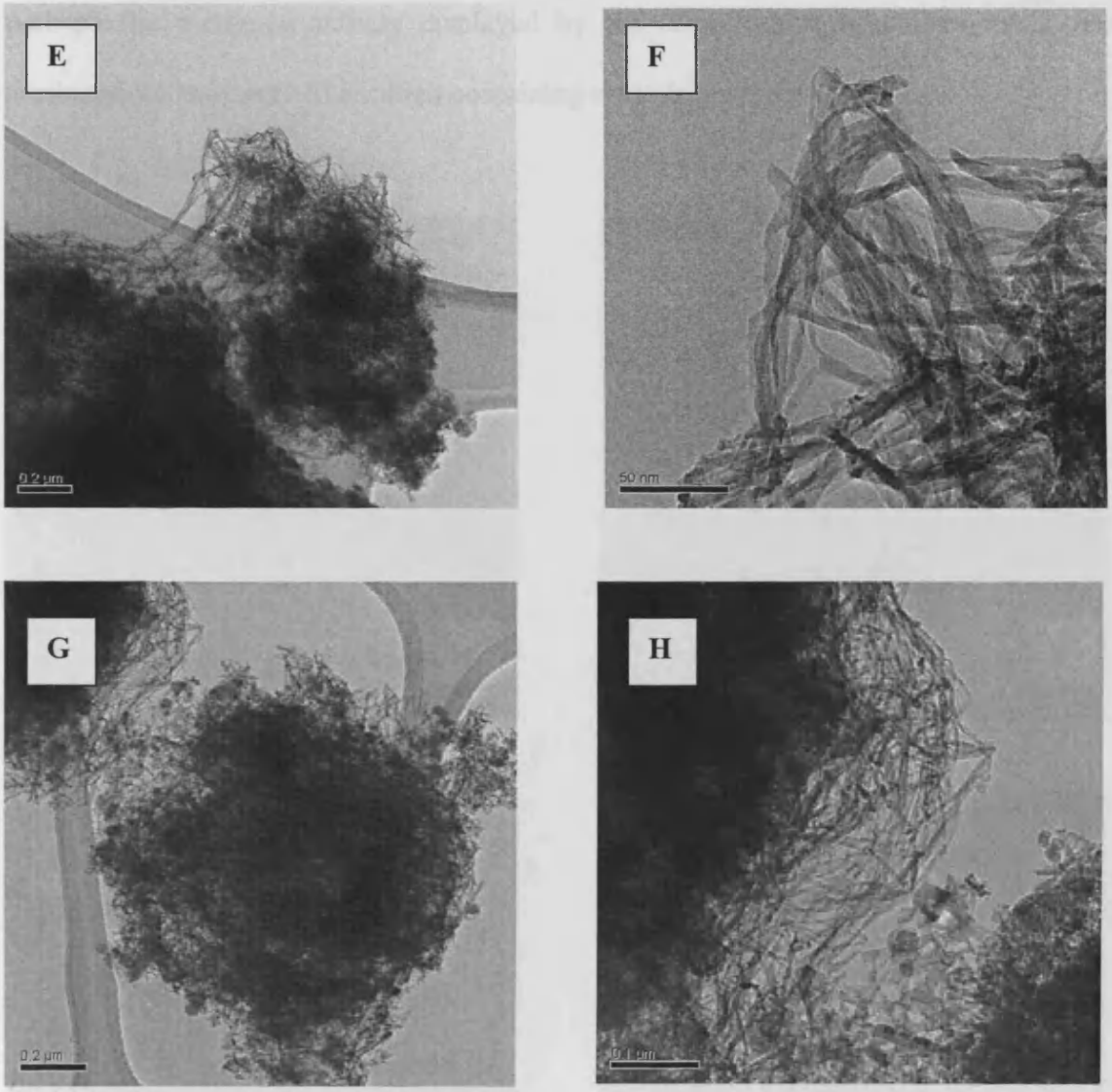


**Figure 5.7.4.2 –TEM analysis of the undoped $CuMnO_x$ catalysts aged for 12h**

The undoped $CuMnO_x$ catalysts possessed a very different morphology to the cobalt doped samples. The major morphology type here was an almost spherical agglomerate

composed of small irregularly shaped material combined with, and in many cases coated with, some of the spindly like material observed in the doped samples. (E-H) This spherical type structure was similar to one reported by Mirzaei in a past study in to copper manganese oxide based catalysts. [3]

A large difference was observed in activity between the doped and un-doped catalysts, perhaps the increased activity displayed by the cobalt-doped hopcalites could be attributed to the needle-like, cobalt containing crystals observed there-in.

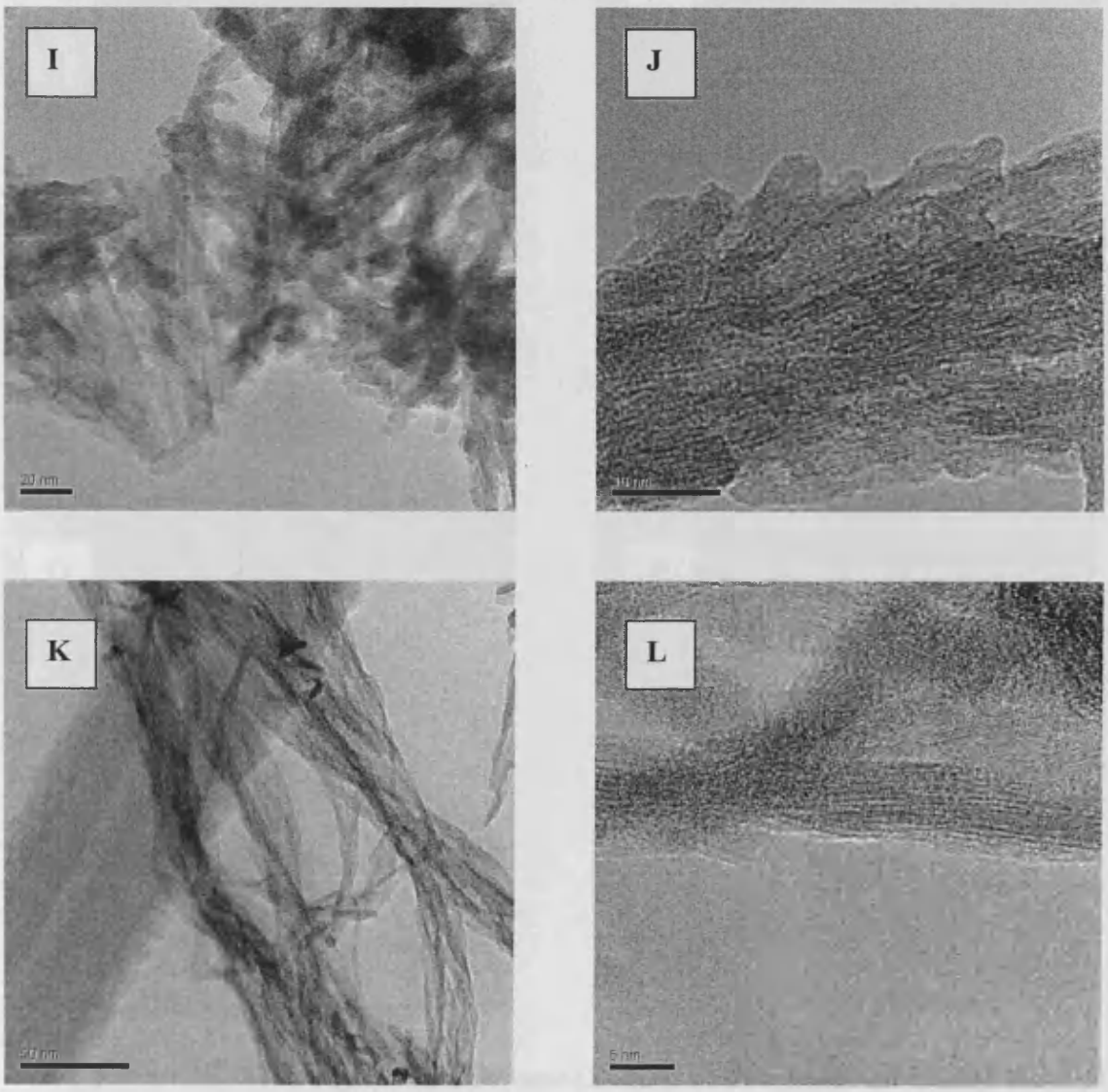


**Figure 5.7.4.3 – TEM analysis of 1% cobalt doped catalyst precursors aged for 12h**

The 1% doped $CuMnO_x$ catalyst precursors were composed of an irregular distribution of needle like fibres. The fibres did not appear to be well defined and were not as crystalline as those fibres observed in the final catalyst after the calcination step had been carried out. When compared to the TEM micrographs of the un-doped catalyst precursors aged for 12h, there were some obvious differences. The poorly formed needle-like structures were again present but on this occasion they were inter-dispersed amongst spherical agglomerates of particles that were the main component of the precursor (see figure 5.7.4.4).

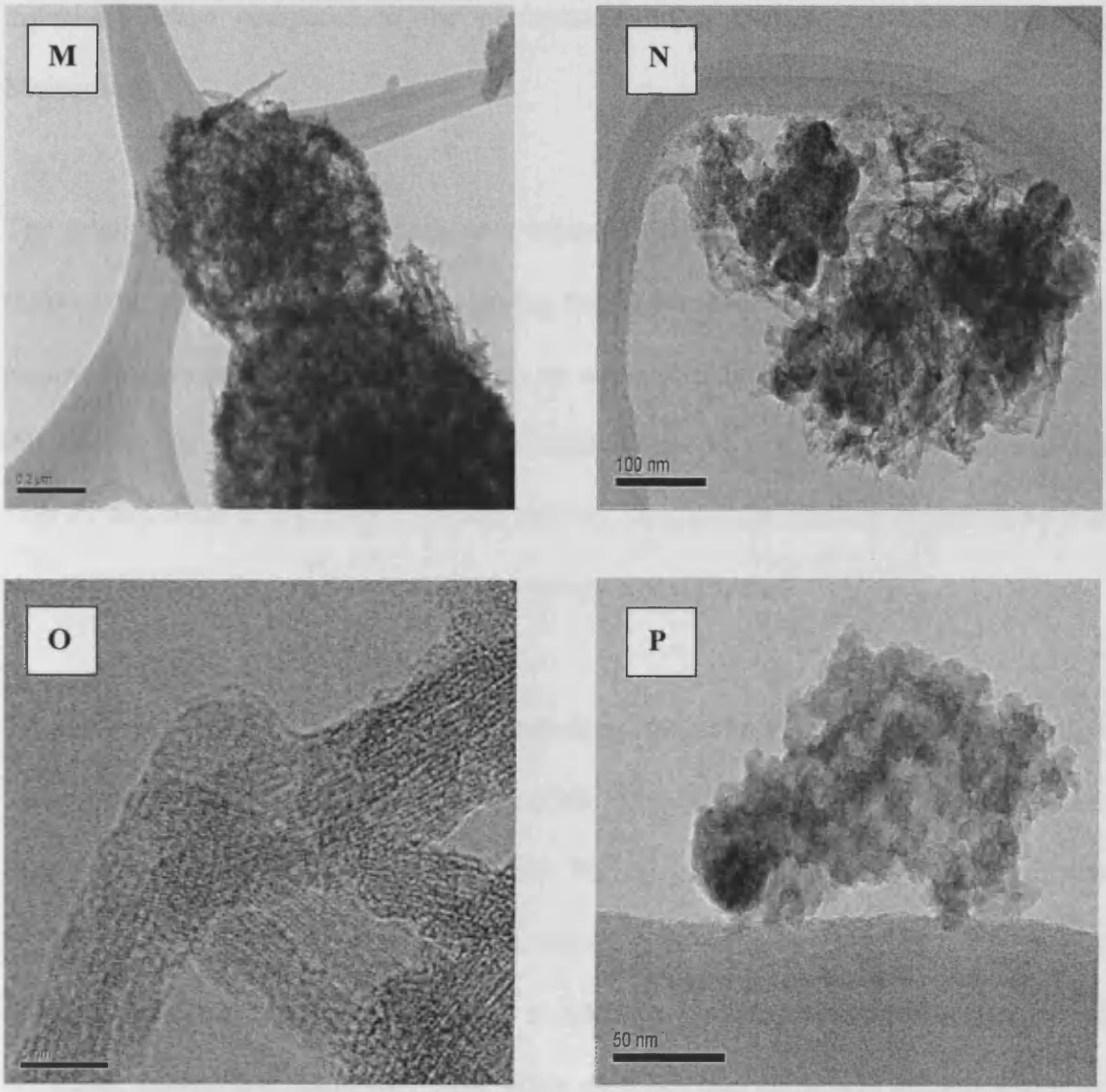


**Figure 5.7.4.4 –TEM analysis of the undoped $CuMnO_x$ catalyst precursors aged for 12h**

The agglomerates were needle-like structures that appeared less well defined in the precursor as compared to the catalyst. This observation underlined the importance of the calcination step during the formation of catalysts active for the oxidation of carbon monoxide.

## 5.8 -Discussion

### 5.8.1 - Activities and Surface Area Adjusted Conversion Rates.

The investigation in to ageing times and cobalt doping yielded some interesting results, especially when compared to the performance of a leading commercial catalyst, Moleculite.

The relative activities and surface area adjusted conversion rates of all the catalysts tested were compared at three times during the 2h test period. Firstly, after 10 minutes on-line to give an indication of the start-up activity of the catalyst, secondly after 30 minutes, as by this point almost all the catalysts tested had reached their maximum activity and were in a period of steady activity, then finally after 2h of testing so that deactivation over the test period could be adequately compared.

On displaying the activities of all the cobalt-doped hopcalites synthesised and discussed in this chapter in a single graph, at a specific time on line, it became easier to draw comparisons between different catalyst sets. Figure 5.8.1.1 shows that after 10 minutes online; a period referred to previously in this study as the start-up activity, only one of the catalysts synthesised during the study rivalled the start-up activity of the commercial hopcalite, Moleculite. However, three other catalysts also displayed activities greater than 50% at this time on line, a level that could be regarded as a benchmark for activity.

The most active of the catalysts at this point during the 2h test period was the standard hopcalite catalyst produced with a 6h ageing time.

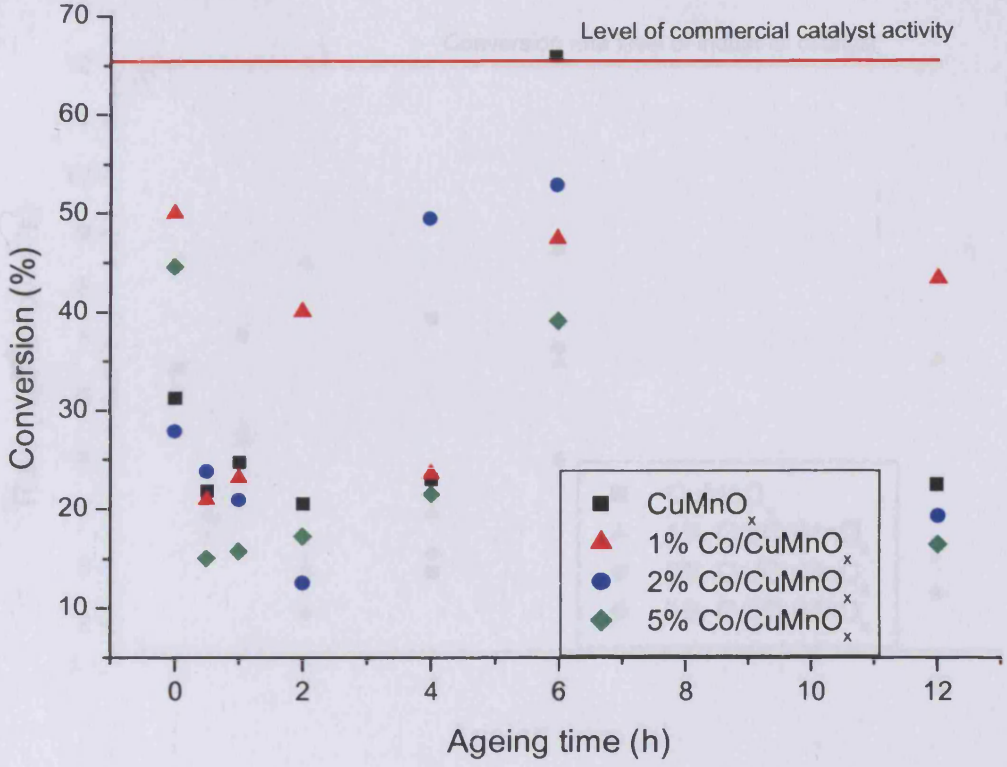


**Figure 5.8.1.1– Comparison of start up activity levels after 10 minutes on-line as a function of ageing time and % cobalt doping**

When the start-up activities were adjusted for differences in surface areas, to give a value that represented the start-up conversion rate, it was interesting to note that none of the catalysts synthesised in this study displayed an initial conversion rate in excess of that of the industrial hopcalite. The highest start-up conversion rate of the catalysts synthesised in this study was exhibited by the 6h aged hopcalite with a conversion rate of $9x10^{-9}$ Mol/m$^2$/s; significantly lower than the $1.2x10^{-8}$ Mol/m$^2$/s rate displayed by Moleculite. For many of the other ageing times investigated, doping with cobalt did have a positive increase on the conversion rate during the start-up period. The effect was particularly noticeable for the 2 and 4h aged experiments where doping with 1 and

2% cobalt respectively had the effect of trebling the conversion shown by the standard hopcalite synthesised for that ageing time.

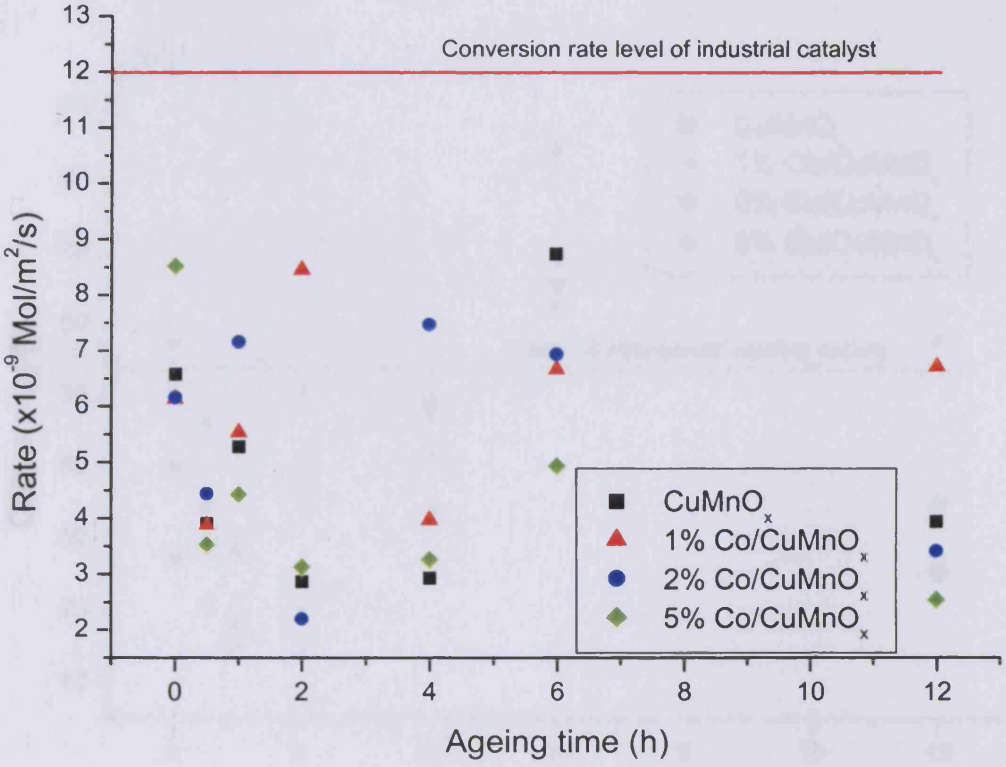


**Figure 5.8.1.2– Surface area adjusted rate of CO conversion after 10 minutes online as a function of ageing time and % cobalt doping**

After a period of 30 minutes on-line, the majority of the catalysts had reached their maximum activity and were in a period of steady state activity. The level of activity at 30 minutes on-line for each of the catalysts synthesised in this chapter is detailed in figure 5.8.1.3. The commercial catalyst Moleculite was in a period of steady deactivation at this time on-line, whereas many of the cobalt-doped catalysts were in a period of stable activity. A larger number of the catalysts discussed in this chapter displayed a greater activity than the Moleculite sample. At that point, the activities of all the catalysts synthesised with a 6h ageing time were greater than both that of hopcalite or any other of the catalysts tested here. The activities of the 1% cobalt doped catalysts aged for 0 and 12 hours were also higher than that of the commercial catalyst, adding

further weight to the theory of a promoting effect of cobalt on hopcalite. A further point of note was that the activities of the 0.5, 1 and 2h aged 1% doped catalysts were also the highest displayed for catalyst in their respective ageing time sets.

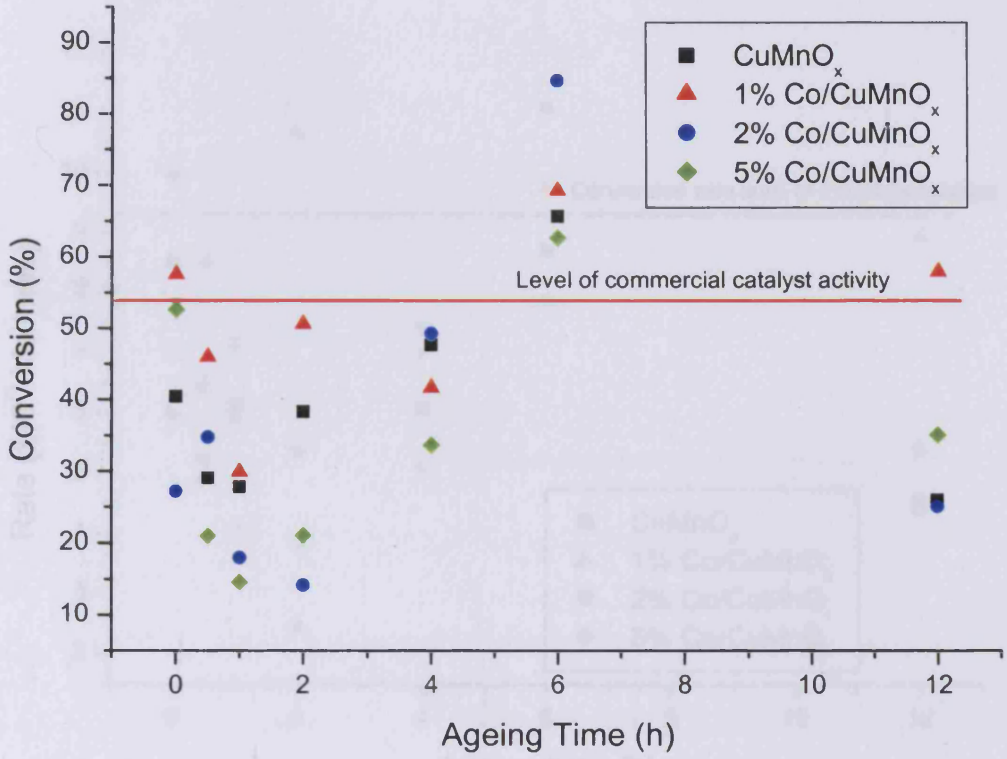


**Figure 5.8.1.3 – Comparison of start-up activity levels after 30 minutes on-line as a function of ageing time and % cobalt doping**

On adjusting the activity at 30 minutes on-line for differences in surface areas to give a rate of CO conversion per $m^2$ per second, four of the catalysts tested displayed increased conversion rates over the industrial catalyst. This, when compared to the fact that none of the catalysts tested reached a conversion rate higher than that of the commercial catalyst at 10 minutes online, was an indication that the cobalt-doped catalyst were becoming more competitive with increased time on-line. The highest conversion displayed here was by the 6h aged 2% cobalt doped catalyst at $1.13 \times 10^{-8}$ Mol/$m^2$/s, closely followed by the 1% Co doped 2h aged catalyst at 1.08 Mol/$m^2$/g. For all the ageing times investigated, at least one or more of the cobalt-doped catalyst displayed a

higher CO conversion than that of the corresponding hopcalite for that ageing time at 30 minutes on-line, thus adding weight to the theory of cobalt acting as a promoter for CO oxidation by hopcalite catalysts.

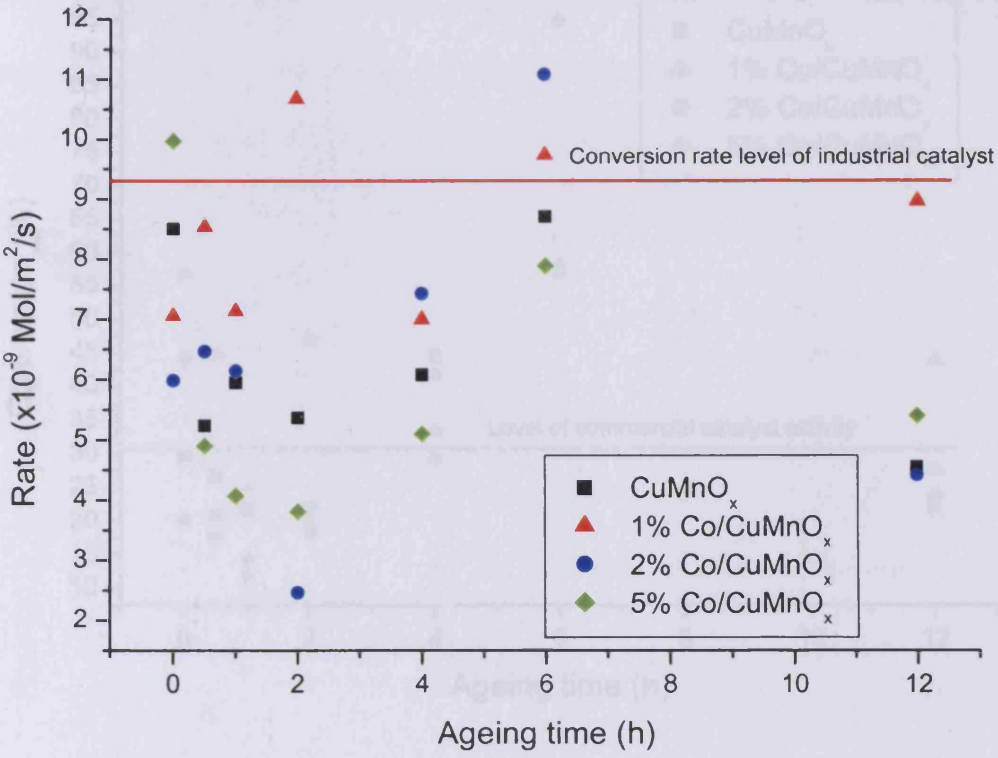


**Figure 5.8.1.4 – surface area adjusted rate of CO conversion after 30 minutes on-line as a function of ageing time and % cobalt doping**

At the end of the 2h test period, when the commercial catalyst activity had fallen to only 31%, eleven of the catalysts synthesised exhibited a higher activity than this level, with five out of these eleven still active to 50% conversion of CO or better. Particularly active were the 1% doped cobalt catalysts, where six out of the seven ageing times investigated yielded catalysts greater in activity than the commercial system. The most active of the 1% cobalt-doped set were the 0 and 6h aged samples both active to a level of 56% conversion. The most active of all the catalysts however was the 6h aged 2% doped sample that exhibited almost total conversion of the CO test mixture even after

the 2h test period finished. The activity of this system remained constant at 95% until 10h on-line, a point at which monitoring ceased. The 2% doped catalyst aged for 6h displayed a conversion level three times greater than that of the commercial catalyst.

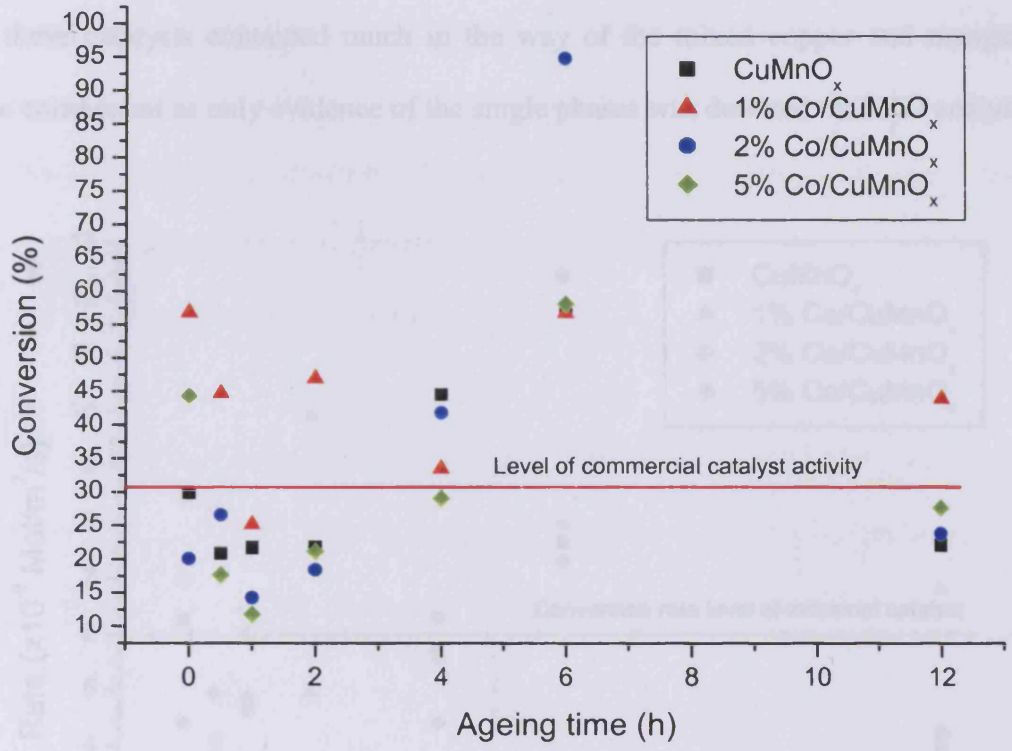


**Figure 5.8.1.5 – Comparison of start up activity levels after 2h on line as a function of ageing time and % cobalt doping**

At the end of the 2h test period, the activity of each of the catalysts synthesised was again adjusted for differences in surface areas. The catalysts were then compared to the conversion of the industrial catalyst at the same time on-line. Twelve of the twenty-eight catalysts synthesised in this study possessed conversion rates greater than that of the commercial hopcalite. In general, the cobalt-doped hopcalites displayed a higher rate of conversion than the un-doped samples as only two of the twelve catalysts which out-performed hopcalite were un-doped samples. The most active sample produced, the 2% doped 6h aged catalyst, displayed a CO conversion rate of $1.25 \times 10^{-8}$ Mol/m$^2$/s compared to only $6 \times 10^{-9}$ Mol/m$^2$/g for the commercial sample. It was interesting to note that almost all of the 1% cobalt-doped samples out-performed both the hopcalite of the

related ageing time and the commercial catalyst at this point of testing. In general, the conversion rates of those catalysts aged for the shorter periods (0.5h, 1h, 2h) were not as high as those of their longer aged counterparts at the conclusion of the test. The conversion rates of the catalysts aged for 0h were also very high but it was not thought that these catalysts contained much in the way of the mixed copper and manganese oxide component as only evidence of the single phases was detected on XRD analysis.

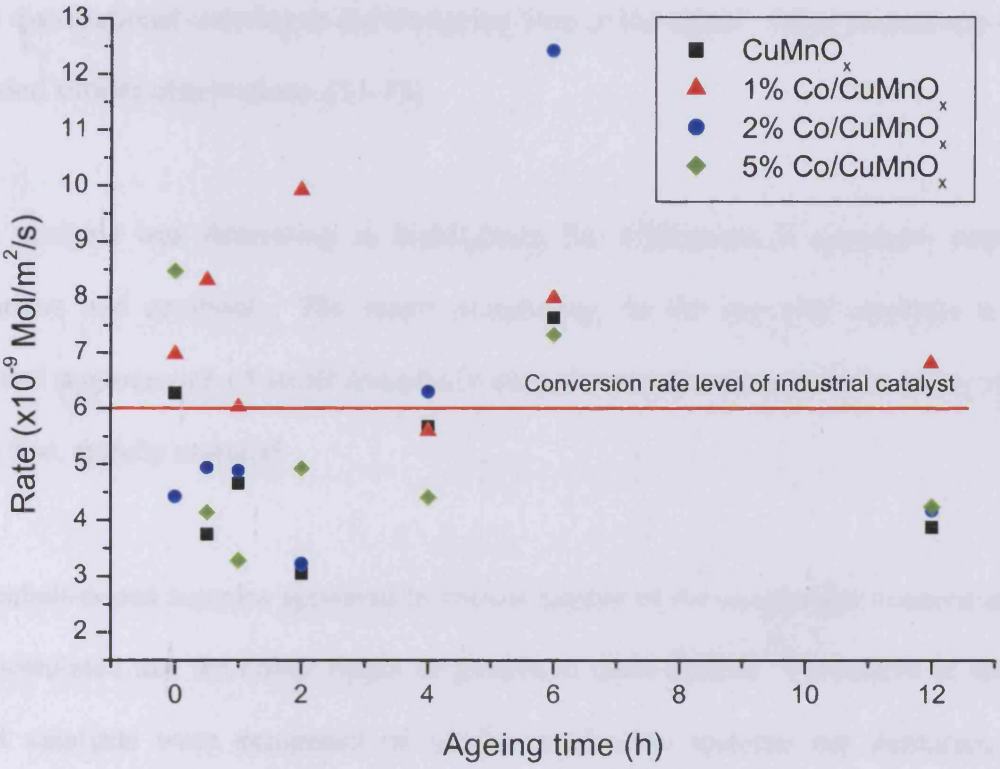


**Figure 5.8.1.6– Surface area adjusted rate of CO conversion at end of test period as a function of ageing time and % cobalt doping**

## 5.8.2 - Surface and Bulk Analysis Studies

On XPS analysis copper was found to be present in a $^{+}2$ oxidation state whereas manganese was detected in a $^{+}3$ and $^{+}4$ oxidation state regardless of whether the catalyst was doped or undoped. These findings were in line with those of Wright *et al.* who found the metals to be present in the same oxidation states in mixed oxides of copper,

manganese and cobalt. [8] It was not possible to confirm the presence of any cobalt on the surface using the XPS technique; however, the cobalt was detected as being present in the catalysts using Atomic Absorption Spectroscopy studies. TEM studies reinforced this theory as cobalt was often observed to be present in the needle-like materials that was a feature of the cobalt-doped catalysts. It was expected that cobalt would have been present in the $^{+}3$ oxidation states as observed by Wright, who observed it to be statistically distributed throughout the cubic form of the $CoMn_2O_x$ spinel and to have some distributional ordering in the tetragonal form of the spinel. Other researchers have recorded similar observations. [11-13]

TEM analysis was interesting in highlighting the differences in structures between precursors and catalysts. The major morphology in the hopcalite catalysts was a spherical agglomerate of small irregularly shaped material, along with, in many cases, some fine, spindly material.

The cobalt-doped samples appeared to consist mainly of the needle-like material and it was postulated that the cobalt might be present in these needles. Precursors of cobalt-doped catalysts were composed of similar needle-like material but definition and increased crystallinity were only achieved on calcination. Particle size identified by TEM was in the region of 5nm; a level approaching the lower detection limit of XRD. This might explain why many of the samples tested appeared amorphous to XRD, when in actual fact, they were microcrystalline in nature.

X-Ray Diffraction studies were again inconclusive in providing definitive bulk structure information. All the precursor samples synthesised possessed similar XRD traces, with the major component being a mixture of the poorly crystalline $CuCO_3$ and $MnCO_3$

along with traces of the single oxides $CuO_x$ and $MnO_x$. However, it was possible to detect subtle changes in the composition of the precursors.

On calcination under the optimum condition of 415°C for 2h in air, highly amorphous or micro-crystalline catalysts were produced. The XRD patterns for these were similar regardless of cobalt content, so much so, that differentiation between samples using this technique proved almost impossible. However, it was possible to detect a subtle decrease in crystallinity of the catalyst precursors as the ageing times were increased. This coincided with the results of Mirzaei who observed a change from a semi crystalline system at 0h ageing for the un-doped hopcalite catalyst but observed crystallinity to decrease as the ageing time was increased. [14] It was likely that during ageing, agglomeration of precipitate particles occurred to form larger particles with the process generally accompanied by a change in morphology of the precipitate. This was again an observation proved by Mirzaei in his own study of copper manganese oxide catalysts. [15] This increase of the amorphous nature of the catalysts resulting from increased ageing times coincided with a general increase in surface area of the catalysts for both the doped and un-doped samples.

### 5.8.3 – Surface Area Analysis

On analysis of the data for surface areas of catalysts as a function of varying composition and ageing times, it became apparent that there was a general increase in the surface area of many of the catalysts tested as the ageing time was increased. The presence of cobalt in the catalyst did not have a profound effect on the surface area of the catalyst. The catalyst set which possessed on average the highest surface areas was the 6h aged group closely followed by the catalysts prepared with ageing of 4h and 12h. In general, there was a correlation between activity and surface area with the highest

surface area species generally being more active. The highest surface area catalysts also tended to be amongst the most active towards the middle and the end of the 2h test period. This lead to the conclusion that perhaps these species contained a greater number of adsorption sites on the catalyst surface and that any deactivation occurring during the test period may have been due to the blocking of active sites. The effect of this would therefore have been more pronounced with time on-line for the catalysts of lower surface area where a smaller number of active sites might have been present. No differences in surface area were evident on analysis of the catalyst before and after use in the micro-reactor against the CO oxidation test reaction.

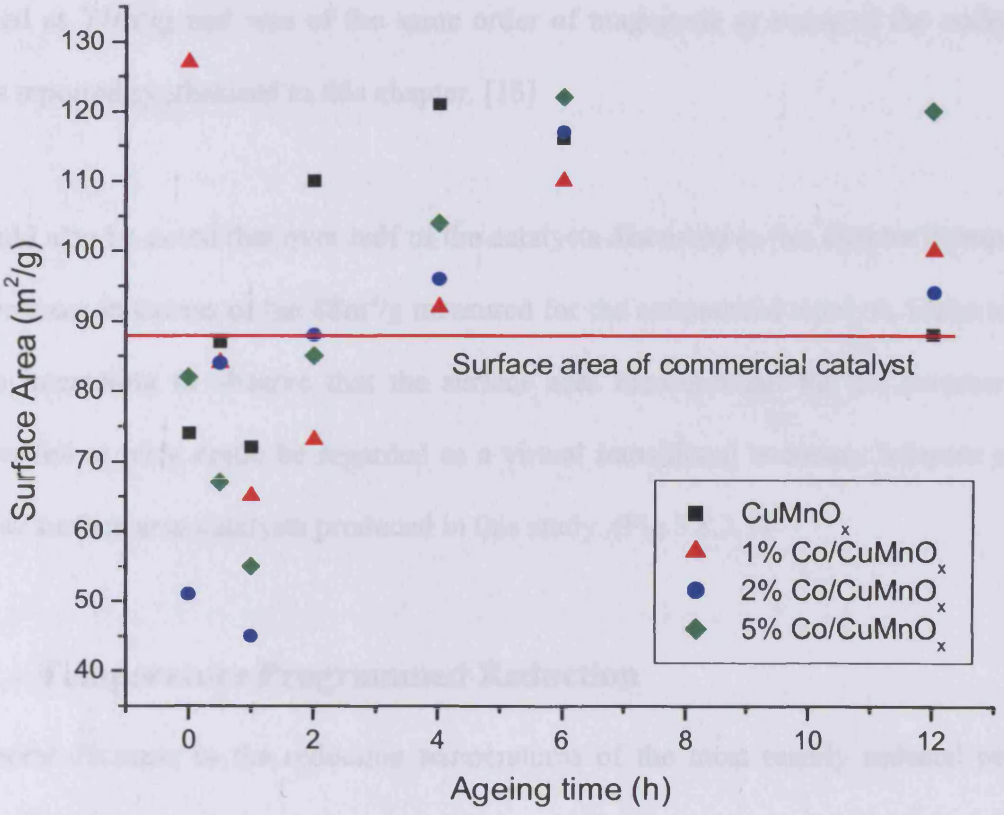


**Figure 5.8.3.1– Surface areas of calcined catalysts as a function of ageing time and % cobalt doping**

In general, all the catalysts produced possessed significantly higher surface areas than reported in other studies of hopcalite catalysts. Mirzaei reported surface areas for

copper manganese oxide catalysts to be in the range 23-31$m^2/g$ for hopcalites produced by co-precipitation of the nitrates at 80°C. [14] The findings of Wright were similar to those presented here with $CuMnO_x$ being prepared by co-precipitation of the metal nitrates at pH=8, 60°C followed by calcination at 420 °C. This procedure gave rise to catalysts with surface areas in the range of 65-79$m^2/g$, depending on the Cu:Mn composition; however, no details were given in terms of any ageing time used. When unspecified quantities of cobalt were added to the reaction mixture, surface areas were seen to increase substantially to greater than 100$m^2/g$. [8] Spassova *et al.* have also reported copper and manganese mixed oxide species prepared by a co-precipitation procedure. The surface area of the mixed oxide with a 2:1, Mn:Cu composition was reported as 77$m^2/g$ and was of the same order of magnitude as many of the undoped oxides reported synthesised in this chapter. [16]

It should also be noted that over half of the catalysts discussed in this chapter possessed surface areas in excess of the 88$m^2/g$ measured for the commercial catalyst, Moleculite. It was interesting to observe that the surface area measurement for the commercial catalyst fell at what could be regarded as a virtual transitional boundary between high and low surface area catalysts produced in this study. (Fig 5.8.3.1)

## 5.8.4 – Temperature Programmed Reduction

A general decrease in the reduction temperatures of the most readily reduced peaks occurred with increasing cobalt content. This might suggest that cobalt had the effect easing the reduction of the copper species in the catalyst during the oxidation of CO. Cocke and Veprek suggested a shift in oxidation state of copper from II to I, on reduction of the catalyst by carbon monoxide. It was highly plausible that the presence of cobalt in catalysts made this reduction step more facile. [9]

The majority of the catalyst produced in this study displayed similar TPR profiles and consisted of a mixture of $CuO_x$, $CuMnO_x$ and $MnO_x$. In some instances, it may have been possible to detect traces of $CoO_x$ in some of the doped catalysts at high T, although this was inconclusive. In general, the longer ageing times produced catalysts consisted of greater quantities of the mixed oxide species and less in the way of the single oxides, especially the $CuO_x$ component. This mixed oxide phase was a strong indicator of good catalytic activity.

Overall, the uptake of $H_2$ during the TPR procedure was a good indicator of catalytic activity. Where the uptake of $H_2$ was highest, this indicated a test catalyst rich in oxide, which generally meant a highly active catalyst. This oxide might have been readily available to take part in the reduction of carbon monoxide via a Langmuir-Hinshelwood type mechanism involving surface or lattice oxide and surface adsorbed CO from the test mixture.

When the most active, 6h aged catalyst set, was investigated using the Kissinger approach, some interesting results were obtained. This approach used data on the reduction temperature of the most easily reduced catalyst component in the catalyst, at a variety of temperature ramping rates to estimate the Activation Energy of the species. The results showed the 5% cobalt-doped to have the lowest $E_a$ (Reduction) followed by the $CuMnO_x$, 2% cobalt-doped and 1% cobalt-doped catalysts. There was little correlation between the $E_a$ values for the catalyst systems and their activity towards the test reaction. This is a good indicator that the CO oxidation may have proceeded with the use of surface adsorbed oxide that would have been more readily available to take part in the reaction.

The values of the $E_a$ (reduction) of the single copper and manganese metals oxides indicated that the value of $E_a$ for the catalyst was not merely an additive effect of the values of its single component oxides, thereby again proving the presence of a mixed oxide phase.

### 5.8.5 - Water Doping Experiments

Any amount of water vapour in the feed gas poisoned both the Moleculite and 2% $Co/CuMnO_x$ catalysts. This was not a surprising result, as it has long been known that water was a potent poison towards hopcalite systems. [17] Water has also been shown to inhibit the adsorption of oxygen on to cobalt oxide catalysts, with the resulting deactivation being attributed to the formation of surface species. [18] The presence of these surface species has been linked to the inhibition of the reduction and the reoxidation process on the metal oxide surface. Takita *et al.* have also discussed the effects of water co-adsorption on the adsorption of oxygen over metal oxide surfaces. They concluded that as the quantity of $H_2O$ was increased over a $Co_3O_4$ surface, the quantity of oxygen that it became possible to populate the surface with decreased. This occurred to level where so much water was present on the surface that it became impossible for $O_2$ to co-adsorb, thereby disabling the oxidising properties of the surface. [19]

On the addition of water to the feed gas, deactivation was quick in all cases, whether the feed gas was fed through a saturator at 0, or at 25°C, and for both the doped and un-doped catalysts. The different % water saturated mixtures caused deactivation of the catalysts at a similar rate, therefore it may indicate that there might have been only a few active sites present in each catalyst and that these became quickly blocked by

hydroxyl groups on water treatment. Deactivation was only temporary indicating that the water was preferentially adsorbing on the active sites on the catalyst surface during the co-feeding experiments. An eventual return to the expected activity levels was observed in all cases but was more rapid in the examples of a dry gas being used. Where the active sites were blocked by the adsorption of water, it would have been impossible for the CO and O species to adsorb also, hence no CO conversion could take place by a surface based mechanism. It was probable that little structural damage occurred during this temporary period of deactivation as the catalyst activity was later observed to return to its expected level. It was probable that the hydroxyl groups were only weakly adsorbed on to the catalyst surface as when returning to a dry feed gas, activity was seen to return. Thormahlen has shown that it was possible to regain the initial activity of cobalt oxide catalysts that had been poisoned by water simply by treatment at high temperature to remove surface adsorbed species. [20]

The return to expected activity was in a different mode of behaviour to results reported by Grillo *et al.* who investigated the influence of $H_2O$ on the activity of $Co_3O_4$ powder and found that it was not possible to attain the original level of CO conversion, even on re-calcination of the sample to remove adsorbed species. [21] It was of course possible that the presence of cobalt along with oxides of copper and manganese lead to a more robust system with respect to the recovery from water poisoning.

It has previously been shown that the use of desiccants in combination with hopcalite type catalysts can prove to be an adequate protector to the catalyst from the effects of water vapour. [22] Adequate protection of hopcalite catalysts from moisture poisoning has been provided in some breathing apparatus systems by the incorporation of a layer of carbon treated with a 50% LiBr solution. [23]

Reactivation towards the initial level of catalytic activity appeared to be quicker when the feed gas used was dry and also when the water content of the deactivating gas was lowest. Further analysis into the mechanism of oxidation over hopcalite catalysts is presented in chapter 6.

The commercial catalyst, Moleculite, deactivated profoundly with time on line. Initially, activity was high but deactivation occurred rapidly after the maximum conversion level was reached early in the lifetime of the catalyst. The addition of water to the feed gas accelerated the deactivation but for this catalyst, activity did not return to its expected level when water doping stopped. This indicated that the poisoning of the industrial catalyst by water was not a temporary feature as it was in the case of the cobalt-doped catalyst. It was possible that the presence of cobalt in the doped catalyst may have contributed to the accelerated return to normal activity in the doped systems.

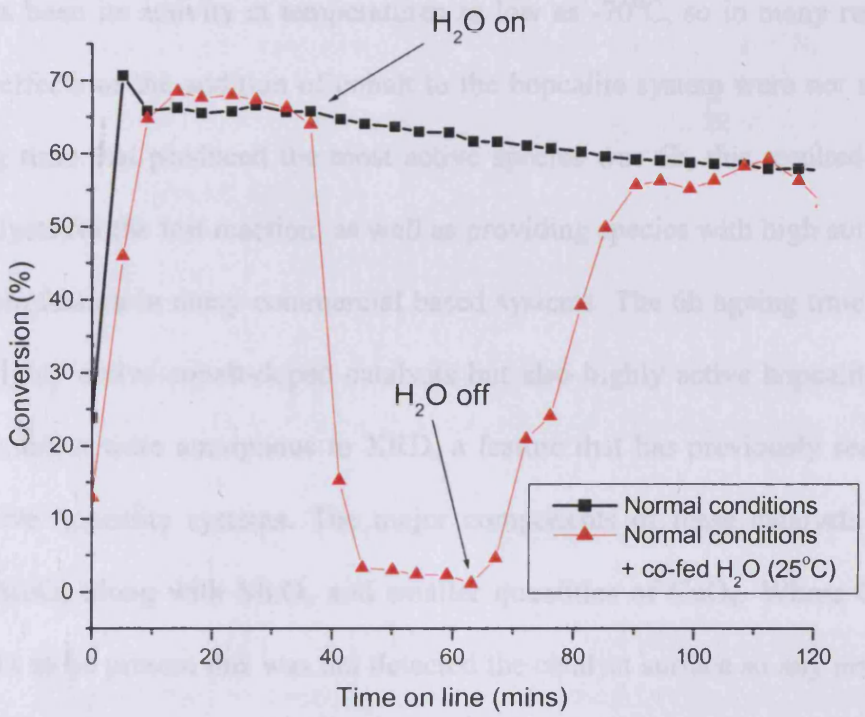


**Figure 5.8.5.1 – Catalytic activity during water co-feeding over 6h aged CuMnOx at 25°C**

In the case of the 2% Co/$CuMnO_x$ catalyst, activity initially increased to a maximum level, from where it declined on treatment with water, and then increased back to a level near the expected maximum when water was removed from the feed gas.

This return to the level of initial activity was not exclusive to the cobalt-doped samples. The 6h aged $CuMnO_x$ sample, after deactivation with water was also observed to return to a level of activity similar to that displayed by the catalyst under normal test conditions for a given time on-line. (Figure 5.8.4.1)

## 5.8.6 - Overall Conclusions

Overall, the doping experiments with cobalt were somewhat of a success in producing active species that rivalled, and in many cases superseded, the activity of a hopcalite catalyst used commercially. The oxidation of carbon monoxide over cobalt oxide has often been reported, [18,24] one of the most attractive features of cobalt as an oxidation catalyst has been its activity at temperatures as low as -70°C, so in many respects the beneficial effects of the addition of cobalt to the hopcalite system were not surprising. The ageing time that produced the most active species was 6h, this resulted in highly active catalysts for the test reaction, as well as providing species with high surface areas – a desirable feature in many commercial based systems. The 6h ageing time produced not only highly active cobalt-doped catalysts but also highly active hopcalite species. All these catalyst were amorphous to XRD, a feature that has previously seen to give rise to active hopcalite systems. The major components of these catalysts were the mixed $CuMnO_x$ along with $MnO_x$ and smaller quantities of $CuO_x$. Where $CoO_x$ was also thought to be present this was not detected the catalyst surface so any promotional effect arising form the presence of cobalt would have involved cobalt dispersed through the bulk phase.

The benefits of doping hopcalite with cobalt not only involved increased activity of many of the systems but also an increase in the stability of the catalyst activity with time on-line. This would be another desirable feature commercially, as increased catalyst lifetime lowers replacement costs and time wastage. However, one feature where the hopcalite and doped hopcalites synthesised in this study, often could not compete was the start-up activity of the catalyst. The induction time leading up to the point of maximum conversion was often slow when compared to the commercial system, thereby limiting the uses of these catalysts in many industrial applications.

Although the exact role of the cobalt in the hopcalite system has not been clearly defined during this chapter, it has been possible to draw some inferences as to its possible function. It has been shown that cobalt was not acting as a structural promoter as if it were, on normalisation of activities for surface areas, all conversion rates would have been the same. It is more likely that the cobalt was acting as an electronic promoter or lattice defect promoter. The Temporal Analysis of Products (TAP) experiments in chapter 6 go some way to identifying the effect that the presence of cobalt in a hopcalite catalyst can have.

## References


[1] W. R. Robinson, J. C. Mol, Appl. Catal. 60 (1990) 61

[2] S. Veprek, D. L. Cocke, S. Kehl and H. R. Oswald, J. Catal, 100 (1986) 250

[3] A. A. Mirzaei, H. R. Shaterian, M. Habibi, G. J. Hutchings, S. H. Taylor, Appli. Cat. A:Gen, 262 (2004)137

[4] H. L. Friedman, in H. G. McAdie (ed.), Proceedings of the 3rd Toronto Symposium on Thermal Analysis, Chemical Institute of Canada, Toronto (1969) 127

[5] H. E. Kissinger, J. Res. Nat. Bur. Stand. 57 (1956) 217

[6] H. E. Kissinger, Anal. Chem. 29, 11 (1957) 217

[7] D. Dollimore, C. Guler, G. R. Heal, Thermochim. Acta, 54 (1982) 187

[8] P. A. Wright, S. Natarajan, J. M . Thomas, P. L. Gai-Boyes, J. Chem Mater. 4 (1992) 5

[9] M. Schwab, S. B. Kanungo, Z. Phys. Chem. N.F, 107 (1977) 109

[10] E. R. S. Winter, Adv Catal. 10 (1958) 196

[11] P Porta, G. Moretti, M. Musicanti, A. Nardella, Catal. Today, 1-2 (1991) 211

[12] P. Porta, G. Moretti, Solid State Ionics, 63-65 (1993) 257

[13] V. Koleva, D. Stoilova, D. Mehandjiev, J. Solid State Chem, 133 (1997) 416

[14] G. J. Hutchings, A. A. Mirzaei, R. W. Joyner, M. R. H. Siddiqui, S. H. Taylor, Appl. Cat. A: Gen 166 (1998) 143

[15] A. A. Mirzaei, PhD Thesis, "Low Temperature Carbon Monoxide Oxidation using Copper Containing Catalysts", University of Liverpool (1998)

[16] I. Spassova, M. Khristova, D. Panayotov, D. Mahandjiev, J. Catal.185 (1999) 43

[17] A. Lamb, W. C. Bray, J. C. W. Fraser, J. Ind. & Chem. Eng. March 1920

[18] D. A. Cunningham, T. Kobayashi, N. Kamijo, M. Haruta, Catal. Lett. 25 (1994) 257

[19] Y. Takita, T. Tashiro, Y. Saito, F. Hori, J. Catal. 97 (1986) 25

[20] P. Thormahlen, E. Fridell, N. Cruise, M. Skoglundh, A. Palmqvist, Appl. Cat. B: Environ. 31 (2001) 1

[21] F. Grillo, M. M. Natile, A. Glisenti, Appl. Cat. B: Environ. 48 (2004) 267

[22] N. Harwood, J. Wojtasik, US Patent 4,925,631, 15th May 1990.

[23] M. J. McGoff, S. J. Rodgers, "Carbon Monoxide Conversion Devices" U. S. Patent 5,038,768, 13th August 1991

[24] P. Thormahlen, M. Skoglundh, E. Fridell, B. Andersson, J. Catal. 188 (1999) 300

# Chapter 6 – Probing the Mechanism of Carbon Monoxide Oxidation over Hopcalite using the Temporal Analysis of Products Technique.

In this chapter the mechanism of the oxidation of CO using copper manganese oxide catalysts is probed using the technique of the Temporal Analysis of Products (TAP).

Steady state experiments have been used widely to evaluate the performance of heterogeneous catalysts. However, mechanistic details arising from these can be limited. [1] On the contrary, non steady state experiments that monitor a transient response can provide a much enhanced understanding of the reaction mechanism.

The early work using transient experiments in heterogeneous catalysis research stemmed from Wagner and Hauffle [2] in 1938 and later from Tamura. [3] In recent years, several transient techniques have found application in heterogeneous catalysis research, a number of which have been developed. [4-6] The most advanced of these is TAP approach. The TAP technique was pioneered in the mid 1980's and for the first time resulted in sub millisecond resolution for heterogeneous catalysis. [7]

## 6.1 - Temporal Analysis of Products:

The TAP II apparatus consists of:

- A high throughput, liquid nitrogen trapped, Ultra High Vacuum system
- Microreactor with T control
- Valve/manifold assembly with T control
- Gas blending station and gas blending oven for preparing samples from gases and liquids
- Quadrupole MS (QMS)

- Computer based control & data acquisition system

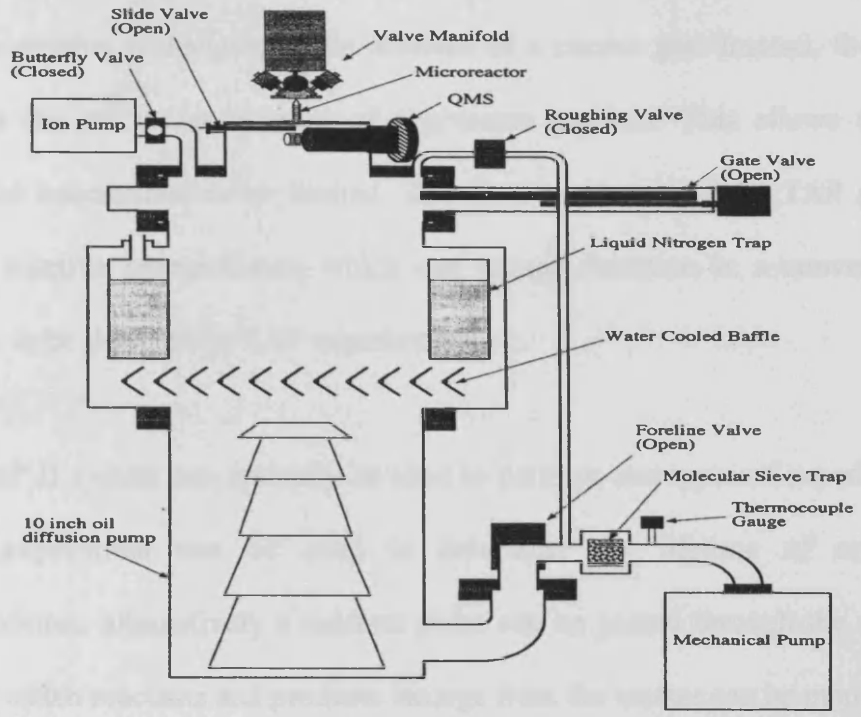


**Figure 6.1.1 – Schematic diagram of a TAP II**

The TAP II equipment allows sub millisecond resolution for heterogeneous catalytic transient experiments. This is achieved by studying the response of a narrow pulse of gas that is injected into one end of a small cylindrical reactor while the other end is continuously evacuated. The pulse moves as a result of the pressure gradient across the reactor, travelling as a molecular beam so that gas phase reactions are eliminated and interactions and reactions on the surface of the test catalyst are predominant. A section of the pulse is intercepted by the quadrupole mass spectrometer with its composition being determined as a function of time. The time resolution can be controlled by changing the length of the catalyst bed. Shortening the bed length will decrease the residence time, providing a better resolution.

The TAP II system can perform transient response & steady state flow experiments in the range $10^{-6}$ to 2500 Torr and 200-900K. The main distinction between TAP and other surface probing techniques is the absence of a carrier gas. Instead, the pulse moves through the reactor as a result of a pressure gradient. This allows the number of gas/solid interactions to be limited. The time resolution of the TAP process allows highly reactive intermediates, which can escape detection in a conventional reactor system, to be detected by TAP experiments.

The TAP II system can typically be used to perform two types of experiment. A pump probe experiment can be used to determine the lifetime of reactive surface intermediates, alternatively a reactant pulse can be passed through the reactor and the time at which reactants and products emerge from the reactor can be monitored.

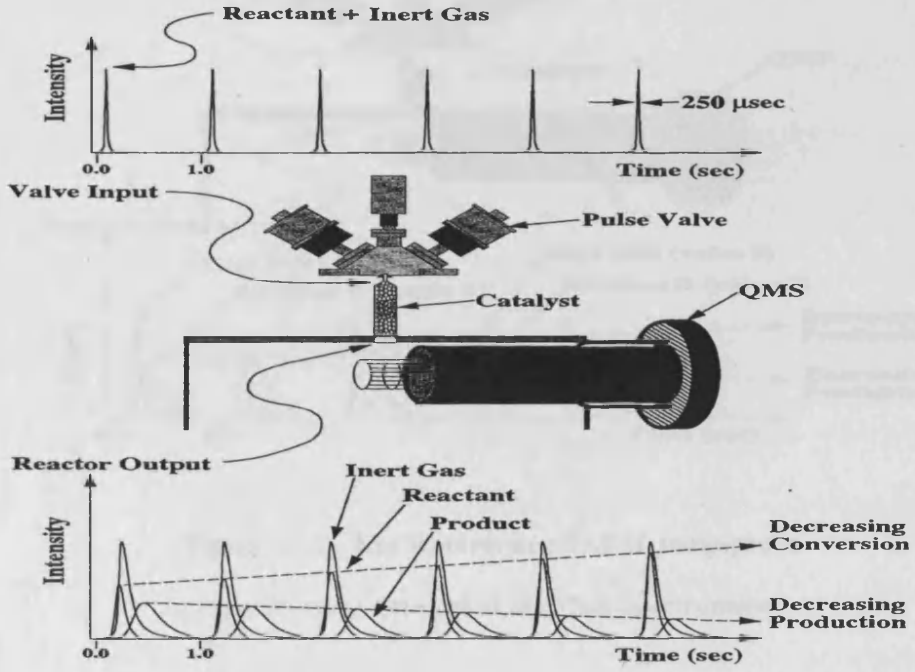


**Figure 6.1.2 – Key features as a TAP II pulsing experiment as detected at the Mass Spectrometer.**

The key experimental features of a TAP reactant pulse response experiment showing a train of input pulses and the transient responses observed at the MS. The signals detected from pulsing one pulse of reactant gas over the catalyst are time limited. The order of elution of the peaks assuming a partial reaction of the reactants over the catalyst would be, Inert (Argon), followed by unconsumed reactant peaks, followed by product peaks arising from interactions between the catalyst and the reactant gas. Product species appear at a later time period due to the period of time taken for adsorption of reactants on the catalyst surface, followed by the surface reaction and the desorption of species produced.

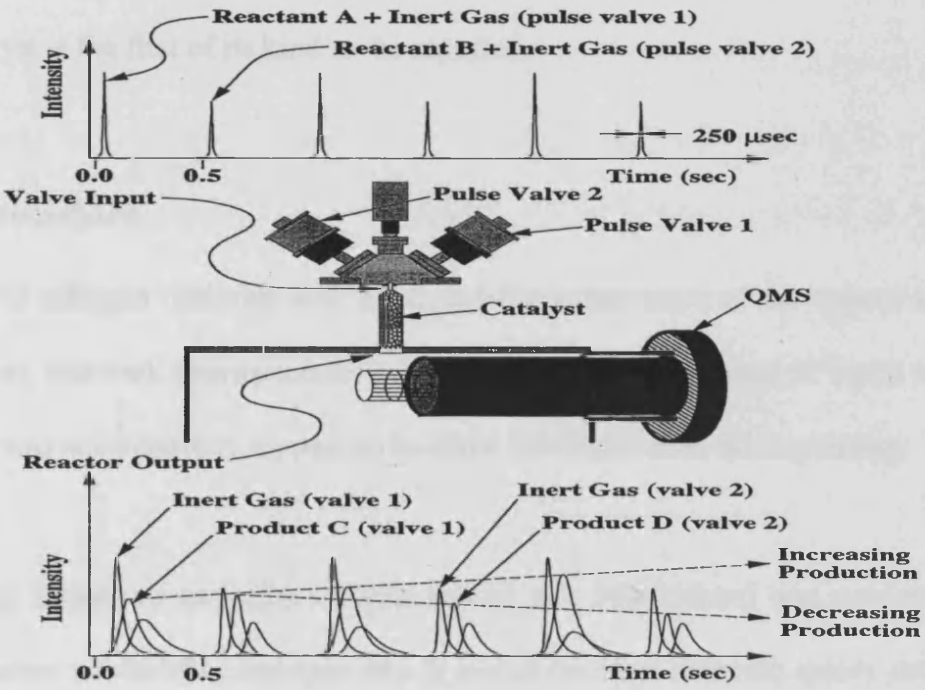


**Figure 6.1.2 – Key features as a TAP II pump-probe experiment as detected at the Mass Spectrometer.**

During TAP pump-probe experiments, two pulsing valves are used. The input train of reactant gas pulses consists of alternating pulses of reactant A and B. Pump probe experiments are designed to determine the lifetime of reactive surface intermediates.

In the TAP reactor the state of the catalyst continuously changes as a consequence of the pulsing. The pulse frequency can strongly influence the results – therefore kinetic information is not easily acquired by TAP. Since the first major publication by Gleaves et al in 1988 [7], the TAP reactor system has been used to explore a variety of heterogeneously catalysed reactions. For instance, methane coupling [8-10], oxidation of methane [11-12], methanol [13], ethene [14], propene [15-16], butane [5,17], and pentene [5] have been studied in the TAP reactor.

To date, there has been virtually no reported work on the oxidation of carbon monoxide using the TAP technique. [18] Consequently this application of TAP using hopcalite as the catalyst is the first of its kind to be reported.

## 6.2 - Procedure

The liquid nitrogen reservoir was filled and the temperature of the system allowed to equilibrate, this took approximately 90 minutes to occur. The level of liquid nitrogen in the reservoir was regularly topped-up to allow for evaporation during testing.

A 100mg sample of hopcalite catalyst (pellet size 250-355$\mu$m) was supported in the microreactor, sandwiched between two layers of the inert material; quartz pellets (250-355$\mu$m). The microreactor was secured in place and the slide valve opened, exposing the sample to the pressure of the TAP system. On pumping down the system, the stabilisation pressure was typically $1.7 \times 10^{-8}$ Torr. A series of mechanism probing experiments were carried out by pulsing mixtures of Ar, CO, $O_2$, and $H_2O$ and associated isotopes of these species, with species detected using a quadrupole mass spectrometer with a Faraday detector. Typically, a pulse of gas from one of pulsing valves contained $5 \times 10^{13}$ molecules of gas, calculated from recording the pressure drop

in the blending tanks for a given number of pulses. All experiments were carried out within the Knudsen diffusion regime as outlined by Yablonsky. [19] All data reported in this chapter is as a result of signal averaging over five pulses of reactant to provide consistency.

## 6.3 – Deactivation of $CuMnO_x$ catalyst

A fresh sample of the hopcalite catalyst was strongly reduced by continuous pulsing of CO/Ar over the catalyst surface (Fig 6.3.1). During the early pulses, activity of the system was good but with time on-line, as in steady state testing, activity was observed to decrease. The very fact that the reactant mixture was oxygen-free and the catalyst was active towards the test reaction indicated that oxygen species from the catalyst must be active in the oxidation cycle in order to form the $CO_2$ product. Oxidation of this type was short lived and had ceased after ~300 pulses, however, pulsing of the CO/Ar mixture continued to ensure the surface was well reduced.

Veprek *et al.* reported that it was possible to re-oxidise a reduced hopcalite surface by pulsing pure oxygen over the catalyst. [21] Experiments carried out during this study, suggested that the surface of the reduced hopcalite catalyst could be re-oxidised by exposure of the reactor to RTP (room temperature and pressure) which resulted in the adsorption of $O_2$ from the air on to the reduced catalyst surface via the following mechanism:

$$CO + O_s \rightarrow CO_2 + S_{reduced} \qquad \textit{(Eq.1)}$$

$$S_{reduced} + \tfrac{1}{2} O_2 \rightarrow O_s$$

During the deactivation experiment, a fresh $CuMnO_x$ catalyst was fully deactivated by pulsing $1.9 \times 10^{19}$ molecules of CO/Ar over it at 25°C (Fig.6.3.1). The catalyst was then removed from vacuum and left at RTP overnight, the next morning, the catalyst was

postulated to have adsorbed water and oxygen from the air resulting in a return of activity, though not to its original level.

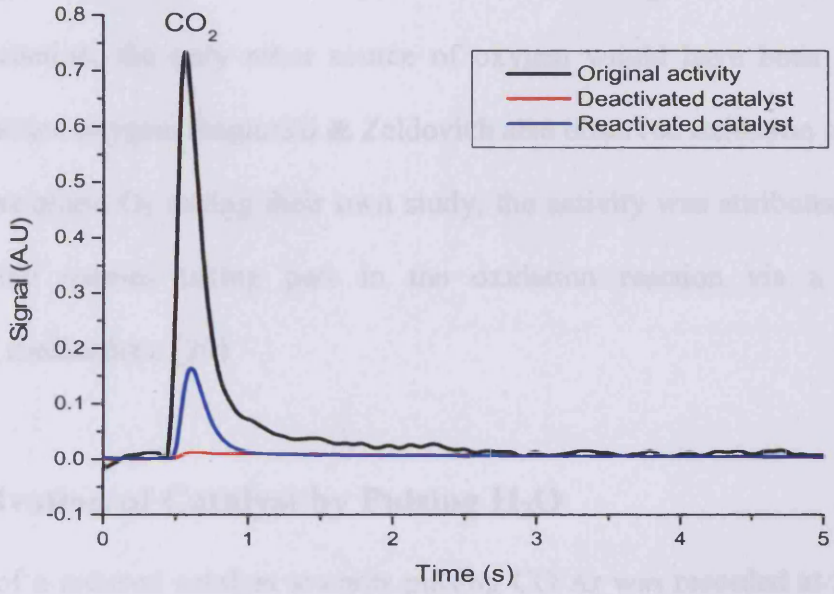


**Figure 6.3.1 – Activity of the hopcalite catalyst as a function of catalyst state**

On pulsing even vast quantities of $O_2$ over a totally reduced catalyst surface, it was not possible to observe any return of activity. However where the catalyst was only partially deactivated, a slight return of activity could be observed. This suggested that lattice oxygen may be responsible for activity during the early period of testing but when the catalyst was deeply reduced, a re-oxidation of the surface was not possible.

The existence of a resonance structure has been proven during the oxidation of CO by hopcalite, so it would be expected that this would be an integral part of the mechanism of oxidation occurring in this case.

$$Mn^{3+} + Cu^{2+} \leftrightarrow Mn^{4+} + Cu^{+} \qquad \textit{(Eq.2)}$$

## 6.4 - Catalytic Oxidation in the Absence of Gas Phase $O_2$.

Experiments where only an Ar/CO gas mixture was pulsed over the hopcalite catalyst still resulted in the production of $CO_2$ by the catalyst. As no gas phase $O_2$ was present during this reaction, the only other source of oxygen would have been the surface adsorbed or lattice oxygen. Roginskii & Zeldovich also observed oxidation of CO in the absence of gas phase $O_2$ during their own study, the activity was attributed to surface adsorbed oxide species taking part in the oxidation reaction via a Langmuir-Hinshelwood mechanism. [20]

## 6.5 - Reactivation of Catalyst by Pulsing $H_2O$

The activity of a reduced catalyst towards pulsing CO/Ar was recorded at 25°C in the TAP reactor. Pulsing a large quantity of CO/Ar pulses, equivalent to 1.04 x $10^{20}$ molecules, had the effect of partially deactivated the catalyst. A similar behaviour was observed by Veprek *et al.* He suggested that pulsing CO over the hopcalite catalyst had the effect of reducing the exposed surface but that the addition of gaseous $O_2$ could reactivate a reduced surface. [21]

The activity of the catalyst was recorded to give a "deactivated" catalyst conversion level (Fig.6.5.1).

In order to test the theory that the catalyst could be regenerated by pulsing water over the surface, water (1.6 x $10^{20}$ molecules) was pulsed over the sample in an initial attempt at restoring activity. A similar mode of activity was suggested by the Bond-Thompson model of oxidation over metal oxide supported, gold nano-particles, where hydroxyl groups were thought to be key to activity. [22] CO/Ar was again pulsed over the surface to record the effect that these 3000 pulses of water had on the catalyst

surface (Fig 6.5.1). It was interesting to observe a partial return of activity as the quantity of $CO_2$ produced on passing CO/Ar over the surface had increased from the level in the "deactivated" catalyst.

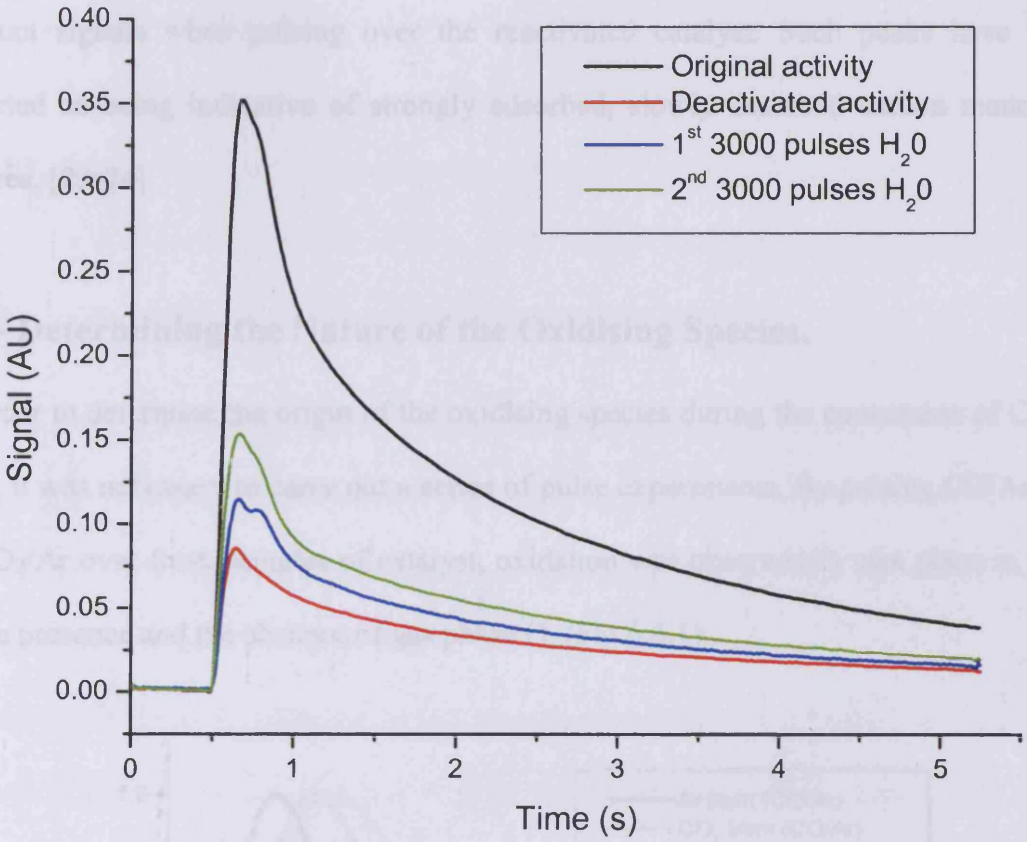


**Figure 6.5.1 – Pulsing CO/Ar over a $H_2O$ regenerated hopcalite catalyst surface.**

Due to the initial positive effect of reactivating the catalyst surface using water vapour, a further 1.6 x $10^{20}$ molecules of $H_2O$ was passed over the surface; equivalent to 3000 pulses. The water used was degassed to remove any dissolved oxygen with the gases used being of high purity to ensure an oxygen-free environment. Once again, an increase in $CO_2$ production was observed when probing the catalyst with a CO/Ar pulse. These observations lead to the conclusion that although water vapour has long been known to poison hopcalite type catalysts, it was possible when using small quantities, to partially regenerate a reduced hopcalite catalyst surface. It should however be noted that

the return to activity was short-lived and that further pulsing of CO/Ar quickly deactivated the surface (Fig.6.5.1).

It was interesting to observe the double maxima of the $CO_2$ peak observed in the product signals when pulsing over the reactivated catalyst. Such peaks have been reported as being indicative of strongly adsorbed, slowly desorbed carbon monoxide species. [23-24]

## 6.6 - Determining the Nature of the Oxidising Species.

In order to determine the origin of the oxidising species during the conversion of CO to $CO_2$, it was necessary to carry out a series of pulse experiments. By pulsing CO/Ar and $CO/O_2/Ar$ over fresh samples of catalyst, oxidation was observed to take place in both in the presence and the absence of gas phase $O_2$ (Fig.6.6.1).

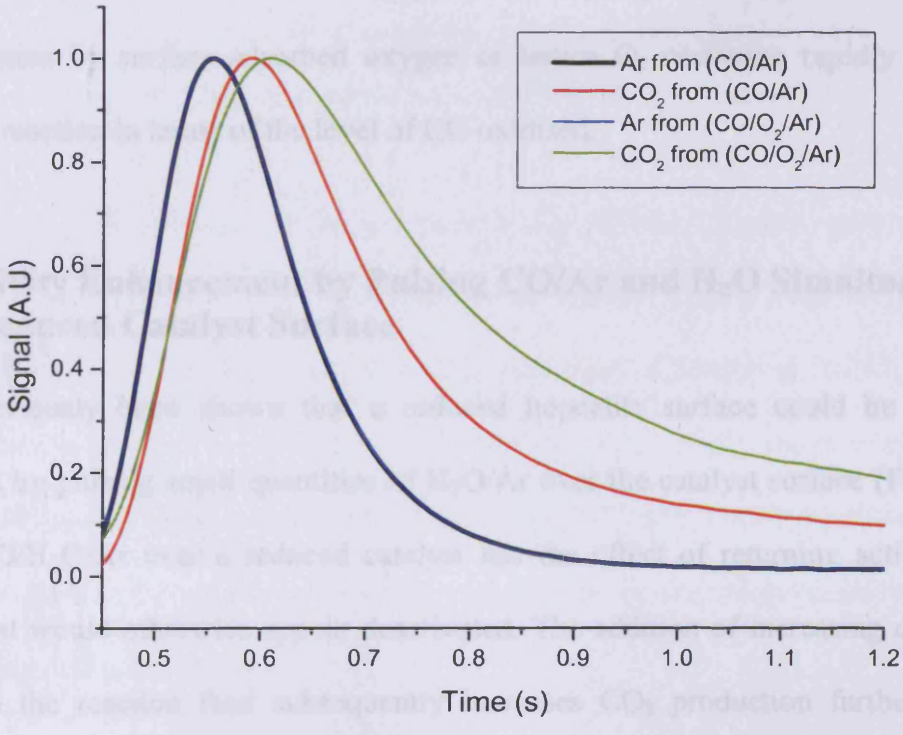


**Figure 6.6.1 – Normalised data, 60ms pulses of CO/Ar and $CO/O_2/Ar$ over $CuMnO_x$ at 25°C**

However, the position of the $CO_2$ product peak maxims were time-staggered with the $CO_2$ formed as a result of passing CO/Ar over the fresh catalyst being eluted before that formed due to the reaction of $CO/O_2/Ar$ over the catalyst. Had these $CO_2$ peaks been exactly super imposable on top of each other it would have indicated that the oxidising species in each case originated from the same source.

However, due to the non super imposable nature of the product peaks, it would seem that both surface adsorbed/lattice oxygen as well as gas phase oxygen were available to take part in the oxidation of carbon monoxide over this catalyst.

On analysis of the raw data, it was evident that the product peak due to the production of $CO_2$ when pulsing $Ar/CO/O_2$ was significantly larger (x 6) in terms of area than was observed when pulsing Ar/CO over the catalyst. It appeared that although two parallel mechanisms of oxidation were present in the hopcalite, one was more dominant. In this case the mechanism of oxidation in the presence of gas phase oxygen was dominant with oxidation by surface adsorbed oxygen or lattice $O_2$ occurring rapidly but as a secondary reaction in terms of the level of CO oxidised.

## 6.7 - Activity Enhancement by Pulsing CO/Ar and $H_2O$ Simultaneously over a Reduced Catalyst Surface

It had previously been shown that a reduced hopcalite surface could be partially reactivated by pulsing small quantities of $H_2O/Ar$ over the catalyst surface (Fig.6.7.1). Pulsing $CO/H_2O/Ar$ over a reduced catalyst has the effect of returning activity to a catalyst that would otherwise appear deactivated. The addition of increasing quantities of $H_2O$ to the reaction feed subsequently increases $CO_2$ production further. When considering the reaction species involved, this perhaps would be symptomatic of a classic water gas shift reaction *(Eq. 3)*. This would not have been the first time that the

water gas shift had been observed at low temperature; however, previous instances of the WGSR occurring at low T involved the use of precious metal catalysts. [25]

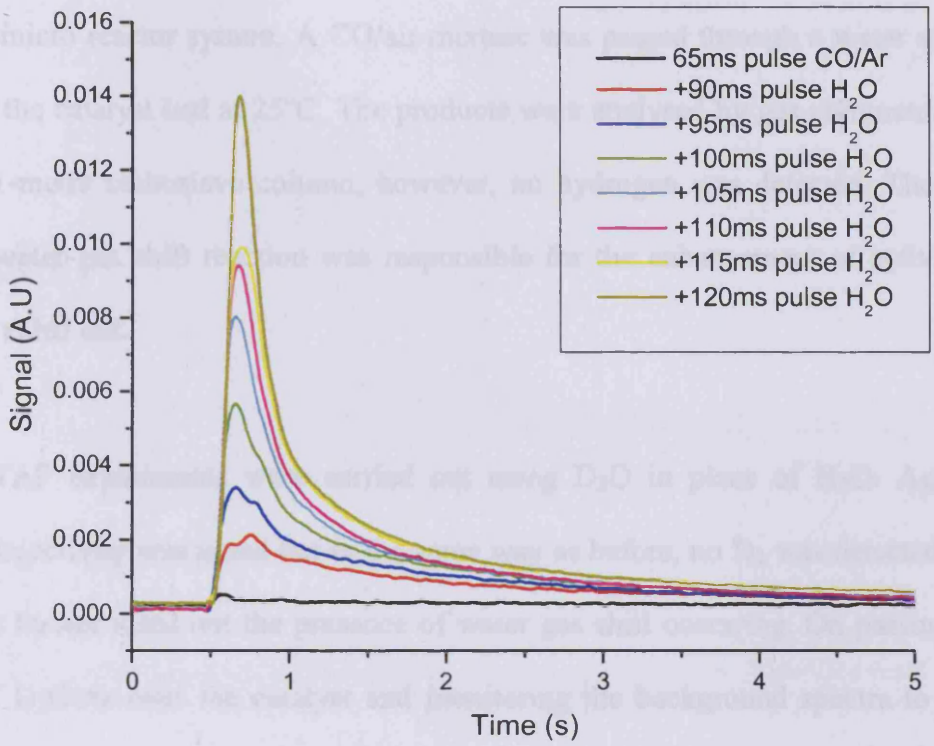


**Figure 6.7.1 – Monitoring the $CO_2$ product peak with pulsing CO/Ar and $H_2O$/Ar simultaneously over the $CuMnO_x$ catalyst at 25°C**

Hutchings *et al.* have reported the presence of the WGSR in spinel type oxides but never at this low temperature. [26] The results of Tanaka indicated the WGSR to take place over a catalyst containing $Cu_{1.5}Mn_{1.5}O_4$ and traces of $Mn_2O_3$ at 200°C. However, after use in the WGSR the species was reduced to Cu and MnO. Activity towards the reaction was shown to increase up to a temperature of 250°C. Other copper-containing spinels, containing metals such as aluminium, iron and chromium were also reported as active at high temperature. [25]

$$CO + H_2O \rightarrow CO_2 + H_2 \qquad \textit{(Eq.3)}$$

However, the theory of a WGSR occurring over the hopcalite in these tests was all but discounted as no hydrogen was detected by the mass spectrometer while the reaction was occurring. These results were verified by carrying out a similar experiment in a standard micro reactor system. A CO/air mixture was passed through a water saturator and over the catalyst bed at 25°C. The products were analysed by gas chromatography, using a 1-metre carbosieve column, however, no hydrogen was detected. The theory that the water-gas shift reaction was responsible for the enhancement of activity was therefore ruled out.

Similar TAP experiments were carried out using $D_2O$ in place of $H_2O$. Again, an increase in activity was noted but in the same way as before, no $D_2$ was detected at *m/e* = 4. This further ruled out the presence of water gas shift occurring. On passing rapid pulses of $D_2O$/Ar over the catalyst and monitoring the background spectra to see all species present, an unknown peak was present at *m/e* = 36. It was possible that this was due to the formation of a peroxo species ($D_2O_2$), having the effect of re-oxidising the catalyst from its reduced state.

## 6.8 - Activity Enhancement by Pulsing CO/Ar and $H_2{}^{18}O$ Simultaneously over a Reduced Catalyst Surface

The catalyst surface was reduced as outlined previously. A similar increase in activity was observed as before where co-pulsing CO/Ar with $H_2{}^{18}O$ reactivated a previously deactivated catalyst. An increase in activity was observed only when using water pulses greater than 90ms in size. On increasing the size of the water pulse, increased activity was observed for $CO_2$ formation.

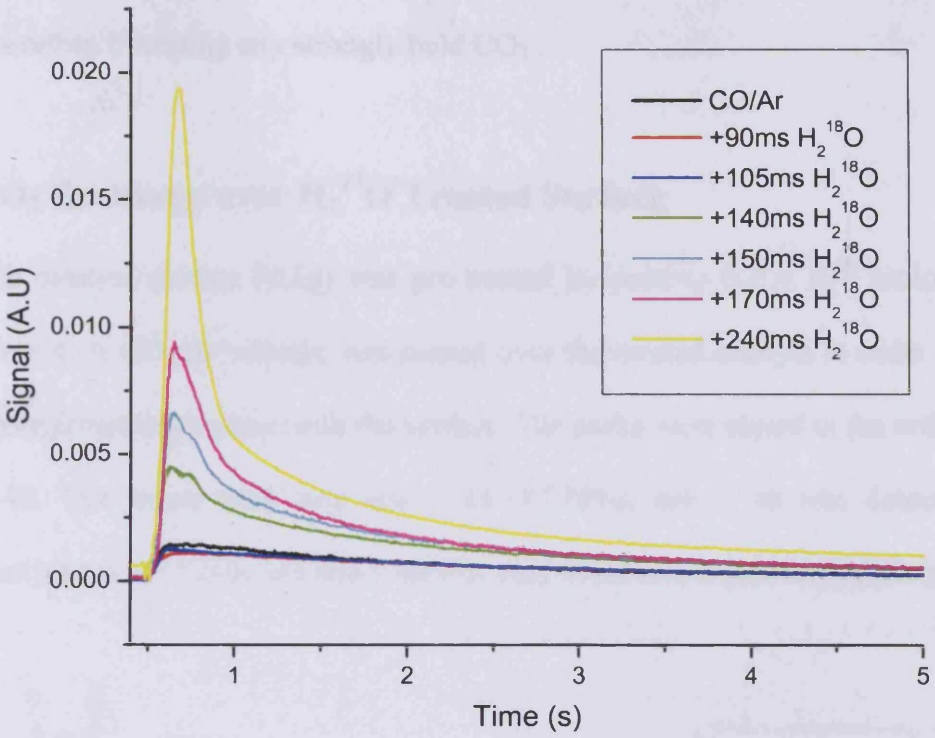


**Figure 6.8.1– Co-pulsing CO/Ar with varying size pulses of Ar/$H_2{}^{18}O$ treated catalyst**

When larger pulses were used (>140ms), $^{16}O_2$ was detected by the mass spectrometer, this might have been due to the larger water pulses displacing $^{16}O$ from the catalyst surface/lattice structure, making $O_2$ available in the gas phase. No *m/e* = 48 peak, owing to the presence of $C^{18}O_2$ was detected. However, some *m/e* = 46 ($C^{16}O^{18}O$) was observed where the water pulse size was equal to, or greater than 160ms. The presence of this species might have been due to the exchange of $^{18}O$ with surface bound $^{16}O$, or more unlikely from $H_2{}^{18}O$ reacting with CO in the gas phase.

A number of the carbon dioxide product peaks exhibited a strongly visible double maximum (Fig.6.8.1), this was indicative of strongly adsorbed and slowly desorbed $CO_2$. [18] However, it remained possible that due to the magnitude of the water pulse being used, that the detection of $CO_2$ by the mass spectrometer was merely as a result of

a displacement reaction occurring when hitting the catalyst surface with large reactant pulses therefore liberating any strongly held $CO_2$ .

## 6.9 - $CO_2$ Exchange over $H_2{}^{18}O$ Treated Surface

The fresh catalyst surface (0.1g) was pre-treated by pulsing 6.2 x $10^{20}$ molecules of $H_2{}^{18}O$ over it. A $CO_2$/Ar mixture was passed over the treated catalyst in order to see if any exchange had taken place with the surface. The peaks were eluted in the order *m/e* = 44, 46, 48. The major peak was *m/e* = 44 *(87.78%)*, *m/e* = 46 was detected in a significant amount *(12.2%)*, but *m/e* = 48 was very small and almost negligible *(0.02%)*.

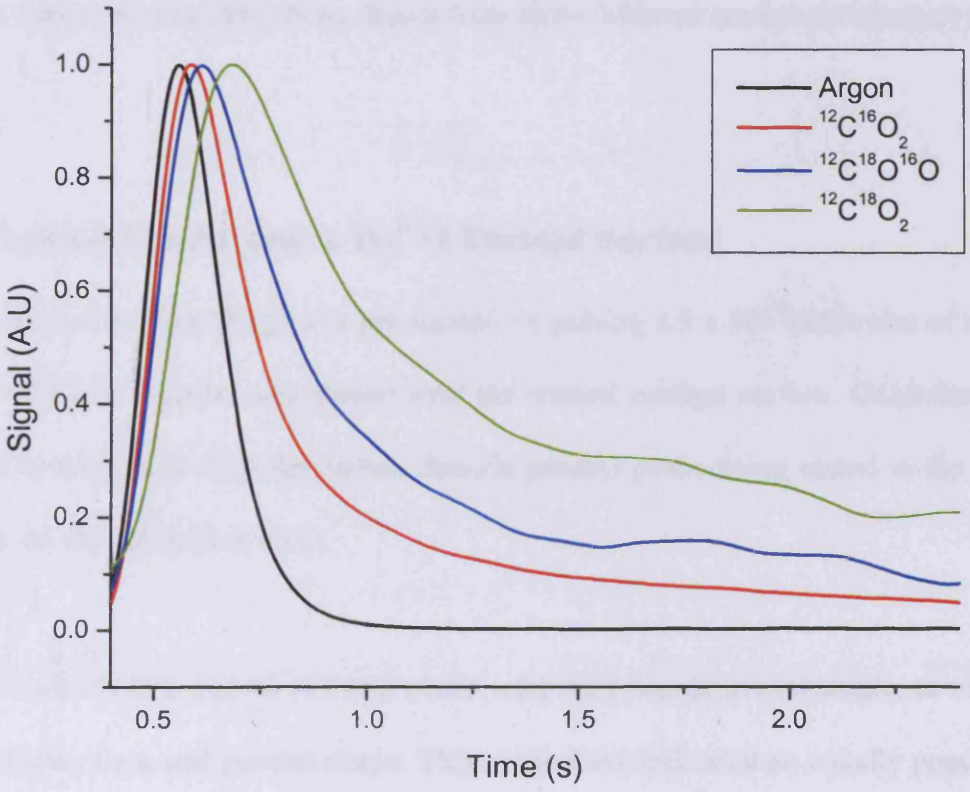


**Figure 6.9.1 – $CO_2$/Ar pulsed over $H_2{}^{18}O$ treated catalyst to test for exchange with surface adsorbed species**

It was therefore possible to deduce that $^{18}O$ at least partially exchanged with the catalyst surface. Only a small quantity of doubley-exchanged $CO_2$, forming the *m/e* = 48 peak

was recorded, indicating that in general only one catalyst surface oxygen atom was incorporated in the final $CO_2$ complex. This result was obviously of some use in ascribing a mechanism for the oxidation of CO over hopcalite, indicating that in general, gas phase $O_2$ would not have taken part in the reaction without at first adsorbing on the catalyst surface. It was therefore unlikely that the mechanism of oxidation was of an Eley-Rideal type:

$$2CO_{(ad)} + O_{2\,(g)} \longrightarrow 2CO_{2\,(ad)} \longrightarrow 2CO_{2\,(g)}$$

The fact that each of the product peaks is time delayed from the other was also an indicator that oxide may have been drawn from three different sources to take part in the reaction.

## 6.10 - Pulsing CO/Ar over a $H_2{}^{18}O$ Treated Surface

A fresh catalyst surface (0.1g) was pre-treated by pulsing $8.5 \times 10^{19}$ molecules of $H_2{}^{18}O$ over it. A CO/Ar mixture was passed over the treated catalyst surface. Oxidation was observed to take place with the carbon dioxide product peaks being eluted in the order *m/e* = 44, 46, 48. (Figure 6.10.1)

The *m/e* = 44 *(44.8%)* and 46 *(47.4%)* peaks were very similar in magnitude, as well as in their elution time and general shape. This might have indicated an equally populated catalyst surface with respect to $^{16}O$ and $^{18}O$ coverage. Certainly, a large quantity of the $H_2{}^{18}O$ must have been involved in exchange reactions with the catalyst surface populating it with $^{18}O$.

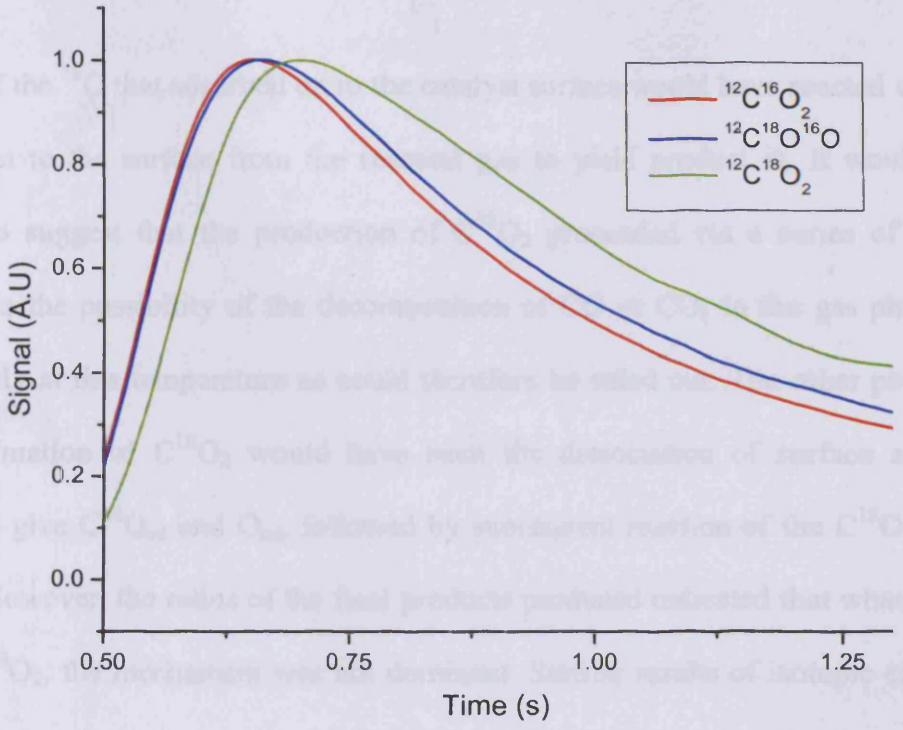


**Figure 6.10.1 – CO/Ar pulsed over $H_2{}^{18}O$ treated catalyst**

The equivalent times of the $C^{16}O_2$ and $C^{18}O^{16}O$ indicated that the products might be derived from a common final step. A small quantity of double-oxygen exchanged $C^{18}O_2$ was also detected at *m/e* = 48 *(0.51%),* but this was time delayed from the peaks of *m/e 44 and 46.* To produce the $C^{18}O_2$ species, dissociation of the $C^{16}O$ reactant must have occurred on the catalyst surface, producing $C^{18}O$ followed by further reaction with $^{18}O$ from $H_2{}^{18}O$ on the catalyst surface through a Langmuir-Hinshelwood type mechanism:

$$C^{16}O_{ad} + {}^{18}O_{ad} \longrightarrow C^{18}O_{ad} + O_{ad}\ \text{(minor species)}\ \mathbf{A}$$

$$\searrow\ C^{18}O^{16}O\ \text{(major product)}\ \mathbf{B}$$

The minor species, A, may then have reacted with further surface adsorbed $^{18}O$ to yield a doubly exchanged carbon dioxide product.

$$C^{18}O_{ad} + {}^{18}O_{ad} \longrightarrow C^{18}O_2 \text{ (minor product)}$$

The bulk of the $^{18}O$ that adsorbed on to the catalyst surface would have reacted with CO adsorbed on to the surface from the reactant gas to yield product B. It would seem plausible to suggest that the production of $C^{18}O_2$ proceeded via a series of surface reactions, as the possibility of the decomposition of CO or $CO_2$ in the gas phase was very unlikely at this temperature so could therefore be ruled out. The other possibility for the formation of $C^{18}O_2$ would have been the dissociation of surface adsorbed $C^{16}O^{18}O$ to give $C^{18}O_{ad}$ and $O_{ad}$, followed by subsequent reaction of the $C^{18}O$ species with $^{18}O$. However, the ratios of the final products produced indicated that whatever the route to $C^{18}O_2$, the mechanism was not dominant. Similar results of isotopic exchange experiments have also been reported by Nijhuis *et al.* who investigated CO oxidation over a platinum sponge. [18]

## 6.11 - Probing the Mechanism of Oxidation over 2% Co/CuMnO$_x$

A similar series of experiments were carried out over the 2% cobalt doped hopcalite catalyst where the precipitation mixture was aged for 6h during the synthesis step. Under steady state experiments this catalyst had proved the most active towards CO oxidation of all those tested in this study.

The product peak due to oxidation of CO over the catalyst in the presence of gas phase $O_2$ was eluted before that was pulsing only Ar/CO over the catalyst. The product peaks were not super-imposable indicating that two mechanisms of oxidation might be occurring and certainly that the source of the oxidising species in each case differed. The product peak in the absence of gas phase $O_2$ was twice as large as that when pulsing

$CO/O_2/Ar$, indicating that although oxidation in the presence of gas phase $O_2$ was quicker, the dominant mechanism involved lattice or surface oxygen species.

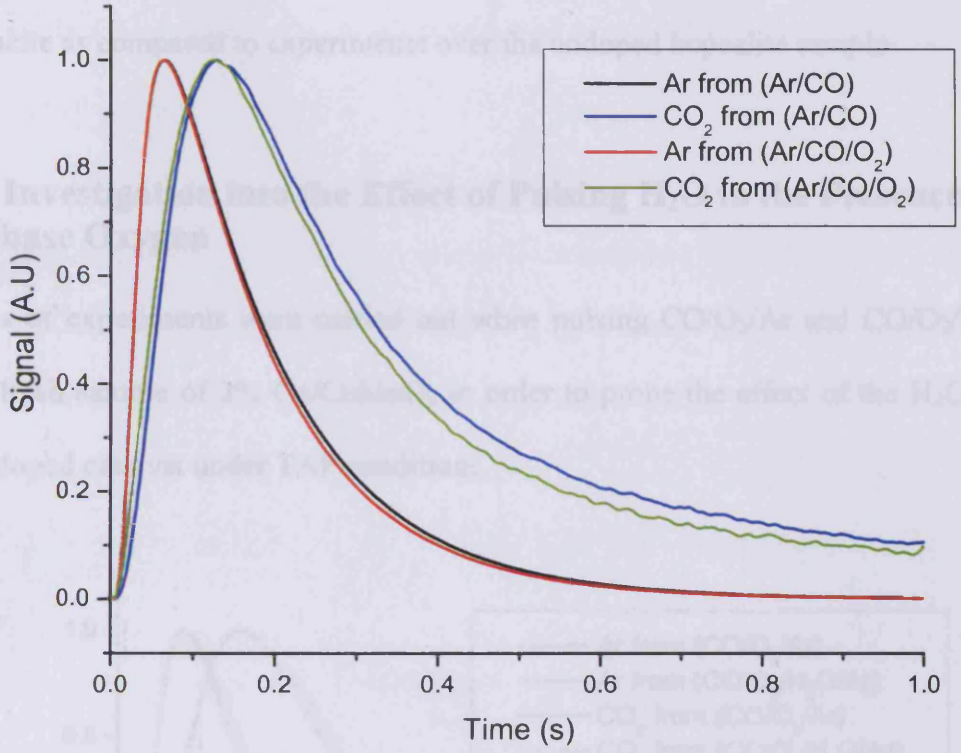


**Figure 6.11.1 – Pulsing CO/Ar and $CO/O_2/Ar$ over fresh 2%Co/$CuMnO_x$ at 25°C to determine the nature of the oxidising species.**

This was in an opposite mode of behaviour to that when pulsing over hopcalite where the dominant mode of oxidation was in the presence of gas phase $O_2$ while the quickest mechanism involved oxidation by lattice or surface adsorbed oxygen. The product peak when pulsing $Ar/CO/O_2$ was considerably larger (factor of 6) than in the absence of gas phase $O_2$.

This indicated that the cobalt might be playing an important part during the oxidation reaction. Its exact role was unclear but it may well have been acting as an adsorption site for oxygen, providing a source of $O_2$ during the reaction. As the surface became

reduced with pulsing CO over the catalyst, reactivation of the surface was continuous with the cobalt acting as an oxygen reservoir thereby facilitating continuous reoxidation of the surface. These factors combined made the reaction in the absence of gas phase $O_2$ more facile as compared to experiments over the undoped hopcalite sample.

## 6.12 - Investigation into the Effect of Pulsing $H_2O$ in the Presence of Gas Phase Oxygen

A series of experiments were carried out when pulsing $CO/O_2/Ar$ and $CO/O_2/H_2O/Ar$ over a fresh sample of 2% $Co/CuMnO_x$ in order to probe the effect of the $H_2O$ on the cobalt-doped catalyst under TAP conditions.

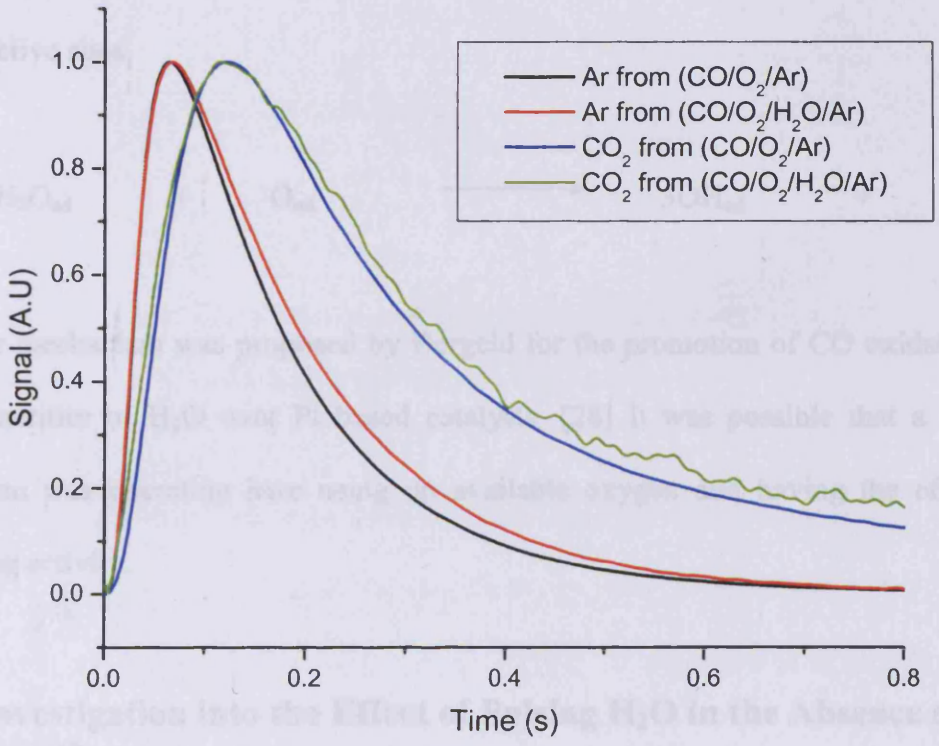


**Figure 6.12.1 – Normalised $CO_2$ response when pulsing $CO/O_2/Ar$ and $CO/O_2/H_2O/Ar$ over fresh 2%$Co/CuMnO_x$ at 25°C**

The peaks due to the production of carbon monoxide were evolved at a similar time, indicating that the oxidation might take place using the same source of oxygen in each

case. It was therefore unlikely that the $H_2O$ was contributing as a source of oxygen for this reaction. Despite the peaks being eluted at a similar time and having similar shape there was a considerable difference in the relative magnitude of the peaks. The peak due to oxidation in the presence of $H_2O$ was a factor of four smaller than during oxidation in the presence of gas phase $O_2$ alone.

It was possible that this was due to preferential adsorption of $H_2O$ over $O_2$ upon the catalyst surface in a competitive adsorption type mechanism. Many authors have previously reported this as a water poisoning effect. [26-27] The effect has been reported to decrease activity as water molecules adsorb on the catalyst surface, scavenging available surface oxygen to form hydroxyl groups, which might block surface active sites.

$$2H_2O_{ad} + O_{ad} \longrightarrow 3OH_{ad} + H_{ad}$$

A similar mechanism was proposed by Bergeld for the promotion of CO oxidation by small quantities of $H_2O$ over Pt based catalysts. [28] It was possible that a similar mechanism was operating here using up available oxygen and having the effect of decreasing activity.

## 6.13 - Investigation into the Effect of Pulsing $H_2O$ in the Absence of Gas Phase Oxygen

When pulsing CO/Ar and $CO/H_2O$/Ar over the cobalt-doped hopcalite, the $CO_2$ product peaks were again almost super-imposable in terms of shape and detection time indicating that the source of the oxidising species in each case was likely to be the same.

The product peak in the presence of $H_2O$ was substantially smaller (7 times) than that obtained when pulsing CO/Ar alone indicating that water was having a detrimental effect on activity over the doped catalyst.

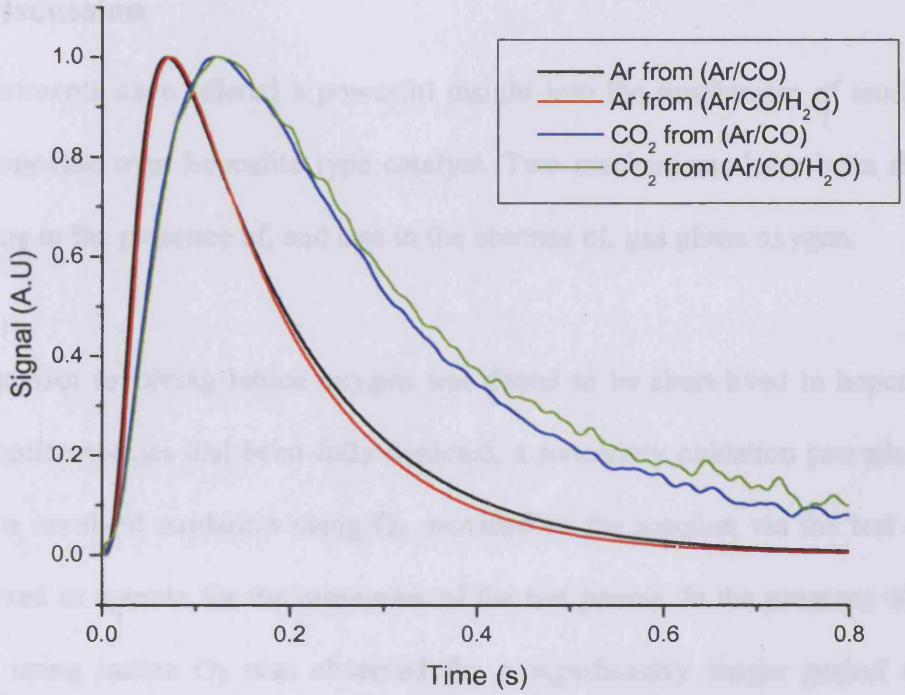


**Figure 6.13.1 – Normalised $CO_2$ response when pulsing CO/Ar and $CO/H_2O/Ar$ over fresh $Co/CuMnO_x$ at 25°C.**

The inclusion of cobalt may have been assisting the CO oxidation reaction by acting as a source of oxygen by assisting in the capture of $O_2$ from the gas phase. This would be via a similar mechanism to that proposed by Huang for oxidation over copper oxide at temperatures above 200°C.

It was postulated that the conversion of CO proceeded using lattice oxygen, thereby creating oxygen vacancies on the surface which could be repopulated by gas phase oxygen. [29] The re-oxidation mechanism proposed where cobalt was present was of a

Mars van Krevelen type which echoed that proposed by Veprek *et al.* in an earlier study. [21]

## 6.14 – Discussion

TAP experiments have offered a powerful insight into the mechanism of oxidation of carbon monoxide over hopcalite type catalyst. Two mechanisms have been shown to operate, one in the presence of, and one in the absence of, gas phase oxygen.

The mechanism involving lattice oxygen was found to be short-lived in hopcalite and once the lattice species had been fully depleted, a secondary oxidation prevailed. This mechanism involved oxidation using $O_2$ provided to the reaction via the test gas and was observed to operate for the remainder of the test period. In the presence of cobalt, oxidation using lattice $O_2$ was observed for a significantly longer period of time, indicating that the cobalt may have been operating as an oxygen donor, having the effect of continuously re-oxidising any oxygen deficiencies in the lattice.

Further evidence that cobalt was acting as a facilitator for the re-oxidation of the catalyst surface came from the reactivation experiments by continually pulsing $O_2$ under TAP conditions. The cobalt-doped catalyst was partially reactivated during these experiments, however, hopcalite could not be. This suggested that there might have been fundamentally different reactivation pathways occurring in each, with the difference being explained by the presence of cobalt in one of the catalyst systems. Both could be reactivated partially by exposure to atmospheric conditions for 12h, indicating that the mechanism of re-oxidation in the hopcalite was perhaps slow and where cobalt was present, this re-oxidation was more facile.

The deactivation of hopcalite species, observed under both steady state and TAP testing can be attributed to the total depletion of surface $O_2$ during the early stages of the reaction. The theory was that the adsorption of gas phase $O_2$ on to the surface was slower, so deactivation was observed in this system but not in the cobalt-doped catalyst.

A reduced hopcalite surface was re-oxidised by pulsing small quantities of $H_2O$ over the species. Incorporation of oxide species on to the catalyst surface from the gas phase was proven by the use of labelling experiments with $^{18}O$ labelled water, where $^{18}O$ was observed in the final $CO_2$ product. Equal quantities of $CO_2$ and $C^{16}O^{18}O$ were observed on pulsing CO/Ar over a $H_2{}^{18}O$ treated surface, indicating a significant level of exchange between the surface $^{16}O$ and the $^{18}O$ of the labelled water or the $^{18}O$ served to satisfy the need of the surface for oxygen in its highly reduced state.

On pulsing $CO_2$/Ar over a $H_2{}^{18}O$ treated surface, $C^{16}O_2$ was the major product (87.8%) but a significant quantity of $C^{16}O^{18}O$ was detected (12%). A very small quantity of $C^{18}O_2$ was detected indicating that a more complex mechanism might also have been occurring in the background, where the $^{16}O$ of the reactant species exchanged with surface $^{18}O$, followed by further reaction with surface adsorbed $^{18}O$.

When combined, these labelling experiments confirmed that it was possible to partially repopulate a catalyst surface using species form the gas phase. The presence of $^{18}O$ in the final $CO_2$ product indicated that the dominant mechanism of oxidation occurring over both the hopcalite and possibly the doped hopcalite was of the Langmuir-Hinshelwood type. This would have involved the adsorption of gas phase CO from the reactant stream, then subsequent reaction with surface bound $^{18}O$. Unfortunately, due to

technical difficulties it was not possible to confirm the similar behaviour of the cobalt-doped catalyst, by completing an identical set of TAP experiments.

In the cases where the surface was deactivated, a greater take up of oxide species was observed. Where a fresh surface was treated with $H_2{}^{18}O$, some exchange with surface oxide was observed but not to the same extent.

Both the cobalt doped catalyst, as well as the hopcalite alone, were sensitive to moisture poisoning on steady state experiments. Poisoning of catalyst activity by $H_2O$ vapour was also recorded with TAP experiments; this observation was not surprising. [30] However, the work reported is the first example of re-oxidising a reduced hopcalite catalyst surface with water vapour leading to a return of activity towards the test reaction.

Some interesting properties were also displayed when pulsing Ar/CO simultaneously with $Ar/H_2O$. High purity gases were used and the water used had been degassed, so the only source of oxygen available would have been the hydrogen bound species of the water molecule. Water has long been known to be a catalyst poison, so perhaps it was surprising that activity was recorded when co-pulsing $CO/H_2O$ over a reduced, deactivated hopcalite surface. The reaction did not occur via a WGSR mechanism as no hydrogen was detected by the mass spectrometer. On heating the catalyst sample to 50°C, hydrogen was evolved from the catalyst surface leading to the conclusion that it had been adsorbed on to the catalyst surface during the deposition of oxygen on the surface. This hydrogen adsorption was only likely to have occurred during the re-oxidation of the deactivated catalyst surface as experiments identified the possibility to regenerate by water pulsing. It has also been shown that $H_2O$ could reactivate a reduced

hopcalite surface so it was likely that a rapid re-oxidation of reduced surface active sites was occurring here which facilitated the oxidation reaction.

These experiments by no means provided a full picture of the complex mechanisms of oxidation and deactivation occurring in hopcalite systems. Some crucial sections of the likely mechanisms have been identified, increasing our understanding of CO oxidation over copper manganese oxide catalysts. Some of the results detailed confirm the thoughts of other researchers but further TAP experiments, outlined in Chapter 7, must be carried out in order to categorically prove some of the postulations made here. Preliminary investigations have indicated that the addition of cobalt to hopcalite catalysts may well strongly influence the surface re-oxidation mechanism leading to a more robust catalytic system.

## References


[1] C. O. Bennett, in Catalysis Under Transient Conditions, Ed. by J. M. Thomas & R. M. Lambert, Wiley, New York, 1980, pg 30

[2] C. Wagner, K. Hauffle, Z. Elektrochem, 44 (1938) 172

[3] K. Tamura, Adv. Catal. 15 (1964) 65

[4] C. O. Bennett, AlChE J. 13 (1967) 890

[5] H. Kobayashu, M. Kobayashi, Catal. Rev. Sci. Eng. 10 (1974) 104

[6] A. Brucato, M. Ciaofalo, F. Grisafi, R. Tocco, Chem. Eng. Sci. 55 (2000) 291

[7] J. T. Gleaves, J. R. Ebner, T. C. Kuechler, Catal. Rev. Sci. Eng. 30 (1988) 49

[8] D. J. Satman, J. T. Gleaves, D. McNamara, P. L. Mills, G. Fornasari, J. R. H Ross, Appl. Catal, 77 (1991) 45

[9] O. V. Buyevskaya, M. Baerns, Catal. Today, 21 (1994) 301

[10] O. V. Buyevskaya, M. Rothaemel, H. W. Zanthoff, M Baerns, J. Catal. 150 (1994) 71

[11] B. Kartheuser, B. K. Hodnett, H. W. Zanthoff, M. Baerns, Catal. Lett, 21 (1993) 209

[12] O. V. Buyevskaya, D. Wolf, M. Baerns, Catal. Lett. 29 (1994) 249

[13] D. S. Lafyatis, G. Creten, G. F. Froment, Appli. Catal. A, 120 (1994) 85

[14] J. T. Gleaves, A. G Sault, R. J. Madix, J. R. Ebner, J. Catal. 121 (1990) 202

[15] D. R. Coulson, P. L. Mills, K. Kourtakis, J. J. Lerou & L. E. Manzier in P. Ruiz & B. Delman (editors). Studies in Surface Science and Catalysis, Vol 72, Elsevier, Amsterdam, 1992, pg 305

[16] D. R. Coulson, P. L. Mills, K. Kourtakis, P. W. J. G. Wijnen, J. J. Lerou, L. E. Manzier, L Gruczi et al (Editors) New Frontiers in Catalysis, Elsevier, Amsterdam, 1993, pg 2015

[17] J. J. Lerou, P. L. Mills, in M. P. C Weijene & A. A Drinkenburg (Editor). Precision Process Technology, Kluwer, Dordrecht, 1993, pg 175

[18] T. A. Nijhuis, M. Makkee, A. D. van Langeveld, J. A. Moulijn, Appl. Cat. A: 164 (1997) 237

[19] G. S. Yablonsky, S. O. Shekhtman, P. Phanawadee, J. T. Gleaves, Catal. Today, 64 (2001) 227

[20] S. Z. Roginskii and Y. Zeldovich, Acta Physicochem, USSR, 1 (1934)

[21] S. Veprek, D. L. Cocke, S. Kehl and H. R. Oswald, J. Catal. 100 (1986) 250

[22] G. C. Bond, D. T. Thompson, Gold Bull. 33 (2000) 41

[23] Y. Schuurman, J. T. Gleaves, Catal. Tod. 33 (1997) 25

[24] J. T.Gleaves, G. S. Yablonski, P. Phanawadee, Y. Schurmann, Appl. Cat. A:160 (1997) 55

[25] Y. Tanaka, T. Utaka, R. Kikuchi, K. Sasaki, K. Eguchi, Appl. Catal. A: 6395 (2002) 1

[26] Y. Takita, T. Tashiro, Y. Saito, F. Hori, J. Catal. 97 (1986) 25

[27] G. J. Hutchings, R. G. Copperthwaite, F. M. Gottschalk, T. Hunter, J. Mellor, S. W. Orchard, T. Sangiorgio, J. Catal. 137 (1992) 408

[28] J. Bergeld, B. Kasemo, D. Chakarov, Surf. Sci. 495 (2001) L815

[29] T. Huang, D. Tsai, Catal. Lett. 87, 3-4 (2003) 173

[30] F. Grillo, M. M. Natile, A. Glisenti, Appl. Cat. B: Environ. 48 (2004) 267

# Chapter 7 – Conclusions

## 7.1 - Optimum Preparation Conditions

The early work centring on the development of a reproducible catalyst synthesis procedure was a critical factor in the development of the active species that we produced and discussed in later chapters. The crude co-precipitation method in chapter 2.1.1 produced some highly active species with comparable activity to the commercial system Moleculite but the synthesis of these species was infrequent despite identical methods being used. This implied that a greater control of reaction parameters was needed, therefore steps were taken to control both pH and temperature in later preparations. The temperature treatment of the precursor was identified as being crucial to the preparation of active species. Where low temperature, short calcinations were employed, final catalysts contained large quantities of amorphous manganese and copper hydroxy carbonates that were inactive as CO oxidation catalysts. In a similar manner, when high temperature long calcination times were used, the crystalline copper manganese spinel, $CuMn_2O_4$ was obtained possessing a low surface area. The inactivity and low surface are was most likely due to harsh thermal treatment of the material breaking down the pores on the catalyst surface that were necessary for activity. Intermediate calcination conditions were employed and gave rise to active species. The most active catalysts also displaying good catalyst surface areas were produced with calcinations conditions of 415°C for 2h in air. On characterisation, this species was shown to be a mixture of copper and manganese single oxides with the mixed phase $CuMn_2O_4$ also being present.

## 7.2 - Effects of Doping with Cations

A synergistic effect was present between the copper and manganese components and the dopant ion, as singularly, all of the metal oxides investigated here were poorly or inactive oxidation catalysts under the test conditions. Only when copper and manganese were in partnership with each other was activity observed; these species were inactive when prepared as single oxides. The addition of small amounts of metal ions gave rise to some further interesting properties of the system.

Doping the hopcalite catalysts with cations, particularly nickel and cobalt contributed to increased stability with time on line. It was likely that the nickel was reacting sacrificially with any water vapour present in the feed gas, thereby protecting the catalyst from water poisoning.

In the cobalt-doped samples, TAP experimentation seemed to suggest that the presence of cobalt in the catalyst system might have been facilitating the replenishment of the surface $O_2$, which was thought to be consumed via a Langmuir-Hinshelwood mechanism during the early time on-line. In many cases when cobalt was present in the catalyst system, no loss of activity due to depletion of lattice $O_2$ would have occurred.

The highest activity catalysts were those identified as being amorphous to XRD analysis, however later TEM studies of cobalt-doped species identified the particle size as being around 5nm which is recognised as being at the lowest limit of sensitivity for XRD studies. TEM micrographs identified the doped materials as having substantial crystalline character all be it of a microcrystalline nature.

Silver doping did not have the same stabilising effect as doping with either nickel or cobalt but an increase in the start-up activity of the catalysts. This again was likely to be due to the excellent properties of silver for $O_2$ storage, however on utilisation of the surface stored $O_2$, an alternative mechanism of for CO oxidation prevailed. The silver-doped catalysts did not appear to provide the same surface $O_2$ replenishment mechanism as was observed for the cobalt-doped samples.

The cobalt-doped samples also possessed good start-up activities and maximum levels of CO conversion, again leading to the conclusion that cobalt was promoting activity in the copper manganese oxide catalyst when present in small quantities. The effect was thought to be electronic rather than due to a structural promotion as on normalisation for differences in surface areas, the cobalt-doped species still displayed better conversion levels than the standard hopcalite catalyst.

In general, all of the doping experiments either offered better activity or enhanced stabilisation over the standard hopcalite but doping with cobalt offered the dual advantage of increased activity and stabilisation during the test period.

## 7.3 - Effects of Percentage Cobalt Doping and Precipitate Ageing Time

The effect of catalysts ageing in terms of the activity of the species produced was quite profound. The catalysts produced with an ageing time of 0h had good activity and were found to be composed mainly of the single metal oxide species. As ageing time was increased, the incorporation of the copper and manganese components into the catalyst mixed phase increase. This was exemplified by the decreasing size of the reduction peaks

of these species on TPR analysis. The size of the TPR reduction peaks was also connected to the oxidising power of the system, where higher volumes of $H_2$ were reacted on TPR analysis; this was in most cases a strong indicator of a highly active catalyst. In general, the catalysts produced with mid range ageing times of the variety investigated produced the most stable catalysts with respect to deactivation with time on line. Many species were produced that were more active than the industrial catalyst, especially at line on-line values of 30 minutes and more. The start-up activities of the cobalt-doped catalysts were lower than the industrial catalyst regardless of the percentage cobalt or ageing time used. However, one robust hopcalite sample was produced with an ageing time of 6h that matched the start-up activity of Moleculite and maintained a consistently high activity throughout the test period. The most active species produced throughout the study was the 2% $Co/CuMnO_x$ species aged for 6h, this species displayed total conversion towards the test period. The start-up activity of this species was however slow compared to the industrial catalysts so other elements such as silver or precious metals which might lead to a quicker start-up time would need to be included in the catalyst formulation to give catalysts suitable for use in personal protective equipment.

Questions remain as to the exact nature of the role that cobalt was playing in the highly active oxidation catalysts produced in this study. For each of the ageing times investigated, the addition of cobalt lead to increased active in all of the 1% doped catalyst tested. It was certain that the promotion of activity was not due to a surface area enhancement, as surface area normalised values still gave rise to different conversion rates. The presence of cobalt was likely to be contributing electronically to the oxidation mechanism or re-oxidation mechanism occurring in the catalyst. TAP experiments indicated oxidation using lattice

oxygen to be longer lasting where the catalyst was cobalt doped. Further evidence as to the role of cobalt in the re-oxidation mechanism of a reduced species came form the fact that the deactivated cobalt-doped catalyst surface was more responsive to re-oxidation experiments than the copper manganese oxide surface alone.

The similarity in size of the $Cu^{2+}$ and $Co^{3+}$ ions meant that a facile replacement of copper ions in the hopcalite framework could take place, causing alterations in the properties of the system due to the different size and charge anions of cobalt. The charge difference especially might have created lattice defects on the catalysts surface, forming interesting sites for catalysis to take place at.

## 7.4 - Water Poisoning

The effect of water doping on the hopcalite system was interesting, water poisoning occurred both in the presence and absence of cobalt as a dopant to an equal measures. It was therefore obvious that the presence of cobalt in the system had no effect in water poisoning prevention. The deactivation that occurred on the addition of water in small quantities to the system was rapid in all cases, whether the sample was doped or not. Reactivation of the species occurred back to its expected level by passing dry gas over the sample. The temporary poisoning effect of the water molecules was likely due to the adsorption of hydroxyl groups on to the catalyst active sites. By pulsing "dry" gas over the catalyst, activity returned at a quicker rate than pulsing the standard reagent gas. The "dry" gas has been passed through a molecular sieve to remove moisture. The rapid return to normal activity without the indicated a temporary poisoning effect where weakly adsorbed OH was possibly disabling the oxidation mechanism. The return towards normal activity

was almost instantaneous once water was withdrawn from the feed gas. Moisture protection must be included for hopcalite type catalysts if intention is for commercial use.

## 7.5 - Mechanistic Insight

In the first application of the TAP technique to hopcalite catalysts, experiments provided important information into the mechanism of oxidation of carbon monoxide and reactivation of reduced hopcalite and doped hopcalite surfaces.

Two mechanisms of oxidation were shown be operating for oxidation over both hopcalite and reduced hopcalite catalysts. A short-lived mechanism was shown to be operating in the absence of gas phase oxygen where lattice oxygen was thought to be oxidant. The addition of cobalt the catalyst was shown to prolong this mechanism. It was thought that the presence of cobalt in the catalyst was fuelling the re-oxidation of the catalyst surface as it became depleted on reaction with carbon monoxide. The re-oxidation of a reduced hopcalite surface was proven using labelling experiments that indicated that the mechanism of CO oxidation occurring over the catalyst was likely to be of a Langmuir-Hinshelwood type. Once lattice oxygen had been depleted, a less active mechanism of oxidation involving gas phase oxygen was still able to operate.

A reduced hopcalite could be re-oxidised to some extent by exposure to atmospheric conditions for 12h, or pulsing of $H_2O$ over a strongly reduced catalyst. It was not possible to re-oxidise a reduced hopcalite surface as quickly as a reduced cobalt-doped hopcalite surface. The fact that a reduced cobalt-doped surface could be reduced by pulsing a

relatively small amount of oxygen over the sample was again a strong indicator of the involvement of cobalt in the re-oxidation mechanism of the catalyst surface.

## 7.6 - Further work

As outlined in the aims of this thesis, promoters will form the future of catalysis. This thesis has gone someway to highlighting the beneficial effects of doping a well established, mature catalyst with small quantities of other elements.

In terms of an immediate follow on to this work, TEM results would be beneficial in discerning how the catalyst structures differ with changing ageing time. XRD has offered only limited use in this work but the application of in-situ XRD might give rise to interesting results on the amorphous to crystalline phase transition temperature that appears to form the boundary between active and inactive hopcalite type catalysts. The technique might also allow catalysts to be tailored to possess a desired level of crystallinity by identifying the heat treatment necessary for active phases to form. XPS might also be applied further to offer evidence of catalyst make-up in terms of the nature of the dopant metals and other surface adsorbed species such as carbonates that might be influencing activity. The application on FTIR or Raman Spectroscopy techniques might also allow further probing of offering important insight as far as surface adsorbed species are concerned, e.g. carbonyl species.

Further TAP experiments must be applied to probe mechanisms of oxidation, reduction and deactivation, especially with respect to cobalt-doped catalysts. Re-oxidation of reduced catalyst surfaces should further be probed, especially with the use of isotopes. The TAP

technique might also be applied to quantify the effect that catalyst ageing time and percentage cobalt content can have on the quantity of lattice $O_2$ present in the sample; a feature that is thought to be crucial to the oxidation mechanism.

The start-up activity of this system will continue to be of interest if the commercial species is to be improved upon. Further doping experiments, possibly extending the silver doping work presenting here or including catalytic quantities of precious metals might hold the key. Incorporation of water protection within the catalyst, again extending some of the initial groundwork identified in this study will be crucial in building a robust catalytic system will commercial applications. The obvious route to moisture protection would be an adsorbent layer to protect the hopcalite, though any inexpensive component added intimately to the catalyst make-up would have wide-ranging applications. Investigations in to the poisoning of the system by other materials such as sulphur or hydrocarbons might also be beneficial to providing a fuller understanding of the catalyst. For any commercial use of the species synthesised in this study, considerable work in to the scaling up of co-precipitation method will need to be carried out so that batches of many hundreds of grams might be produced. Early indications were that scale-up experiments could be successful in the production of 20-30g batches, but this work will need to be build upon further.